A NEW PROCEDURE FOR DETERMINING BOND ORDERS IN POLAR MOLECULES, WITH APPLICATIONS TO PHOSPHORUS AND NITROGEN CONTAINING SYSTEMS

By
MAGGIE A. AUSTEN, B.Sc.

A Thesis
Submitted to the School of Graduate Studies
in Partial Fulfilment of the Requirements
for the Degree
Doctor of Philosophy

McMaster University

A PROCEDURE FOR DETERMINING BOND ORDERS IN POLAR MOLECULES

DOCTOR OF PHILOSOPHY (2003) McMaster University
(Chemistry) Hamilton, Ontario

TITLE: A New Procedure for Determining Bond Orders in Polar Molecules, with Applications to Phosphorus and Nitrogen Containing Systems
AUTHOR: Maggie A. Austen, B.Sc. (Dalhousie University)
SUPERVISOR: Dr. R. F. W. Bader
NUMBER OF PAGES: x, 288, A1-12, A2-14, A3-16, A4-11.

Abstract

This thesis introduces a newly discovered relationship between calculated values of the delocalization index and Lewis bond orders, for polar bonds. Using the methods of the Theory of Atoms in Molecules, properties of individual atoms - defined as regions of real space - can be calculated from numerical molecular wavefunctions. In addition to determining the number of electrons in an atom, and thus the atomic charge, one can also calculate the extent to which the charge density on a given atom is delocalized to the each of the other atoms in the molecule. This property is known as the delocalization index.

For a non-polar bond (equal sharing of electrons), the delocalization index calculated from a Hartree-Fock wavefunction is found to correspond closely with the bond order predicted by the Lewis model of chemical bonding. The delocalization index decreases, however, as the bond polarity increases. The relationship between the decreasing delocalization index and the increasing atomic charges is quantified in this work. A simple quadratic relationship is observed between the delocalization index, $\delta(A,H)$ and the charge transfer, $q(H)$, across the A-H bond in a series of hydrides, AH_n. The same relationship, $\delta = 1-q^2$, is shown to be derived from the Hartree-Fock expressions for the delocalization index and the atomic charges and can be generalized to more than one pair of electrons. The same derivation applies to two other definitions of bond order proposed by other workers.

A method for employing these correlations, along with other calculated properties, to establish the Lewis bond order for a series of related molecules, with differently polarized bonds, is presented. The method is applied to seven series of phosphorus containing molecules and three series of nitrogen containing molecules. The octet rule is found to be more important for the nitrogen systems than for the phosphorus systems.

Acknowledgements

I would like to acknowledge the contributions of the many people with whom I have interacted during my years at McMaster, without whom this project would not have been successful. First, I would to thank Richard Bader for providing me with the freedom to explore this topic and for his guidance and continuing enthusiasm. Other members of the Bader group have made invaluable contributions to this thesis, both in developing the computer programs used and in providing moral support and camaraderie over the years.

I would like to thank my family and friends for their encouragement and understanding. This includes the many chemistry and physics students who started graduate school at the same time I did, and who made arriving alone in a new province fun and exciting, rather than terrifying. It also includes all those older friends who continued to keep in touch, even at a distance, no matter how many times I forgot to write back or return the phone call. Thank you Magda! And of course it includes all those new friends I've made over the years. I would particularly like to acknowledge my fellow freshman chemistry instructors who have been continuously supportive, both personally and professionally, as I try to hold down two 'jobs' at once.

Critical readings of the various manuscripts were by Richard Bader, Ron Gillespie, Gary Schrobilgen, David Chettle, David Brown, Russell Boyd and Stephen Cool. Their suggestions were greatly appreciated and made the thesis infinitely better than it otherwise would have been.

Thank you again to my family, who made me the person I am, and to Steve, who was there, every day, through it all. I love you.

Table of Contents

Table of Figures

See also Appendix A4 in the Table of Contents, above.

Table of Tables

See also Data Tables sections in the Table of Contents, above.

1. Introduction

For over 85 years chemists have been describing the bonding in molecules using cartoons consisting of atomic symbols, dots and (later) lines, known as Lewis structures (Lewis, 1916). This system of dots and dashes is the Morse code of chemistry, conveying large amounts of information in an easily transmitted message. The dots represent valence electrons, which are normally paired together as a colon. Some of the electrons may be localized on a single atom. These are referred to as non-bonding electrons, or lone pairs. In Lewis's model, connected atoms share one or more pairs of electrons, so that there are normally eight electrons (an octet) surrounding each atom. These shared pairs later came to be represented by lines and eventually became almost synonymous with the lines of force binding the atoms together. The shared pairs are therefore also known as bonding pairs.

The number of electron pairs binding two atoms together is called the *bond order*. In some cases, more than one Lewis structure is needed to adequately represent the molecular properties. The structures are then referred to as *resonance structures* and they are drawn with a double-headed arrow connecting them. This resonance arrow indicates that the true properties of the molecule are in some way an average, or superposition, of the properties indicated by each of the structures drawn. For example, ozone (O_3) requires two resonance structures, and the two O-

O bonds each have an average bond order of one and a half (3/2).

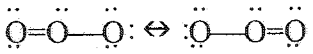

$$O{=}O{-}O \leftrightarrow O{-}O{=}O$$

1.1. The problem

This work began with an interest in the degree of multiple bonding -- and therefore the extent of electron delocalization – in the phosphenium cations, PR_2^+. Like the related carbenes, CR_2, many of the most easily isolable members of this class have a planar amino group, NY_2, as one or both of the substituent R groups.

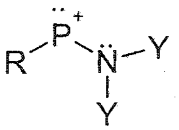

The observed planarity of the amino groups suggests that the 'lone pair' on nitrogen is being partially donated to the formally electron deficient[*] phosphorus atom. This interaction can be described by the following resonance structures, in which the phosphorus atom has a complete octet – eight valence electrons.

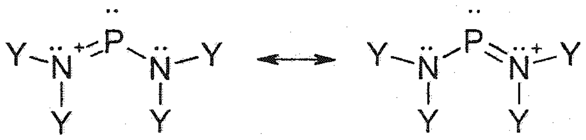

These structures suggest that the P-N bond has partial multiple-bond character, *i.e.* a bond order greater than one. That conclusion raises two questions. 1) How much double bond character does the P-N bond have? 2) Is this double bond character the (main/only) reason for the particularly effective stabilization of

---

[*] The phosphorus is electron deficient in the sense that it has less than a full octet of electrons in its valence shell.

amino-phosphenium cations? In order to answer the second of these questions we must establish whether the extent of multiple bonding in amino-phosphenium cations is in fact greater than in other phosphenium cations, and whether that is the only major difference between the cations.

The questions have now become: 1) What is the extent of multiple bonding in phosphenium cations in general? 2) Is it exceptionally high in amino-phosphenium cations? 3) Do amino-phosphenium cations exhibit any other major differences relative to less stabilized phosphenium cations? Again, let us start with the last of these. We should ask what other factors are likely to contribute to stabilization of phosphenium cations besides strong multiple bonding character. There could be kinetic effects involved in making amino-substituted phosphenium cations relatively easy to isolate. The amino group may protect the electrophillic phosphorus from nucleophillic attack,[*] making it less labile. However, hydride transfer energies, ΔE_H, indicate that the amino groups are among the most effective *thermodynamic* stabilizers of phosphenium cations (Gudat, 1998; Schoeller and Tubbesing, 1995) and it is this stabilization we wish to explain.

$$PH_2^+ + HPR_2 \rightarrow PH_3 + PR_2^+ + \Delta E_H$$

Along with double bond character through 'lone pair donation' comes a spreading out of the positive (formal) charge, over the phosphorus and substituent atoms. In addition, the doubly bonded Lewis structures obey the 'octet rule' for all

---

[*] This could include steric protection and/or electronic effects such as the destabilization of the low-energy, unoccupied p_π - like orbital.

atoms. Chemists tend to associate both of these properties of Lewis structures (spreading out of formal charge and agreement with the octet rule) with chemical stability. It is questionable whether either of these factors has any physical significance, let alone an effect on the energy of the cation. In any case, both can be seen as secondary effects of the double bond formation and cannot really be separated from multiple bonding as stabilizing factors in this system.[*]

Another factor that may contribute to stability is bond polarity. While polar bonds tend to be more labile than non-polar bonds, the electrostatic attraction between a positively charged atom and a negatively charged atom gives thermodynamic stability. This is reflected in the larger bond dissociation energies of polar bonds relative to otherwise similar non-polar bonds. The electronegativity difference between P and N is significant and the P-N bonds are thus quite polar. It has been suggested (Gudat, 1998) that the exceptional cation-stabilizing ability of the amino substituent is due to the best combination of π-donation (which should increase from F to NH_2 but is absent in CH_3) and electrostatic attraction.[†] Similar push-pull effects are thought to stabilize the related carbene molecules (Bourissou *et al.*, 2000), though in these systems the ideal substituents are thought to be those that maintain electroneutrality, the stabilization being explained in terms of orbital interactions.

---

[*] Sigma donation (reversal or reduction of bond polarity) may also help spread out the positive charge.

[†] Gudat uses Natural Population Analysis charges on the atoms P and E to determine the electrostatic attractions. The N has the largest charge, due to the combined bond polarity of the P-N and two N-H bonds. The attraction is further enhanced by the shorter P-N bonds relative to P-S and P-Cl bonds, which should have similar polarities.

The strength of a bond tends to be well correlated with the bond length, for a given pair of atoms. Even for different sets of bonded atoms, longer bonds tend to be weaker. We might then expect bond strengthening (and thus molecular stabilization) to be reflected in bond shortening. Other properties of the bond that may be relevant are the accumulation and distribution of electron density in the bonding region. The questions posed above will be explored, and answered, in Chapter 8.

1.2. The Approach to a Solution

To summarize, the properties to be investigated are bond length, bond polarity as measured by atomic charges, the distribution of electron density in the bonding region and the extent of multiple bonding. The Theory of Atoms in Molecules (Bader, 1990) will give us the tools to calculate and analyse these properties and the appropriate methods will be described in Chapters 2 and 3. However, it is very difficult to make meaningful comparisons of bond properties when the atoms involved are different in each molecule or ion. As the size and electronegativity of the substituent atoms change, all the other properties change also. The approach adopted in this thesis is therefore to study a *series* of 'typical' phosphorus-element (*P-E*) bonds represented by the phosphines: H_2PR, HPR_2 and PR_3. The substituent groups used are the same as those to be studied in the phosphenium cations: R = H, F, OH, NH_2, CH_3, Cl, SH, PH_2 and SiH_3.

Since one of the main goals of this thesis is to ascertain the extent of multiple bonding in the cations, a series of 'standard double bonds' is also studied. The question of what constitutes a 'double bond' will be considered in more detail below, but for now we will assert that the series HP=X involves phosphorus-element double bonds to O, N, C, S, P and Si, where X = O, NH, CH_2, S, PH and SiH_2, respectively. These four series, H_2PR, HPR_2, PR_3 and HPX allow us to establish how the bond lengths, atomic charges and bonding density vary as the substituent group changes and as the bond order increases from one to two. We may then determine how the trends in phosphenium cation bonds compare to these 'standard' trends. To ensure that the observed differences in the P-E bonds are significant, the effects of substitution at P and/or E as well as rotation about the P-E bond are studied for the phosphines in order to establish how much variation is present within, for example, the set of 'standard P-N single bonds.'

1.2.1. Expanding the investigation to other systems

Once the groundwork had been laid, in terms of determining the methods to be used and establishing standard parameters for P-E bonds, two other series of phosphorus molecules were added to the study. The extent of multiple bonding in these systems is also a matter of debate and presents an opportunity to extend the application of the tools developed in this thesis. The two additional series are H_3PX and HPX_2, where X = O, NH, CH_2, S, PH and SiH_2, as in HPX. Both series have a pentavalent phosphorus atom and *the question of P-E bond order arises from the question of what Lewis structure to draw.* Taking X = O as an example, Lewis's 'rule of eight', *i.e.* the octet rule, suggests the structure on the left for H_3PO, below. The existence of systems such as PCl_5 shows that phosphorus may have an 'expanded octet' and the structure on the right is thus possible.

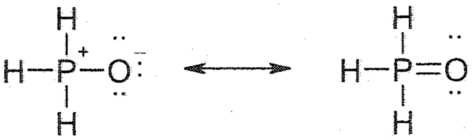

There is a school of thought that holds that reducing the number of formal charges[*] is more important than satisfying the octet rule. Indeed this is a topic much debated in the chemical education literature with some articles supporting the octet rule[†] and others supporting the 'minimization of formal charge' approach[‡] in which multiple bonds are made to the central atom if, and only if, there is a positive charge on the central atom and a negative charge on a neighbouring atom. A slightly different approach must then be taken for non-polar molecules such as N_2 or $H_2C{=}CH_2$. Still others suggest that both structures are important and that both should be included, with the 'true structure' being a (weighted) resonance average, though the weighting factors are generally unknown.

All approaches to drawing Lewis structures tend to require that the

---

[*] The formal charge on an atom is the charge it *would* have is all bonding electrons were *equally* shared between two atoms. In the formal charge minimization procedure, electronegative terminal atoms always receive a complete octet.

[†] Typically this position is held on the basis of large negative charges calculated for O atoms, or simply for simplicity. See for example: L. Suidan, J. K. Badenhoop, E. D. Glendening, F. Weinhold,. "Common Textbook and Teaching Misrepresentations of Lewis Structures," *J. Chem. Edu.*, 1995, **72**, 583. See also J. Cioslowski and P.R. Surjan, *THEOCHEM*, 1992, 87, 9.

[‡] Typically this position is held on the basis of large electron densities and strong, short bonds, suggestive of double bonds. See for example: G. H. Purser, *J. Chem. Educ.* 2001 **78** 981; G. H. Purser, "Lewis Structures Are Models for Predicting Molecular Structure, Not Electronic Structure," *J. Chem. Edu.*, 1999, **76**, 1013; D. K. Straub, "Lewis Structures of Oxygen Compounds of 3p-5p Nonmetals," *J. Chem. Edu.*, 1995, **72**, 889.

terminal atoms in any structure be given a complete octet and that second period elements (Li - Ne) not exceed the octet. This last rule is usually justified by the lack of experimentally known molecules, such as NCl_5 or OCl_6, with a coordination number greater than four on the second period atom. In order to check the validity of the octet rule for second period elements, in contrast to third period elements, the series of molecules H_3NX was also studied, and compared to H_2NR and HNX. Thus three more series of molecules were added to the study.

1.2.2. Is this a soluble problem?

It remains to be asked, ***"Exactly what do we mean by a 'shared pair of electrons'?"*** The Lewis model is an inherently local model in which electrons are assumed to be localized on one or two atoms. A shared pair of electrons is then a pair that contributes to the valence shell of two atoms. When more resonance structures are needed for an adequate description, as in benzene, chemists take this as an indication that the electrons are more delocalized than usual. Certainly electron sharing relates to the delocalization of electrons between two atoms. A quantum mechanical description, however, implies that all the electrons are inherently delocalized. In the molecular orbital model, pairs of electrons 'occupy' orbitals that are delocalized over the entire molecule, and in fact over all space. In any quantum mechanical description that obeys the Pauli Principle, all the electrons are indistinguishable and thus exchanging with each other and so are delocalized over the entire molecule. What can the terms *localized*, *delocalized* and *shared* mean within this context?

This is one example of an oft-cited problem with detailed quantum mechanical calculations. The complex mathematical descriptions of molecules (or ions or solids) may be very accurate, but appear to have little relationship to the simple chemical concepts of atom, charge, lone pair, bond, bond order, *etc.*, in terms of which most chemists tend to think. Molecular orbital descriptions can be quite helpful in understanding chemical reactivity and electron properties such as absorption and ionization energies. In-depth analysis of wavefunctions and their constituent orbitals can become quite unphysical however, and thus arbitrary and counterproductive. The Theory of Atoms in Molecules allows us to analyze a calculated wavefunction in terms of the observable properties it predicts, including localization and delocalization of electrons, rather than in terms of the orbitals used to construct the wavefunction.

In the early stages of this work, it was unclear whether a meaningful answer could be found to the question of how much double bond character was present in a given molecule. Indeed it was not clear that the question was meaningful, as bond order was not clearly related to any observable that could be calculated from the wavefunction or measured experimentally. Rather, bond order is a model-dependent concept, rooted most deeply in the Lewis model of chemical bonding. This thesis therefore seeks specifically to determine the extent of multiple bonding as measured by the *Lewis* bond order.

The assignment of a Lewis bond order is not straightforward when a single

Lewis structure is insufficient to describe the bonding, as seems to be the case for the phosphenium cations. In that case, the bond order is assumed to be *somewhere* between the different bond orders predicted by the various structures. The model is further complicated by conflicting ideas about which Lewis structures best describe the bonding in molecules that may, or may not, obey Lewis's rule of eight, such as HPX_2, H_3PX and H_3NX. The octet rule has evolved from an empirical observation to a guiding principle that some chemists take as a universal law of chemical structures. Thus resonance schemes such as ***A*** and ***B*** are not uncommon.

A.

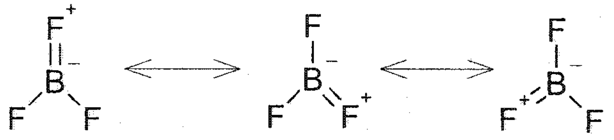

B.

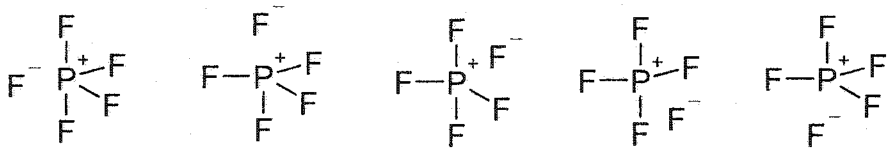

Chemists who find these 'octet' structures unhelpful or misleading use a different rule of thumb to replace the octet rule on central atoms. This guideline suggests the judicious placement of double bonds to reduce the number of opposing formal charges within a molecule or ion. Thus while the octet rule requires $^{+}\!:C\equiv O:^{-}$ (bond order = 3), the formal charge minimization procedure gives $:C=\ddot{O}:$ (bond order = 2) for the Lewis structure of carbon monoxide.* It is

---

* In CO, C is considered a central atom, while electronegative O is terminal.

therefore unclear, even within the Lewis model, what the bond order is in CO, and many other molecules. A more detailed discussion of various definitions of bond order and their relation to specific models of chemical bonding is given in Appendix 3.2. The method proposed in this thesis will help to resolve the issue of what Lewis structures best represent the sharing of electrons in polar bonds, without reference to the octet rule, or to any predetermined limits on the formal charge.

1.2.3. The meaning of bond order

When deciding among these various resonance schemes, or attempting to determine weighting factors, the most important question one should ask is, *"**What does each particular Lewis structure mean?**"* In other words, what physical/chemical properties are we trying to represent and what value does each structure intend to assign to each property? When Lewis introduced his dot diagrams to describe chemical bonding each line or pair of dots was meant to represent a pair of valence electrons. The fact that electrons generally come in pairs is the source of Lewis's 'rule of two.' A pair of dots associated with just one atom is mean to represent a pair of electrons located primarily on that atom (a lone pair), while a line between two atoms is meant to represent a shared pair of electrons. This shared (or bonding) pair participates in the valence shell of both atoms and is thought to constitute, in some way, the bond.

However, the electron pair need not be shared equally when the atoms have different electronegativities. Thus even the extremely polar LiF could be described as having one very unevenly shared pair of electrons. At some (not well defined) point along the polarity scale, we normally say that the 'bonding pair' has become essentially *localized* on the more electronegative atom. The definition of Lewis bond orders becomes even more complicated by the issue of bond polarity; how equal does the sharing have to be before we call it sharing, and thus count the pair towards the bond order? There does not seem to be any simple answer to that question. For multiple bonds, the question of bond polarity is closely connected to resonance schemes such as that shown above for H_3PO, and repeated here.

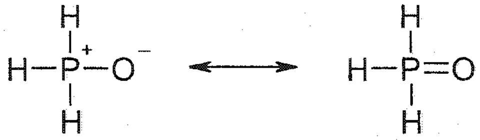

Clearly, this is meant to represent that at least one pair of electrons is *partially* shared between P and O and *partially* localized on O. However, this is no different from saying that the pair is unequally shared, *i.e.* polar. One might then conclude that the structures are meant to represent the equal sharing of one electron pair and the unequal sharing of another, but this is not a reasonable description of the bonding.* The only reasonable interpretation seems to be that the two polar bonds have different polarities, but it is questionable whether the chemists who draw such structures really have this interpretation in mind. Two (equally) polar bonds would be better represented by the resonance scheme shown below.

---

* It is questionable whether the two shared pairs can be meaningfully distinguished from each other, but if they can then they are surely both polar, though not necessarily equally so.

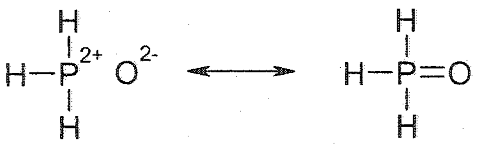

The polarity need not be explicitly shown in this way and was already assumed by Lewis. Two (equally) polar bonds can be adequately represented by a single Lewis structure [$H_3P{=}O$] if we choose to interpret the Lewis structure in this way. Similarly, we do not usually write non-bonded resonance structures to represent the polar O-H bonds in water. Rather we assume that a single structure, [H-O-H], giving a bond order of one, is adequate.

1.3. Delocalization and the Theory of Atoms in Molecules

The Theory of Atoms in Molecules (Bader, 1990) has been developed to analyse and interpret calculated wavefunctions in terms of physical observables and simple chemical concepts. The details of this theory will be given in more depth in Chapter 2. The most important aspect of this theory is that it divides the molecule into atoms that are defined as open regions of real space, and it does so in a non-arbitrary manner. These atoms have well defined properties and obey equations of motion analogous to those obeyed by the total system. This allows the non-arbitrary calculation of properties such as atomic population and energy. Of these, atomic charge will be most important to this thesis, as a measure of bond polarity.

The theory also allows the calculation of atomic localization, the number of electrons that are *localized* within a given atom and the associated delocalization index, $\delta(A,B)$, which measures the number of electron pairs *delocalized* between atoms A and B. Here, the words *localization* and *delocalization* are related to the concept of electron exchange, as required by the Pauli principle, see below.

1.3.1. The chemistry of the delocalization index

As this work began, the most promising *observable* for relating calculated values to bond orders was the delocalization index, δ. Its physical interpretation is 'the number of electron pairs delocalized (shared) between two regions of space (atoms).' This property will be defined and discussed in more detail in chapter 3. For non-polar bonds, the Hartree-Fock value of δ corresponds closely to the bond order predicted from standard Lewis structures (Fradera *et al.*, 1999). There are two objections, however, to equating δ with bond order.

The first is that the delocalization index is non-zero for atoms that are not directly bonded to each other. Thus electron sharing takes place between every pair of atoms in a molecule, while bonding - defined as the accumulation of electron density along a bond path (Bader and Essen, 1984) - occurs only between atoms that are normally assumed to share electrons in the localized Lewis model. Identifying δ with bond order would therefore entail assigning non-zero bond orders to pairs of atoms that are not bonded together.

The second obstacle to identifying δ with bond order is that, for polar bonds, δ is less than the bond order predicted by Lewis structures. For some chemists this may not appear to be a problem, since they choose to interpret Lewis diagrams as non-polar representations, as if the formal charge were meant to reflect the true atomic charge. Given this interpretation of Lewis structures, the atomic charges in water require at least two of the resonance structures shown below.

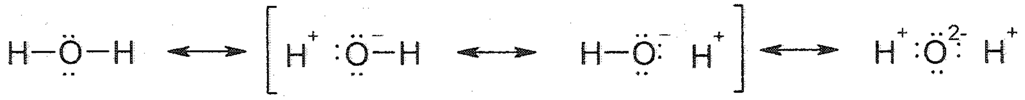

Those who interpret Lewis structures in this way would not be surprised to learn that the delocalization index (or bond order) is less than one for polar bonds. For those whose concept of bond order allows for bond polarity within the Lewis structure [H-O-H], an indicator that gives a bond order of one for water is desirable, so that the question of bond order in other molecules can be meaningfully answered.

When this research began, no such observable property (experimental or calculated) was known. The first step was therefore to search for ways to distinguish between single, double and partial bonds based on quantitative or qualitative differences in the calculable properties of the molecules and their constituent atoms. Thus a number of properties were studied for a wide range of molecules involving phosphorus. The definition and interpretation of many of these properties will be discussed, in the context of the Theory of Atoms in Molecules, in Chapter 2.

Many discussions of the nature of particular bonds of interest have been based on empirical classification schemes relating to properties of the electron density. Since these properties vary with the size, electronegativity and period of the atoms involved, it was important to establish parameters for typical phosphorus-element single bonds and double bonds before attempting to consider systems with potentially partial multiple bonding. Indeed, such 'baseline' values are important for any study of the properties of atoms in molecules. A secondary purpose of this thesis is therefore to establish a database of the properties of phosphorus atoms in molecules, at a common computational level, for use in future studies.

As the data were collected and analyzed, molecules were compared within each series and the series were compared to each other. Correlations were sought between the various properties of interest. A simple plot of the dependence of delocalization index, δ, on bond polarity, as measured by group charges, q, revealed an empirical quadratic relationship. Such a relationship is easily derived theoretically from the mathematical expressions for δ and q at the Hartree-Fock level of theory, as will be shown in Chapter 3. This relationship allows the delocalization to be 'corrected' for the bond polarity effects, affording the hypothetical 'non-polar' bond order. This represents the first quantitative measure of Lewis bond orders for polar bonds that does not involve interpretation of specially optimized (localized) orbital representations. We therefore look more closely at the physical interpretation of the delocalization index in the next section.

1.3.2. The physics of the delocalization index

The electronic structure of a molecule can be described in terms of a molecular wavefunction. One of the most fundamental observable properties that can be obtained from the wavefunction is the electron density, the distribution of charge through space. Another property obtained from the wavefunction is the Fermi density, or Fermi hole, $h^{\sigma}(\mathbf{r}_1, \mathbf{r}_2)$. This Fermi hole describes how the σ-spin density at one position, $\mathbf{r}_1$, is spread out, or delocalized, to other positions, $\mathbf{r}_2$.

At the Hartree-Fock level of theory, the only type of electron correlation accounted for is that due to the Pauli exclusion principle. At this level, there is no correlation between electrons of the same spin. Thus α-spin electrons and β-spin electrons may be treated as two independent, but equivalent, sets of electrons. Within the set of α-spin electrons, the density at position $\mathbf{r}_1$ excludes density from the surrounding region, as it spreads out through space, as described by the Fermi hole. An identical principle holds for the β-spin electrons, while there is no exclusion of β-spin electrons due to α-spin electrons. Both α and β valence electrons are attracted to the bonding regions, thus α,β pairs may result, as hypothesized in the Lewis model.

For an electron at a given reference position, the Fermi hole may be very localized, meaning that the probability of finding another same-spin electron is nearly zero in nearby regions but is unaffected further from the reference position, or the Fermi hole may be delocalized, in that there is significant reduction in the probability far from the reference position. It is in this sense that the words localization and delocalization shall be used throughout the rest of this thesis; ***an electron is localized if its Fermi hole is localized and is delocalized to the extent***

that its Fermi hole is delocalized (Bader and Stephens, 1975). It has been shown (Bader *et al.*, 1996a/b) that this definition of delocalization determines a large range of phenomena generally attributed by chemists to electron delocalization, including aromatic substituent effects and spin-spin coupling of vicinal hydrogen atoms.

Integration of the Fermi hole (weighted by the electron density), as prescribed by the Theory of Atoms in Molecules, results in a delocalization index between two atoms, or groups of atoms. For a non-polar bond the delocalization index, calculated at the Hartree-Fock level of theory,* corresponds very closely with the predicted bond order from a Lewis structure, *i.e.* it equals the predicted number of equally shared electron pairs. As the bond becomes increasingly polar, the electrons become more localized on the more electronegative atom and the calculated delocalization index decreases. This polarity may be assumed to exist within the covalent Lewis description, [A-B], or may be made explicit with an ionic resonance contributor, [$^{+}$A :B^{-}]. For a polar 'doubly-bonded' structure, [A=B], the delocalization index is less than two and if it is very polar it may be less than one. Should we then say that there is one slightly polar bond or two very polar double bonds? The answer is often not clear. If we wish to translate our results into the language of Lewis structures should we write [A=B $\leftrightarrow$ A^{2+} :B:$^{2-}$], [A^{+}-B:$^{+}$], or simply [A=B]? Again the answer depends mainly on how we choose to interpret the Lewis structures. The physical quantities of interest, the charge and extent of electron delocalisation, are already known from the calculation.

---

* Fradera *et al.* (1999) found that correlation significantly lowers $\delta(A,B)$ for primarily covalent interactions.

1.4. Introduction of a New Computational Approach

The author of this thesis chooses to interpret Lewis structures in such a way that a single Lewis structure suffices for the description of water, giving an O-H bond order of one. Furthermore, if two shared electron pairs have similar polarity, as is typically the case, the *Lewis* bond order is taken to be two, as might be expected between C and O in an unconjugated ketone, $R_2C=O$, for example. Such interpretations seem, to the author, to be in closest accord with the understanding of experimental chemists, who use the language of Lewis structures to communicate, and help explain, their results.

This thesis introduces a newly discovered relationship between calculated values of the delocalization index and the Lewis bond order, for polar bonds. The reduction in the delocalization index, $\delta^{HF}(A,B)$, due to bond polarity is related in a simple way to the charge transferred to the more electronegative atom, q(B) = -q(A). The relationship will be derived and demonstrated in Chapter 3. We will see that in the simple one-orbital two-electron case, the delocalization index depends on the square of the charge transferred, $\delta(A,B)=1-q(A)^2$, and that the maximum delocalization of 1.0 thus occurs for the non-polar case, $q(A) = 0$. We will also see that the coefficient of q^2 can be varied by interactions with other orbitals. The relationship will be verified empirically using previously published data. ***A procedure for using this relationship to determine bond orders in a series of related molecules will be introduced.*** This procedure will be applied to the series H_2PR, HPR_2, PR_3, HPX, HPX_2, H_3PX, PR_2^+, H_2NR, NR_3, HNX and H_3NX. For the phosphenium cations, the extent of multiple bonding in $P(NH_2)_2^+$ will be compared to that in other members of the series in order to ascertain whether there is a significant difference and whether this difference is likely to account for the much greater stability of $P(NH_2)_2^+$ as measured by hydride transfer energies.

1.5. Outline of the Thesis

In Chapter 2, a brief review of the basic postulates of quantum mechanics is given, followed by a description of the philosophy and methods of the Theory of Atoms in Molecules. This includes the definition of an atom as a proper open system and formulae for calculating local and group contributions to total system properties. The topological description of chemical structure is also included. Details of some relevant derivations are given in Appendix 2.

In Chapter 3, some basic descriptions of chemical bonding are discussed. Calculated local and atomic properties can be used to characterize the bonding within the context of one or more such frameworks. Interpretations of the properties at characteristic points, known as bond critical points, are discussed. Mathematical details of the delocalization index are given and the relationship between charge transfer and the delocalization index is derived. The extraction of bond orders and formal charges from an extrapolation of the calculated data on a series of related molecules is introduced. A tutorial on density matrices is given in Appendix 3, along with a discussion of several previous definitions of bond order based on calculated wavefunctions.

In Chapters 4 through 8, the results of geometry optimizations and Atoms in Molecules analyses of the computed wavefunctions are presented. In chapter 4, three series of differently substituted phosphines (PH_2R, PHR_2 and PR_3) and a series of amines (NH_2R) are studied, along with a few additional substituted amines and phosphines. These series establish the 'baseline' properties of P-E and N-E single bonds. The effects of electron correlation, substitution and rotation about the P-E bonds are explored. In chapter 5, the properties of P-E and N-E double bonds are established by a study of two series of molecules, HP=X and HN=X.

In Chapters 6 and 7, some hypervalent compounds are studied: $H_3N{=}X$, $H_3P{=}X$ and $HP({=}X)_2$. The P-E and N-E bond orders in these systems are investigated using the method established in the previous chapters. In chapter 8, the formally hypovalent phosphenium cations, R_2P^+ are studied. As described at the beginning of this chapter, the bond order in these systems is expected to be between one and 1.5. The bond order of these systems is investigated and the stabilizing role of amino substituents is explored.

Chapter 9 makes some final comparisons between the various series and summarizes the findings of the investigation. The data from each series are plotted together in a series of Figures, found in Appendix 4. The reader is referred to these figures to get a simple, visual overview of the major trends discovered in Chapters 4 – 8. Appendix 1 gives a glossary of the specialized terms and symbols used in this thesis.

1.6. A Note on Notation

Throughout this thesis I will refer to the second row atoms (C, N, O, F) as L and to the third row atoms (Si, P, S, Cl) as M, consistent with their valence shells being the L and M shells, respectively. Both second and third row atoms will be represented by E. When referring to a 'monovalent' substituent *group* (-CH_3, -SH, *etc.*), I will use the symbols R, EH_n, LH_n or MH_n. When referring to 'divalent' substituent groups (=SiH_2, =NH, *etc.*), I will use the symbols X, EH_{n-1}, LH_{n-1} or MH_{n-1}. On occasion, Pn is used to refer to the central pnictogen, be it P or N.

1.7. Computational Methods

1.7.1. Previous related work

Some organophosphorus compounds have been previously studied by the Atoms in Molecules method (Bachrach, 1989 and Howard *et al.*, 1995, 1996), as have phosphorus-oxygen 'double bonds' (Chestnut, 1998 and Dobado *et al.*, 1998). An important result of the paper by Bachrach (1989) relates to basis set and correlation effects. He finds that polarization (d) functions are necessary for good reproduction of experimental organophosphorus species geometries. His Hartree-Fock geometries for phosphines were in good agreement with experiment, but for multiply bonded systems electron correlation (MP2) was needed to get good agreement. In the present study a much larger basis set is used, and some correlated results are included to study the effects on the observed trends.

A study of correlation and basis set effects on the delocalization index was included in the paper by Fradera *et al.* (1999). The basis set 6-311++G(2d,2p) was found to give no significant change relative to 6-311+G(2d,2p) though there were small differences compared to smaller basis sets. Correlation (at the CISD level) was found to have the largest effects on non-polar covalent interactions, which showed reductions of 27% for N_2 and up to 16% for main group hydrides (CH_4 and SH_2). The effects on polar covalent interactions were smaller and ionic interactions showed small increases in the delocalization indices. The correlation effect on the P-H delocalization index of PH_3 was found to be a decrease from 0.839 to 0.774.

1.7.2. Programs and parameters used

All the molecules studied in the present work were geometry-optimized at the restricted Hartree-Fock level of theory. Many molecules were also optimized at the MP2 level and a few at the QCISD level to determine the effects of correlation. All analyzed wavefunctions were calculated at the same level of theory as the geometry optimization. A revised version of gaussian94 was used (*Virial*: Keith, 1995), which implements self-consistent virial scaling (SCVS, Löwdin 1959; Douglas and Murdoch, 1982) to ensure that the wavefunction satisfies the virial theorem.* The convergence criteria for the geometry optimizations and virial scaling procedures are given in Table 1-1.

---

* In a few cases the MP2 wavefunctions could not be converged using the SCVS method, so these were calculated using the standard (unscaled) gaussian94 package.

Table 1-1: Convergence criteria for the geometry optimizations and virial scaling procedures*

Parameter	**Threshold**
Maximum Force	2×10^{-6}
Root Mean Square Force	1×10^{-6}
Maximum Displacement	6×10^{-6}
Root Mean Square Displacement	4×10^{-6}
$(V / T) - 2$	1×10^{-8}

The Atoms in Molecules analysis of the resulting wavefunctions was performed using the *AIMPac* suite of programs. Critical points in the electron density were located and analyzed using *Extreme94B* or *Extreme96*. Atomic properties, including atomic overlap matrices (AOM's) were integrated using *PAIM96*, which accounts for virial scaling. The (de)localization indices were calculated at the Hartree-Fock level only, from the atomic overlap matrices using the *Bindx* and *Bond* programs. Critical points in the Laplacian of the density were analyzed using *Bubble* and *Extreme*.

Figures were generated with a variety of programs. The contour plots of the Laplacian of the density were generated using the *Gridv* and *Contor* routines of *AIMPac*. Gradient vectors of the density were traced using *Gridvec*. The isovalue envelopes of the Laplacian were generated using *Nabla2* and displayed using the *Scian* visualization package. Graphs of the numerical data were plotted using *Microsoft Excel*, and the equations of the best-fit quadratic curves, for the δ *versus* *q* graphs, were found using the built-in regression analysis tools. References for all programs used can be found in the bibliography below.

---

* Requested convergence on root mean square density matrix = 1.00×10^{-8} within 64 cycles. Requested convergence on maximum density matrix = 1.00×10^{-6}.

Bibliography

SOFTWARE USED:

Freely available and/or internally developed:

AIMPac (Including: Extreme9x, Gridv, Gridvec and Contor): available for download at: http://www.chemistry.mcmaster.ca/aimpac/.

Bindx Version 96, Revision C: Copyright by Todd. A. Keith, 1996.

Bond: M. Austen and F. Martin, McMaster University, 1997.

Bubble: Paul Krug, McMaster University, 1990.

Nabla2: S. Noury, Université Pierre et Marie Curie, Paris, France. (See also: Noury, S.; X. Krokidis, F. Fuster and B. Silvi (1999). *Computers & Chemistry (Oxford)* **23**, 597.)

PAIM96, Version 96, Revision C: Copyright by Todd. A. Keith, 1996.

Virial: Todd. A. Keith, McMaster Unviersity, 1995.

Commercially Available:

Gaussian94, Revision B.3: M. J. Frisch, G. W. Trucks, H. B. Schlegel, P. M. W. Gill, B. G. Johnson, M. A. Robb, J. R. Cheeseman, T. Keith, G. A. Petersson, J. A. Montgomery, K. Raghavachari, M. A. Al-Laham, V. G. Zakrzewski, J. V. Ortiz, J. B. Foresman, C. Y. Peng, P. Y. Ayala, W. Chen, M. W. Wong, J. L. Andres, E. S. Replogle, R. Gomperts, R. L. Martin, D. J. Fox, J. S. Binkley, D. J. Defrees, J. Baker, J. P. Stewart, M. Head-Gordon, C. Gonzalez, and J. A. Pople, Gaussian, Inc., Pittsburgh PA, 1995.

Microsoft® Excel 2000: Copyright © 1985-1999, Microsoft Corporation. Regression analysis: Analysis Toolpack.

Scian: E. Pepke, J. Murray, J. Lyons and T.-Z. Hwu. *Scian*; Supercomputer Computations Research Institute; Florida State University: Tallahassee, FL, 1993.

REFERENCES

References are listed alphabetically by first author and then by date.

Bachrach, S.M. (1989). *J. Comp. Chem.* **10**, 392.

Bader, R.F.W. and M.E. Stephens (1975). *J. Am. Chem. Soc.* **97**, 7391.

Bader, R.F.W. and H. Essen (1984). *J. Chem. Phys.* **80**, 1943.

Bader, R.F.W. (1990). Atoms in Molecules: a quantum theory. Oxford: Oxford University Press.

Bader, R.F.W.; S. Johnson, T.-H. Tang and P.L.A. Popelier (1996a). *J. Chem. Phys.* **100**, 15396.

Bader, R.F.W.; A. Streitweiser, A. Nuehaus, K.E. Laidig and P. Speers (1996b). *J. Am. Chem. Soc.* **118**, 4959.

Bourissou, D.; O. Guerret, F.P. Gabbat and G. Bertrand (2000). *Chem. Rev.* **100**, 39.

Chestnut, D.B. (1998). *J. Am. Chem. Soc.* **120**, 10504.

Douglas, E. and J.R. Murdoch (1982). *Int. J. Quantum Chem.* **22**(6), 1249.

Dobado, J.A.; H. Martínez-García, J.M. Molina and M.R. Sundberg (1998). *J. Am. Chem. Soc.* **120**, 8461.

Fradera, X., M.A. Austen and R.F.W. Bader (1999). *J. Phys. Chem. A* **103**, 304.

Gudat, D. (1998). *Eur. J. Inorg. Chem.* **1998**, 1087.

Howard, S.T. and J.A. Platts (1995). *Inorg. Chem.* **99**, 9027.

Howard, S.T., J.P. Foreman and P.G. Edwards (1996). *Inorg. Chem.* **35**, 5805.

Lewis, G.N. (1916). *J. Am. Chem. Soc.* **38**, 762.

Löwdin, P.O. (1959). *J. Mol. Spectrosc.* **3**, 46.

Schoeller, W.W. and U. Tubbesing (1995). THEOCHEM **343**, 49. [ab initio RHF/SCF level with inclusion of electron correlation treatment (MP4SDTQ(fc)/6-31+g(d)).]

2. Atoms in Molecules Theory – a primer

A brief review of quantum mechanical principles is followed by an outline of the Atoms in Molecules description of open systems and chemical structure.

2.1. Quantum Mechanical Description of Chemical Systems

2.1.1. The state function

The state of a quantum mechanical system is described in terms of the *eigenvalues* of a set of *commuting operators* (observables) acting on an element of *Hilbert space* (a *state vector*). A commuting set must be used, since only these will have sharp, rather than average, *expectation values*, so only these observables will define the state. Typically, the commuting set includes the Hamiltonian operator, $\hat{H}$, which appears in the Schrödinger equation, Equation 2-1.

$$\frac{\partial|\Psi\rangle}{\partial t}=-\frac{i}{\hbar}\hat{H}|\Psi\rangle \qquad \frac{\partial\langle\Psi|}{\partial t}=\frac{i}{\hbar}\hat{H}\langle\Psi|$$

Equation 2-1

A state vector, $|\Psi\rangle$, contains all the information about the probability of observing each of the *eigenvalues* of every operator. Chemical systems are typically described by a *wavefunction*, $\Psi(\mathbf{x},\mathbf{X},t)$; the projection of the state vector onto the electron spin coordinates (σ_i) and the real space coordinates of the electrons ($\mathbf{x}_i = \mathbf{r}_i, \sigma_i$) and nuclei ($\mathbf{X}_\alpha = \mathbf{R}_\alpha$) in the system. For a *stationary state* the Hamiltonian operator and the observables are independent of time. The eigenvalues are *constants of motion*. The eigenvalue of the Hamiltonian operator is energy, E. The wavefunction, Ψ, may be factored into a spin and space dependent wavefunction, ψ, and a time dependent factor, as in Equation 2-2.

$$\Psi(\mathbf{x},\mathbf{X},t) = \psi(\mathbf{x},\mathbf{X})\exp(-iEt/\hbar)$$
$$\hat{H}\psi(\mathbf{x},\mathbf{X}) = E\psi(\mathbf{x},\mathbf{X}) \qquad \hat{H}\psi^{*} = E\psi^{*}$$

Equation 2-2

The possible eigenvalues of the position operator form a continuous set, and the wavefunction is not an eigenfunction of the particle positions. The position operator does not commute with the Hamiltonian, so the positions of the particles do not have sharp values; rather they are spread out over all space, in accordance with Heisenberg's uncertainty principle. The probabilistic interpretation of the wavefunction is that, when properly normalized, $\psi(\mathbf{x},\mathbf{X})^{*}\psi(\mathbf{x},\mathbf{X})d\tau$ equals the probability of finding the particles (electrons and nuclei) in the multidimensional infinitesimal volume, $d\tau$. Thus for a system consisting of one electron, $\psi(\mathbf{r})^{*}\psi(\mathbf{r})$ equals the electron density.

Using the Born-Oppenheimer approximation, the nuclear coordinates can be separated out, giving $\psi(\mathbf{x},\mathbf{X}) \approx \psi_{nuc}(\mathbf{X})\psi_{el}(\mathbf{x};\mathbf{X})$. The nuclear coordinates become parameters in the electronic Hamiltonian and the electronic wavefunction. Once the approximate stationary-state electronic wavefunction $\psi_{el}(\mathbf{x})$ has been obtained for a given nuclear configuration, $\mathbf{X}$, the properties of interest can be calculated. Like any quantum system consisting of fermions, molecules and other 'closed' chemical systems must be described by *antisymmetric* wavefunctions that obey the boundary conditions that ψ_{el} and $\nabla\psi_{el}$ approach zero at infinity, or at some other bounding surface.

For many-electron systems only approximate solutions to the Schrödinger equation can be found. Numerical methods now allow for very good approximations, depending on the level of theory used, and on the size and flexibility of the *basis set* used for expansion. Approximate solutions generally take the form of *Slater determinants* of molecular orbitals (MO's) or, at higher levels of theory, linear combinations of determinants. The MO's themselves are usually written as linear combinations of basis functions. Typical basis sets consist of atomic orbital-like functions of varying size (diffuseness) and polarization.[*]

2.1.2. Operators and observables

Quantum mechanical operators (observables) can be defined, through the correspondence principle, in terms of their classical analogues. In the potential energy operator, the positions, **r**, are simply replaced by the multiplicative position operator. In the kinetic energy operator, the momentum is replaced by the momentum operator, $\hat{p} = -i\hbar\nabla$.

The set of operators that commute with the Hamiltonian (and are thus the state-defining properties of the system) will depend on the form of the Hamiltonian. For most chemical systems a simple, non-relativistic Hamilton is used. In Equation 2-3, the total non-relativistic nuclear plus electronic Hamiltonian is shown,

---

[*] This is the linear combination of atomic orbitals to form molecular orbitals (LCAO-MO) method.

assuming no external forces. A and B refer to nuclei, while i and j refer to electrons. M_A and m refer to nuclear and electron masses, respectively, while Z_Ae and e refer to their charges. The inter-particle distances are denoted by r, and ε_o is permittivity.

$$\hat{H} = \sum_A \frac{\hat{p}_A^2}{2M_A} + \sum_i \frac{\hat{p}_i^2}{2m} + \sum_{A,B} \frac{Z_A Z_B e^2}{4\pi\varepsilon_\circ r_{AB}} + \sum_{A,i} \frac{Z_A e^2}{4\pi\varepsilon_\circ r_{Ai}} + \sum_{i,j} \frac{e^2}{4\pi\varepsilon_\circ r_{ij}}$$

Equation 2-3

For operators that commute with the Hamiltonian, eigenvalue equations ($\hat{A}\psi = a\psi$) are obeyed locally and throughout the entire Hilbert space. For any non-commuting operator $\hat{A}$, only the average (expectation) value $<A>$ can be obtained for the total system. Any system property, A, can be written as the integral of a property density, $\rho_A(\mathbf{r})$, in real space, see Equation 2-4. The definition of this local contribution will be developed below.

$$\langle A \rangle = \left\langle \psi \middle| \hat{A} \middle| \psi \right\rangle = \int d\tau\, \psi(\mathbf{x}) \hat{A} \psi(\mathbf{x}) = \int d\mathbf{r} \rho_A(\mathbf{r})$$

Equation 2-4

2.1.3. *Local property densities*

The first property density we will consider is the non-uniform N-electron density, $\rho(\mathbf{r})$. This can be calculated as a function of real space, $\mathbf{r}$, by considering the probabilistic interpretation of the wavefunction and the indistinguishability of the electrons. For a given nuclear configuration, the probability $P(d\mathbf{r}_1)$ of finding a particular electron, electron 1, in the volume $d\mathbf{r}_1$ with *either* spin, and the remaining electrons in *any* configuration is determined by summing or integrating over all the 'arbitrary' variables.

$$P(d\mathbf{r}_1) = \rho(\mathbf{r}_1)d\mathbf{r}_1 = d\mathbf{r}_1 \sum \mathbf{spins} \int d\mathbf{r}_2 \int d\mathbf{r}_3 \ldots \int d\mathbf{r}_N \psi^*(\mathbf{x})\psi(\mathbf{x}) = d\mathbf{r}_1 \int d\tau' \psi^*(\mathbf{x})\psi(\mathbf{x})$$

Equation 2-5

In Equation 2-5, **x** includes both spin and spatial coordinates for the electrons. The sum is over α and β for the spins of all N electrons, and the integration is over the spatial coordinates of all electrons but one; all of this is represented by $\int d\tau'$.

The probability of finding *any* one of the N indistinguishable electrons in the same volume dr is N times this value. To obtain the electron density we simply drop the infinitesimal volume factor. The nuclear coordinates can be shown as parameters, and the density depends only on the spatial coordinates, **r**, of any one of the N electrons.

$$\begin{aligned}\rho(\mathbf{r};\mathbf{X}) &= N \sum \mathbf{all\ spins} \int d\tau_2 \int d\tau_3 \ldots \int d\tau_N \psi^*(\mathbf{x};\mathbf{X})\psi(\mathbf{x};\mathbf{X}) \\ &= N \int d\tau' \psi^*(\mathbf{x};\mathbf{X})\psi(\mathbf{x};\mathbf{X})\end{aligned}$$

Equation 2-6

Integrating the electron density over all space, we get the total number of electrons, N. The above discussion leads to the realization that the number of electrons in any particular volume of space Ξ *should **not*** be calculated as $N \int_{\Xi} d\tau \psi^*(\mathbf{x})\psi(\mathbf{x})$, *but rather as* $N(\Xi) = N \int_{\Xi} d\mathbf{r} \int d\tau' \psi^*(\mathbf{x})\psi(\mathbf{x})$. The electron density is a local one-electron property, dependent on the mean field of the remaining electrons *over all space.* Using this kind of integration, we will now define other property densities. In each case the local contribution to the property will be N times the one-electron value.

We can write an expression for the local contribution to a given property A,[*] similar to that in Equation 2-6. *As a first guess* we could write for a one-electron operator:

$$\begin{aligned}\rho_A(\mathbf{r};\mathbf{X}) &= N\sum \textbf{all spins} \int d\tau_2 \int d\tau_3 \ldots \int d\tau_N\, \psi^*(\mathbf{x};\mathbf{X})\hat{A}\psi(\mathbf{x};\mathbf{X}) \\ &= N\int d\tau' \psi^*(\mathbf{x};\mathbf{X})\hat{A}\psi(\mathbf{x};\mathbf{X})\end{aligned}$$

Equation 2-7

The integral of such a local property density over some system gives the value for the system, as in Equation 2-4. For the one-electron case the property density reduces to simply $\psi\hat{A}\psi$. In many cases, however, Equation 2-7 is not sufficient.

While all physical observables for a closed system are Hermitian, $\langle A\rangle = \int d\tau\psi^*(\hat{A}\psi) = \int d\tau(\hat{A}\psi)^*\psi$, some (such as kinetic energy) are not Hermitian locally, or over an arbitrary open system, *i.e.* $\int_{\Xi} d\mathbf{r} \int d\tau' \{\psi^*(\hat{A}\psi) - (\hat{A}\psi)^*\psi\} \neq 0$. For example, consider the Hamiltonian operator averaged over an arbitrary open system. Here the kinetic energy is represented by $\frac{\hbar^2}{2m}\sum_j \nabla_j^2 = \hat{K}$. Letting $\int d\tau_j''$ indicate "summation over all spins and integration over all the spatial coordinates except those of electron 1 and electron j" we can write:

$$\int_{\Xi} d\mathbf{r} \int d\tau' \{\psi^*(\hat{H}\psi) - (\hat{H}\psi)^*\psi\} = \frac{\hbar}{2mi}\int_{\Xi} d\mathbf{r}_1 \int d\tau' \sum_j \{\psi^*\nabla_j^2\psi - (\nabla_j^2\psi)^*\psi\}$$

---

[*] A is a sum of one-electron operators, which can be replaced by N times a single one-electron operator.

$$
\begin{aligned}
&= \frac{\hbar}{2mi} \oint dS_{\Xi} \int d\tau' \left(\psi^* \nabla_1 \psi - \psi \nabla_1 \psi^* \right) \cdot \mathbf{n} + \sum_{j \neq 1} \frac{\hbar}{2mi} \oint dS_j \int_{\Xi} d\mathbf{r}_1 \int d\tau_j'' \left(\psi^* \nabla_j \psi - \psi \nabla_j \psi^* \right) \cdot \mathbf{n} \\
&= \frac{\hbar}{2mi} \oint dS_{\Xi} \int d\tau' \left(\psi^* \nabla_1 \psi - \psi \nabla_1 \psi^* \right) \cdot \mathbf{n}
\end{aligned}
$$

Equation 2-8

The potential energy operator is still Hermitian, and those terms cancel. The volume integrals are converted to surface integrals by Gauss's theorem. The $\nabla_{j \neq 1}$ terms vanish for all systems because $\nabla_j \psi = 0$ at infinity, the bounding surface for the coordinates of all electrons but one. Similarly, the final expression of Equation 2-8 reduces to zero for a closed system, since the wavefunction and its gradient approach zero at the boundary surface. For integration over an arbitrary open system bounded by the surface, S_{Ξ}, the two terms in the final expression of Equation 2-8 are not equal, and the expectation values arising from each of these terms may be complex. Thus, we have not determined a meaningful property density. This leads to a modification of the expression for the local property density given in Equation 2-7. By taking the average of the expression in Equation 2-7 and its complex conjugate, we can assure that the property is real. Equation 2-9 defines a real property density, which may be integrated over an open system.

$$
\rho_A(\mathbf{r}) = \frac{N}{2} \int d\tau' \left\{ \psi^*(\mathbf{x}) \hat{A} \psi(\mathbf{x}) + \left(\hat{A} \psi(\mathbf{x}) \right)^* \psi(\mathbf{x}) \right\}
$$

Equation 2-9

2.2. Open systems

The Theory of Atoms in Molecules is a development of the quantum mechanics of an open system (Srebrenik and Bader, 1975; Bader and Nguyen-

Dang, 1981; Bader, 1990). Its name reflects the chemical seeds of this theory, but it applies to any open system, that is, any system that exchanges matter and/or energy with its surroundings. The Theory of Atoms in Molecules seeks to define, and thus enable the evaluation of, quantum mechanical properties of open systems. Any measurement, *e.g.* of a force exerted, involves a measurement of the exchange of energy (and/or matter) with the surroundings, *i.e.* the measuring device. If such a measurement can be made, then surely we can define the properties being measured (see for example, Bader *et al.*, 2000).

Open systems are regions of real space, bounded by surfaces that divide them from the surroundings, *i.e.* from other open systems (Bader, 1990, 1994). The fundamental observation that 'like pieces of matter have like properties' leads one to the conclusion that two open systems with the identical distributions of matter (electrons and nuclei) will have identical properties, regardless of the matter distribution in neighbouring systems. The interaction with the surroundings can be accounted for by a *surface contribution* to the total properties. For extensive properties, the sum over many neighbouring but non-overlapping subsystems gives the property for the larger system, which may still be open.[*]

It is this additivity of open system properties and the near transferability of charge distributions in many chemical systems that lead to *empirical* additivity schemes for properties such as heats of reaction and polarizability, having specific,

---

[*] The internal surface terms must vanish, since the sum of basin terms alone must equal the integral of the property density over the total system.

nearly fixed contributions from the functional groups present within larger molecules.[*] The transferability of the charge distribution also leads to the conservation of spectroscopic (Bader *et al.*, 2000) and reactivity properties of functional groups as they appear in various environments.

2.2.1. Definition of a proper open system

Having ensured that all property densities and their integrals over an open system are real (Equation 2-9) does not guarantee that they will be physically meaningful. Again we can consider the case of the kinetic energy. There are two expressions for the local kinetic energy, both of which have the same integrated value for the total system. While G appears in Schrödinger's energy functional, K appears in the Hamiltonian operator.

$$\langle T\rangle = \langle K\rangle \equiv \frac{1}{2m}\langle \Psi \mid \hat{p}^2\Psi\rangle = \frac{1}{2m}\langle \hat{p}^2\Psi \mid \Psi\rangle = \langle G\rangle \equiv \frac{1}{2m}\langle \hat{p}\Psi \mid \hat{p}\Psi\rangle$$

Equation 2-10

The different definitions give different values for an arbitrary open system, leading to a poorly defined kinetic energy. One simple approach to resolving this dilemma would be to choose one definition over the other, or to concoct some combination of the two. An alternative is to find some definition of an open system over which the two kinetic energies do have the same average. We will see that defining a *proper* open system, rather than imposing an arbitrary definition of the

---

[*] See for example: K. B. Wiberg, R. F. W. Bader and C. D. H. Lau (1987) "A Theoretical Analysis of Hydrocarbon Properties II: Additivity of Group Properties and the Origin of Strain Energy" *J. Am. Chem. Soc.* **109**, 985; R. F. W. Bader, K. M. Gough, K. E. Laidig and T. A. Keith (1992) "Properties of Atoms in Molecules: Additivity and Transferability of Group Polarizabilities" *Mol. Phys.* **75**, 1167.

local kinetic energy density, leads to a very satisfying result. The same open system that has a well defined energy also has a well defined value for the virial of the forces acting on the system and obeys a meaningful form of the virial theorem, as extended to open systems.

Since the potential energy term, $\hat{V}$, in the Hamiltonian is a function of the particle positions, it does not commute with the kinetic energy operator $\hat{K}$, which involves derivatives with respect to those positions. Thus neither the potential nor the kinetic energy operator commutes with the Hamiltonian, $\hat{H} = \hat{K} + \hat{V}$, and the state function is an eigenfunction of neither. However, for closed systems at equilibrium (no net forces) there is a relationship between the total energy, E, and the *average (expectation) values* $\langle T\rangle = \langle K\rangle = \langle G\rangle$ and $\langle V\rangle$. For equilibrium systems involving Coulombic (1/r) potentials only: $\langle V\rangle = -2\langle T\rangle = 2E$. This is the quantum mechanical expression of the virial theorem. We wish to extend this theorem to an open quantum mechanical system.

To define a system for which the difference between the two expressions ($\langle K\rangle_{\Xi} - \langle G\rangle_{\Xi}$) vanishes, we first consider the Laplacian operator:

$$\nabla^2(\psi^*\psi) = \nabla\cdot\{(\nabla\psi^*)\psi + \psi^*(\nabla\psi)\} = (\nabla^2\psi^*)\psi + \psi^*(\nabla^2\psi) + 2\nabla\psi^*\cdot\nabla\psi$$

Equation 2-11

Extension of the operators to the many electron case, multiplication by $\frac{-\hbar^2}{4m}$ and integration over all the coordinates but one, gives a local property density (Bader and Beddall, 1972). Each of the integrals in Equation 2-12, below, corresponds to a local property density as follows: $L(r) = K(r) - G(r)$.

$$L(\mathbf{r}) \equiv \frac{-\hbar^2}{4m} N \int d\tau' \nabla^2 \left(\psi^* \psi\right)$$
$$= \frac{-\hbar^2}{4m} N \int d\tau' \left\{ \left(\nabla^2 \psi^*\right)\psi + \psi^* \left(\nabla^2 \psi\right) \right\} - \frac{\hbar^2}{2m} N \int d\tau' \nabla \psi^* \cdot \nabla \psi$$

Equation 2-12

Thus, the kinetic energy of an open system Ξ, bounded by a surface S, is well defined when $\int_{\Xi} d\mathbf{r} L(\mathbf{r}) = -\frac{\hbar^2}{4m} \int_{\Xi} d\mathbf{r} \nabla^2 \rho(\mathbf{r}) = -\frac{\hbar^2}{4m} \int dS \nabla \rho(\mathbf{r}) \cdot \mathbf{n}(\mathbf{r}) = 0$, where $\mathbf{n}(\mathbf{r})$ is the unit vector normal to the surface. The surface integral is obtained by using Gauss's theorem. A system for which this integral vanishes is a proper open system, and we will use Ω in place of Ξ to denote such systems. We will see this definition of a proper open system again, but it can be more rigourously derived by using the calculus of variations (Appendix A2.3).

2.2.2. *Variational definition of a proper open system*

In classical mechanics there are *equations of motion* that describe the variation of the properties, A, with time. All of these equations of motion can be derived from a single principle: the principle of stationary action (Feynman *et al.*, 1964). In quantum mechanics, a similar set of equations of motion applies to a closed system.

$$\frac{d\langle \hat{A} \rangle}{dt} = \left(\frac{i}{\hbar}\right) \left\langle \Psi, \left[\hat{H}, \hat{A}\right] \Psi \right\rangle + \left\langle \frac{\partial \hat{A}}{\partial t} \right\rangle$$

Equation 2-13

This equation of motion can be derived from the definition of the expectation value and the time-dependent Schrödinger equation, which tells us that the Hamiltonian operator is the generator of time-development. See Appendix A2.1b for details. We will be concerned only with operators that have no explicit time dependence, so the final term in Equation 2-13 can be dropped. For stationary states the expectation values are independent of time and we arrive at the hypervirial theorem, Equation 2-14.

$$0 = \left(\frac{i}{\hbar}\right)\left\langle \psi, \left[\hat{H}, \hat{A}\right]\psi \right\rangle$$

Equation 2-14

It is desirable to find open systems whose properties obey analogous equations of motion. Open systems with well-defined properties and behaviour will be called ***proper open systems***. The theory of Atoms in Molecules extends Schwinger's quantum mechanical principle of stationary action (Schwinger, 1951) to systems with variable spatial *and* temporal boundaries. By using a variational method, one arrives at a natural criterion for the surface of a proper open system. See Appendix A2.4 for the development of this argument for the time-independent case. The criterion one discovers is that the integral of the flux through the bounding surface, $\oint dS\, \nabla\rho\cdot\mathbf{n}$, must be zero. This happens to be identical to the criterion for a well-defined kinetic energy. We further require that the flux be zero at *every* point on the surface, so that the criterion holds for *any variation* in the surface, S.

$$\nabla\rho(\mathbf{r}_S)\cdot\mathbf{n} = 0; \quad \forall \mathbf{r}_S \in \mathrm{S}(\mathbf{r}_S)$$

Equation 2-15

This definition of a proper open system also reproduces the partitioning that has been observed to lead to maximum transferability of group properties in chemical systems, thus leading to a natural definition of an atom in a molecule (Bader and Beddall, 1972).

2.2.3. *Open system properties and atomic theorems*

Each property, A, has a corresponding *property density, ρ_A*, defined in Equation 2-9. The property density is integrated with respect to the final coordinate, $d\tau$, over the proper open region, Ω, to obtain the value of the property for the open region; this is the *basin contribution* to the atomic value of A.

$$A(\Omega) = \langle A \rangle_\Omega = \int_\Omega d\tau\, \rho_A(\mathbf{r})$$

Equation 2-16

For many properties, the equations of motion tell us that the interactions with the surroundings can be accounted for through a surface integral of a related function. The general equation of motion is:

$$\frac{d\langle A \rangle_\Omega}{dt} = \frac{1}{2}\frac{d\left\{\left\langle \Psi^* \hat{A}\Psi \right\rangle_\Omega + \left\langle \left(\hat{A}\Psi\right)^* \Psi \right\rangle_\Omega\right\}}{dt}$$

$$= \frac{N}{2}\left\{\left(\frac{i}{\hbar}\right)\left\langle \left[\hat{H}, \hat{A}\right]\right\rangle_\Omega + cc\right\} - \frac{1}{2}\left\{\oint dS(\Omega)\mathbf{J}_{\mathbf{A}} \cdot \mathbf{n} + cc\right\} + \oint dS(\Omega)\left(\frac{\partial S}{\partial t}\right)\rho_A$$

Equation 2-17

This equation is the open system analogue to Equation 2-13 and can be derived similarly, see Appendix A2.2c. The explicit time dependence of $\hat{A}$ is again assumed to be zero and is not shown here, but now we have additional terms accounting for the *flux*[*] in property A through the bounding surface, $S(\Omega)$, which involves the property *current density*, $\mathbf{J}_A = N\,\mathbf{j}_A$. The definition of the one-electron current density of A is:

$$\mathbf{j}_A(\mathbf{r}) = \left(\frac{\hbar}{2mi}\right)\int d\tau' \left\{\Psi^*\nabla\left(\hat{A}\Psi\right) - \left(\nabla\Psi^*\right)\hat{A}\Psi\right\}$$

Equation 2-18

There is also a final term in Equation 2-17 accounting for the time derivative of the surface, which is required to vary in such a way as to maintain the condition of zero-flux. Both these additional terms vanish for a closed system. For a stationary state, the time derivatives of all atomic properties vanish along with the time derivative of the surface. Therefore Equation 2-17 simplifies to the open-system hypervirial theorem, Equation 2-19.

$$\frac{N}{2}\left\{\left(\frac{i}{\hbar}\right)\left\langle\left[\hat{H},\hat{A}\right]\right\rangle_{\Omega} + cc\right\} = \frac{1}{2}\left\{\oint dS(\Omega)\mathbf{J}_A \cdot \mathbf{n} + cc\right\}$$

Equation 2-19

Equation 2-17 and Equation 2-19, can be derived from Schrödinger's equation and the definition of A(Ξ) for *any* arbitrary open system. However, there is no guarantee that the mathematical expressions will be physically meaningful. Using a variational approach one can relate the surface terms in these equations to a variation in Schrödinger's energy functional for a stationary state, Equation 2-20 (or variations in the atomic action integral for time-dependent systems, Equation 2-21), generated by the operator $\varepsilon\hat{G}/i\hbar$. See Appendix A2.4 for this derivation.

---

[*] The local flux equals the dot product of the current, **J**, into the surface normal, **n**.

$$\delta \mathcal{G}[\psi,\Omega] = -\frac{\varepsilon}{2}\oint dS(\Omega,\mathbf{r})\mathbf{j}_G(\mathbf{r})\cdot\mathbf{n}(\mathbf{r}) + cc = -\frac{\varepsilon}{2}\frac{i}{\hbar}\left\langle \psi \middle| \left[\hat{H},\hat{G}\right] \psi \right\rangle_{\Omega} + cc$$

Equation 2-20

$$\begin{aligned}\frac{N}{\varepsilon}\delta \mathcal{W}_{12}[\Psi,\Omega] &= G(\Omega,t_2) - G(\Omega,t_1) - \int_1^2 dt \oint dS(\Omega,\mathbf{r})\frac{\partial S}{\partial t}\rho_G(\mathbf{r},t) \\ &+ \frac{1}{2}\int_1^2 dt \oint dS(\Omega,\mathbf{r})(\mathbf{J}_G(\mathbf{r})\cdot\mathbf{n}(\mathbf{r}) + cc) \quad = -N\int_1^2 dt\left\{\frac{1}{2}\frac{i}{\hbar}\left\langle \Psi \middle| \left[\hat{H},\hat{G}\right] \Psi \right\rangle_{\Omega} + cc\right\}\end{aligned}$$

Equation 2-21

The first equality in each expression above holds *only* if the local zero-flux condition is imposed as a variational constraint. Only for proper open systems can the time development of the system's properties be seen as arising from the operation of infinitesimal *generators*. We have seen that some properties are only well defined for proper open systems. We see here that the equations of motion for a given operator can be written for any open system, but are only variationally meaningful for proper open systems.

By inserting an operator of interest into Equation 2-20 or Equation 2-21 one can derive an associated atomic theorem. For example, when $\hat{A} = \hat{\mathbf{r}}\cdot\hat{\mathbf{p}}$, we arrive at the atomic virial theorem for a proper open system.

$$\begin{aligned}\frac{N}{2}\left\{\frac{i}{\hbar}\left\langle\left[\hat{H},\hat{\mathbf{r}}\cdot\hat{\mathbf{p}}\right]\right\rangle + cc\right\} &= 2\left\langle\hat{K}\right\rangle + \left\langle -\mathbf{r}\cdot\nabla\hat{V}\right\rangle \\ \frac{1}{2}\left\{\oint dS(\Omega)\mathbf{J}_{\mathbf{r}\cdot\mathbf{p}}\cdot\mathbf{n} + cc\right\} &= -\oint dS(\Omega)\left\{\mathbf{r}\cdot\vec{\boldsymbol{\sigma}} + \frac{\hbar^2}{4m}\nabla\rho(\mathbf{r})\right\}\cdot\mathbf{n}\end{aligned}$$

Equation 2-22

The stress tensor is defined as $\vec{\boldsymbol{\sigma}} = \frac{\hbar^2}{4m}\left\{\Psi^*\nabla(\nabla\Psi) + \nabla\left(\nabla\Psi^*\right)\Psi - \nabla\Psi^*\nabla\Psi - \nabla\Psi\nabla\Psi^*\right\}$.

For a stationary state, we substitute these results into Equation 2-20 and rearrange the resulting equation.

$$
\begin{aligned}
&2K(\Omega)+V_b(\Omega)=-V_S(\Omega)-L(\Omega)\\
&V_b(\Omega)+V_S(\Omega)=-2K(\Omega)-L(\Omega)=-2G(\Omega)+L(\Omega)
\end{aligned}
$$

Equation 2-23

For a proper open system, we recall that the two definitions of kinetic energy are equal (K = G = T). The Laplacian integrates to zero and we can define the total atomic virial, *V(Ω)*, Equation 2-24. We see that the atomic virial has a basin contribution, equal to the volume integral of the local virial density; and a surface term, accounting for the interactions with the surroundings. The sum is equal to negative two times the kinetic energy, as for the total system.

$$
\begin{aligned}
&V(\Omega)\equiv V_b(\Omega)+V_S(\Omega)=-2T(\Omega)\\
&V_b(\Omega)\equiv N\int_\Omega d\tau\int d\tau'\psi\left(-\mathbf{r}\cdot\nabla\hat{V}\right)\psi\\
&V_S(\Omega)\equiv\oint dS(\Omega,\mathbf{r})\mathbf{r}\cdot\overleftrightarrow{\boldsymbol{\sigma}}(\mathbf{r})\cdot\mathbf{n}(\mathbf{r})
\end{aligned}
$$

Equation 2-24

2.3. Chemical Structure

Having derived expressions for properties of open systems, and having discovered which open systems obey meaningful equations of motion, some general characteristics of open systems can be observed. In chemistry, the smallest proper open systems that can normally be defined consist of one nucleus,* which is a local maximum in ρ(**r**), and a surrounding region. The surrounding region – called the attractive basin of the nucleus – is defined as the space mapped out by all the trajectories of the density gradient (∇ρ(**r**)) that terminate at that nucleus. These

---

* In a few systems maxima occur at non-nuclear positions, thus acting as attractors for 'pseudo-atoms'.

are non-overlapping regions that one can identify with atoms – as they exist in molecules. Being proper open systems, these atoms have well defined properties that obey their respective equations of motion. An alternative definition of an atom in a molecule, equivalent to the zero-flux condition, is then 'the union of a nucleus and its attractive basin.'

Having defined atoms in molecules, we can also identify the other components of molecular structure: *bonds*, rings and cages. To do this we should consider further the topology of the electron density, as described in terms of the critical points and the gradient vector field, $\nabla\rho(\mathbf{r})$. A critical point, $\mathbf{r}_c$, in the scalar electron density field has a gradient vector, $\nabla\rho(\mathbf{r}_c)$, equal to zero. The vector field consists of trajectories, or paths, which originate at low electron density (a critical point, or infinite distance) and follow the direction of maximum increase until they reach another critical point (or cusp) of higher density.

It was mentioned above that there is a maximum in the electron density at each nucleus. We should note here that while the nuclei correspond to maxima in the electron density, they are not proper critical points. There is a cusp condition (Kato, 1957) that makes $\nabla\rho(\mathbf{r}_\alpha)$ undefined at these positions. These *behave* as critical points in the electron density, and each is the terminus for an infinite number of gradient trajectories that define the basin. The other common types of critical points for functions of real space are minima, and two kinds of saddle points. Critical points are classified by their rank (ω, the number of non-zero curvatures) and signature (σ, the sum of the signs of those curvatures). In this (ω,σ) classification system a maximum is a (3,-3) critical point, having three negative curvatures. We will consider only critical points of rank 3. Lower ranks are a sign of structural instability.

The first kind of saddle point, a (3,-1) critical point, is the origin of two trajectories departing in antiparallel directions, and terminating at two different nuclei. This pair of trajectories is referred to as the *bond path* linking the two nuclei A and B. The same saddle point is the terminus for an infinite number of trajectories, which approach the saddle in a plane orthogonal to the bond path. These trajectories define the *interatomic surface*; the surface of zero-flux that divides the two atoms A and B. The saddle point is known as a *bond critical point (BCP)* and its presence, linking two nuclei in an equilibrium geometry, is the necessary and sufficient condition for those two atoms to be 'chemically bonded' (Bader and Essen, 1984). While it is tempting to identify a bond path with a bond, it is best to restrict ourselves to the verb and say that two atoms *are bonded.* This focuses attention on the forces holding the atoms together, rather than on some hypothetical physical entity, or region of real space, called 'a bond'. While atoms are regions of space, 'bonds', along with rings and cages, are merely aspects (or characteristics) of the topology of the electron density.

The second kind of saddle occurs when a ring of bonded atoms is present. The *ring critical point (RCP),* a (3,+1) critical point, is the origin for a set of trajectories that depart in a single plane and terminate at the nuclei or bond critical points defining the ring. This set of trajectories defines a *ring surface*. The ring critical point is the terminus for a pair of trajectories that approach in antiparallel directions, orthogonal to the plane defined by the ring surface. This pair of trajectories defines the ring axis. When a set of rings encloses a 3-dimensional space, a cage is formed. Inside this cage is a minimum in the electron density, known as a *cage critical point (CCP)* or a (3,+3) critical point.

2.4. Summary

We have seen that the Theory of Atoms in Molecules provides a definition of the quantum mechanical properties of an open system and the equations of motion determining those properties. From the criterion for a proper open system, we derive a definition of atoms within molecules and define topological features corresponding to all the elements of chemical structure. While the Theory of Atoms in Molecules is now known to have much wider applicability, this thesis will focus on chemical applications of this theory. In the next chapter we will see how a few integrated properties of atoms in molecules (open systems) and several topological features of the electron density allow us to characterize the chemical bonding in a molecule.

Bibliography

References are listed alphabetically by first author and then by date.

Bader, R.F.W. and P.M. Beddall (1972). *J. Chem. Phys.* **56**, 3320.

Bader, R. F. W. and T.T. Nguyen-Dang (1981). *Adv. Quantum Chem.* **14**, 63.

Bader, R.F.W. and H. Essen (1984). *J. Chem. Phys.* **80**, 1943.

Bader, R.F.W. (1990). Atoms in Molecules: a quantum theory. Oxford: Oxford University Press.

Bader, R.F.W. (1994). *Int. J. Quant. Chem.* **49**(3), 299.

Bader, R.F.W. (1998). *Can. J. Chem.* **76**, 973.

Bader, R.F.W. (2000). *Phys. Rev. B* **61**(11), 7795.

Bader, R.F.W.; D. Bayles and G.L. Heard (2000). *J. Chem. Phys.* **112**, 10095.

Born, M. and J.R. Oppenheimer (1927). *Ann. Physik* **84**, 457.

Feynman, R.P. (1948). *Rev. Mod. Phys.* **20**, 367.

Feynman, R.P.; R.B. Leighton and M. Sands (1964). The Feynman Lectures on Physics, Vol. II, Chapter 19. Reading, MA: Addison-Wesley.

Kato. W.A. (1957). *Commun. Pure Appl. Math.* **10**, 151.

Schwinger, J. (1951). *Phys. Rev.* **82**, 914.

Srebrenik, S. and R.F.W. Bader (1975). *J. Chem. Phys.* **63**, 3945.

3. Characterization of Chemical Bonding

3.1. Basic Methods

Chemists have described the chemical bond in many ways. The bond can be characterized by its length, its strength, its strain, and its conjugation to other bonds, in terms of the fragments from which it was formed or in terms of electronic structure. A review of concepts in chemical bonding (DeKock, 1987) gives the following list of descriptors which have been applied to bonds (in a different order): polar, nonpolar, semipolar, bridged, bifurcated, localized, delocalized, single, double, triple, quadruple, electron-pair, one-electron, two-center, three-center, protonated, sigma, pi, delta, phi, bent, unusual, dangling, weak, strong, agostic, dative, coordinate covalent, covalent, ionic, metallic, van der Waals, and hydrogen. To this list, we might add the concepts of aromaticity, resonance, back bonding and hyperconjugation, among others. Many of these descriptions are only meaningful within a given model, some are mutually exclusive and some appear so from a particular perspective.

3.1.1. Experimentally accessible properties

While one can see energetic evidence of conjugation and other aspects of electronic configuration in the ultraviolet spectrum of a molecule, the most experimentally accessible properties of most bonds are the average bond length and bond strength. The bond length may be determined using a variety of techniques, including X-ray diffraction, neutron diffraction, electron diffraction and microwave spectroscopy, each of which involves a different kind of time averaging (Ebsworth *et al.*, 1987). The bond strength may be described by the bond dissociation energy, which is only well defined for diatomic species,[*] and/or by the vibrational stretching frequency, which again is only bond-specific for diatomic molecules.[†] Deeper potential wells tend to have higher stretching frequencies. Shorter bonds are typically stronger by both measures than longer bonds between the same two atoms. Both of these parameters – strength and length – are usually correlated with a third: bond order.

3.1.2. The Lewis model

In the early nineteenth century, the working model of how atoms were held together was essentially an ionic model, with positive and negative atoms bound by electrostatic forces (Stranges, 1984). Later in the century the ever-expanding realm of organic chemistry brought this model into question. J. J. Thompson's discovery of the electron in 1897 led to a new interest in models of chemical bonding. Just before the advent of quantum mechanics, G. N. Lewis gave a description in terms of the equal *or* unequal sharing of a pair of electrons,

---

[*] For polyatomic species, the dissociation energy will include contributions due to the relaxation of the remaining bonds. We may want to consider both homolytic and heterolytic cleavage.

[†] In polyatomic species all vibrational frequencies correspond to vibrational modes that are linear combinations of various stretches, bends, twists, *etc.* However, many modes are due predominantly to one stretch or bend, which is why we can use infrared spectroscopy to identify functional groups.

which explained the structure of molecular systems (Lewis, 1916). This led to the ideas of *covalent bonding* for relatively equal sharing of electron pairs and *ionic bonding* for very unequal sharing. These ideas are still in use as the most accessible model of chemical bonding. A shared pair of electrons has come to be identified with *a bond*.[*] When more than a single pair is shared between two atoms in the Lewis model, the bond is said to be a *multiple bond*. When a single Lewis structure cannot account for observed properties, an average of resonance structures is invoked. The Lewis model is a localized model of electron density. Each pair of electrons is considered to occupy a specific region of space within the molecule. When more than one Lewis structure is needed, the electrons are usually said to be *delocalized*.

As was mentioned above, chemists tend to categorize bonds involving a non-metal as 'non-polar covalent', 'polar covalent' or 'ionic'.[†] As pointed out by Lewis, these are differences only in degree, not differences in kind (Lewis, 1916). Any bond in the Lewis sense can be described as the sharing of a pair of electrons. As the electronegativity difference increases between the two atoms, the electrons are less equally shared. Polar bonds, which include most bonds in inorganic systems, have a large covalent component, but electrostatic interactions can also play a significant role. Very few bonds are entirely non-polar and none are purely ionic. The ideal extreme of ionic bonding, where the only binding

---

[*] Note that the focus shifted from bonding forces to physical entities within the molecule. Many chemistry students, and indeed chemists, think of a bond as a line connecting two atoms in a Lewis structure.

[†] Metallic bonding will not be discussed in this thesis.

forces are electrostatic, would be an example of a closed-shell interaction. Other examples are van der Waals interactions between closed shell molecules or atoms.

3.1.3. Quantum models: valence bond theory, and VSEPR

Pauling (1931*a/b/c*, 1932*a/b* 1960) and Slater (1931*a/b*; 1932) introduced the ideas of directed valence bond (VB) theory, describing bonds as the overlap of atomic orbitals. The idea of orbital hybridization was introduced to maximize the orbital overlap by having the atomic orbitals point along the bond axis. While Lewis makes little reference to geometry, the choice of hybridization states requires that the bond angles are known. One can alternatively describe the bonding in terms of localized electrons, shared and unshared as in the Lewis model, without appealing to atomic orbitals.

Because of Pauli repulsion, electrons of the same spin, in the valence shell of a given atom, will tend to keep as far apart as possible. This is the basis of the Valence Shell Electron Pair Repulsion (VSEPR) model of molecular geometry (Gillespie and Nyholm, 1957; Gillespie and Hargittai, 1991). Thus in the typical case of four same-spin electrons, the most stable arrangement is at the corners of a tetrahedron. When two or more bonds are formed, the α-spin and β-spin tetrahedra are brought into coincidence and electron pairs are formed, each occupying a domain in real space (Gillespie and Popelier, 2001; Linnett, 1961, 1964). When two pairs of electrons are shared between the same two atoms, the two pairs are pulled closer together due to their attraction for the positively charged nuclei. The two distorted tetrahedra share an edge. The more electronegative the atoms, the more effectively they can overcome the Pauli repulsion and the more stable the 'double' (or 'triple') bonds will be. If the atoms are not sufficiently electronegative, Pauli repulsion will dominate, and multiple bonds will not be formed (Malcolm *et al.*, 2002). For polar covalent systems the second electron pair is likely to be localized on the more electronegative atom.

In the electron domain model we could describe a double bond as being made up of two 'banana bonds' or 'bent bonds', while in the hybridized-orbital version of the valence bond approach a double bond is described in terms of the end-to-end (σ) overlap of sp^2-hybridized atomic orbitals and the side-to-side (π) overlap of unhybridized p-type atomic orbitals. In either model, the electron pairs are seen as localized to one or two atoms, as in the Lewis model, and bond order simply refers to the number of shared pairs (or half the number of shared electrons) between two atoms. These quantum mechanical models are useful for molecules that are well described by a single Lewis structure.

3.1.4. Quantum models: molecular orbitals

In the same era that valence bond theory appeared, Mulliken (1928*a/b*, 1932*a/b*, 1935) and Hund (1931*a/b*, 1932, 1940) introduced the ideas of molecular orbital (MO) theory, which considers the quantum states of the entire molecule. While valence bond theory gave a good description of 'localized' or 'directed' bonds, MO theory explained 'conjugated' or 'unsaturated' systems well (Coulson and Longuet-Higgens, 1947 and 1948).

One simple example of an molecular orbital (MO) description is the Hückel treatment of conjugated polyenes, in which the π system is described as a linear combination of the carbon p orbitals. When the p_z-like functions on many neighbouring carbon atoms are 'coupled' by off-diagonal terms in the Hamiltonian matrix, the π-system is said to be *conjugated,* or delocalized, in the sense that a single Lewis structure is not sufficient to describe the electron sharing.

Ab initio wavefunctions of great accuracy and complexity can now be determined. These numerical results can be difficult to interpret within the simple framework of the Lewis model or valence bond concepts. Most computational methods today start with an MO model of the molecular wavefunction. Each canonical molecular orbital corresponds to a symmetry representation of the molecular point group. The many-electron wavefunction is written as an antisymmetrized product (Slater determinant) of MO's. In some types of analysis, the canonical orbitals are transformed into maximally localized orbitals, more reminiscent of the valence bond description. Approaches for relating the calculated wavefunction to chemical concepts of atomic charge and bond order are discussed in the following sections, and in Appendix A3.2.

3.2. A Topological Approach: properties at the bond critical point

The properties of the electron density at the bond critical point (BCP), including the density, Laplacian, ellipticity, energy densities, and distance to the nuclei have all previously been used to characterize the bonding in some way. It is assumed that the properties at this one point can summarize the interaction between the two atoms (Bader *et al.*, 1983). One way to think about this summary is to consider the electron density of a diatomic system, and take as our zeroth-order approximation the overlap of two spherical 'atomic densities', which decay approximately as $\exp(-\alpha r)$. Such a model is shown in Figure 3-1.

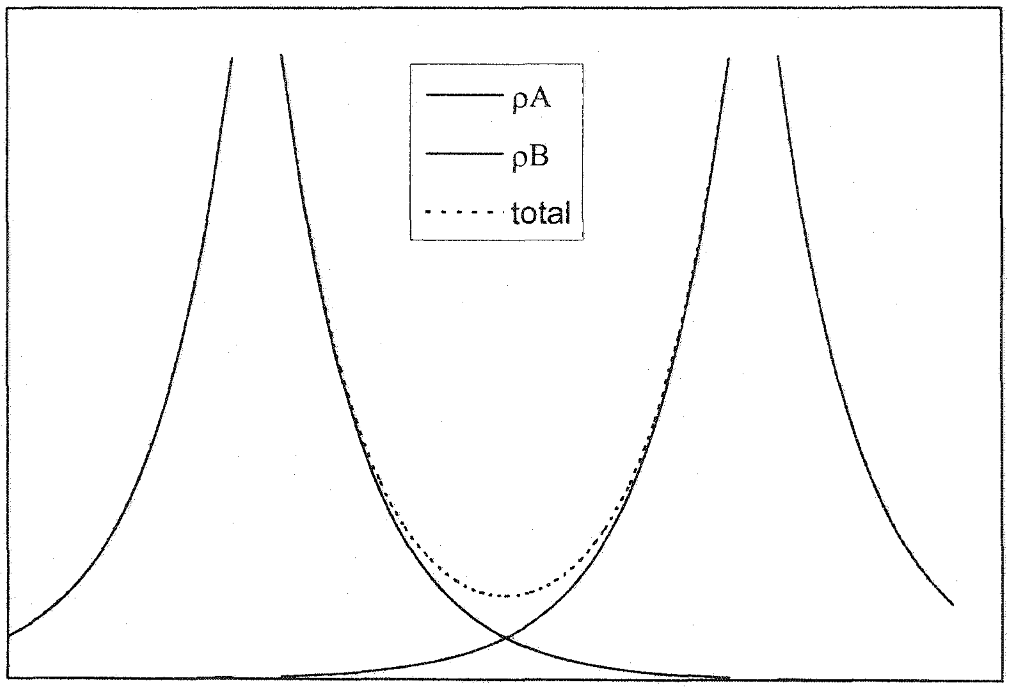

Figure 3-1. A profile of the simple overlap of two spherical, exponentially decaying atomic densities.

3.2.1. Density – bond order / bond strength

In a diatomic molecule, AB, the path of maximum density between the nuclei (the bond path) is along the internuclear axis, by symmetry. The closer the nuclei approach, the higher the density will be at the lowest point along the bond path (*i.e.* at the bond critical point). For the simple overlap model, where the distances from the BCP to the nuclei are A-r_b and B-r_b, the density at the bond critical point, $\rho(\mathbf{r}_b)$, is:

$$\rho(\mathbf{r}_b) = \rho_A(\mathbf{r}_b) + \rho_B(\mathbf{r}_b) = ae^{-\alpha(A-r_b)} + be^{-\beta(B-r_b)}$$

Equation 3-1

A correction to this model would account for the rearrangement (relaxation) of the electron density in response to the perturbation. In covalent interactions, there is an increase in electron density along the bond axis, beyond that in the overlap model. The covalent sharing of electrons pulls more electron density into the region between the nuclei, stabilizing the interaction. In interactions between closed shell molecules (van der Waals forces) or between closed shell ions (electrostatic forces), electrons repel each other away from the internuclear region.* So for closed shell interactions the density at the BCP is lower than that expected for simple overlap at the given internuclear distance. If the bond is polar covalent, the electrostatic attraction between the atoms or groups will shorten the bond and thus increase the density at the BCP, making the bond appear even more covalent – if we have not accounted for the change in bond length.

Empirical equations have been proposed to relate the bond order to the density at the bond critical point (Bader *et al.*, 1983). These formulae depend parametrically on the two atoms involved and generally have an exponential

---

[*] Both electrostatic repulsion and Pauli exclusion contribute to this repulsion.

dependence on $\rho(\mathbf{r}_b)$ (Boyd *et al.*, 1988). Since $\rho(\mathbf{r}_b)$ depends exponentially on bond length with a small 'chemical adjustment', it seems more straightforward to relate the bond order directly to bond length, as originally proposed by Coulson (1951). This measure would include both covalent and ionic contributions to the length (and strength) of the bond. This may be exactly the property one is interested in considering, and if so one could simply stop at the bond length rather than going through the trouble of analyzing the density. One could compare the expected density to the calculated or observed density to discover if there was any *unexpected additional* covalent character. (This idea is similar to the density difference maps often seen for experimental densities.) If one has no access to integration programs, this parameterized method could be of use, but since it contains information for only one point and is empirical, it is preferable to have a more global definition of bond order.

3.2.2. Laplacian – covalence / ionicity

The Laplacian, $\nabla^2\varphi = \frac{\partial^2\varphi}{\partial x^2} + \frac{\partial^2\varphi}{\partial y^2} + \frac{\partial^2\varphi}{\partial z^2}$, of any scalar field φ is an indication of local concentration or depletion (Morse and Feshbach, 1951). If the value of the electron density is higher than the average value at neighbouring points, the Laplacian of the density, $\nabla^2\rho(\mathbf{r})$, will be negative; if the value of $\rho(\mathbf{r})$ is lower than the local average, its Laplacian will be positive. The Laplacian is invariant to rotation of the frame of reference, and the tensor $\nabla\nabla\rho(\mathbf{r})$ (the Hessian of ρ) can be diagonalized by choosing an appropriate coordinate system.

At a bond critical point (BCP) the appropriate system is one with the z-axis along the bond axis. The component of $\nabla\nabla\rho(\mathbf{r})$ in this direction (*the curvature,* λ_3) will be positive. The other two components of the diagonalized tensor will correspond to axes that lie in the interatomic surface and both these curvatures (λ_1 and λ_2) will be negative. The BCP Laplacian, $\nabla^2\rho(\mathbf{r}_b)$, can be seen as an indicator of the competition between accumulating density from the surface towards the bond path (negative components), indicative of covalence, and accumulation of density at the nuclei (positive component), associated with closed-shell interactions. When the Laplacian is negative at the BCP, this indicates that the accumulation of density in the bonding region dominates.

A map of the Laplacian of a free atom reveals more structure than the simple exponential decay seen in a density plot. Spherical shells of alternating sign are observed. Each radial minimum corresponds to a quantum mechanical shell ($n = 1, 2, 3\ldots$). At distances far removed from the nucleus the Laplacian is positive, while at distances associated with the valence region $\nabla^2\rho(\mathbf{r})$ is negative. Moving in towards the nucleus, we encounter another sphere of positive $\nabla^2\rho(\mathbf{r})$, which can be associated with the beginning of the core region.

Empirically it is seen that shared (covalent) interactions between atoms in the second row have negative values of $\nabla^2\rho(\mathbf{r}_b)$ with magnitudes on the order of one atomic unit (1 au). Conversely, bonds that are normally considered ionic (or closed shell) have positive values of $\nabla^2\rho(\mathbf{r}_b)$, with magnitudes closer to 0.1 au. For third row atoms these values are somewhat different and the long bonds favour more positive values of the Laplacian, particularly for polar bonds. We will see other important information contained in the Laplacian field in Section 3.3.

3.2.3. Distance to the nuclei - polarity

Another indicator of bond polarity is the distance of the BCP to each of the connected nuclei. This will of course be strongly determined by the characteristic size of the atoms involved, but for a given atom, as the BCP moves closer to the nucleus, less electron density is associated with that atom and more with the neighbouring (bonded) atom. Thus as the BCP shifts away from some 'neutral' position, the bond is becoming more polar. The Laplacian will concomitantly become more positive as the BCP moves closer to the core region of the electropositive atom, where $\nabla^2\rho(\mathbf{r}) > 0$.

3.2.4. Ellipticity – sigma / pi contributions

In most organic molecules and some inorganic systems, particularly planar molecules, we can describe multiple bonds as being made up of one σ-like and one (or two) π-like 'bonds'. We may use any other set of equivalent orbitals, such as two (or three) bent bonds, in our description. In the case of a double bond in a planar molecule, the density is observed to be greater in the plane containing the π-like bond than in a perpendicular plane containing the bond axis. A single or triple bond has more cylindrical symmetry. This accumulation of density in the 'π-plane' may be measured using the ellipticity at the BCP. The ellipticity is defined as the ratio of the two negative curvatures minus one, $\varepsilon = (\lambda_1 / \lambda_2) - 1$. When the bond is cylindrically symmetric, $\lambda_1 = \lambda_2$ and $\varepsilon = 0$. When there is significant 'π-character' in the plane corresponding to λ_2 the density in that plane is more 'flat' and $\lambda_1 > \lambda_2$, so $\varepsilon > 0$. Ellipticity is a good indicator of the presence of a single π-like bond or orbital, but it is important to remember that not all multiple bonds are well described as the sum of one σ bond and one π bond.*

3.3. The Laplacian, Lewis and VSEPR

The Lewis model is recognizable in the Laplacian of the electron density, which is the sum of the three curvatures of the density. The Laplacian is a measure of how concentrated or depleted the density is, relative to neighbouring points. As mentioned above, the Laplacian is negative at points where the density is locally concentrated and positive at points where it is locally depleted (Morse and Feshbach, 1951). Contour maps and isovalue envelopes of $\nabla^2\rho(\mathbf{r})$ show regions of charge concentration ($\nabla^2\rho(\mathbf{r}) < 0$) in the positions where Lewis structures and VSEPR theory predict localized electron pairs. Bonding charge concentrations (CCs) are observed between covalently bonded atoms, and non-bonding CCs are observed where 'lone pairs' are predicted. Connected bonding and non-bonding (lone pair) regions can be seen in a contour plot of the Laplacian

---

* Consider for example the double bond in cylindrically symmetric molecular oxygen, $^3O_2$.

for P_4, Figure 3-2.

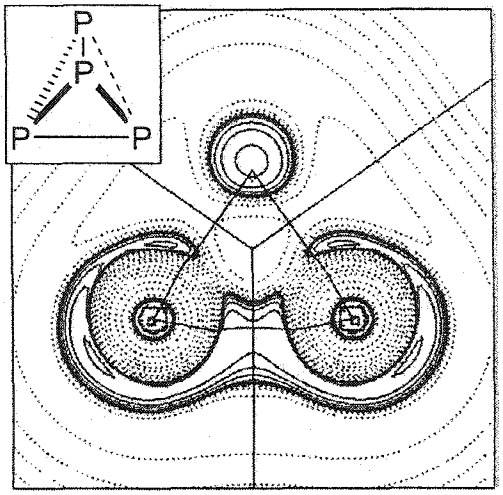

Figure 3-2: Contour map of $\nabla^2\rho(\mathbf{r})$ in a symmetry plane of tetrahedral P_4. Solid contours indicate negative values (concentration) and dashed lines indicate positive values (depletion). The outermost contour is +0.002 au. Isovalue contours increase and decrease from the $\nabla^2\rho(r) = 0$ contour in the order $\pm 2\times 10^n$, $\pm 4\times 10^n$, $\pm 8\times 10^n$, beginning with $n = -3$ and increasing in steps of unity.
The curved line forming the base of a triangle is a bond path between the two in-plane nuclei. The two sides of the triangle are intersections of the plane with ring surfaces. They meet at a bond critical point. The three lines forming a Y are intersections of the plane with the interatomic surfaces. The bond path crosses the interatomic surface at a bond critical point.

This connection between concentration and localization has recently been explained (Bader and Heard, 1999), by noting that *if* the reference electron is totally localized within some region, the magnitude of the α-Fermi hole $\left|h^{\alpha}(\mathbf{r}_1,\mathbf{r}_2)\right|$ will equal the α-electron density $\rho^{\alpha}(\mathbf{r}_2)$ within that region and be zero outside. Outside this region, the *conditional pair probability* (see below), $\delta^{\alpha\alpha}(\mathbf{r}_1,\mathbf{r}_2)=\rho^{\alpha}(\mathbf{r}_2)-\left|h^{\alpha}(\mathbf{r}_1,\mathbf{r}_2)\right|$, will exactly equal the α-electron density and the Laplacians of the two fields will also be equal. The same will be true of the β-spin electrons. Thus when the electrons are *reasonably* localized, the Laplacian shows the regions in which the localization is concentrated.

For a given Lewis structure, VSEPR theory predicts the arrangement of the shared and unshared electron pairs around each atom. The preferred arrangement arises from the minimization of Pauli repulsion between same-spin electrons (see Section 3.1.3). In the most typical case of four electron pairs, the same-spin electrons arrange themselves such that their most probable locations are at the corners of a tetrahedron. When the atom in question is sharing two or more pairs with other atoms, the tetrahedra are fixed in position. If an atom is sharing two pairs with the same neighbouring atom, the two pairs are pulled closer together than the ideal tetrahedral angle, by electrostatic attraction for the positive cores. The two domains overlap to give a single high-density region along the bond axis. One region of charge concentration is observed, regardless of the bond order.

As the bond polarity increases, the electron pairs become more localized on a single atom. If only one of the (potential bonding) pairs is localized on the atom of interest, while the other is more equally shared, we expect one charge concentration along the bond path and one at a near-tetrahedral angle, giving a pyramidal bonding arrangement. If the geometry around the more electronegative atom is constrained to be planar, there should be charge concentrations above and below the plane, and there will also be a bonding concentration associated with the more equally shared electron pair.

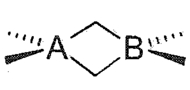

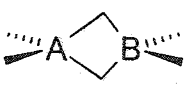

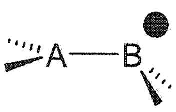

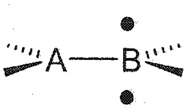

Such an arrangement of charge concentrations, combined with an energetic preference for a pyramidal arrangement, is evidence that one or both bonded atoms are insufficiently electronegative to attract two pairs of electrons and bring them into close proximity, against the Pauli repulsion effects. A single bond is preferred in such cases.

The number, location and properties of the maxima give us some clues to the appropriate Lewis structure(s) with which to describe a molecule. The number of non-bonding maxima gives an indication of the number of lone pairs (and thus the number of bonding pairs, by deduction). However, one must take care when counting the maxima. For singly bonded terminal atoms, the unshared electrons are not localized into pairs. Rather the six electrons form a torus of unshared density (Gillespie and Popelier, 2001). The molecular symmetry may also place restrictions on the number and location of maxima, so that they do not correspond to the expected Lewis structures. For example, linear molecules must have cylindrical symmetry, so lone pairs must appear as a single 'cap' or as a torus. Molecules with C_3v symmetry must have one or three - never two - equivalent maxima for atoms lying on the axis. Therefore, we will never observe two lone pairs on the oxygen atom, in the Laplacian map of H_3PO. In a case such as this, the two (hypothetical) lone pairs cannot become localized into two separate, well-defined regions of space.

In regions where the density is quite 'flat', a single region of charge concentration can sometimes exhibit more than one maximum, with a saddle in between. Bader and Heard (1999) have suggested a method for determining whether two charge concentrations are associated with the same 'localized' pair of electrons, by studying maps of the conditional pair density. A more simplistic approach is taken in the current study. If the density and Laplacian at the saddle are very similar to those at the maxima, we can conclude that the two maxima represent a single region of charge concentration. If the properties at the saddle point are quite different, there may be two pairs of electrons present.

A bonding charge concentration may show a local maximum in the valence shell of one or both bonded atoms. The number of bonding charge concentrations gives no indication of the bond order as all the bonding pairs are localized in the same region. However, an unexpected non-bonding charge concentration is an indication that the bond order is less than expected. Analysis of the topology of the Laplacian will be helpful for deducing the appropriate Lewis description of a molecule when the delocalization index approach, described below, gives inconclusive results. This will be the case particularly when one member of a series has an unusual bonding arrangement.

3.4. Atoms in Molecules Approach to Population Analysis

We have seen that in order to partition many-particle properties, such as potential energy, into atomic contributions we must use a mean field approach. *Dressed operators* are obtained by integrating the 'property' over all the electronic coordinates but one and summing over all the electronic spins. This procedure is denoted by $\int d\tau'$. Taking the average of this dressed operator and its complex conjugate accounts for the local non-Hermicity of some operators. Multiplication by the number of electrons, N, results in a property density, which is a function of real space. To calculate the atomic contribution to a property, the property density is integrated over the basin of the open system. This operation is denoted by $\int_{\Omega} dr$.

3.4.1. *Population and charge*

One of the easiest atomic properties to calculate is the electron population, N(Ω). This depends only on the electron density, $\rho(\mathbf{r})$. From this the atomic charge, $q(\Omega) = Z_{\Omega} - N(\Omega)$, is easily accessible, and a good indication of the polarity of the bonding is obtained. In later chapters, when various substituents are compared, the charge on the entire substituent will be calculated to avoid the complications of increased charge on a substituent atom due to its increased coordination number.

3.4.2. *Localization and the Fermi hole*

The population of an atom or group may be determined using only the one-electron density, while the kinetic energy depends on the *first-order density matrix*. See Appendix A3.1 for a description of density matrices. Both population and energy can be expressed in terms of property densities in real space. In contrast, the localization of electrons within an atom or group, and the delocalization of electrons between two groups depend on the *pair density*, $\rho(\mathbf{r}_1,\mathbf{r}_2)$ which is proportional to the diagonal elements of the *second-order density matrix*. These properties depend on the coordinates of *two* electrons and can be integrated over two regions of space.

The relationship between electron pair localization and the Lewis model of molecular structure has been discussed by Fradera *et al.* (1999) and was introduced in Chapter 1. Due to anti-symmetrization, an electron at some reference position, $\mathbf{r}_1$, will exclude density of the same spin from the region around it. For wavefunctions at correlated levels of theory, electrons of different spin also exclude each other due to Coulomb correlation. Both of these correlations are described by the correlation function, $f^{\sigma\sigma'}(\mathbf{r}_1,\mathbf{r}_2)$, which is defined in terms of first- and second-order density matrices by Equation 3-2.

$$\rho^{\sigma\sigma'}(\mathbf{r}_1,\mathbf{r}_2) = \tfrac{1}{2}\rho^{\sigma}(\mathbf{r}_1)\rho^{\sigma'}(\mathbf{r}_2)\left[1 + f^{\sigma\sigma'}(\mathbf{r}_1,\mathbf{r}_2)\right]$$

Equation 3-2

Thus the correlation function relates the probability of finding an electron of spin σ at position $\mathbf{r}_1$ *and* an electron of spin σ' at position $\mathbf{r}_2$ to the probabilities of those events occurring independently. At the Hartree-Fock level of theory, there is no Coulomb correlation and so the opposite-spin correlation functions are zero. We define the *conditional* same-spin pair density, $\delta^{\sigma\sigma}$, as the probability of finding an electron at $\mathbf{r}_2$ given that an electron of the same spin is present at $\mathbf{r}_1$.

$$\delta^{\sigma\sigma}(\mathbf{r}_1,\mathbf{r}_2) = 2\frac{\rho^{\sigma\sigma}(\mathbf{r}_1,\mathbf{r}_2)}{\rho^{\sigma}(\mathbf{r}_1)} = \rho^{\sigma}(\mathbf{r}_2) + \rho^{\sigma}(\mathbf{r}_2)f^{\sigma\sigma}(\mathbf{r}_1,\mathbf{r}_2) = \rho^{\sigma}(\mathbf{r}_2) + h^{\sigma}(\mathbf{r}_1,\mathbf{r}_2)$$

Equation 3-3

The Fermi hole, $h^{\sigma}(\mathbf{r}_1,\mathbf{r}_2)$, is a measure of how much density is excluded at $\mathbf{r}_2$ due to the presence of a *reference* electron at $\mathbf{r}_1$. The Fermi hole is equal to the same-spin correlation function multiplied by the spin density, $\rho^{\sigma}(\mathbf{r}_2)$, and to the *conditional* same-spin pair density minus the spin density, see Equation 3-3. The more localized the Fermi hole, the more localized is the reference electron at $\mathbf{r}_1$ (Bader and Stephens, 1975). For a closed shell system, the Fermi holes of α and β electrons are *independent and equal* so that α,β pairs result. At the Hartree-Fock level of theory, the Fermi hole reduces to the *exchange density* divided by the reference density.

$$h^{\sigma}(\mathbf{r}_1,\mathbf{r}_2) = \rho^{\sigma}(\mathbf{r}_2) f^{\sigma\sigma}(\mathbf{r}_1,\mathbf{r}_2) = \frac{-\sum_{i}^{\sigma}\sum_{j}^{\sigma} \phi_i^*(\mathbf{r}_1)\phi_i(\mathbf{r}_2)\phi_j^*(\mathbf{r}_2)\phi_j(\mathbf{r}_1)}{\rho^{\sigma}(\mathbf{r}_1)}$$

Equation 3-4

$$\int d\mathbf{r}_2 h^{\sigma}(\mathbf{r}_1,\mathbf{r}_2) = \int d\mathbf{r}_2 \rho^{\sigma}(\mathbf{r}_2) f^{\sigma\sigma}(\mathbf{r}_1,\mathbf{r}_2) = -1$$

Equation 3-5

For a given reference position, the Fermi hole integrates to –1 over all space, corresponding to the exclusion of one electron. If the Fermi hole is integrated over an atom, the result is the fraction of an electron excluded from the atom by that reference position or, equivalently, how localized the reference electron is within the atom. If the result is also integrated over the atom *with respect to the reference position*, weighted by the electron density, $\rho(\mathbf{r}_1)$, the result is the number of electrons localized within the atom. The sum of the alpha and beta localizations is called the atomic localization index, $\lambda(\Omega)$.

$$\int_{\Omega} d\mathbf{r}_1 \rho^{\sigma}(\mathbf{r}_1) \int_{\Omega} d\mathbf{r}_2 h^{\sigma}(\mathbf{r}_1,\mathbf{r}_2) = \int_{\Omega} d\mathbf{r}_1 \rho^{\sigma}(\mathbf{r}_1) \int_{\Omega} d\mathbf{r}_2 \rho^{\sigma}(\mathbf{r}_2) f^{\sigma\sigma}(\mathbf{r}_1,\mathbf{r}_2) = F^{\sigma}(\Omega,\Omega)$$

Equation 3-6

$$\lambda(\Omega) = F(\Omega,\Omega) = F^{\alpha}(\Omega,\Omega) + F^{\beta}(\Omega,\Omega)$$

Equation 3-7

Alternatively, the reference position may be integrated over a different atom, and the result is the number of electrons in the reference atom that are delocalized onto another atom.

$$\int_{\Omega'} d\mathrm{r}_1 \rho^{\sigma}(\mathrm{r}_1) \int_{\Omega} d\mathrm{r}_2 h^{\sigma}(\mathrm{r}_1,\mathrm{r}_2) = \int_{\Omega'} d\mathrm{r}_1 \rho^{\sigma}(\mathrm{r}_1) \int_{\Omega} d\mathrm{r}_2 \rho^{\sigma}(\mathrm{r}_2) f^{\sigma\sigma}(\mathrm{r}_1,\mathrm{r}_2) = F^{\sigma}(\Omega',\Omega)$$

Equation 3-8

The delocalization of Ω into Ω' must necessarily equal the delocalization of Ω' into Ω, and the total *delocalization index*, $\delta(\Omega,\Omega')$, between the pair of atoms is the sum of these contributions.

$$\delta(\Omega,\Omega') = 2F(\Omega,\Omega') = 2[F^{\alpha}(\Omega,\Omega') + F^{\beta}(\Omega,\Omega')]$$

Equation 3-9

At the closed-shell Hartree-Fock level, the delocalization index can be calculated as $\delta(\Omega,\Omega') = 4\sum_{ij}S_{ij}(\Omega)S_{ij}(\Omega')$; where $S_{ij}(\Omega) = \int_{\Omega} dr\Phi_i\Phi_j(r)$ is known as an atomic overlap integral. At this level of theory the delocalization index is equal to the bond indices proposed by Fulton (1993) and by Ángyán, Loos and Mayer (1994), see Appendix A3.2. For post-Hartree-Fock wavefunctions there will also be contributions from the opposite spin correlation functions and, due to differences in the basic definitions, the equality with other indices no longer holds.

3.5. Interpretation of the Delocalization Index

3.5.1. Delocalization and bond orders.

While the delocalization index, $\delta(\Omega,\Omega')$, does count the number of electrons shared between two atoms, it does not directly measure the number of contributing *Lewis pairs* of electrons. An equally shared pair of electrons will donate 1.0 to $\delta(\Omega,\Omega')$, but an unequally shared pair will donate less. For example, the delocalization index in H_2 is 1.0, while that in LiF is about 0.1, though both bonds can be described by the sharing of one pair of electrons (Fradera *et al.*, 1999). Conversely, a delocalization index near one may reflect one equally shared pair or more unequally shared pairs. Furthermore, $\delta(\Omega,\Omega')$ has a non-zero value for atoms that do not share a bond path and are therefore not bonded to each other according to the topological definition. Fradera *et al.* (1999) therefore argue that $\delta(\Omega,\Omega')$ should not be identified with a bond order.

To get an indication of the number of Lewis electron pairs involved in bonding, Fradera *et al.* undertook an orbital-based analysis. For molecules with cylindrical or planar symmetry, electrons in orbitals of σ or σ-like symmetry can be rigourously separated from electrons in π or π-like orbitals. Thus the σ-like and π-like delocalization indices can be calculated separately. In the case of moderately polar covalent molecules with multiple bonding it was seen that the two contributions are similarly (but not identically) polarized.

3.5.2. Derivation of a new relationship between $\delta^{HF}(A,B)$ and $q^{HF}(B)$

For non-polar molecules at the Hartree-Fock level of theory, $\delta(\Omega,\Omega')$ is very close to the bond order determined by Lewis structures. For example, the delocalization index $\delta(C,C)$ in $H_2C{=}CH_2$ is 1.89, slightly below 2.00 due to interaction with the H atoms. For polar molecules, the delocalization index decreases as the charge transfer from Ω to Ω' (measured by the charge on Ω)

increases. See section 3.5.3 for examples.

Let us look at three simple cases; a polar molecule with one unequally shared pair of electrons, and a polar molecule with two or three unequally shared pairs of electrons, occupying molecular orbitals (Φ) of different symmetry in the canonical molecular orbital description.

Case 1. Let the core charge on each atom be +1 and the total charge on the molecule be zero. The core electrons are assumed to be completely localized and do not contribute to the delocalization, so for the purposes of this treatment we can write the single-determinantal wavefunction as: $\psi = \left|\Phi_1 \overline{\Phi}_1\right|$. *I.e.*, assume all other atomic overlap integrals $S_{ij}(A)$ and $S_{ij}(B) = 0$ or 1 and all other products $S_{ij}(A)S_{ij}(B) = 0$.

The population on each atom (due to the orbital of interest) is $N(A) = 2\int_A dr\Phi^2(r) = 2S(A)$ and $N_\Phi(B) = 2\int_B dr\Phi^2(r) = 2S(B)$. For neutral atoms, we would require that each atomic population was one. The charges are thus $q(A) = 1\text{-}N(A) = 1\text{-}2S(A)$ and $q(B) = 1\text{-}N(B) = 1\text{-}2S(B) = -q(A)$.

Rearranging these expressions to isolate the overlap integrals gives $S(A) = \dfrac{1-q(A)}{2}$ and $S(B) = \dfrac{1-q(B)}{2} = \dfrac{1+q(A)}{2}$.

Substituting these expressions into the delocalization index gives:

$$\delta(A,B) = 4S(A)S(B) = 4\left(\frac{1-q(A)}{2}\right)\left(\frac{1+q(A)}{2}\right) = 1 - q(A)^2 .$$

Equation 3-10

We see that, in this simple case, the delocalization does indeed depend on the square of the charge transferred, and that the maximum delocalization of 1.0 occurs for the non-polar case ($q = 0$), as expected. We will see below that the coefficient of q^2 can be varied by interactions with other orbitals.

Case 2. We now consider the case for a diatomic molecule, XY, with a second pair of shared electrons in a molecular orbital of *different symmetry* (*e.g.* one σ-like and one π-like) and core charges of +2. The determinantal wavefunction is then $\psi = \frac{1}{\sqrt{4}}\left|\left(\Phi_i^{\alpha}(r_1)\Phi_i^{\beta}(r_2)\Phi_j^{\alpha}(r_3)\Phi_j^{\beta}(r_4)\right)\right|$.

Again we define the population of each atom due to the two orbitals of interest.

$$N(Y) = \int_Y dr\rho(r) = 2\int_Y dr\left\{\Phi_i^2(r) + \Phi_j^2(r)\right\} = 2S_{ii}(Y) + 2S_{jj}(Y)$$

$$N(X) = \int_X dr\rho(r) = 2\int_X dr\left\{\Phi_i^2(r) + \Phi_j^2(r)\right\} = 2S_{ii}(X) + 2S_{jj}(X)$$

Since the neutral atoms would each have populations of two, the charges are:

$q(Y) = 2\text{-}N(Y) = 2\text{-}\ 2S_{ii}(Y) - 2S_{jj}(Y)$ and $q(X) = 2\text{-}N(X) = 2\text{-}\ 2S_{ii}(X) - 2S_{jj}(X) = -q(Y)$.

Assuming the two orbitals are *equally polarized*, we can define new overlap terms: $S_{ii}(Y) = S_{jj}(Y) \equiv S(Y)$ and $S_{ii}(X) = S_{jj}(X) \equiv S(X)$. This allows us to rearrange and substitute as before.

$$S(Y) = \frac{2-q(Y)}{4} \text{ and } S(X) = \frac{2-q(X)}{4} = \frac{2+q(Y)}{4}$$

The delocalization index for this system can be written as

$\delta(Y,X) = 4\left\{S_{ii}(Y)S_{ii}(X) + 2S_{ij}(Y)S_{ij}(X) + S_{jj}(Y)S_{jj}(X)\right\}$ where

$S_{ij}(Y) = \int_Y dr \Phi_i \Phi_j(r) = 0$ and $S_{ij}(X) = \int_X dr \Phi_i \Phi_j(r) = 0$ due to symmetry.*

Finally, we can write,

$$\delta(Y,X) = 8S(Y)S(X) = 8\left(\frac{2-q(Y)}{4}\right)\left(\frac{2+q(Y)}{4}\right) = \frac{2^2 - q(Y)^2}{2} = 2 - \frac{q(Y)^2}{2}.$$

Equation 3-11

We see again the quadratic dependence on the charge transfer with the expected maximum value for a non-polar system, but this time with a different coefficient in front of q^2. Since the charges are equal and opposite either $q(X)$ or $q(Y)$ may be used in this expression, and in Equation 3-10.

Expressing the total charge transfer as the sum of the two orbital polarities, we can rewrite Equation 3-11 as $\delta(Y,X) = 2 - \frac{(2p)^2}{2} = 2 - \frac{4p^2}{2} = 2\left(1 - p^2\right)$; where $q = 2p$. Similarly, for three orbitals of different symmetry but the same polarity, p, we can write q = 3p and then, generalizing the previous expression,

$$\delta(Y,X) = 3\left(1 - p^2\right) = 3 - 3\left(\frac{q}{3}\right)^2 = 3 - \frac{q^3}{3}.$$

3.5.3. Verification of the new relationship.

Case 1 above can be verified by plotting the period 2 hydride, AH_n, data published by Fradera *et al.* (1999), see Figure 3-3. The seven molecules (A = Li

---

* It should be noted that this vanishing only occurs when the nuclei of *X* and *Y* coincide with the symmetry element that distinguishes the symmetry of the two orbitals. For example if one orbital is symmetric and the other antisymmetric with respect to a symmetry plane $S_{ij}(X) = 0$ only if the nucleus of *X* lies in the symmetry plane.

- F) give a curve whose best-fit equation is $\delta(A,H) = 0.99 - 0.97q^2(H)$, with $R^2 = 0.999$, in excellent agreement with the equation derived above.

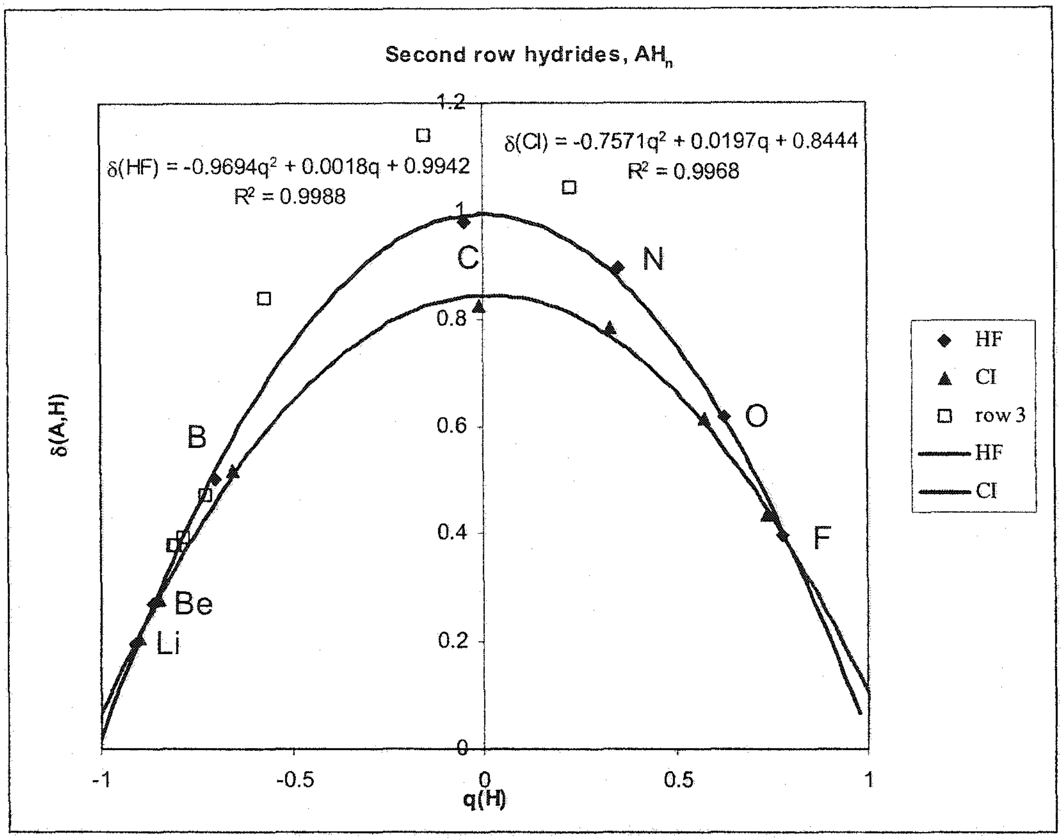

Figure 3-3: A graph of delocalization index *versus* charge transfer for the second row hydrides, at two levels of theory: Hartree-Fock (HF, ◆) and Configuration Interaction (CI, ▲). Each series is fitted to a quadratic function and the equations are displayed on the graph. Hartee-Fock data for the third-row hydrides are also shown, as open squares. The data are those published by Fradera *et al.* in 1999. Note that there is an error in Table 3 of the paper by Fradera *et al.* The $2D_2(H,H')$ value has also been reported as $N(H)$. The correct value, based on $N(N)$ is q(H) = 0.651.

The Hartree-Fock level data for the third period hydrides are shown on the same graph. The metals and metalloids (A = Na – Si) fall on or near the curve described for the second row hydrides. PH_3, SH_2 and HCl form their own curve above the first. This can be most easily explained as additional delocalization of the 'lone pair' electrons from the large moderately electronegative central atom to the neighbouring hydrogen atoms. Similar lone pair effects will be seen in the phosphorus and nitrogen systems studied in this thesis.

Figure 3-3 also shows that a quadratic relationship is maintained when correlation is included, though the curve is lower for the covalent systems. The two curves (HF and CI) cross when the magnitude of the charge transfer is approximately 0.8 electrons. The two essentially ionic hydrides, LiH and BeH_2 show little change when correlation is included. For CH_4 and NH_3 the major effect is a reduction of the delocalization index. For BH_3 and H_2O the major effect is a decrease in the charge transfer. The expected reduction in δ due to correlation is apparently compensated by the concomitant reduction in bond polarity. For hydrogen fluoride, the reduction in polarity dominates and the delocalization index actually increases with inclusion of correlation. The most dramatic reduction in $\delta(\Omega,\Omega')$ observed in the 1999 study was for N_2 where $\delta(N,N')$ dropped from 3.04 at the Hartree-Fock level to 2.22 at the CISD level. As pointed out by Fradera *et al.*, the Hartree-Fock wavefunction, which describes the molecule in terms of electron pairs, moving in the average field of the other electrons, corresponds more closely to the simple Lewis picture than does a correlated wavefunction.

In order to determine whether a triple-bond description was in fact reasonable for the 14-electron species: CO, CN^- and NO^+, the data reported by Fradera *et al.* for these systems and for N_2 were supplemented by newly calculated data for P_2, PN and PCH, where the CH group is treated as a single atom. All of these systems have ten valence electrons.

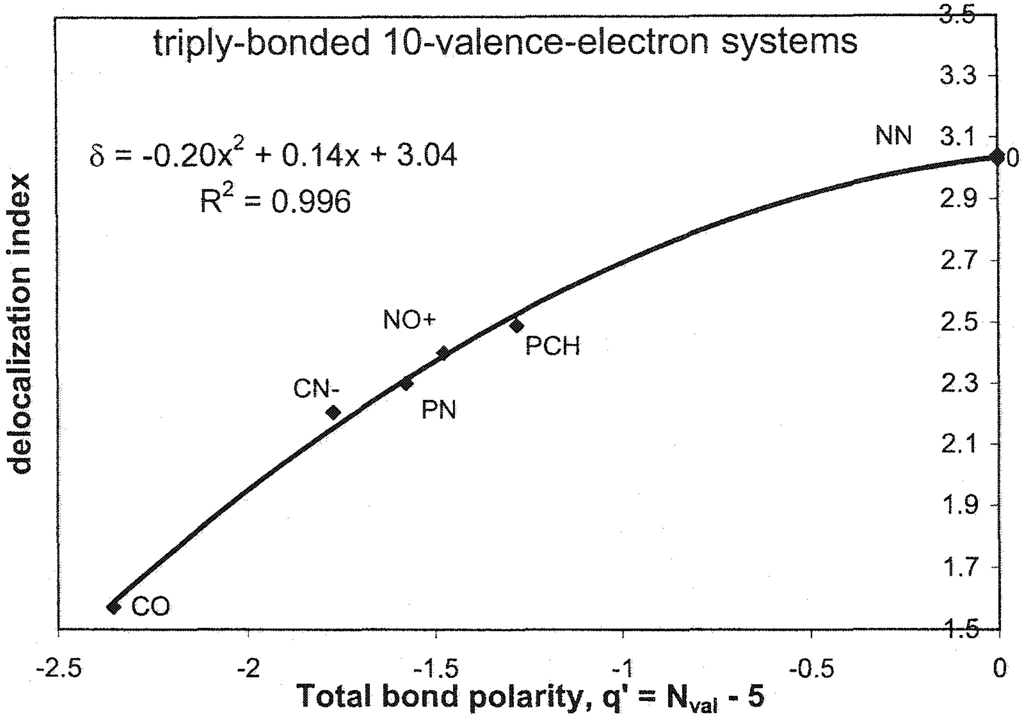

Figure 3-4: A graph of delocalization index *versus* charge transfer, q′, for a set of ten-valence-electron 'diatomic' systems, assuming five valence electrons for each atom, in the 'non-polar' case. The data are fitted to a quadratic function and the equation is displayed on the graph. The data for CO, CN^-, NO^+, and N_2 are those published by Fradera *et al.* in 1999. All wavefunctions were calculated at the HF/6-311++G(2d,2p) level of theory.

It was initially assumed that the bonds are all triple bonds and thus each atom would have five valence electrons in the non-polar case. The total bond polarization, $q' = 3p$, was thus calculated relative to this non-polar reference, as $q' = \{N(\Omega) - N(\text{core}) - 5\}$, rather than simply using atomic charges, which would not be a direct measure of charge transfer for the ionic species. The resulting graph is shown in Figure 3-4.

All the points fall close to a best-fit quadratic function, $\delta = 3.04 + 0.14q - 0.20q^2$, whose curvature is not in agreement with the equation derived above, $\delta = 3.00 - 0.33q^2$. The maximum is at (0.35, 3.06), close to the expected (0, 3) and the delocalization of three pairs is attained for the non-polar NN (0, 3.04) and PP (0, 3.03) molecules. The deviation may be explained by the additional delocalization of lone pairs and by the fact, established by Fradera *et al.*, that the three contributing orbitals are not equally polarized. Given these complications it is encouraging that a quadratic function with approximately the expected maximum is attained. More data points would help strengthen the conclusion that these molecules do indeed involve polar triple bonds.

The results of this analysis highlight the importance of determining the δ *vs.* q (or p) relationship for an entire of series of molecules, related to a system of interest, before making conclusions regarding the bond order. We also note that such a fitting procedure reveals differences that may be present in one or a few members of a series, but not in others, such as additional lone pair delocalization.

3.5.4. Extracting bond orders and formal charges from the data

For the purposes of this thesis the term *bond order* will refer to the Lewis sense of '*number of shared pairs of electrons,*' whether the sharing is equal or unequal. A pair of electrons will be considered 'shared' when there is significant delocalization of electrons between two atoms, as measured by the delocalization index. The bond order is then assumed to be the same for a series of molecules that differ mainly in the polarity of the bond of interest, and which can be fit to a simple quadratic function when plotting $\delta(A,B)$ *vs*. $q(B)$. The bond order will be taken as the maximum point on the quadratic curve, as this represents the delocalization index when the pairs are most equally shared. The charge at the maximum will be identified with the formal charge, as this point best matches the definition of formal charge as the hypothetical charge on the atom when all the bonding pairs are equally shared. This has been done for each series studied in this thesis. Each series can be fitted to a different quadratic curve, with varying quality of fit.

We expect the maximum delocalization index to occur when the electron pairs are equally shared, *i.e.* when the bond is non-polar. Thus if the maximum delocalization index for the H_3PX series was two and occurred when $q(X) = 0$, we would conclude that the best Lewis structure was $H_3P{=}X$ and that the polar bond consisted of two unequally shared electron pairs. If on the other hand the maximum delocalization was one and it occurred when $q(X) = -1$, we would conclude that the best Lewis structure for the series was $H_3P^{+}\text{-}X{:}^{-}$ and that the P-X bond consisted of one shared pair of electrons while the second pair was localized almost exclusively on X.

If the maximum delocalization occurs at some intermediate ($q(X)$, $\delta(P,X)$) point we should conclude that the bond consists of two differently polarized, shared pairs of electrons. Returning to our derived relationship for the equally polarized pairs, $\delta = 2(1-p^2)$, we could write for unequally polarized pairs $\delta = 2 - p_1^2 - p_2^2$. If the two polarities, $p_1 + p_2 = q$, are never both zero, the delocalization index will never reach a maximum value of two. Furthermore, if the maximum occurs for q(X) < 0 we must conclude that some of the density remains localized on X, even as the bond polarity reverses, so that while one shared pair is becoming more localized on P, and thus reducing the delocalization index, the second pair remains more localized on X, so that there are never two equally shared pairs of electrons, regardless of the bond polarity. In this case, the bond order must be less than two, and should again be identified with the maximum delocalization index.

Having determined a common bond order and formal charge distribution for a series of molecules, a Lewis structure will be proposed which best reflects these properties. We then appeal to Lewis's original intention that the bonds represented be either polar or non-polar so that the Lewis structure is a sufficient representation of all members of the series, regardless of polarity. In the case that a single resonance structure cannot represent the calculated properties, *i.e.* the bond order and formal charges are non-integer, one or more resonance schemes will be proposed to *describe* the observed properties, keeping in mind that what is important, in the end, are the resonance averages and not the individual weightings of specific resonance structures. Thus a bond order of 1.5 and formal charge of 0.5 can be *equally* well represented *either* as 50% [A=B] + 50% [A^+–B:$^-$] *or* as 75% [A=B] + 25% [A^{2+} :B:$^{2-}$], for example.

This approach will be taken for the series H_2PR, HPR_2, PR_3, HPX, HPX_2, H_3PX, PR_2^+, H_2NR, NR_3, HNX and H_3NX. For the phosphenium cations, the extent of multiple bonding in $P(NH_2)_2^+$ will be compared to that in other members of the series in order to ascertain whether there is a significant difference and whether this difference is likely to account for the much greater stability of $P(NH_2)_2^+$ as measured by hydride transfer energies. A ($q(NH_2)$, $\delta(P,NH_2)$) point well above the curve representing other members of the series would be evidence of additional bonding in this system. Such an observation seems possible given the hydride results, though similar increases could be expected for R = Cl, SH and PH_2. Conversely, the data for R = H, CH_3 and SiH_3 are expected to fall below the curve for the other substituents as these have no lone pairs available to donate.

Bibliography

References are listed alphabetically by first author and then by date.

Ángyán, I.; M. Loos and I. Mayer (1994). *J. Phys. Chem.* **98**, 5244.

Bader, R.F.W. and M.E. Stephens (1975). *J. Am. Chem. Soc.* **97**, 7391.

Bader, R.F.W.; T.S. Slee, D. Cremer and E. Kraka (1983). *J. Am. Chem. Soc.* **105**, 5061.

Bader, R.F.W. and G.L. Heard (1999). *J. Chem. Phys.* **111**, 8789.

Boyd, R.J.; O. Knop and S.C. Choi (1988). *J. Am. Chem. Soc.* **110**, 7299.

Coulson, C.A. (1947). *Quart. Revs. (London)* **1**, 144.

Coulson, C.A. and H.C. Longuet-Higgins (1947). *Proc. Roy. Soc. (London)* **A191**, 39.

Coulson, C.A. (1951). *Proc. R. Soc.* **A207**, 91.

DeKock, R.L. (1987). *J. Chem. Edu.* **64**, 934.

Ebsworth, E.A.V., D.W.H. Rankin and S. Craddock (1987). Structural Methods in Inorganic Chemistry. Edinburgh: Blackwell.

Fradera, X.; M.A. Austen and R.F.W. Bader (1999). *J. Phys. Chem. A* **103**, 304.

Fulton, R.L. (1993). *J. Phys. Chem.* **97**, 7516.

Gillespie, R.J. and R.S. Nyholm (1957). *Q. Rev. Chem. Soc.* **11**, 339.

Gillespie, R.J. and I. Hargittai (1991). The VSEPR Model of Molecular Geometry. Allyn and Bacon.

Gillespie, R.J. and P.L.A. Popelier (2001). Chemical Bonding and Molecular Geometry. New York: Oxford University Press.

Hund, F. (1931*a*). *Z. Physik* **73**, 1.

Hund, F. (1931*b*). *Z. Physik* **73**, 565.

Hund, F. (1932). *Z. Physik* **77**, 12.

Hund, F. (1940). *Z. Physik* **117**, 1.

Lewis, G.N. (1916). *J. Am. Chem. Soc.* **38**, 762.

Linnett, J.W. (1961). *J. Am. Chem. Soc.* **83**, 2643.

Linnett, J.W. (1964). The Electronic Structure of Molecules. London: Methuen.

Longuet-Higgins, H.C. (1948). *Proc. Phys. Soc. (London)* **60**, 270

Malcolm, N.O.J., R.J. Gillespie and P.L.A. Popelier (2002). *J. Chem. Soc. Dalton Trans.* **2002**, 3333.

Morse, P. and H. Feshbach (1953). Methods of Theoretical Physics, Part 1. New York: McGraw-Hill.

Mulliken, R.S. (1928*a*). *Phys. Rev.* **32**, 186.

Mulliken, R.S. (1928*b*). *Phys. Rev.* **32**, 761.

Mulliken, R.S. (1932*a*). *Phys. Rev.* **40**, 55.

Mulliken, R.S. (1932*b*). *Phys. Rev.* **41**, 49.

Mulliken, R.S. (1935). *J. Chem, Phys.* **3**, 375.

Pauling, L.C. (1931a). *Phys. Rev.* **37**, 1185.

Pauling, L. (1931b). *J. Am. Chem. Soc.* **53**, 1367.

Pauling, L. (1931c). *J. Am. Chem. Soc.* **53**, 3225.

Pauling, L. (1932a). *J. Am. Chem. Soc.* **54**, 988.

Pauling, L. (1932b). *Proc. Natl. Acad. Sci.* **18**, 293.

Pauling, L.C. (1960). The Nature of the Chemical Bond and the Structure of Molecules and Crystals. An Introduction to Modern Structural Chemistry. 3rd ed. Ithaca, N.Y.: Cornell University Press.

Slater, J.C. (1931*a*). *Phys. Rev.* **37**, 481.

Slater, J.C. (1931*b*). *Phys. Rev.* **38**, 1109.

Slater, J.C. (1932). *Phys. Rev.* **41**, 255.

Stranges, A.N. (1984). *J. Chem. Edu.* **61**, 185.

4. Phosphine Results

Phosphines, PR_3, are the classic trivalent environment for phosphorus atoms. The Lewis description requires only a single structure with three single bonds and one lone pair at phosphorus. The P-E bonds studied in this chapter will serve as a 'singly-bonded' reference point for comparison with double bonds and partial multiple bonds studied in the later chapters.

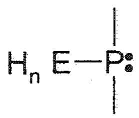

It is hoped that these data may also prove useful to other workers in the field. Some comments are included on the usefulness and reliability of various density-based bond characterization schemes. Appendix 4 shows graphs for most of the properties discussed in the following chapters, as a function of substituent atom. All seven phosphorus series are shown on the same graphs for easy comparison. For a visual exposition of the important trends in the calculated properties, the reader is referred to Figures A4-1 through A4-8 in the Appendix. Figure A4-9 shows the delocalization index versus charge transfer curves for each series. Each chapter includes complete data tables and some Laplacian maps for the systems studied.

4.1. Geometry

In order to simplify the analysis, only reasonably high symmetry conformations were considered. Specific geometries are illustrated below. Optimized bond lengths and bond angles about P are given in Table 4-1, along with experimental values, where known. Table 4-2 gives the corresponding values for amines. Graphs of the P-E bond lengths are shown in Figure A4-1.

The phosphines show a gradual increase in bond length from fluorophosphine through methylphosphine and from chlorophosphine to silylphosphine. The monosubstituted amines, NH_2R, on the other hand exhibit a step-like trend, with all the N-L bonds being 140 ± 5 pm long and all the N-M bonds being about 170 pm long. The trisubstituted amines show slightly greater variation, with the N-F bond shortening to 132 pm.

In addition to the expected increase in bond lengths in going from second to third row atoms, the bond angles are much smaller for the phosphines than for the amines. This observation can be understood in terms of Gillespie's valence shell electron pair repulsion (VSEPR) and ligand close packing (LCP) models (Gillespie and Popelier, 2001). The VSEPR model considers repulsions between the electron pairs while the LCP model considers repulsions between the ligands. In both models the lone pair, which is closer to the central atom, takes up as much space as possible. Since the phosphorus-ligand bonds are longer (and more polarized towards the ligands) than the nitrogen-ligand bonds, the angles can be smaller. The lone pairs in the phosphines are effectively more sterically active than those in the amines.

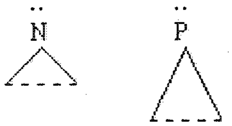

To determine a baseline of P-E bonding characteristics it is important to know how variable the bonding properties are. The effects of rotation about the P-E bond and of substitution at P and E are considered. The lowest energy rotamers studied are discussed in more detail when making comparisons with other systems.

4.1.1. Effect of rotation about P-E bonds.

Different conformational isomers were considered for the monosubstituted phosphines to determine the effects of rotation about the P-E bond. The variations in bond lengths and angles, along with the relative energies of these conformers are shown in Table 4-1A.

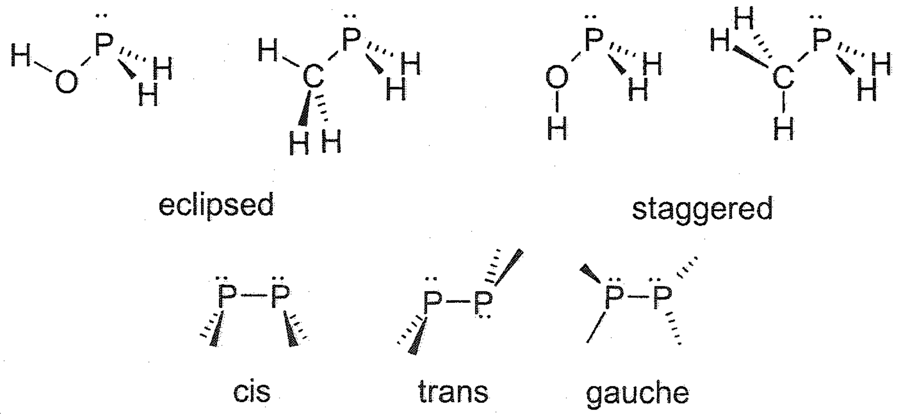

Figure 4-1: Sketches of the conformational isomers studied for the mono-substituted phosphines. For PH_2CH_3 and PH_2SiH_3 the eclipsed form is lower in energy than the staggered form. For PH_2OH and PH_2SH the anti-eclipsed form is lower in energy than the syn-staggered form. NH_2OH and NH_2SH also prefer the anti-eclipsed conformation. The 'dipnictogine' molecules, PH_2PH_2, PH_2NH_2 and NH_2NH_2 all prefer the gauche conformation, with the *cis* conformation being higher in energy than the *trans*.

For the phosphines H_2P-CH_3 and H_2P-SiH_3, the lowest energy C_s rotamer is the 'staggered' conformation. A C_1 conformation converges to the 'anti-eclipsed' form for H_2P-OH and H_2P-SH and the lowest energy C_s rotamer is the 'anti-eclipsed' conformation. For H_2P-NH_2 and H_2P-PH_2, the lowest energy rotamers have the C_2 'gauche' conformation, as observed experimentally. The '*cis*' and '*trans*' C_s rotamers were also studied.

For the doubly substituted phosphines, two C_s rotamers of $HP(OH)_2$ were studied. The rotamer with the hydroxy hydrogens 'up' towards the phosphorus lone pair, but not quite eclipsed, was lower in energy by 4.5 kJ/mol than that with the hydrogen atoms 'down', in line with the energy differences in the monosubstituted phosphines.

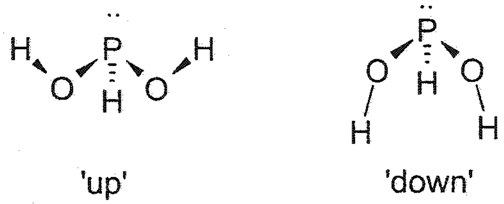

Figure 4-2: Sketches of the 'H-up' and 'H-down' conformers of $PH(OH)_2$.

The extent of rotation about the P-E bond is measured by the dihedral angles that the substituent hydrogen atoms make with the assumed location of the phosphorus lone pair when looking down the P-E bond. The lone pair is assumed to lie on a plane bisecting the HPH angle in the PH_2R as is required by symmetry in all but the gauche conformations. The same definition of the dihedral angle is used in the more substituted phosphines – with the HPH angle being replaced by the HPE or EPE angle - though this definition is quite arbitrary in these cases. For the disubstituted phosphines the substituent hydrogen atoms tend to lie closer to the other substituent than to the hydrogen atom.[*]

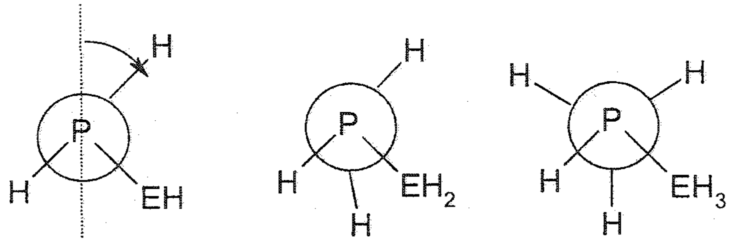

Figure 4-3: Newman projections of the studied conformations of disubstituted phosphines, $PH(EH_n)_2$. The 'H-up' conformation is preferred by $PH(OH)_2$ and $PH(SH)_2$. The amino hydrogen atoms in $PH(NH_2)_2$ lie closer to the other amino group in the optimized geometry. A staggered conformation is studied for $PH(CH_3)_2$ and $PH(SiH_3)_3$. The lone pair on the phosphorus atom is assumed to lie in the plane bisecting the HPE angle. The dihedral angles reported in Table 4-2 are measured relative to this plane, as indicated in the $PH(EH)_2$ sketch.

For the monosubstituted phosphines, the P-E bond length varies by about 1 to 2 pm between different conformers. The P-P and P-N bonds are shortest in the gauche conformations, which give the lowest energies. The anti-eclipsed conformers have longer P-E bonds than the staggered conformations, as might be expected due to steric effects. It is interesting that the eclipsed conformer is lowest in energy for PH_2OH and PH_2SH despite the longer bonds. The energy differences upon bond rotation are very small for both these molecules. Similarly, the 'H-up' conformer of $PH(OH)_2$ has longer P-O bonds and lower energy than the 'H-down' conformer. We will see that bond length is strongly correlated with other bonding properties.

---

[*] This may be an artefact of the initial-guess geometry in some cases, however, in $PH(NH_2)_2$ the initial guess started with the H atom further from the NH_2 group.

4.1.2. Effects of substitution

The P-E bond lengths can be easily compared in the PH_2R, PHR_2 and PR_3 series by a quick glance at Figure A4-1, or by comparing the values in Tables 4-1A, 4-1B and 4-1C. Increasing the degree of substitution at phosphorus has little effect on the bond lengths when the substituent is a methyl, thio or phosphino group. Other substituents tend to shorten the P-E bond length, and this can be understood in terms of electrostatic effects. For silyl-phosphines the slight P-Si bond shortening is probably due to increased negative charge on phosphorus and thus increased electrostatic attraction for the positively charged silicon atom, $P^{\delta-}$ - $Si^{\delta+}$. One would therefore expect that silyl substitution at phosphorus would lengthen P - $E^{\delta-}$ bonds, and this is indeed observed for the P-H bonds.

For increasing fluoro, hydroxy and chloro substitution, the P-E and P-H bonds shorten as the charge on phosphorus becomes more positive, and thus more attractive to the negatively charged substituents. The P-F bond shortens from 159.0 pm in PH_2F to 154.6 pm in PF_3. Fluorination at the substituent atom was also investigated for methyl- and amino-phosphines. See Table 4-1D. Fluorination at E increased P-E bond lengths as would be expected for more positive substituent atoms bonded to positive P atoms. The P-N bond lengthens by 5.5 pm when the N is perfluorinated. The P-C bond lengthens by 2.2 pm when the C is perfluorinated.

Only a few trisubstituted amines were studied: NR_3; R = F, Cl. CH_3 and SiH_3, see Table 4-2B. Replacing H with CH_3 or Cl had a small effect (-1 pm) on the N-E bond length. Increased fluorination of nitrogen shortened the N-F bond by

6 pm, due to the change from negative to positive charge on nitrogen when bound to negatively charged fluorine. Trisilylamine is nearly planar (in agreement with experiment), when restricted to a C_3v symmetry, and the N-Si bond is 2 pm longer than in silylamine. A planar, C_3h geometry was also calculated for $N(SiH_3)_3$, which has a slightly shorter N-Si bond length and is 7.4 kJ/mol *lower* in energy.

4.1.3. Low energy conformers compared to experiment.

Some experimental geometrical parameters are included in Tables 4-1 and 4-2, for comparison with the calculated values. The calculated amine bond lengths are generally too small, with correspondingly large bond angles, Table 4-2. This is typical for Hartree-Fock geometries, and including correlation at the MP2 level of theory generally increases bond lengths and decreases bond angles (DeFrees *et al.*, 1979). The Hartree-Fock optimized P-H bonds are shorter than the experimental values by up to 1.5 pm. The P-C bonds are in excellent agreement with experiment, as was found by Bachrach (1989). The calculated P-F bonds in PF_3 are also short, but when the substituent group is Cl, PH_2 or SiH_3, the optimized P-M bonds are too long by about 2 pm.

Thio- and hydroxyl-phosphines, Y_2PEH where E = O or S, undergo tautomerization to phosphine chalcogenides, $Y_2HP{=}E$, in solution (Walker, 1972, *p*.48; Hamilton and Landis, 1972). *Ab initio* calculations generally show that the phosphine tautomer is more stable in the gas phase (Kwiatkowski and Leszczynski, 1992). The hypothetical compound $P(OH)_3$ can be used as a model for $P(OR)_3$, which does exist under normal conditions. Interestingly, $N(OR)_3$ does not exist, but instead decomposes to give RON=O (Cotton and Wilkinson, 1988).

No directly comparable experimental values were found for the P-N, P-O or P-S bond lengths. However, substituted derivatives were found for amino-, alkoxy- and thio-phosphines and these are included in Table 4-1C. The optimized P-N bond lengths are in excellent agreement with the experimental bond length for $P(NMe_2)_3$. The optimized NPN angle in $P(NH_2)_3$ is large, despite the expected difference in steric bulk of the amino group *vs.* the dimethyl amino group.

Single bonds between S and trivalent P are rare, but two acyclic thiophosphines have been structurally characterized. The optimized P-S bond length in $P(SH)_3$ is in fair agreement with the electron diffraction value for $P(SMe)_3$ (Tuzova *et al.*, 1981) and in slightly better agreement with the experimental solid state geometry for $P(SPh)_3$ (Burford *et al.*, 1990). The difference of 2 pm is consistent with the errors in the other P-M bonds. Again the optimized bond angle is larger than the experimental value, despite the expected steric differences. While most of the P-E bond lengths are greater than the experimental values, the calculated P-O bond length in $P(OH)_3$ is 2 pm shorter than the experimental result for $P(OMe)_3$ (Zaripov *et al.*, 1974)[*], similar to the P-F bond length error. All the calculated bond angles are larger than those found experimentally, except in $P(OH)_3$, PF_3 and in NH_2SH. The dihedral angles in hydrazine and diphosphine are

---

[*] Electron diffraction for P(OMe)3, dihedral = 76.7°.

well reproduced at the HF level. The dihedral angle is defined in the literature relative to the '*cis*' conformation and for hydrazine it is 91° ± 2° (Kohata *et al.*, 1982), while for diphosphine it is 74.0° ± 2.2° (Durig *et al.*, 1974). The corresponding Hartree-Fock values are 90° and 77°.

At the HF level, N-H and N-E bond lengths are underestimated by 1 to 5 pm, except N-S and N-Si bonds, which are well reproduced. The near-planar angles in $N(SiH_3)_3$ are also well reproduced. Most other angles are overestimated by 1 to 5 degrees. As for the phosphines, MP2 is expected to increase the bond lengths and decrease the bond angles.

4.1.4. Effects of correlation (MP2 results)

Going from the HF to the MP2 level of theory gives the expected changes in geometry for most bonds and angles (DeFrees *et al.*, 1979). However, for the bonds between two third row atoms, this worsens the agreement with experiment. P-L bonds lengthen by 2 to 4 pm, except P-C which only lengthens by 0.3 pm. The already overestimated P-M bond lengths increase by about 1 pm - with the exception of the P-Si bond, which shortens by 1 pm, giving better agreement with experiment. The HPO angle in H_2POH is greatly reduced, but most angles decrease by only a few degrees. Another exception is that the PF_3 bond angle is increased, again improving agreement with experiment. The QCISD geometry of PH_3 is much closer to experiment than are the HF and MP2 geometries, having angles of 93.5° and bond lengths of 141.2 pm.

While the optimized geometries are not in perfect agreement with the experimental values, the agreement is good and it is reasonable to expect that the calculated trends in other properties will be reliable. Adding correlation at the MP2 level does not reliably improve the agreement.

4.2. Position of the interatomic surface

Figure 4-6 shows plots of the Laplacian of the density, $\nabla^2\rho(\mathbf{r})$ in a plane of each PH_2XH_n molecule containing the P-X bond and an X-H bond, except PH_2PH_2, which is shown in a plane containing the two P nuclei and the C_2 axis. Corresponding amine plots are shown in Figure 4-7. In all but PH_2PH_2, NH_2NH_2 and PH_2NH_2 this is a plane of symmetry. These plots are overlaid with the corresponding bond paths and the intersections of the interatomic surfaces with the plane. Bond critical points are found between all atoms that we expect to be bonded. Properties of the P-E and N-E BCPs are given in Tables 4-3 (phosphines) and 4-4 (amines). There are no ring or cage critical points in the phosphine or amine molecules studied.

4.2.1. Position of the bond critical point

It can be seen, in Figure 4-6, as we move across the phosphine series from F to CH_3 and from Cl to SiH_3 that the interatomic surface moves away from the phosphorus atom, and more electron density enters the phosphorus basin. This trend can be quantified by the distance between the P nucleus and the BCP, given in Table 4-3. This distance can be identified with the *bonding radius* of the phosphorus atom, $r_b(P)$. The bonding radius of P in the P-H bond lies between the values for the P-C and P-N bonds. We will see that calculated charges correlate with this trend. Bonding radii of the substituent atoms, $r_b(E)$, are also given in Table 4-3. The bonding radii of the phosphorus and substituent atoms are plotted, along with those for the other phosphorus series, in Figures A4-2 and A4-3.

The P-E bond length increases in the expected order (H < F < N < O < C < Cl < S < P < Si) for the expected size of the atoms and the bonding radius of phosphorus follows the expected trend as charge is transferred to the substituent. The bonding radii of the substituents follow a different trend, however. From simple periodic trend arguments, one would expect that the size of the atoms would decrease across a row (see Figure 4-4A below), and this is indeed observed for the second row substituents. For the third row however, the trend is reversed with Si having the smallest bonding radius and Cl the largest. (See Figure 4-4B below.)

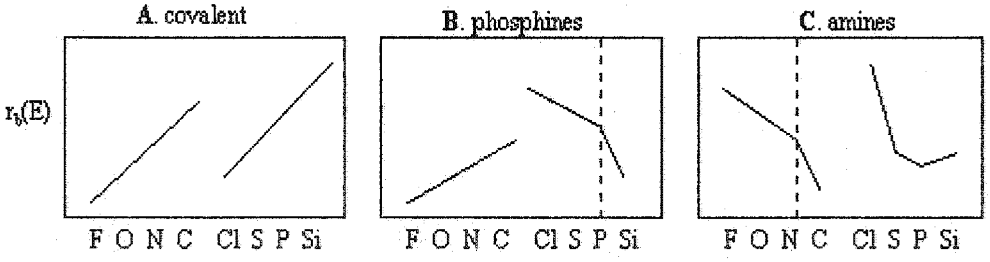

Figure 4-4: Sketches of the expected and observed trends in substituent bonding radii. **A)** The expected periodic trend in covalent radii, assuming non-polar bonds. **B)** The observed trend in $r_b(E)$ for the monosubstituted phosphines, PH_2EH_n. **C)** The observed trend in $r_b(E)$ for the monosubstituted amines, NH_2EH_n. The non-polar bonding cases are indicated with a dashed vertical line.

It seems that the effect of charge transfer has dominated the effective nuclear charge in the third row. This is consistent with the small differences between q(F) and q(Me) compared to the large differences between q(Cl) and q(SiH_3). The changes in r_b(M) are compensated by even larger opposing changes in r_b(P) to give the expected trend in bond length.

4.2.2. Comparison with amines

Switching our attention to the amines, the r_b(N) values given in Table 4-4 follow a very similar trend to the r_b(P) values, nitrogen radii being just a few tenths of an atomic unit smaller. The substituent bonding radii in the amines follow a different pattern than they do in the phosphines. In the amines both the second and third row atoms show a trend opposite to the expected (neutral atom) radius trend (see Figure 4-4C). Again this must be due to differences in atomic charge (*i.e.* bond polarity) across each row.

Note the 'elbows' at the purely non-polar P-P and N-N bonds. Increasing polarity in either direction effectively shortens r_b(E). While charge transfer shifts the position of the bond critical point it also has a secondary shortening effect on both bonding radii – due to increased electrostatic attraction. Thus polar bonds are shorter than the hypothetical non-polar bonds between the same two atoms.

While in the phosphines the unexpected r_b(M) trend is overcompensated by the r_b(P) trend, this is not the case for the amines. The increasing bonding radius of nitrogen matches the decreasing r_b(L) values so that the overall trend in N-L bond lengths is a very slight increase from fluoroamine to methylamine. For the third row substituents however, the shrinking radius from chlorine to silicon dominates the slow increase in $r_b(N)$ so that the bonds actually shorten slightly from the nearly non-polar N-Cl bond to the very polar N-P and N-Si bonds. Interestingly, tri-substitution shortens N-Cl and lengthens N-Si so that the expected ordering of these bond lengths returns.

4.2.3. MP2 correlation effects

For the electronegative substituents, MP2 correlation lengthens the bonding radius of P by 0.05 to 0.1 atomic units. The increase is only 0.01 au for PH_2PH_2, and in PH_2SiH_3 the bonding radius of P decreases by 0.1 au. This is consistent with a decrease in the degree of polarity with inclusion of correlation.

Again consistent with decreasing polarity, the bonding radius of Si increases, while those of S, Cl, C and H decrease, in effect shifting the interatomic surface closer to the electronegative atom. The nitrogen atom has no significant change, while the O and F atoms increase their bonding radii, so that in PH_2F, PH_2OH, PH_2NH_2 and PH_2PH_2, both atoms contribute to the increasing bond length, but phosphorus more so than F, O or N.

4.3. Bond Critical Point Properties

Having determined the position of the bond critical point, we now consider its properties, which are summarized in Tables 4-3 and 4-4, for phosphines and amines, respectively.

4.3.1. Density

The P-E bond critical point densities in the phosphines are compared to $\rho(\mathbf{r}_b)$ for the other phosphorus series in Figure A4-4. Typically phosphorus-hydrogen BCPs have $\rho(\mathbf{r}_b)$ values near 0.165-0.170 au, P-L BCPs have $\rho(\mathbf{r}_b)$ values ranging from 0.155 to 0.180 au, and P-M BCPs have $\rho(\mathbf{r}_b)$ values ranging from 0.09 to 0.13 au, see Table 4-3. The lower density between third row elements is consistent with the longer bonds. BCP densities in the amines are much higher than in the corresponding phosphines, again due to the much shorter bonds, Table 4-4. The phosphine BCP densities closely mirror the bond lengths. Just as increased substitution has a significant effect on the polar P-F, P-O and P-Cl bond lengths, these same bonds show variation in BCP density of up to 15% with increasing substitution.

The correlation between bond length and density is only strictly observed when comparing bonds between the same two atoms. Bonds to F have slightly lower $\rho(\mathbf{r}_b)$ values than the bonds to O. A similar trend is seen for the density at P-Cl *vs.* P-S bond critical points, but not for N-Cl and N-S BCPs, which have very similar densities, as do the N-O and N-N BCPs. It has been noted above that the amines have little variation in bond length, though the individual bonding radii change significantly, across a row. The increasing bond polarity from thio- to phosphino- to silyl-amine is accompanied by a large decrease in the BCP density.

Correlation at the MP2 level lowers the bond critical point density, again consistent with the lengthening of optimized bond distances. Another factor may be a shift of the BCP away from the high-density core of P and towards the valence region of the substituent.

The BCP density varies only slightly with rotation about the P-E bond. The eclipsed and staggered rotamers of PH_2OH, PH_2CH_3 and PH_2PH_2 vary in the third decimal place (1 to 2%). This is similar to the variation with degree of substitution for methyl phosphines, and much less than the substitution effect in the fluoro- and hydroxyl-phosphines. In most (but not all) cases, the variation within a set of P-E BCP densities is smaller than the difference between bonds to different substituents.

4.3.2. Laplacian

The value of the Laplacian at the P-E bond critical point is plotted, as a function of the substituent atom, in Figure A4-5. The values of $\nabla^2\rho(\mathbf{r}_b)$ at P-H BCPs range from -0.086 au to –0.184 au in PH_2SiH_3 and PH_2F, respectively. The values of $\nabla^2\rho(\mathbf{r}_b)$ at P-M BCPs range from -0.07 in H_2P-SiH_3 to –0.19 in $P(SH)_3$, see Table 4-3. The negative values are consistent with covalent bonding, but typical Laplacian values for second row – second row bonding are several times larger, as can be seen in the amine data, Table 4-4.

Phosphorus-carbon BCPs have $\nabla^2\rho(\mathbf{r}_b)$ about –0.2, while P-N, P-O and P-F BCPs in phosphines have positive Laplacian values ranging from +0.2 in $P(NH_3)_3$ to +0.9 in PF_3. Such positive Laplacian values are typically assumed to reflect a largely ionic bond, particularly when the BCP density is low. By considering the contour plot of the Laplacian overlaid with the bond path, shown in Figure 4-6, we see that the interatomic surface and the bond critical point lie just at the edge of the core region of the electronegative ligand. Thus the Laplacian is positive at this point even when a significant region of bonding concentration (negative Laplacian) exists, as in PH_2OH and PH_2NH_2. These bonds are better described as highly polar than as ionic.

MP2 correlation tends to make $\nabla^2\rho(\mathbf{r}_b)$ more negative (or less positive), consistent with a decrease in polarity, as measured by the shift in the BCP away from the phosphorus (or silicon) core. Exceptions to this are PCl_3, PH_2PH_2 and PH_2SH, which become less negative with inclusion of correlation. At the MP2 level, all the BCPs in PH_2MH_n have a Laplacian value of about –0.11 au, with PH_2SH being slightly lower.

When using the Laplacian at the bond critical point as an indicator of bond polarity it is very important to consider the row to which each atom belongs. Let us consider NH_2NH_2, NH_2Cl, and PH_2PH_2, each of which exhibits no significant charge transfer. The $\nabla^2\rho(\mathbf{r}_b)$ values are –0.51, –0.18 and –0.16 respectively. Clearly, when two second-row atoms are involved in a relatively non-polar covalent bond the Laplacian is much more negative than when one or more heavier atoms are involved. These differences can be traced to the differences in the valence shell concentration in the free atoms. There are also considerable differences across the rows. Therefore the polarity of a bond does not display a monotonic relationship with the Laplacian. Consider some weakly polar L-M bonds; in NH_2SH, PH_2CH_3 and $P(CH_3)_3$, the $\nabla^2\rho(r_b)$ values are -0.38, -0.25 and -0.21 respectively – all are more negative than in the essentially non-polar NH_2Cl. Similarly the N-C BCP Laplacian in NH_2CH_3 is –0.88, considerably more negative than in non-polar NH_2NH_2.

Thus if the property of interest is the bond polarity (charge-transfer across the interatomic surface), a more reliable measure is the bonding radius of either atom. Of course, these must be compared to the radii of the valence shell in the free atoms or to bonding radii in non-polar systems, as each element has a different size. In a polyatomic system the atomic charges are affected by more than one bond polarity and are more time consuming to calculate than bond critical point properties. Thus the simplest single indicator of bond polarity remains the Laplacian, but this must be interpreted with caution and does not help distinguish slightly polar from non-polar bonds.

4.3.3. Ellipticity

The ellipticities of P-H bond critical points are about 0.1 to 0.2, and other phosphine BCPs have ellipticities up to 0.17, see Table 4-3. The variability of this property is demonstrated by the difference between the 'gauche' ($\varepsilon = 0.02$) and '*trans*' ($\varepsilon = 0.08$) conformers of P_2H_4 which have quite similar values of $\rho(r_b)$ and $\nabla^2\rho(r_b)$. As a comparison, the ellipticity of the C-C bond in ethane is 0.0 (as required by the 3-fold symmetry), while that in ethene is 0.45. Bachrach (1989) finds ellipticities of 0.01 to 0.16 for single P-C bonds, 0.26 for phosphabenzene, and 0.50 to 0.60 for P-C double bonds in phosphaalkenes. The ellipticity of N-E bonds in the amines, Table 4-4, ranges up to 0.2, but is generally less than 0.1.

4.4. Integrated properties

Atomic and group charges and energies ($K = G = -2V = -E$) are given in Table 4-5 for phosphines and in Table 4-6 for amines. The quality of the numerical integration is indicated by the value of the integrated Laplacian, L, which should ideally equal zero for a precise integration. The uncertainty in atomic charges is generally of the same order of magnitude as L. For example, an initial integration of the P atom in H_2POH gave an L value of –0.015 au. Improving the integration to give L(P) = -0.007 increased the charge on P by 0.009e, and changed K(P) by less than 0.001 au. Note that the difference between K(P) and G(P) is still 0.007 au. Results of some initial integrations are shown in Table 4-5A, in brackets, to illustrate this. Improving the integrated value of L from 5×10^{-3} to 5×10^{-4} typically gave changes in q(P) of less than 0.01 electrons, and changes in K(P) of less than 0.005 au – the largest differences being for the gauche conformation of P_2H_4. In this particular case the true q(P) values can be estimated, from the more precise q(H) values $\{L(H) < 10^{-4}\}$, to be between the two integrated values.

Delocalization indices, δ(P,E) and δ(P,R), are shown in Table 4-3. For the amines, δ(N,E) and δ(N,R), are shown in Table 4-4. The typical improvements in the integrated values of L(P) change the value of the delocalization indices by about

0.001 atomic units. The delocalization index δ(P,O) in PH_2OH was lowered by 0.007 for the larger integration improvement mentioned above.

4.4.1. Population and charge transfer

The charges on phosphorus atoms, q(P), and substituent groups, q(R), are plotted in Figures A4-6 and A4-7, respectively. While the hydrogen atoms in NH_3 donate electron density to nitrogen, Table 4-6, hydrogen atoms bonded to phosphorus accept approximately 0.6 electrons each, Table 4-5, due to the differences in electronegativity. Looking at the trisubstituted systems, the second row phosphines $P(LH_n)_3$ have significant charge transfer, with q(P) ranging from +1.9 (CH_3) to +2.5 (F). The charge transfer in the third row phosphines, $P(MH_n)_3$, is much smaller, with q(P) becoming negative in $P(SiH_3)_3$. The substituent group charges, q(R), are nearly invariant to the degree of substitution, while the phosphorus charge, q(P), changes greatly upon replacement of a hydrogen atom with an electronegative (second row) or electropositive (third row) substituent. Only chloro- and methyl-phosphines see little change in q(P) with increased substitution.

The phosphorus charges are about 0.2e smaller than those calculated by Howard and Platts (1995). It is interesting to note that Howard *et al.* (1996) found that alkyl groups accepted more charge from phosphorus than hydrogen, but that the effect was less at a larger basis set {6-311G(d,p)}. This led them to conclude that the effect would vanish at the Hartree-Fock limit, and in fact the present calculations show that the trend is reversed with H accepting slightly more electron density than a methyl group using the 6-311++G(2d,2p) basis set. Including correlation decreases the degree of charge transfer. The QCISD charge on P in PH_3 (1.448) is even smaller than the MP2 charge.

4.4.2. Dipole moment

The atomic dipole of the central atom is discussed only for the trisubstituted systems, for which the dipole moment must be directed along the C_3 axis. The atomic dipole of the phosphorus in PR_3 is an order of magnitude larger than the atomic dipole of nitrogen in NR_3. In all but the bromo and silyl substituted systems the negative end of the dipole points towards the lone pair.

These findings can be rationalized by first noting that the phosphine lone pair is much more diffuse and has its maximum concentration further from the nucleus than the amine lone pair. Also, the nitrogen atoms have considerable density in the bonding region. The dipole reverses direction for the trisilylamine, trisilylphosphine and tribromophosphine because in these cases there are three large bonding charge concentrations *within the basin of the central atom*, on the side of the atom opposite to the lone pair. As the electronegativity of the substituent increases, the polarization of the phosphorus atom generally increases - away from the substituent. However, PF_3 has a less polarized phosphorus atom than $P(OH)_3$, perhaps because this phosphine has the most compact lone pair, see Table 4-9c.

These findings (except for PBr_3) are consistent with the observation that in *diatomic* systems atomic dipoles always oppose the charge transfer dipole (Gough *et al.*, 1996). This can be understood in terms of the valence electrons on a given atom being repelled by a neighbouring anion, or attracted by a neighbouring cation. For multivalent atoms, the valence electrons are more localized into bonding and non-bonding regions. In the case of phosphines and amines, the non-bonding concentration is more important than the bonding concentrations, except when the bonding concentrations within the basis are very large, as they are for silyl and bromo substituents.

4.4.3. Localization and delocalization

Plots of the delocalization index, δ(P,R), are shown in Figure A4-8. Values for δ(P,E) and δ(P,R) are shown in Table 4-3. Values for δ(N,E) and δ(N,R) are shown in Table 4-4. The localization of the central phosphorus atom, λ(P), in phosphines ranges from 11.66 (93%) to 15.52 (92%). The *percent* localization drops to 88% in the nearly neutral central atom of triphosphinophosphine, $P(PH_2)_3$. The delocalization index between directly bonded phosphorus and hydrogen atoms ranges from 0.79 to 0.96. The very ionic phosphines with fluoro and silyl substituents have low P-E delocalization indices, around 0.5 to 0.6, when the hydrogen atoms are not included. The less polar phosphines (with phosphino and thio substituents) have delocalization indices, δ(P,E), near one. See Table 4-3.

Including the hydrogen atoms of the substituents lowers the variation between substituents, and increases the delocalization values, δ(P,R) *vs.* δ(P,E), overall. There is, of course, no increase for F and Cl, but the $\delta(P,SiH_3)$ value is 0.84 in H_2PSiH_3, similar to δ(P,H) in PH_3 and to δ(P,Cl) in PCl_3. This summed index gives a better indication of the total delocalization of the central atom onto the substituent with less effect from E-H bond polarity. It is this delocalization index and the corresponding charge transfer q(R) that will be considered in the quadratic fitting procedure.

Rotation about the P-E bonds leads to small changes in the delocalization. It was noted at the beginning of this chapter that PH_2OH and PH_2SH prefer the eclipsed conformation even though this has a longer bond (and a lower BCP density). The delocalization indices, δ(P,E) and δ(P,R) are greater in this conformer. The relative energy ordering follows the delocalization index ordering for the monosubstituted phosphines. The one exception is methyl phosphine which has the same δ(P,Me) value, within integration errors, for both conformers. For silicon and the second row substituents, the higher energy conformer has a higher atom – atom delocalization index, δ(P,E). When the substituent H atoms are included, all the monosubstituted phosphines have the highest δ(P,R) for the lowest energy conformer. It seems that extent of delocalization may be an important factor in determining the relative stability of the conformers, along with steric effects.

While $\delta(P,LH_n)$ decreases with increasing substitution, $\delta(P,MH_n)$ increases with increasing substitution. For a given substituent, the delocalization indices δ(P,R), generally increase with the population of P. An exception is the silylphosphines, in which the charge transfer to P lowers the value of δ(P,Si) relative to δ(P,P) while increasing the charge on P. Fluorination of the substituent increases charge transfer across the P-E bond and thus lowers the delocalization index, δ(P,EY_n). See Tables 4-3D and 4-5D. Fluorination of phosphorus also increases charge transfer to E and decreases δ(P,E) but these effects are much smaller than seen for fluorination of the substituent. The charge on phosphorus is much higher in PF_3 than in PH_2F. They have very similar values of q(F), while the delocalization index decreases slightly upon increased fluorination.

The correlation between δ(P,R) and q(R), discussed in the next section, is much stronger than between δ(P,R) and q(P), confirming that the polarity of the P-E bond is the most important determining factor. Transfer of charge from phosphorus to other substituents has a much smaller effect, which may account for the small deviations from a simple parabola, in the graphs of δ(P,R) *vs.* q(R) below.

4.5. Variation of delocalization with charge transfer: bond order

Plots of the delocalization index *vs.* the charge on the substituent for the phosphine and amine series are shown in Figure 4-5. Each series is plotted separately and a quadratic function is fit to each curve.

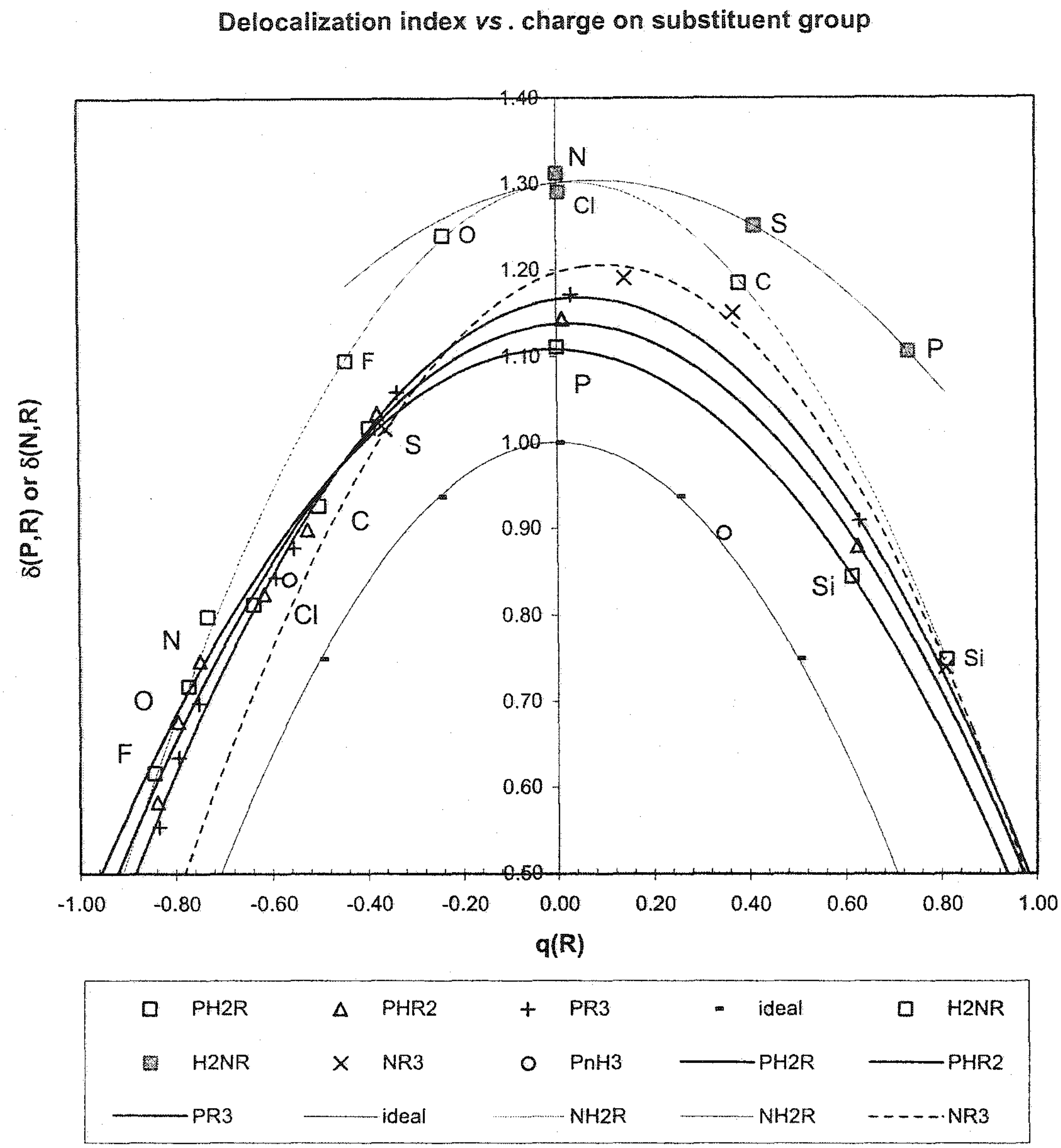

Figure 4-5: Plot of delocalization index *versus* charge transfer for PH_3, PH_2R, PHR_2, PR_3, NH_3, NH_2R and NR_3. The curves correspond to best-fit quadratic equations. Substituent atoms are labeled near the corresponding data points for the PH_2R and NH_2R series. The ideal curve, $\delta = 1-q^2$, is also shown, for comparison. The PH_3 data point lies near the phosphine curves, while the NH_3 data point lies near the ideal curve, open circles, PnH_3.

Increasing the degree of substitution shifts the maximum in the curve up by about 0.03 per substitution and slightly towards positive substituent charges. The $\delta(P,R)$ *vs.* $q(R)$ curves cross between methyl and thio substituents. The PH_3 data point lies slightly below these three curves. All the data points lie well above the ideal $\delta = 1-q^2$ curve. The best-fit curves have the following equations, where the subscript represents the degree of substitution:

$$\delta_1 = -0.6781q^2 - 0.0131q + 1.1084, R^2 = 0.9799;$$

$$\delta_2 = -0.7116q^2 + 0.0347q + 1.1381, R^2 = 0.9858;$$

$$\delta_3 = -0.7663q^2 + 0.0744q + 1.1666, R^2 = 0.9968.$$

The aminophosphine data point clearly lies above the PH_2R curve. The data for phosphorus and sulfur substituents are seen to be exceptional in many of the phosphorus series studied (Figure A4-8), reminiscent of the exceptional PH_3 and SH_2 data in the hydride curves, Figure 3-3. Removing the PH_2NH_2, PH_2PH_2 and PH_2SH data, gives a best-fit curve, $\delta_1' = -0.646q^2 + 0.0004q + 1.087$, $R^2 = 0.991$, slightly below the curve for the total data set.

The NR_3 data are slightly above the phosphine curves. The NH_2R curve is considerably higher than the phosphine curves. In the NH_2R series, the data for R = PH_2 and SH are clearly on a different curve than the CH_3 and SiH_3 data. Two curves are plotted, with the NH_2Cl and NH_2NH_2 data included in both. For the electron rich systems (R = NH_2, Cl, SH, PH_2), the best-fit curve is $\delta = -0.453q^2 + 0.066q + 1.301$, $R^2 = 0.990$. For the systems with less available lone pairs (R = F, OH, NH_2, CH_3, Cl, SiH_3) the best-fit curve is $\delta = -0.907q^2 + 0.052q + 1.300$, $R^2 = 0.999$. An additional 0.3 is apparently added to the delocalization index due to 'lone pair' involvement in the bonding in amines. The phosphines, on the other hand, only have an additional 0.1 contribution from 'lone pair' delocalization.

The overall trends are consistent with varying inequality in the sharing of one pair of electrons - as expected from the usual Lewis structures drawn for these molecules. The maxima in the $\delta(P,R)$ *vs.* $q(R)$ curves are slightly greater than one, indicating that the 'lone pairs' are somewhat delocalized. A similar effect occurs in the amines, where several of the $\delta(N,R)$ values are greater than one, as a result of less polar bonding and more 'lone pair' delocalization. It is open for interpretation whether this extra delocalization should be counted towards the total bond order. Correlation is expected to lower the values of these indices. However, the calculated delocalization index at higher levels of theory (such as CI) is more difficult to interpret in the Lewis context of localized bonding electron pairs.

4.6. Topology of the Laplacian: Bonding and Electron Localization

The position and some properties of the P-E bonding charge concentrations are given Table 4-7. The corresponding amine data are in Table 4-8. The position and some properties of the non-bonded charge concentration on phosphorus are given Table 4-9. The corresponding amine data are in Table 4-10.

As described above, Figure 4-6 shows contour plots of the Laplacian of the density, $\nabla^2\rho(\mathbf{r})$, in a plane of the phosphines, PH_2R. Corresponding amine plots are shown in Figure 4-7. These plots are overlaid with the corresponding bond paths and the intersections of the interatomic surfaces with the plane. The Laplacian contour maps show two contributions to the variations in $\nabla^2\rho(r_b)$: the movement of the bond critical point relative to phosphorus, and the changing size and shape of the bonding charge concentration. The bonding region of concentration (negative $\nabla^2\rho$, solid lines in the contour maps) is continuous with the non-bonding ('lone pair') region for the third row and methyl substituents, but shrinks as the electronegativity increases, disappearing for fluorophosphine, which has an essentially spherical valence charge concentration about fluorine.

4.6.1. Bonding charge concentrations

The topology of the Laplacian may be analyzed in terms of critical points, as is the topology of the density. A bonding maximum may be found in the valence shell of one atom or the other, but not necessarily in both. For each of the P-P bonding regions, a maximum is found 1.47 or 1.48 au from each phosphorus nucleus, with $\nabla^2\rho = -0.25$. The Laplacian at the phosphorus bonding charge concentration (CC) is more negative in $P(NH_2)_3$ (-0.32) and $P(CH_3)_3$ (-0.34), but less negative for the remaining phosphines. In PH_2F, and even more so in PF_3, the P-F bonding charge concentration in the phosphorus valence shell is closer to the phosphorus nucleus than in the other phosphines, and has a positive Laplacian value. It may be misleading to say that these concentrations are in the valence shell of phosphorus, since in fact they lie in the atomic basin of the neighbouring second row atom, for R = F, OH, NH_2 and CH_3. Similarly, the P-Si bonding charge concentration in PH_2SiH_3, which is nominally in the valence shell of silicon, is actually in the atomic basin of phosphorus. See Figure 4-6 and the bonding radii in Table 4-3.

In all the mono-substituted amines except NH_2Cl, a bonding charge concentration is found in the valence shell of nitrogen, and these are all in the atomic basin of nitrogen. The trends are more clear-cut in this series. The bonding charge concentration generally moves further from the N nucleus as the substituent becomes more electronegative. The distance to N ranges from 0.82 to 0.91 au in the second row amines and from 0.80 to 0.84 au in the third row amines. The Laplacian of the bonding charge concentration becomes less negative as it moves further from the N nucleus, and the density decreases. The interatomic surface moves away from nitrogen much more quickly than the bonding charge concentration, so that the nitrogen atomic basin encompasses part of the valence shell of the least electronegative substituents, SH, PH_2 and SiH_3.

4.6.2. Non-bonding charge concentrations

A search of the valence shell of each substituent atom shows that the number of non-bonding charge concentrations does not always agree with the expected number of lone pairs in the Lewis model, as explained in Chapter 3. For example, the terminal F atom in PH_2F has only two non-bonding charge concentrations, both in the plane of symmetry, rather than the expected three.

Gillespie and Popelier, (2001) have pointed out that for terminal atoms there is no constraint for the non-bonding electrons to be localized and thus they form a torus of charge concentration rather than three distinct lone pairs. The properties at the maxima are similar to those at the intervening saddle points, suggesting a slight distortion in the torus. The maxima are 0.577 au from F and have $\nabla^2\rho = -9.01$, $\rho = 1.46$. The in- and out-of-plane saddle points are 0.580 au from F and have $\nabla^2\rho = -8.56$, $\rho = 1.43$. In PHF_2, where the topology around F is not constrained by molecular symmetry, the two non-bonding maxima have very similar properties to those in PH_2F. A pattern of three maxima is seen around Br in PBr_3. The oxygen in PH_2OH and the sulfur atom in PH_2SH exhibit the expected two non-bonding maxima, in and out of the plane of symmetry, due to the localizing effects of the two bonding Lewis pairs on O and S, respectively.

Looking at the non-bonding maxima on the central atom, the phosphorus has the expected one charge concentration in each phosphine, Table 4-9. These maxima are much closer to the nucleus than are the bonding maxima. The more electronegative substituents draw the maximum closer the P nucleus. The value of the Laplacian becomes more negative (more concentrated charge) and the 'lone pair' becomes less diffuse (as measured by the radial curvature in $\nabla^2\rho$, μ_3).

Comparing the non-bonding maxima of the amines (Table 4-10) to those of the phosphines, we see very different properties. The amine maxima are much closer to the nucleus, being in the second shell rather than the third. The density and Laplacian values are thus bigger by a factor of about five, while the radial curvatures are bigger by a factor of ten or more. The monosubstituted amines each show a single non-bonding maximum, as expected from the Lewis structure.

The two trisubstituted third row amines studied, NCl_3 and $N(SiH_3)_3$, exhibit two non-bonding maxima, lying on the C_3 axis, on opposite sides of the nitrogen atom. This is not particularly surprising in $N(SiH_3)_3$ which is nearly planar (the data shown in Table 4-10 are for the C_{3v} geometry, not the C_{3h} geometry). The planarity arises from a lack of localization of the valence electrons on nitrogen. The electronegativity difference is very large between N and Si, so that the charge on SiH_3 is +0.80, see Table 4-6. The valence electrons on the nearly spherical nitrogen are only weakly polarized towards the substituents. Thus the non-bonding electron pair is also non-localized, so that a planar rather than trigonal pyramidal arrangement is preferred, with two very similar non-bonding maxima.

In NCl_3, the bond angles are almost perfectly tetrahedral, and a 'lone pair' concentration appears in the expected position, with properties comparable to those the other amines. Yet there is a second concentration of charge lying between the three chlorine atoms, with similar properties to the maxima in $N(SiH_3)_3$. The atomic charges in NH_2Cl and NCl_3 are very small, indicating that these N-Cl bonds are not very polar, and that the chlorine should be sufficiently electronegative to localize the bonding electrons. The maximum lies out of the plane of the three chlorine atoms, towards the nitrogen atom. It may be that the concentration is simply an artefact of the four relatively electronegative atoms in NCl_3 contributing density from their valence shells to the same region of space.

The unlocalized non-bonding electron pair on $N(SiH_3)_3$ is instructive for later chapters, where we will again see examples of poorly localized electron pairs, when the atoms are insufficiently electronegative to pull the bonding electrons completely into the bonding region.

4.7. Conclusion

Substituted phosphines have a range of bond polarities, depending on the substituent. The electronegative elements F, O and N give strongly polar phosphines, with charge transfer of greater than 0.7 electrons to the substituent group, XH_n. The P-F bond might almost be considered ionic, given the nearly spherical symmetry about F. However, the delocalization index is still considerably higher than in the ionic LiF. Methyl, chloro and thio substituents are less polar, with a charge transfer of less than 0.7 electrons. There is equal sharing of electrons with phosphino substituents and significant (0.6e) electron transfer *from* the silyl group *to* phosphorus. The variation of the delocalization index with charge transfer is consistent with the unequal sharing of one pair of electrons, plus a small additional delocalization of the lone pairs both on the central pnictogen atom and on the substituent atoms, to the neighbouring atoms.

4.8. Laplacian contours

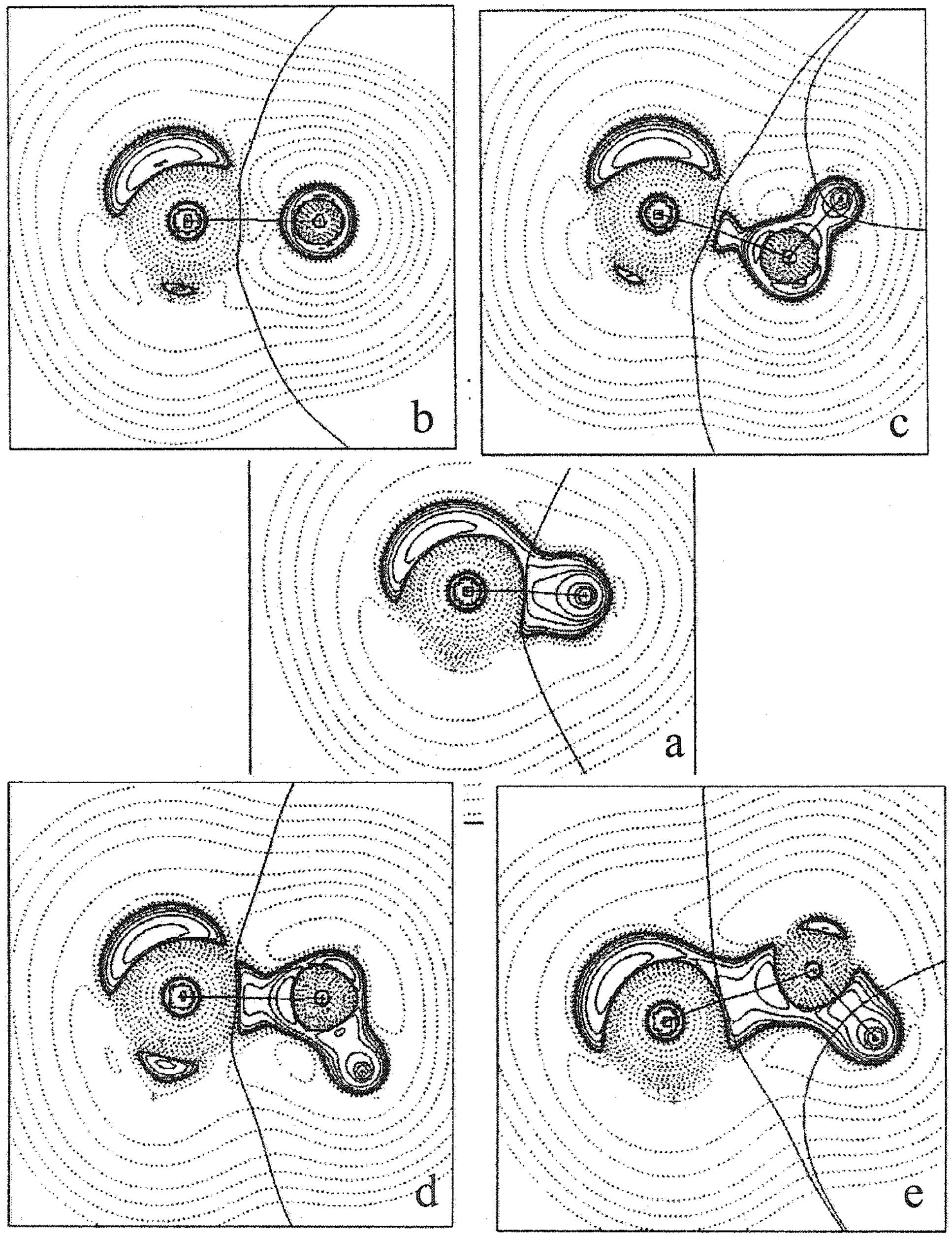

Figure 4-6: Continued on the next page.

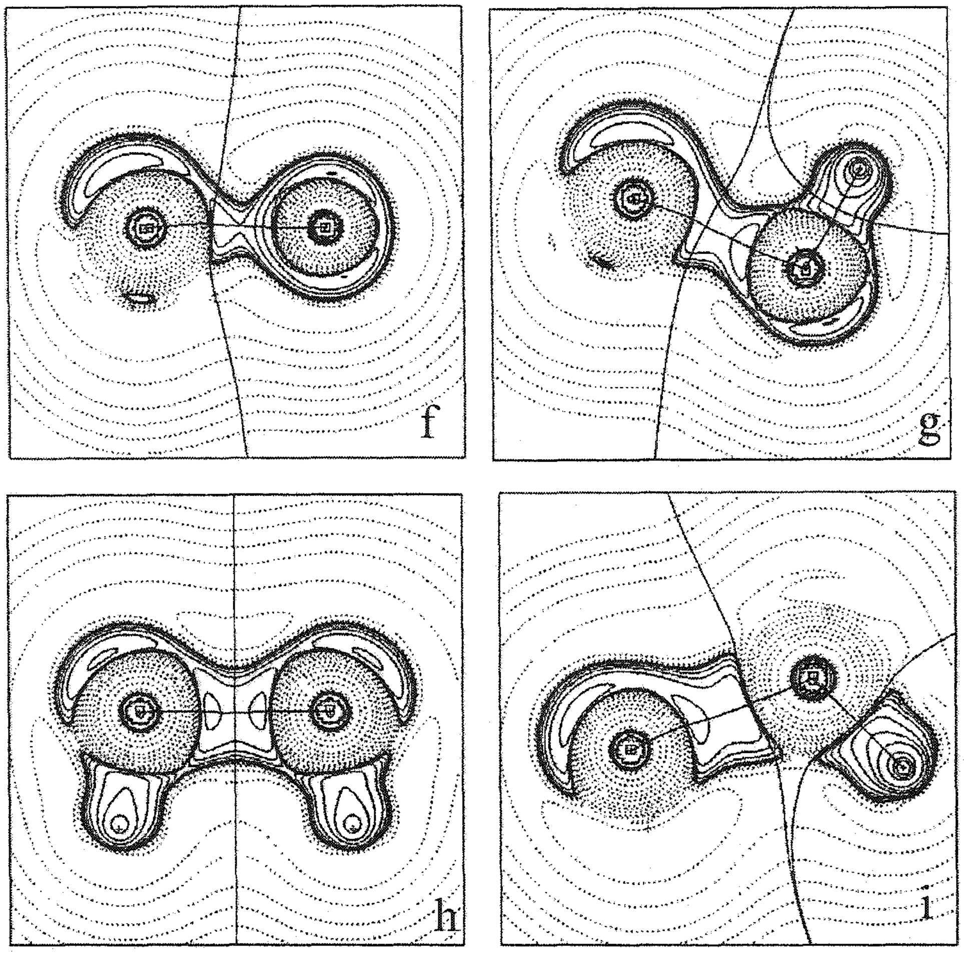

Figure 4-6 Contour map of $\nabla^2\rho(r)$ in a plane of PH_3 and PH_2R. a) PH_3, b) PH_2F, c) PH_2OH, d) PH_2NH_2, e) PH_2CH_3, f) PH_2Cl, g) PH_2SH, h) PH_2PH_2, i) PH_2SiH_3. The displayed plane is the symmetry plane for all phosphines except PH_2PH_2 and NH_2PH_2. Solid contours indicate negative values (concentration) and dashed lines indicate positive values (depletion). The outermost contour is +0.002 au. Isovalue contours increase and decrease from the $\nabla^2\rho(r) = 0$ contour in the order $\pm2\times10^n$, $\pm4\times10^n$, $\pm8\times10^n$, beginning with $n = -3$ and increasing in steps of unity. Each map is overlaid with the bond paths and with the intersection of the interatomic surfaces with the displayed plane.

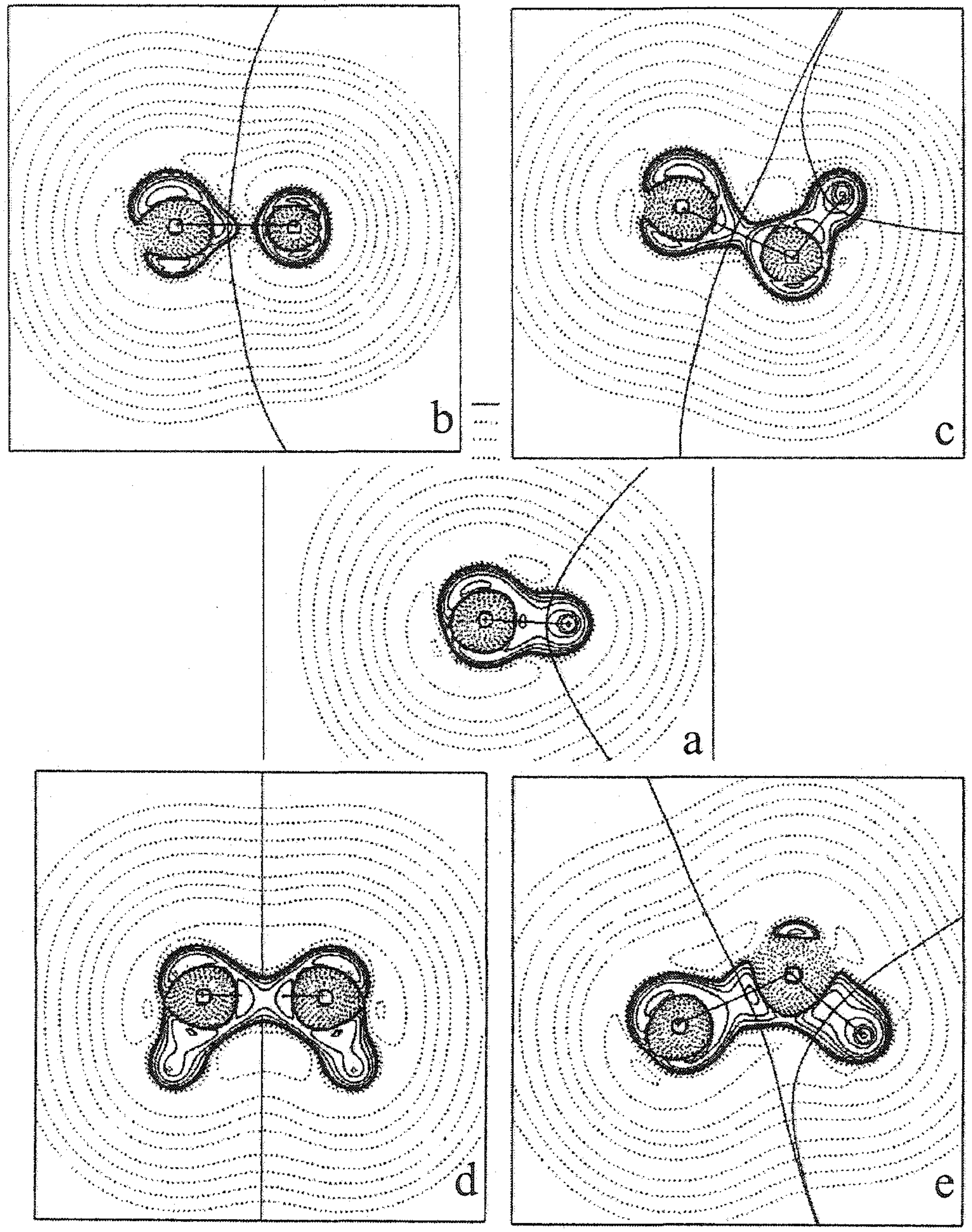

Figure 4-7: Continued on the next page.

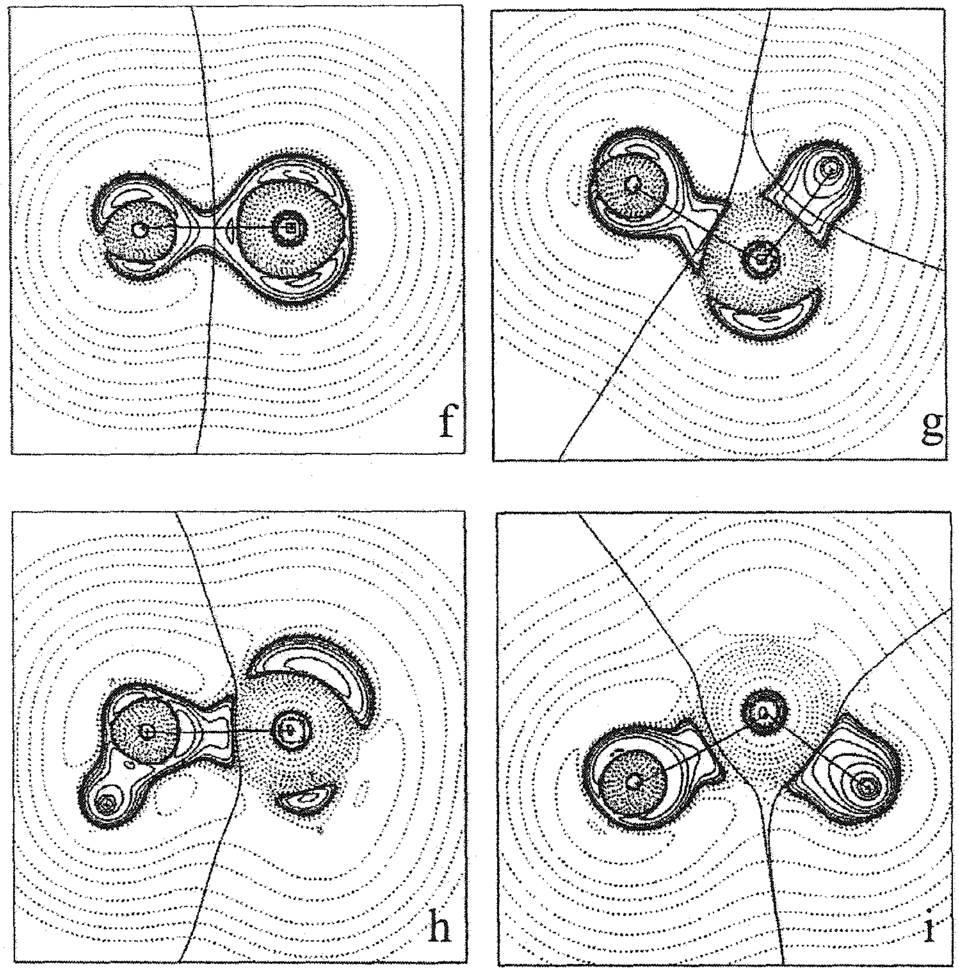

Figure 4-7: Contour map of $\nabla^2\rho(\mathbf{r})$ in a plane of NH_3 and NH_2R. **a)** NH_3, **b)** NH_2F, **c)** NH_2OH, **d)** NH_2NH_2, **e)** NH_2CH_3, **f)** NH_2Cl, **g)** NH_2SH, **h)** NH_2PH_2, **i)** NH_2SiH_3. The displayed plane is the symmetry plane for all amines except NH_2NH_2 and NH_2PH_2. Solid contours indicate negative values (concentration) and dashed lines indicate positive values (depletion). The outermost contour is +0.002 au. Isovalue contours increase and decrease from the $\nabla^2\rho(\mathbf{r}) = 0$ contour in the order $\pm 2\times10^n$, $\pm 4\times10^n$, $\pm 8\times10^n$, beginning with $n = -3$ and increasing in steps of unity. Each map is overlaid with the bond paths and with the intersection of the interatomic surfaces with the displayed plane.

4.9. Data Tables

Table 4-1(a-d). Optimized geometries of phosphines at HF/6-311++G(2d,2p) and at MP2 (in italics). Experimental values are given where available.

Table 4-1a: Monosubstituted phosphines, PH_2EH_n.

Phosphine	**r(P-E)**	**r(P-H)**	**∠ HPH**	**∠ HPE**	**Dihedral wrt ln pr**	**-Energy /au**	**ΔE / kJ/mol**
PH_2F	159.04	140.42	93.8	98.0		441.39091	
	162.77	*140.89*	*92.02*	*97.55*		*441.91838*	
PH_2OH	163.72	140.29	94.17	99.07	0.0	417.38418	0
eclipsed	*167.51*	*140.70*	*92.65*	*98.12*	*0.0*	*417.90559*	
PH_2OH *staggered*	163.09	140.88	93.55	101.17	180.0	417.38408	+0.26
PH_2NH_2	170.01	140.94 / .20	94.33	103.47,99.55	28, 164	397.54171	0
gauche	*171.88*	*141.33/0.51*	*93.04*	*103.29,98.39*	*30, 162*	*398.04008*	
PH_2NH_2 *trans*	174.10	140.46	106.52	110.50	±22.0	397.53328	22.1
PH_2NH_2 *cis*	173.83	140.92	93.03	100.27	±118.1	397.53042	29.6
PH_2CH_3	185.60	140.47	94.99	98.94	±58.6,180	381.53164	0
staggered	*185.88*	*140.75*	*93.35*	*97.42*	*±58.4,180*	*381.99787*	
Exp't[a]	186.3	141.4	93.4	97.5			
Exp't[b]	185.8 ± .3	142.3 ± .7		(96.5 ass'd)			
PH_2CH_3 *eclipsed*	186.99	140.34	94.45	99.41	±119.7, 0.	381.52842	+8.5
PH_2Cl	208.53	140.03	94.28	97.05		801.43433	
	209.40	*140.52*	*92.37*	*96.38*		*801.92595*	
PH_2SH	214.02	140.07	94.94	98.04	0.0	740.04060	0
eclipsed	*214.86*	*140.48*	*93.23*	*97.00*	*0.0*	*740.60053*	
PH_2SH *staggered*	213.74	140.10	95.54	99.74	180	740.03937	+3.2
PH_2PH_2	222.71	140.25	95.71	100.69,96.19	54.5,151.5	683.81489	0
gauche	*223.48*	*140.57/.56*	*93.97*	*99.47,94.37*	*55.4,150.2*	*684.36404*	
Exp't[c]	221.91±.04	141.7/.4±.2	92.0±.8	99.1 ± .1,			
Exp't[d]	221.8 ± .4	145.1 ± .5	91.3±.1.4	95.2 ± .6			
PH_2PH_2 *trans*	224.27	140.52	94.40	95.41	±47.5	683.81358	+3.4
PH_2PH_2 *cis*	226.73	140.28	94.71	97.98	±132.0	683.80727	+20.0
PH_2SiH_3	227.79	140.57	95.62	96.23	±59.1,180	632.59584	0
staggered	*226.92*	*140.87*	*93.47*	*93.27*	*±59.0,180*	*633.12489*	
Exp't[e]	224.9 ± 0.3	143.8 ± 2.0	91 ± 3	91 ± 3			
PH_2SiH_3 *eclipsed*	229.24	140.43	95.35	96.32	0, ±131.9	632.59358	+5.9

- Bond lengths are in picometers and angles are in degrees. Absolute energies are given in hartrees and relative energies of conformers are given in kJ/mol.

Table 4-1b: Disubstituted phosphines, $PH(EH_n)_2$

Phosphine	**r(P-E)**	**r(P-H)**	**∠ EPE**	**∠ HPE**	**Dihedral wrt 'ln pr'**	**-Energy /au**
PHF_2 Exp't [a]	156.64 158.2 ± .2	140.42 141.2 ± .6	98.37 99.0 ± .2	96.18 96.3 ± .5		540.31882
$PH(OH)_{2\,up}$	162.06	139.47	103.40	95.23	23	492.30498
$PH(OH)_{2\,dn}$	161.87	141.28	104.60	97.99	167	492.30328
$PH(NH_2)_2$	169.58	139.70	110.42	96.19	37,176	452.61275
$PH(CH_3)_2$ Exp't [b] Exp't [c]	185.09 184.8 ± .3 185.3 ± .3	140.52 141.7 ± .5 144.5 ± 2.	101.26 99.72 ± .3 99.2 ± .6	98.13 96.95 ± .3 (96.5 ass'd)	58, 60, 179	420.58297
$PHCl_2$	206.83	139.55	102.33	95.43		1260.38876
$PH(SH)_{2\,up}$	213.62	139.54	106.47	94.52	21	1137.60038
$PH(PH_2)_2$	222.19	140.07	109.45	96.69	56, 153	1025.14810
$PH(SiH_3)_2$	227.29	140.71	100.59	96.81	58, 60, 179	922.71156

- Bond lengths are in picometers and angles are in degrees.
- Absolute energies are given in hartrees.

Table 4-1c: PH_3 and trisubstituted phosphines, $P(EH_n)_3$

Phosphine	**r(P-E)**	**∠ EPE**	**Dihedral wrt lone pair**	**-Energy /au**
PH_3 Exp't [a]	140.43 *140.71* 141.15 ± .05	95.44 *93.52* 93.36 ± .08		342.47746 *342.76703*
PF_3 Exp't [b]	154.56 *158.25* 156.1 ± .1	97.29 *97.53* 97.7 ± .2		639.26520 *640.28613*
$P(OH)_3$ *up* Deriv.Exp't[c]	160.49 (162.0 ± .2)	93.37 (100.5 ± .6)	34.75	567.23488
$P(NH_2)_3$ *gch* Deriv Exp't[d]	170.00 (170.0 ± .5)	102.13 (96.5 ± 1.)	43.7, 172.2	507.68293
$P(CH_3)_3$ *stag* Exp't [e] Exp't [f]	184.71 184.3 ± .3 184.65 ± .3	100.41 98.9 ± .2 98.6 ± 0.3	±58.9, 180.0	459.63590
PCl_3 Exp't [g] Exp't [h]	205.78 *207.15* 203.9 ± 1.4 204.3 ± .3	100.44 *100.26* 100.27 ± .09 100.1 ± .3		1719.34260 *1720.26144*
$P(SH)_3$ *up* Deriv Exp't[i]	213.91 (211.5 ± .4)	99.24 (94.0 ± .6)	36.1	1535.15595
$P(PH_2)_3$ *gch*	222.20	102.60	62.5, 159.6	1366.48179
$P(SiH_3)_3$ *stag* Exp't [j]	226.88 224.8 ± .3	100.90 96.45 ± .50	±59.3, 180.0	1212.82894
PBr_3	223.88	101.23		

- Bond lengths are in picometers and angles are in degrees.
- Absolute energies are given in hartrees.

Table 4-1d: Fluorinated phosphines.

Phosphine	**r(P-E)**	**r(P-Y)**	**∠YPY**	**∠YPE**	**Dihedral wrt ln pr**	**-Energy /au**
PH_2NH_2 *trans*	174.10	140.46	106.52	110.50	±22.0	397.53328
PF_2NH_2 *trans*	168.03	156.17	99.19	96.84	±63.6	595.40075
PH_2NF_2 *trans*	179.62	140.08	94.85	93.09	±53.9	595.14881
PH_2CH_3 *stag*	185.60	140.47	94.99	98.94	±58.6, 180	381.53164
PF_2CH_3 *stag*	181.46	157.24	97.45	98.14	±59.2, 180	579.38299
PH_2CF_3 *stag*	187.81	140.11	95.81	94.81	±59.3, 180	678.19921

- Y represents H or F, whichever is bonded to P.
- Bond lengths are in picometers and angles are in degrees.
- Absolute energies are given in hartrees.

Table 4-1a references

a) Kojima, Breig and C.C. Lin (1961). Microwave, ‘plausible’ structure, no uncertainties.
b) Bartell (1960). (electron diffraction) HPC angle assumed to be 96.5°
c) Durig, Carreira and Odom (1974). Microwave, external HPPH dihedral = 81°.
d) Beagley *et al.* (1972). Electron diffraction.
e) Glidewell, *et al.* (1972). Electron diffraction, axial symmetry of SiH_3 group assumed, all phosphorus angles assumed equal.

Table 4-1b references

a) Kuczkowski (1968). Microwave.
b) Nelson, R. (1963). Microwave.
c) Bartell, L.S. (1960). Electron diffraction, HPC angle assumed to be 96.5°.

Table 4-1c references

a) Chu, F.Y.; Oka, T. (1974). Microwave, $r_a = 142.73 \pm .01$ $\angle_{av} = 93.28 \pm .02$.
b) Kawashima, Y. and P.A. Cox (1977). Microwave.
c) *Electron diffraction for* ***$P(OMe)_3$*** Zaripov, Naumov and Tuzova (1974). Dihedral = 76.7°.
d) *Electron diffraction for* ***$P(NMe_2)_3$*** Vilkov and Khaikin (1969).
e) Bryan and Kuczkowski (1971). Microwave.
f) Bartell and Brockway (1960). Electron diffraction.
g) Hedberg and Iwasaki (1962). Electron diffraction.
h) Kisliuch and Townes (1950). Microwave.
i) *Electron diffraction for* ***$P(SMe)_3$*** Tuzova *et al.* (1981). Dihedral = +5.6, -5.6, 180°. Compare: *X-ray for* ***$(PhS)_3P$*** Burford, Royan and White (1990). 212.2 ± 0.1pm, 97.45± 0.05°, C_3.
j) Beagley, Robiette and Sheldrick (1968). Electron diffraction.

Table 4-2(a-c): Optimized geometries of amines at HF/6-311++G(2d,2p). Experimental values are given where available.

Table 4-2a: Monosubstituted amines, NH_2EH_n

Amine	**r(N-X)**	**r(N-H)**	**∠HNH**	**∠HNE**	**-E (SCF)/au**
NH_2F	138.05	100.04	106.86	103.0	155.02038
NH_2OH *ecl*	139.92	99.82	107.06	105.41	131.04002
Exp't[a]	145.3 ± .2	101.6 ± .8	107.1 ± .5	103.25 ± .5	
NH_2OH *stag*	139.29	99.87	108.75	108.37	131.03316
NH_2NH_2	141.26	99.78, 99.51	108.63	112.36, 108.45	111.22331
Exp't[b]	144.9 ± .2	102.1 ± .3	(106.6 ass'd)	112 ± 2, 106 ± 2	
NH_2CH_3	145.32	99.71	107.19	111.07	95.25075
Exp't[c]	147.14	100.96	107.13	110.27	
NH_2Cl	173.20	99.86	107.31	105.19	515.09876
Exp't[d]	174.80 ± .01	101.7 ± .5	107 ± 2	103.68 ± .37	
NH_2SH *ecl*	170.59	99.48	110.06	110.97	453.73527
Exp't[e]	170.5 ± .3	100.8 ± 1.3	111.6 ± 2.1	112.7 ± .9	
NH_2SH *stag*	169.44	99.43	111.07	113.12	453.73514
NH_2PH_2	170.01	99.32, 99.27	111.33	119.50, 114.56	397.54171
NH_2SiH_3	171.49	99.33	110.56	120.19	346.34365

- Bond lengths are in picometers and angles are in degrees.

a) Tsuneka (1972). Microwave.
b) Kohata,. Fukuyama and Kuchitsu (1982). Electron diffraction and microwave, HNH angle is assumed, NH bond length is an average.
c) Takagi and Kojima (1971). Microwave, no uncertainties reported.
d) Cazzoli, Lister and Favero (1972). Microwave.
e) Lovas, Suenram and Stevens (1983). Microwave.

Table 4-2c: NH_3 and trisubstituted amines, $N(EH_n)_3$.

Amine	**r(N-E)**	**∠ENE**	**-Energy / au**
NH_3	99.84	107.89	56.21864
Exp't[a]	101.56	107.28	
NF_3	132.07	102.85	352.66243
Exp't[b]	136.5 ± .2	102.37 ± .03	
$N(CH_3)_3$	144.42	111.72	173.32725
Exp't[c]	145.1 ± .3	110.9 ± .6	
NCl_3	172.55	109.37	1432.84216
Exp't[d]	175.9 ± .2	107.1 ± .5	
$N(SiH_3)_3$	173.87	119.82	926.59524
Exp't[e]	173.4 ± .2	119.7 ± .1	
$N(SiH_3)_3$	173.34	120.0	926.59807

- Bond lengths are in picometers and angles are in degrees.

a) Helminger, P., F.C. DeLucia and W. Gordy (1971). Microwave. no uncertainties reported.
b) Otake, M., C. Matsumura and Y. Morino (1968). Microwave.
c) Wollrab, J.E. and V. W. Laurie (1969). Microwave.
d) Bürgi,, H.B., D. Stedman and L.S. Bartell (1971). Electron diffraction.
e) Beagley, B. and A.R. Conrad (1970). Electron diffraction.

Table 4-3(a-d): Properties of P-X bond critical points and delocalization indices in phosphines, MP2 values in italics. All values are given in atomic units.

Table 4-3a: Monosubstituted phosphines.

Phosphine	$\rho(r_b)$	$\nabla^2\rho(r_b)$	$\varepsilon(r_b)$	**r(P-r$_b$)**	**r(E-r$_b$)**	**δ(P,E)**	**δ(P,R)**
PH_2F	0.156	+0.780	0.060	1.21	1.79	0.617	0.617
	0.146	*+0.530*	*0.067*	*1.25*	*1.83*		
PH_2OH *ecl*	0.165	+0.552	0.016	1.22	1.88	0.708	0.718
MP2	*0.153*	*+0.341*	*0.015*	*1.26*	*1.91*		
PH_2OH *stag*	0.166	+0.570	0.012	1.22	1.87	0.686	0.703
PH_2NH_2 *gau*	0.166	+0.252	0.010	1.25	1.97	0.755	0.799
MP2	*0.158*	*+0.139*	*0.009*	*1.28*	*1.97*		
PH_2NH_2 *trans*	0.159	+0.140	0.155	1.27	2.02	0.757	0.789
PH_2NH_2 *cis*	0.159	+0.143	0.163	1.27	2.02	0.725	0.764
PH_2CH_3 *stag*	0.155	-0.250	0.114	1.39	2.12	0.826	0.927
MP2	*0.148*	*-0.261*	*0.080*	*1.49*	*2.03*		
PH_2CH_3 *ecl*	0.152	-0.267	0.121	1.41	2.13	0.829	0.928
PH_2Cl	0.115	-0.091	0.137	1.46	2.49	0.816	0.816
MP2	*0.113*	*-0.113*	*0.072*	*1.58*	*2.38*		
PH_2SH *ecl*	0.122	-0.188	0.001	1.68	2.36	0.976	1.018
MP2	*0.115*	*-0.119*	*0.043*	*1.80*	*2.26*		
PH_2SH *stag*	0.123	-0.190	0.021	1.67	2.37	0.958	1.005
PH_2PH_2 *gau*	0.117	-0.157	0.019	2.10	2.10	0.947	1.111
MP2	*0.107*	*-0.110*	*0.016*	*2.11*	*2.11*		
PH_2PH_2 *trans*	0.114	-0.152	0.083	2.12	2.12	0.943	1.103
PH_2PH_2 *cis*	0.111	-0.145	0.112	2.14	2.14	0.917	1.069
PH_2SiH_3 *stag*	0.096	-0.066	0.019	2.80	1.50	0.518	0.845
MP2	*0.093*	*-0.109*	*0.019*	*2.71*	*1.58*		
PH_2SiH_3 *ecl*	0.095	-0.072	0.032	2.82	1.51	0.521	0.838

- All properties, including distances from nuclei to bond critical points, r(A-r$_b$), are given in atomic units.

Table 4-3b: Disubstituted phosphines.

Phosphine	$\rho(r_b)$	$\nabla^2\rho(r_b)$	$\varepsilon(r_b)$	**r(P-r$_b$)**	**r(E-r$_b$)**	**δ(P,E)**	**δ(P,R)**
PHF_2	0.167	+0.862	0.087	1.19	1.77	0.583	0.583
$PH(OH)_2$ *up*	0.172	+0.597	0.040	1.21	1.86	0.668	0.677
$PH(OH)_2$ *dn*	0.171	+0.601	0.038	1.21	1.85	0.635	0.653
$PH(NH_2)_2$	0.168	+0.267	0.032	1.24	1.96	0.705	0.748
$PH(CH_3)_2$	0.156	-0.230	0.127	1.37	2.13	0.803	0.900
$PHCl_2$	0.121	-0.123	0.168	1.46	2.45	0.825	0.825
$PH(SH)_2$	0.124	-0.190	0.039	1.69	2.34	0.994	1.035
$PH(PH_2)_2$	0.117	-0.156	0.046	2.11	2.09	0.976	1.144
$PH(SiH_3)_2$	0.095	-0.058	0.036	2.79	1.51	0.535	0.880

- All properties, including distances from nuclei to bond critical points, r(A-r$_b$), are given in atomic units.

Table 4-3c: PH_3 and trisubstituted phosphines.

Phosphine	$\rho(r_b)$	$\nabla^2\rho(r_b)$	$\varepsilon(r_b)$	$r(P-r_b)$	$r(E-r_b)$	$\delta(P,E)$	$\delta(P,R)$
PH_3	0.165	-0.107	0.116	1.30	1.35	0.843	0.843
	0.162	*-0.170*	*0.094*	*1.34*	*1.32*		
PF_3	0.179	+0.930	0.049	1.18	1.74	0.554	0.554
	.167	*+0.639*	*0.054*	*1.22*	*1.77*		
$P(OH)_3$	0.180	+0.613	0.063	1.20	1.84	0.624	0.635
$P(NH_2)_3$	0.170	+0.224	0.065	1.24	1.97	0.657	0.698
$P(CH_3)_3$	0.157	-0.214	0.134	1.36	2.13	0.785	0.878
PCl_3	0.127	-0.164	0.118	1.47	2.42	0.844	0.844
	0.122	*-0.136*	*0.071*	*1.61*	*2.30*		
$P(SH)_3$	0.127	-0.190	0.119	1.74	2.30	1.018	1.059
$P(PH_2)_3$	0.117	-0.155	0.046	2.12	2.08	1.000	1.172
$P(SiH_3)_3$	0.094	-0.051	0.022	2.78	1.51	0.546	0.909
PBr_3	0.110	-0.114	0.065	1.81	2.42	1.035	1.035

- Distances from nuclei to bond critical points, $r(A-r_b)$, are given in atomic units.

Table 4-3d: Fluorinated phosphines

Phosphine	$\rho(r_b)$	$\nabla^2\rho(r_b)$	$\varepsilon(r_b)$	$r(P-r_b)$	$r(E-r_b)$	$\delta(P,E)$	$\delta(P,EY_n)$
PH_2NH_2 *trans*	0.159	+0.140	0.155	1.27	2.02	0.757	0.789
PH_2NF_2 *trans*	0.148	+0.118	0.160	1.29	2.11	0.631	0.747
PF_2NH_2 *trans*	0.184	+0.177	0.178	1.23	1.94	0.672	0.699
PH_2CH_3 *stag*	0.155	-0.250	0.114	1.39	2.12	0.827	0.927
PH_2CF_3 *stag*	0.153	-0.121	0.154	1.34	2.21	0.679	0.846
PF_2CH_3 *stag*	0.178	-0.368	0.076	1.36	2.07	0.730	0.816

- Distances from nuclei to bond critical points, $r(A-r_b)$, are given in atomic units.

Table 4-4(a, c): Properties of N-X BCPs and delocalization indices in amines.

Table 4-4a: Monosubstituted amines

Amine	$\rho(r_b)$	$\nabla^2\rho(r_b)$	$\varepsilon(r_b)$	$r(N-r_b)$	$r(E-r_b)$	$\delta(N,E)$	$\delta(N,R)$
NH_2F	0.298	-0.380	0.063	1.10	1.51	1.095	1.095
NH_2OH *ecl*	0.318	-0.467	0.041	1.21	1.43	1.219	1.240
NH_2NH_2	0.318	-0.508	0.0002	1.34	1.34	1.229	1.312
NH_2CH_3	0.274	-0.875	0.0305	1.65	1.10	0.979	1.185
NH_2Cl	0.205	-0.178	0.059	1.58	1.69	1.290	1.290
NH_2SH *ecl*	0.201	-0.381	0.214	1.87	1.35	1.174	1.251
NH_2PH_2	0.166	+0.252	0.010	1.97	1.25	0.756	1.106
NH_2SiH_3	0.137	+0.566	0.125	1.95	1.29	0.416	0.749

- Distances from nuclei to bond critical points, $r(A-r_b)$, are given in atomic units.

Table 4-4c: NH_3 and trisubstituted amines.

Amine	$\rho(r_b)$	$\nabla^2\rho(r_b)$	$\varepsilon(r_b)$	$r(N-r_b)$	$r(E-r_b)$	$\delta(N,E)$	$\delta(N,R)$
NH_3	0.361	-1.880	0.045	1.38	0.51	0.895	0.895
NF_3	0.377	-0.850	0.122	1.08	1.41	1.016	1.016
$N(CH_3)_3$	0.284	-0.924	0.048	1.63	1.10	0.957	1.151
NCl_3	0.209	-0.189	0.060	1.63	1.63	1.191	1.191
$N(SiH_3)_3$	0.128	+0.492	0.057	1.98	1.31	0.412	0.740

- Distances from nuclei to bond critical points, $r(A-r_b)$, are given in atomic units.

Table 4-5(a-d): Atomic and group properties in phosphines, MP2 values in italics. All values are given in atomic units.

Table 4-5a: Monosubstituted phosphines, PH_2EH_n. q(H) refers to the H atoms bonded to P.

Phosphine	**q(P)**	**q(E)**	**q(EH$_n$)**	**q(H)**	**K(P)**	**L (P)**	**L (E)**
PH_2F	+1.992	-0.845	-0.845	-0.574	339.927	-6.4 e-3	3.8 e-3
MP2	*+1.779*	*-0.782*	*-0.782*	*-0.500*	*340.279*	*-3.1 e-3*	*5.8 e-5*
PH_2OH *ecl*	+1.951	-1.438	-0.773	-0.584	339.928	-7.0 e-3	-8.9 e-6
	+1.942				339.928	-1.5 e-2	
MP2	*+1.727*	*-1.307*	*-0.710*	*-0.509*	*340.297*	*-1.6 e-3*	*2.1 e-5*
PH_2OH *sta*	+1.977	-1.442	-0.801	-0.593	339.923	-2.9 e-3	-6.5 e-3
PH_2NH_2 *gau*	+1.918	-1.489	-0.733	-0.600, -0.589	339.948	-4.5 e-4	-5.4 e-5
	+1.922				339.949	2.5 e-3	
MP2	*+1.690*	*-1.388*	*-0.654*	*-0.524, -0.514*	*340.317*	*-1.6 e-3*	*-3.5 e-4*
PH_2NH_2 *trn*	+1.866	-1.426	-0.701	-0.578	339.991	6.1 e-3	2.0 e-4
PH_2NH_2 *cis*	+1.887	-1.453	-0.711	-0.585	339.985	7.9 e-3	-3.0 e-3
PH_2CH_3 *sta*	+1.661	-0.422	-0.503	-0.582	340.119	4.4 e-4	-2.5 e-4
	+1.667				340.1193	5.3 e-3	
MP2	*+1.396*	*-0.432*	*-0.386*	*-0.502*	*340.506*	*3.8 e-3*	*-1.7 e-4*
PH_2CH_3 *ecl*	+1.646	-0.409	-0.475	-0.582	340.125	4.8 e-3	6.0 e-4
PH_2Cl	+1.759	-0.638	-0.638	-0.562	340.019	-1.7 e-3	3.7 e-3
MP2	*+1.497*	*-0.533*	*-0.533*	*-0.484*	*340.361*	*-3.6 e-3*	*2.9 e-3*
PH_2SH *ecl*	+1.534	-0.255	-0.397	-0.568	340.145	6.1 e-4	-2.4 e-4
	+1.541				340.145	6.0 e-3	
MP2	*+1.278*	*-0.219*	*-0.300*	*-0.489*	*340.494*	*-3.5 e-4*	*-2.2 e-4*
PH_2SH *sta*	+1.551	-0.257	-0.404	-0.570	340.141	5.3 e-3	-8.6 e-4
PH_2PH_2 *gau*	+1.131	+1.131	0.000	-0.570, -0.567	340.310	7.9 e-4	7.9 e-4
	+1.141	+1.141			340.305	3.3 e-3	3.3 e-3
MP2	*+0.979*	*+0.979*	*0.000*	*-0.488, -0.487*	*340.540*	*2.9 e-3*	*8.8 e-5*
PH_2PH_2 *tran*	+1.138	+1.138	0.000	-0.565	340.311	5.9 e-3	5.9 e-3
PH_2PH_2 *cis*	+1.134	+1.134	0.000	-0.566	340.303	1.5 e-3	1.5 e-3
PH_2SiH_3 *sta*	+0.499	+2.797	+0.613	-0.559	340.543	6.0 e-4	5.7 e-3
	+0.505				340.544	5.0 e-3	
MP2	*+0.427*	*+2.566*	*+0.516*	*-0.472*	*340.836*	*-2.5 e-4*	*2.0 e-5*
PH_2SiH_3 *ecl*	+0.509	+2.790	+0.620	-0.558	340.536	5.3 e-3	5.0 e-3

- In some cases two sets of values have been given for q(P), K(P) and L(P), to show the effect of improving the precision of the integration.
- The charge transfer, q(EH$_n$), is zero by symmetry in PH_2PH_2.
- For *gauche* P_2H_4, the q(P) value deduced from q(H) (where $L(H) < 10^{-4}$) is +1.137

Table 4-5b: Disubstituted phosphines, $PH(EH_n)_2$. q(H) refers to the H atom bonded to P.

Phosphine	**q(P)**	**q(E)**	**q(EH_n)**	**q(H)**	**K(P)**	**L (P)**	**L (E)**
PHF_2	+2.266	-0.839	-0.839	-0.588	339.725	-3.3 e-3	3.3 e-5
$PH(OH)_2$ *up*	+2.183	-1.443	-0.795	-0.596	339.746	-3.3 e-3	-2.2 e-5
$PH(OH)_2$ *dn*	+2.224	-1.440	-0.802	-0.619	339.741	7.7 e-4	-4.4 e-4
$PH(NH_2)_2$	+2.114	-1.491	-0.750	-0.605	339.804	7.5 e-3	1.3 e-3
$PH(CH_3)_2$	+1.657	-0.435	-0.526	-0.596	340.124	4.9 e-3	1.8 e-3
$PHCl_2$	+1.803	-0.617	-0.617	-0.563	339.947	4.4 e-3	3.6 e-3
$PH(SH)_2$ *up*	+1.326	-0.240	-0.380	-0.563	340.202	3.1 e-3	-1.4 e-4
$PH(PH_2)_2$	+0.546	+1.145	+0.012	-0.568	340.523	3.0 e-3	-1.0 e-3
$PH(SiH_3)_2$	-0.694	+2.794	+0.625	-0.555	340.975	2.3 e-3	-1.2 e-4

Table 4-5c: PH_3 and trisubstituted phosphines, $P(EH_n)_3$.

Phosphine	**q(P)**	**q(E)**	**q(EH_n)**	**μ(P)**	**K(P)**	**L (P)**	**L (E)**
PH_3	+1.695	-0.564	-0.564	-2.20	340.100	1.6 e-3	5.7 e-5
	+1.458	*-0.485*	*-0.485*	*-2.03*	*340.458*	*1.8 e-3*	*6.6 e-5*
PF_3	+2.512	-0.836	-0.836	-2.42	339.513	4.5 e-3	2.5 e-5
	+2.345	*-0.780*	*-0.780*	*-2.26*	*339.857*	*4.4 e-3*	*6.3 e-5*
P(OH)	+2.386	-1.448	-0.794	-2.67	339.556	1.3 e-3	1.7 e-4
$P(NH_2)_3$	+2.253	-1.473	-0.751	-2.52	339.694	2.1 e-3	1.2 e-4
$P(CH_3)_3$	+1.662	-0.445	-0.554	-2.33	340.120	4.4 e-3	2.6 e-3
PCl_3	+1.780	-0.592	-0.592	-1.92	339.890	3.8 e-3	3.3 e-3
	+1.423	*-0.473*	*-0.473*	*-1.60*	*340.295*	*3.5 e-3*	*1.6 e-3*
$P(SH)_3$	+1.013	-0.205	-0.337	-1.54	340.302	-3.0 e-7	1.8 e-4
$P(PH_2)_3$	-0.089	+1.160	+0.030	-0.63	340.758	-4.1 e-4	-1.6 e-4
$P(SiH_3)_3$	-1.887	+2.805	+0.629	+1.39	341.404	3.5 e-3	6.5 e-3
PBr_3	+1.095	-0.365	-0.365	+1.31	340.178	2.3 e-4	-4.0 e-3

- A negative dipole, μ, has the negative end pointing away from the substituents.

Table 4-5d: Fluorinated phosphines

Phosphine	**q(P)**	**q(E)**	**q(H)**	**q(F)**	**q(EY_n)**	**K(P)**	**L (P)**	**L (E)**
PH_2NH_2 *trans*	+1.866	-1.426	-0.578		-0.701	339.991	6.1 e-3	2.0 e-4
PH_2NF_2 *trans*	+1.883	+0.075	-0.553	-0.420	-0.764	340.116	6.7 e-3	6.7 e-3
PF_2NH_2 *trans*	+2.401	-1.497		-0.846	-0.710	339.589	4.6 e-3	1.8 e-4
PH_2CH_3 *stag*	+1.661	-0.422	-0.582		-0.503	340.119	4.4 e-4	-2.5 e-4
PH_2CF_3 *stag*	+1.756	+1.585	-0.550	-0.744 / 5	-0.648	340.200	4.4 e-3	4.7 e-3
PF_2CH_3 *stag*	+2.222	-0.526		-0.846	-0.530	339.743	4.3 e-3	-4.5 e-5

- Note: q(H) refers to the H atoms bound to P, q(EY_n) refers to EH_n or EF_n as appropriate.

Table 4-6(a, c). Atomic and group properties in amines. All values are given in atomic units.

Table 4-6a: Monosubstituted amines, NH_2XH_n, q(H) refers to the H atoms bonded to N.

Amine	q(N)	q(X)	$q(XH_n)$	q(H)	K(N)	L (N)	L (X)
NH_2F	-0.316	-0.445	-0.445	+0.381	54.416	2.6 e-4	6.5 e-5
NH_2OH *e*	-0.478	-0.869	-0.239	+0.359	54.495	3.1 e-4	1.9 e-4
NH_2NH_2	-0.683	-0.683	0.000	+0.330, 0.354	54.602	2.1 e-4	2.1 e-4
NH_2CH_3	-1.052	+0.549	+0.382	+0.335	54.801	2.5 e-4	3.0 e-4
NH_2Cl	-0.795	+0.004	+0.004	+0.393	54.618	-4.3 e-3	1.2 e-4
NH_2SH *e*	-1.179	+0.572	+0.414	+0.383	54.823	-5.7 e-5	6.6 e-4
NH_2PH_2	-1.489	+1.922	+0.733	+0.377, 0.383	54.991	-5.4 e-5	2.5 e-3
NH_2SiH_3	-1.563	+3.015	+0.810	+0.377	54.986	1.2 e-5	-3.4 e-4

Table 4-6c: NH_3 and trisubstituted amines, NH_2XH_n.

Amine	q(N)	q(X)	$q(XH_n)$	μ(N)	K(N)	L (N)	L (X)
NH_3	-1.044	+0.348	+0.348	-0.17	54.745	7.0 e-5	2.7 e-5
NF_3	+1.092	-0.362	-0.362	-0.11	53.523	8.2 e-3	2.0 e-4
$N(CH_3)_3$	-1.109	+0.542	+0.370	-0.25	54.935	5.2 e-3	8.4 e-4
NCl_3	-0.422	+0.142	+0.142	-0.31	54.330	5.8 e-3	9.9 e-5
$N(SiH_3)_3$	-2.425	+3.003	+0.808	+0.08	55.336	1.7 e-3	2.5 e-3

- A negative dipole has the negative end pointing away from the substituents.

Table 4-7(a, c): Properties of bonding maxima in phosphines.

Table 4-7a: Monosubstituted phosphines

Phosphine	**$r(P-r_b)$**	**$r(E-r_b)$**	**$\nabla^2\rho(r_b)$**	**$\rho(r_b)$**
PH_2F	1.527	1.479	+0.080	0.205
PH_2OH *e*	1.564	1.532	-0.173	0.207
PH_2NH_2 *g*	2.407	0.816	-1.678	0.449
PH_2CH_3 *s*	2.529	0.979	-0.813	0.244
PH_2Cl	2.695	1.249	-0.518	0.240
PH_2SH *e*	2.679	1.378	-0.384	0.177
PH_2PH_2 *g*	2.665	1.548	-0.253	0.127
PH_2SiH_3 *s*	2.528	1.778	-0.180	0.099
PH_2SH *e*	1.572	2.476	-0.201	0.123
PH_2PH_2 *g*	1.548	2.665	-0.253	0.127
PH_2PH_2 *t*	1.547	2.701	-0.250	0.125

- The bolded element is the atom in whose valence shell the charge concentration is located.
- The shaded rows correspond to the maxima in the valence shells of substituent atoms.
- All properties, including distances from nuclei to maxima, $r(A-r_b)$, are given in atomic units.

Table 4-7c: Trisubstituted phosphines

Phosphine	**$r(P\text{-}r_b)$**	**$r(E\text{-}r_b)$**	**$\nabla^2\rho(r_b)$**	**$\rho(r_b)$**
PF_3	1.503	1.420	+0.253	0.240
$P(OH)_3$	1.537	1.498	-0.229	0.228
$P(NH_2)_3$	1.553	1.664	-0.320	0.192
$P(CH_3)_3$	1.544	1.946	-0.341	0.160
PCl_3	2.651	1.247	-0.532	0.245
$P(SH)_3$	2.680	1.371	-0.390	0.179
$P(PH_2)_3$	2.653	1.548	-0.248	0.127
$P(PH_2)_3$	1.547	2.653	-0.253	0.128
$P(SiH_3)_3$	1.541	2.749	-0.249	0.127
PBr_3	1.555	2.676	-0.167	0.113
PBr_3	2.365	1.870	-0.071	0.131

- The bolded element is the atom in whose valence shell the charge concentration is located.
- The shaded rows correspond to the maxima in the valence shells of substituent atoms.
- All properties, including distances from nuclei to maxima, $r(A\text{-}r_b)$, are given in atomic units.

Table 4-8: Properties of bonding maxima in NH_3 and monosubstituted amines.

Amine	**$r(N\text{-}r_b)$**	**$r(E\text{-}r_b)$**	**$\nabla^2\rho(r_b)$**	**$\rho(r_b)$**
NH_3	0.830	1.057	-2.204	0.481
NH_2F	0.910	1.701	-0.590	0.311
NH_2OH *e*	0.879	1.766	-1.037	0.359
NH_2NH_2	0.851	1.820	-1.418	0.405
NH_2CH_3	0.824	1.923	-1.741	0.445
NH_2SH *e*	0.840	2.386	-1.268	0.394
NH_2PH_2	0.816	2.407	-1.678	0.449
NH_2SiH_3	0.801	2.456	-1.891	0.478
NH_2OH *e*	1.904	0.741	-1.852	0.612
NH_2NH_2	1.820	0.851	-1.418	0.405
NH_2CH_3	1.747	1.000	-0.945	0.275
NH_2Cl	2.001	1.274	-0.459	0.235
NH_2SH *e*	1.826	1.399	-0.392	0.201

- The bolded element is the atom in whose valence shell the charge concentration is located.
- The shaded rows correspond to the maxima in the valence shells of substituent atoms.
- All properties, including distances from nuclei to maxima, $r(A\text{-}r_b)$, are given in atomic units.

Table 4-9(a, c): Properties of non-bonded maxima on P in phosphines.

Table 4-9a: Monosubstituted phosphines.

Phosphine	**$r(P\text{-}r_{nb})$**	**$\nabla^2\rho(r_{nb})$**	**$\rho(r_{nb})$**	**$\mu_3(r_{nb})$**
PH_2F	1.420	-0.414	0.146	-11.50
PH_2OH	1.426	-0.402	0.143	-11.02
PH_2NH_2	1.430	-0.385	0.140	-10.61
PH_2CH_3	1.438	-0.359	0.136	-9.98
PH_2Cl	1.430	-0.376	0.139	-10.62
PH_2SH	1.438	-0.350	0.134	-9.93
PH_2PH_2	1.444	-0.331	0.131	-9.47
PH_2SiH_3	1.450	-0.310	0.127	-8.97

Table 4-9c: PH_3 and trisubstituted phosphines. MP2 values in italics.

Phosphine	$\mathbf{r(P\text{-}r_{nb})}$	$\nabla^2\rho(\mathbf{r}_{nb})$	$\rho(\mathbf{r}_{nb})$	$\mu_3(\mathbf{r}_{nb})$
PH_3	1.443	-0.340	0.132	-9.58
	1.448	*-0.292*	*0.126*	*-8.94*
PF_3	1.389	-0.506	0.163	-14.61
	1.399	*-0.421*	*0.151*	*-13.13*
$P(OH)_3$	1.400	-0.489	0.159	-13.52
$P(NH_2)_3$	1.410	-0.458	0.153	-12.45
$P(CH_3)_3$	1.430	-0.387	0.141	-10.59
PCl_3	1.412	-0.417	0.148	-12.19
	1.422	*-0.340*	*0.137*	*-10.85*
$P(SH)_3$	1.427	-0.373	0.140	-10.76
$P(PH_2)_3$	1.446	-0.315	0.129	-9.20
$P(SiH_3)_3$	1.468	-0.249	0.117	-7.67
PBr_3	1.419	-0.380	0.141	-11.37

- $\mu_3(\mathbf{r}_{nb})$ is the radial curvature of the Laplacian.
- All properties, including distances from nuclei to maxima, $r(A\text{-}\mathbf{r}_{nb})$, are given in atomic units.

Table 4-10(a, c): Properties of non-bonded maxima on N in amines.

Table 4-10a: Monosubstituted amines.

Amine	$\mathbf{r(N\text{-}r_{nb})}$	$\nabla^2\rho(\mathbf{r}_{nb})$	$\rho(\mathbf{r}_{nb})$	$\mu_3(\mathbf{r}_{nb})$
NH_2F	0.722	-3.713	0.640	-217.81
NH_2OH *e*	0.730	-3.387	0.616	-199.42
NH_2NH_2	0.737	-3.087	0.595	-183.90
NH_2CH_3	0.744	-2.814	0.572	-171.32
NH_2Cl	0.731	-3.238	0.608	-194.25
NH_2SH *e*	0.744	-2.735	0.568	-168.47
NH_2PH_2	0.757	-2.337	0.535	-147.55
NH_2SiH_3	0.766	-2.113	0.514	-136.24

- $\mu_3(\mathbf{r}_{nb})$ is the radial curvature of the Laplacian.
- All properties, including distances from nuclei to maxima, $r(A\text{-}\mathbf{r}_{nb})$, are given in atomic units.

Table 4-10c: NH_3 and trisubstituted amines.

Amine	$\mathbf{r(N\text{-}r_{nb})}$	$\nabla^2\rho(\mathbf{r}_{nb})$	$\rho(\mathbf{r}_{nb})$	$\mu_3(\mathbf{r}_{nb})$
NH_3	0.748	-2.649	0.556	-165.70
NF_3	0.693	-5.378	0.450	-307.38
$N(CH_3)_3$	0.741	-3.029	0.593	-178.59
NCl_3	0.712	-4.100	0.673	-240.49
	-0.804	-1.139	0.398	-91.32
$N(SiH_3)_3$	0.789	-1.486	0.460	-107.23
	-0.799	-1.266	0.441	-96.55

- $\mu_3(\mathbf{r}_{nb})$ is the radial curvature of the Laplacian.
- All properties, including distances from nuclei to maxima, $r(N\text{-}\mathbf{r}_{nb})$, are given in atomic units.
- A negative distance indicates that the non-bonded maximum is on the same side of the nitrogen as are the substituents.

Bibliography

References are listed alphabetically by first author and then by date, with the references in the Data Tables sections listed separately.

Bachrach, S.M. (1989). *J. Comp. Chem.* **10**, 392.

Burford, N., B.W. Royan and P.S. White (1990). *Acta Crystallogr., Sect. C: Cryst. Struct. Commun.* **C46**, 274.

Cotton, F.A. and G. Wilkinson (1988). Advanced Inorganic Chemistry, 5th ed. New York: Wiley.

DeFrees, D.J.; B.A. Levi, S.K. Pollack, W.J. Hehre, J.S. Binkley and J.A. Pople, (1979). *J. Am. Chem. Soc.* **101**, 4085.

Durig, J.R., L.A. Carreira and J.D. Odom (1974). *J. Am. Chem. Soc.* **96**, 2688.

Gatti, C., P.J. MacDougall and R.F.W. Bader (1988). *J. Chem. Phys.* **88**, 3792.

Gillespie, R.J. and P.L.A. Popelier (2001). Chemical Bonding and Molecular Geometry. New York: Oxford University Press.

Gough, K.M., M.M. Yacowar, R.H. Cleve and J.R. Dwyer (1996). *Can. J. Chem.* **74**, 1139.

Hamilton, L.A. and P.S. Landis (1972). *Phosphinous Acids and Derivatives*, in Organic Phosphorus Compounds , Volume 4. G. M. Kosolapoff and L. Maier eds. New York: Wiley Interscience.

Howard, S.T. and J.A. Platts (1995). *Inorg. Chem.* **99**, 9027.

Howard, S.T.; J.P. Foreman and P.G. Edwards (1996). *Inorg. Chem.* **35**, 5805.

Kohata, K., T. Fukuyama and K. Kuchitsu (1982). *J. Phys. Chem.* **86**, 602.

Kwiatkowski, J.S. and J. Leszczynski (1992). *Mol. Phys.* **76**, 475.

Tuzova, L.L., V.A. Naumov, R.M. Galiakberov, E.N. Ofitserov and A.N. Pudovik (1981). *Dokl. Akad. Nauk. SSSR* **256**, 891.

Walker, B. J (1972). Organophosphorus Chemistry. London: Penguin Books.

Zaripov, N.M., V.A. Naumov and L.L. Tuzova (1974). *Dokl. Akad. Nauk SSSR* **218**, 1132.

Table References

Bartell, L.S. (1960). *J. Chem. Phy.* **32**, 832.

Bartell, L.S. and L.O. Brockway (1960). *J. Chem. Phys.* **32**, 512.

Beagley, B., A.G. Robiette and G.M. Sheldrick (1968) *J. Chem. Soc. (A)* **1968**, 3002.

Beagley, B. and A.R. Conrad (1970). *Trans. Faraday Soc.* **66**, 2740.

Beagley, B. *et al.* (1972). *J. Mol. Struct.* **11**, 371.

Bryan, P.S. and R.L. Kuczkowski (1971). *J. Chem. Phys.* **55**, 3049

Burford, N.; B.W. Royan and P.S. White (1990). *Acta Crystallogr., Sect. C: Cryst. Struct. Commun. C46,* 274.

Bürgi,, H.B., D. Stedman and L.S. Bartell (1971). *J. Mol. Struct.* **10**, 31.

Cazzoli G., D.G. Lister and P.G. Favero (1972). *J. Mol. Spectrosc.* **42**, 286.

Chu, F.Y.; Oka, T. (1974). *J. Chem. Phys.* **60**, 4612

Durig, J.R., L.A. Carreira and J.D. Odom (1974). *J. Am. Chem. Soc.* **96**, 2688.

Glidewell, C., P.M. Pinder, A.G. Robiette and G.M. Sheldrick (1972). *J. C. S. Dalton Trans.* **1972**, 1402.

Hedberg, K. M. Iwasaki (1962). *J. Chem. Phys.* **36**, 589.

Helminger, P., F.C. DeLucia and W. Gordy (1971). *J. Mol. Spectrosc.* **39**, 94.

Kawashima, Y. and P.A. Cox (1977). *J. Mol. Spectrosc.* **65**, 319. Kisliuch, P. and C.H. Townes (1950). J. Chem Phys. 18, 1109.

Kohata, K.T. Fukuyama and K. Kuchitsu (1982). *J. Phys. Chem.* **86**, 602.

Kojima, T., E.L. Breig and C.C. Lin (1961). *J. Chem. Phys.* **35**, 2139.

Kuczkowski, R.L. (1968). *J. Am. Chem. Soc.* **90**, 1705.

Lovas, F.J., R.D. Suenram and W.J. Stevens (1983). *J. Mol. Spectrosc.* **100**, 316.

Nelson, R. (1963). *J. Chem. Phys.* **39**, 2382.

Otake, M., C. Matsumura and Y. Morino (1968). *J. Mol. Spectrosc.*, **28**, 316.

Takagi, K. and T. Kojima (1971). *J. Phys. Soc. Jpn.* **30**, 1145.

Tsuneka, S. (1972). *J. Phys. Soc. Jpn.* **33**, 167.

Tuzova, L.L. *et al.* (1981). *Dokl. Akad. Nauk SSSR*, **256**, 891.

Vilkov, L.V. and L.S. Khaikin (1969). *Zh. Stukt. Khim.* **10**, 978.

Wollrab, J.E. and V. W. Laurie (1969). *J. Chem. Phys.* **51**, 1580.

Zaripov, N.M., V.A. Naumov, L.L. Tuzova (1974). *Dokl. Akad. Nauk SSSR*, **218**, 1132.

5. Phosphinylidene Results

5.1. History of double bonds to phosphorus

Until about 35 years ago[*] double bonds to and between main group atoms of the third row and higher were thought to be too unstable to exist, due in part to weak *p-p* π-like overlap (Gusel'nikov and Nametkin, 1979; Kutcha and Parkin, 1998). This belief, sometimes called the 'classical double bond rule', is similar to the one that noble gases could not form compounds, in that an observation (or lack thereof) was generalized, then rationalized and then became set in stone. Like the inert gas 'rule', it was broken when researchers synthesized examples of the 'non-existent'[†] molecules. Multiple bonds to phosphorus and silicon are indeed quite reactive, but as early as 17 years ago, a large number of relatively stable phosphinylidenes (RP=X, $X \neq O, S$), silenes ($R_2Si{=}CR_2$) and disilenes ($R_2Si{=}SiR_2$) were known (Cowley, 1986) and the number has grown since then. The area of multiple bonds to heavy main group elements has recently been extensively reviewed by Power (1999) in terms of experimental results and theoretical models. He points out that the chemistry and structure of compounds of second row elements are the exception, rather than the rule.

---

[*] Phosphabenzene was discovered in 1966 and this renewed interest in the chemistry of low-coordinate phosphorus, see Neicke and Gudat, 1991.

[†] These molecules were included in the oft-cited book by W. E. Dasent (1965) *Non Exisitent Compounds – Compounds of Low Stability*, Marcel Dekker: New York.

With the exception of some phosphoranes, $Y_3P{=}X$ (which can be written in a singly-bonded zwitterionic form – see chapter 6), compounds exhibiting formal multiple bonds to phosphorus are usually only isolable when the bond is sterically protected by large substituents and/or electronically stabilized. Phosphorus typically has a coordination number of three or four, and sometimes five or six. The first stable examples of phosphinylidenes, YP=X and bis(ylene)phosphoranes $YP(=X)_2$ (chapter 7) were synthesized in 1973 and 1974 (see chapter 1 of Scherer and Regitz, 1990).

5.2. Energy and reactivity of double bonds to phosphorus

The ratio of double bond strength to single bond strength is much smaller for M-M bonds than for L-L bonds, with M-L bonds in between (Schoeller *et al.*, 1997). The heavier atoms are less electronegative and are less effective at stabilizing two electron pairs in close proximity in the bonding region (Malcolm *et al.*, 2002). The heavier atoms are also less sterically crowded at higher coordination number. These factors together favour dimerization or oligomerization over double bond formation for heavy atoms. With very similar energies for the two highest energy molecular orbitals (Schoeller, 1990), phosphinylidenes, HP=X, show significant reactivity at both functional groups: the double bond and the lone pair.

The phosphorus atom in YP=X is coordinatively unsaturated and thus very reactive. In fact, though P=S and P=O bonds are extremely strong when the phosphorus is pentavalent, trivalent YP=O and YP=S are extremely unstable.* No trivalent examples have been definitively structurally characterized, though infrared vibrational frequencies have been measured where Y is a halogen or hydroxyl group. A few examples of $YP=SY_2$ are known where S is substituted with a siloxyl group (Zurmühlen and Regitz, 1987). The related $YP=PY_3$ systems will be discussed in Chapter 6. Phosphines readily react with chalcogens to form phosphine oxides and sulfides (Chapter 6). A similar reaction can convert phosphinylidenes into bis(ylene)phosphoranes (Appel, 1990, p.160) – see Chapter 7. Alternatively, oxidative 1,1-addition to phosphinylidenes leads to phosphoranes (Niecke, 1990, p.306), such as $Y_3P=NY$ – see Chapter 6.

Common reactions of phosphinylidenes that involve the double bond are cycloadditions and addition of dipolar compounds (Regitz and Scherer, 1990). Iminophosphines also oligomerize and react with Lewis acids and bases. Phosphaalkenes may undergo elimination to form phosphaalkynes. The non-polar diphosphenes also add X_2 or H_2 and the weak P-P bond may be cleaved when HCl is added.

While neutral tetracoordinate pentavalent nitrogen is not usually observed (with the exception of F_3NO), imine derivatives (YN=X) are relatively well known. Conversely, phosphinylidenes, YP=X, are fairly reactive but phosphoranes, $Y_3P=X$, are much more stable, especially when the X group is electronegative. Based on the similarities in the molecular orbital energies, the switch in chemical stability

---

* Note that *single* bonds between sulfur and trivalent phosphorus are also very rare.

from trivalent N to pentavalent P seems to have more to do with maximum coordination number (and thus the *effective* reactivity of the lone pair on phosphorus *vs.* nitrogen) than with the reactivity of the double bond. Since the products of the addition reactions to YP=X are more stable than the products from addition to YN=X, YN=X is readily observed, while YP=X is not.

The calculated geometric and electronic structures of the unsubstituted HP=X and HN=X species will serve as a baseline for comparison with other systems in later chapters. The Lewis structures exhibit double bonds with no formal charges, while obeying the octet rule. While the P-E bond may be polar, few chemists would argue that the bond order, in the Lewis sense, is anything other than two.* This will be verified by the delocalization index data below. In later chapters, less clear-cut bonding situations will be investigated.

5.3. Geometry

5.3.1. General features – planar species

Optimized bond lengths and bond angles about P are given in Table 5-1, along with experimental values for some related systems. Table 5-2 gives the corresponding values for imines. The P-E bond lengths are plotted in Figure A4-1, and compared to the other phosphorus species studied. Where both *cis* and *trans* isomers are possible, the *trans* isomer is lower in energy by 2 to 15 kJ/mol. This is

---

* Some would argue that for more electropositive atoms, such as silicon, the bond order in systems such as $H_2Si=SiH_2$ is less than two, due to incomplete localization of the bonding electrons in the bonding region, see Malcolm *et al.*, 2002.

the observed geometry for most experimental systems (Power, 1990), however previous calculations have predicted that the *cis* isomer of YP=NY′ will be favoured by electronegative substituents (Schoeller *et al.*, 1990). Electron-withdrawing groups on P shorten the P=N bond, while on N they lengthen it.

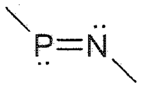
trans


cis

For the series of planar species, in addition to the expected increase in bond lengths in going from second to third row atoms, the bond angles around P are smaller for the phosphinylidenes than the bond angles around N for the imines. The doubly bonded species have similar angles to the singly bonded species because the ligand non-bonding radii are similar. There is a trend of increasing HNX angle as the size of X, as measured by bond length[*], increases. The ligands around phosphorus are less crowded and show the opposite trend; the bond angle generally decreases as the bond length increases. In both cases, the *cis* isomers have angles about 5° larger than the *trans* isomers. These larger bond angles allow for a shorter P=N bond length in the less stable *cis* isomer. The P=P and N=N bonds are longer in the *cis* arrangement.

The bond lengths in the phosphinylidenes are generally 20 to 23 pm shorter than the corresponding phosphine bond lengths. The imine (N=E) bonds are shorter than the amine (N-E) bonds by a similar amount. The smallest change is for

---

[*] The size, as measured by N-E bond lengths, decreases from left to right across a period, in contrast with calculated bonding radii.

the P-N bond, which shortens by only 16 pm. In general, the N-M and P-L bonds shorten less than the N-L and P-M bonds. This suggests that multiple bond formation is less effective between elements in different rows of the periodic table.

5.3.2. Comparison with experiment and correlation effects

Table 5-1 shows the geometrical parameters calculated at both the Hartree-Fock and MP2 levels of theory. Experimental values are shown where available. Including correlation at the MP2 level of theory generally increases bond lengths and decreases bond angles (DeFrees *et al.*, 1979). For the systems studied here, MP2 increases the P=E bond lengths by about 5 pm and increases the P-H bond lengths by about 1 pm. For phosphines and amines, it was found that HF gave short bonds compared with experiment, except bonds between two third row elements, which were too long, and even longer at MP2.

The only reliable experimental phosphinylidene geometry available for direct comparison is $HPCH_2$. The MP2 geometry is significantly closer to the experimentally determined P-C bond length and HPC bond angle. A microwave spectrum of HPO has been obtained, but no structure was elucidated (Saito *et al.*, 1986). The geometry had previously been elucidated from rotational analysis of an electronic transition (Larzilliere *et al.*, 1980). That study shows that the present MP2 calculation overestimates the P-O bond length by 2 pm. The structure fit to the experimental data is somewhat uncertain due to a lack of isotopic substitution data, but is in reasonable agreement with a structure calculated using the CASPT2 method (Luna *et al.*, 1995).

Comparison with experimental geometries of substituted (YP=NY, YP=PY and YP=SiY$_2$) phosphinylidenes shows that the experimental P=N and P=P bond lengths lie between the HF and MP2 values, while the calculated P=Si bond is 1 pm too short at MP2 and 3 pm too short at the HF level. These comparisons are only rough indicators as steric, crystal packing and electronic effects may be important, particularly for the P=Si bond where the Si atom is phosphino-substituted and slightly pyramidal. When the phosphorus atom is silyl substituted the silylene group is planar (Power, 1999) and the experimental P=Si bond length (206.2 pm) is closer to the Hartree-Fock value.

In summary, MP2 increases the Hartree-Fock bond length and thus the error for P-M single bonds lengths, which are overestimated, and P-N bonds, which are well reproduced at HF. MP2 overcompensates for the error in P=O, P=N and P=P double bond lengths, which are underestimated at HF, while P=Si is underestimated even at MP2 and P=C is well reproduced at MP2.

The imines HN=O and HN=CH$_2$ have been structurally characterized by microwave spectroscopy. Like P=O and P=C bonds, N=O and N=C bond lengths are underestimated by about 4 pm at Hartree-Fock. This is on the order of the variation between P-E (or N-E) bond lengths as the degree of substitution is changed, and about half the variation in P-E bond lengths as E is changed, say from O to N. These differences, in turn, are about half the difference between the single bond length and double bond length for a given E. Therefore, while there is some error in the calculated geometries, and thus in the densities and other calculated properties, it should not be enough to obscure the trends within a series of molecules, nor to hide the important differences between one series and another.

5.3.3. Non-planar species

Most phosphaalkenes are planar, with a significant barrier to rotation about the P-C bond. In fact, *E/Z* isomers of Mes*P=CHPh have been isolated (Yoshifuji *et al.*, 1983, 1985; Appel *et al.*, 1986). However, a class of related compounds have much freer rotation about the P-C bond (Arduengo *et al.*, 1997*a/b*). These may be described as 1,3-imidazol-2-ylidene complexes of PR (or AsR), with a C-P distance of about 176 pm. When the R group is large and R′ is electron withdrawing, the dihedral angle is non-zero. The NMR chemical shift gives evidence of significant shielding at P, relative to other phosphaalkenes.

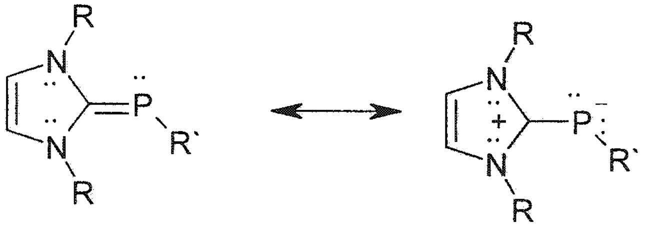

In order to investigate this phenomenon, a planar amino-substituted phosphalkene was studied, $(NH_2)_2C{=}PH$. The bond length was found to agree well with experiment, being 175.4 pm, about halfway between the $H_2C{=}PH$ double bond, and the P-C single bond lengths. The HPC angle narrows, suggesting increased lone pair density at phosphorus.

To investigate the effects of rotation about the P=E bond, C_s-twisted geometries of $HPCH_2$, and $HPSiH_2$ were investigated. The singlet twisted species are found to be higher in energy than the planar species by 375 kJ/mol for C and by 114 kJ/mole for Si. This confirms a strong π-like interaction in the planar species. In both of these species, the bond lengths are just slightly longer than the planar double bond lengths, so the bond is still being shortened, by either residual π-like overlap, electrostatic attraction, or both. The twisted geometries have angles about C and Si summing to 320.7° (less than tetrahedral) and 359.4° (planar), respectively. This suggests the presence of a lone pair on the carbon atom and a zwitterionic structure for this hypothetical molecule. Clearly the amino groups are important for donating electron density to carbon in the imidazol derivative above, otherwise the phosphorus atom would be deshielded, not shielded.

In the twisted $HPSiH_2$, the near planar-silicon atom could be described as sp^2 hybridized, but the (negatively charged) H atom bound to phosphorus is shifted over to interact with the silicon atom. The P-H bond stretches from the typical 141 pm to 155 pm. The Si-P-H bond angle is only 56°. The H--Si distance is only 176 pm, while the directly bound H atoms are 147 pm from the Si atom. However, no ring critical point is found and no bond path is found between Si and the H bound to phosphorus. A zwitterionic form with a positive charge on silicon and two lone pairs on phosphorus would best describe this hypothetical system.

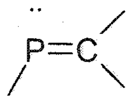

planar

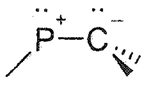

twisted

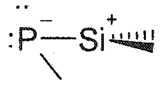

twisted

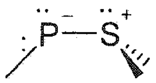

hypervalent

A potentially 'hypervalent'* $HP{=}SH_2$ molecule was also optimized. Experimental examples of this structure have a siloxy group on the sulfur (Zurmühlen and Regitz, 1987). The electronegative $OSiR_3$ substituent supports the 'hypervalent' bonding arrangement about S, by removing electron density.

The calculated P-S bond length in $HPSH_2$ is 5 pm *greater* than the single bond length in the phosphines, suggesting that the bond is essentially a single bond. The PSH angles are 109.5° and the HSH angle is 94.3°. The P-H bond length and HPS angle are quite similar to those in planar $HPSiH_2$. This suggests that there is electron transfer towards the PH group. The high valence (4 *vs.* 2) of sulphur reduces its effective electronegativity. Since it already has a complete octet, it will not pull more density from phosphorus. This conclusion will be further supported by an analysis of the electron density distribution below.

5.4. Bond Paths and Interatomic surfaces

Bond critical points (BCPs) are found between all atoms that we expect to be bonded. Properties of the BCPs are given in Tables 5-3 (P-L, P-M) and 5-4 (N-L, N-M). There are no ring or cage critical points in the molecules studied. Figure 5-4 shows plots of the Laplacian of the electron density, $\nabla^2\rho(\mathbf{r})$, in the symmetry plane of each phosphinylidene. These plots are overlaid with bond path trajectories and the intersection of the interatomic surface with the plane.

---

* A simple definition of a hypervalent molecule is one in which a (non-metallic) atom has more than four pairs of electrons in its valence shell, see Noury *et al.*, 2002.

5.4.1. Position of the bond critical point

Bonding radii of the phosphorus and substituent atoms are plotted in Figures A4-2 and A4-3, respectively. The values are reported in Table 5-3. Corresponding imine data are reported in Table 5-4. As in the phosphines, $r_b(P)$ decreases and the BCP draws closer to phosphorus as the electronegativity of X increases. The trends in $r_b(P)$ and $r_b(E)$ are similar to those in the phosphines, see Figure 5-2 and Figure 5-3. The probable reasons for these trends were discussed in Chapter 4.

As in the second row amines, the nitrogen bonding radius increases while the radius of L decreases (particularly between N and C), so that the N=L bond length increases steadily from O to C. In the third row imines the N radius decreases slightly and the M radius increases slightly, again leading to a slow increase in the N=M bond lengths from S to Si. This behaviour is opposite to the P=M bonds. Remarkably, in both singly and doubly bonded species, the phosphorus atom is smaller than the nitrogen atom when bonded to S or C. Similarly Si is smaller than C when bonded to phosphorus and S is smaller than O when bonded to nitrogen. Again this can be explained based on the variations in bond polarity.

5.4.2. Comparison with single bonds

See Figure 5-2 and Figure 5-3 for plots of phosphorus, nitrogen and substituent bonding radii in comparison with the singly bonded species. Relative to the phosphines, the distance from the phosphorus atom to the BCP decreases by 0.21 au to 0.35 au in the third row species, but only by 0.09 au to 0.17 au in the second row phosphinylidenes, where the interatomic surface is already within the core region of phosphorus. This is a decrease of 7% to 12% in each case but HP=S, where it is a 19% decrease in the bonding radius. The $r_b(E)$ values are about 0.2 au (10%) less than the phosphine values, though $r_b(S)$ and $r_b(Si)$ shorten by less than 0.1 au (5%), so the P-S and P-Si bond shortening is almost entirely in the P atom. For P and C the shortening is about equally shared. The bonding radii of N and O in HPO and HPNH are shortened more than twice as much as P, relative to H_2PR. In summary, the decrease in bond length *usually* (except in P-S) occurs by greater shortening of the more electronegative atom, in essence decreasing the polarity of the bond.

There is not such a clear reason for the trend in the imines relative to the amines. Both bonding radii shorten by about 0.2 au in NHO and NHNH. The majority of shortening occurs on C and S for $NHCH_2$ and NHS, but on N for NHPH and $NHSiH_2$.

5.4.3. Correlation effects

All the bonding radii in PHX are longer at the MP2 level than at the HF level, with the exceptions of S in PH=S and P in $PH{=}SiH_2$, which are shorter. The bonding radius of C in $PH{=}CH_2$ is changed very little. Thus, in $PH{=}CH_2$, PH=S and $PH{=}SiH_2$, the major effect of correlation is to shift the BCP towards the more electronegative atom, decreasing the polarity, while the bond lengthens. When X = O, NH and PH, MP2 correlation increases both bonding radii by about 0.05 au.

5.5. Properties at the Bond Critical Point

5.5.1. Density, $\rho(r_b)$

The density at the P-E bond critical point is plotted in Figure A4-4. The values are reported in Table 5-3. For the phosphinylidenes, P-L BCPs have $\rho(\mathbf{r}_b)$ values ranging from 0.20 to 0.26 au, compared with 0.155 to 0.166 au in the corresponding phosphines (H_2PR), and P-M BCPs have $\rho(\mathbf{r}_b)$ values ranging from 0.12 to 0.17 compared to 0.10 to 0.12 au in the phosphines. The increase in density over the phosphines is most pronounced for the P-O bond. For the imines, BCP densities of N-M bonds are in line with P-L bonds, ranging from 0.18 to 0.27 au. The N-L bonds have much higher densities, from 0.41 to 0.58 atomic units – an 80% increase for the N-O bond, relative to H_2NOH. The greater shortening of the less polar P-M bonds is accompanied by a smaller increase in $\rho(\mathbf{r}_b)$, while the N-L $\rho(\mathbf{r}_b)$ values increase the most.

The twisted geometries of $HPCH_2$ and $HPSiH_2$ again give surprising results. While the P-E bonds are slightly longer than in the planar systems, the BCP density in the twisted HP-CH_2 is actually higher than in the planar system, and in HP-SiH_2, $\rho(\mathbf{r}_b)$ is just a little lower than for the planar case. Clearly there is a strong interaction in these systems, which might be consistent with a double bond, despite the lack of *p-p* π-type overlap. While the energy increases greatly upon rotation about the P-E bond, the extent of overlap apparently does not change significantly. Substitution at C, on the other hand, has a significant effect on the P-C bond. The P-C bond length in $HP{=}C(NH_2)_2$ is halfway between $HP{=}CH_2$ and $H_2P\text{-}CH_3$. The P-C BCP density in the diamino-substituted phosphaalkene is only slightly higher than in methylphosphine.

5.5.2. Laplacian

The trends in the BCP Laplacian values will be discussed as they relate to the BCP's position relative to the bonding charge concentration in the valence shell of each atom. The trend in P-E $\nabla^2\rho_b$ values is plotted in Figure A4-5. The values are reported in Table 5-3. In the phosphinylidenes, $\nabla^2\rho_b$ of the P-L bonds is much more positive than in the phosphines, and decreases from 1.59 for O to 0.26 for C. The BCP lies inside the core region of the phosphorus atom, so shortening the bond, and the bonding radius of P, moves the BCP to a region of even more positive Laplacian values.

For the third row substituents, the BCP Laplacian varies between -0.02 and -0.23, with the most negative value for the non-polar HP=PH. In HPS, the BCP lies just 0.15 au inside the valence shell maximum of phosphorus. In HPPH, it is 0.4 au from each bonding charge concentration. In $HPSiH_2$ the BCP lies 0.3 au inside the valence maximum of Si. The relative positions are similar in PH_2MH_n except that the BCP is just 0.1 au *outside* the valence maximum in PH_2SH. It is interesting that while the P-P BCP Laplacian is slightly more negative and the P-Si

BCP Laplacian is slightly less negative, the P-S BCP is almost unchanged on going from a single bond to a double bond.

Since the Laplacian picks up subtle variations in the density, it is important to have an accurate density distribution before reading too much into the observed trends (or lack thereof). The MP2 values are generally much more negative than the HF values, with the exception of HP=PH. At the MP2 level, a different trend arises for P=M bonds: $\nabla^2\rho_b$ becomes more negative as the electronegativity increases, opposite to the trend for the P=L bonds. All these trends are consistent with the observed variations in bond polarity, as measured by bonding radii and atomic charges.

5.5.3. Ellipticity

The planar symmetries of these species are conducive to larger ellipticities than those found in the phosphines. Large ε values are typically taken as evidence of significant π-like bonding, with increased density in the π-bonding plane. Such bonding is certainly anticipated for these structures and the observed curvatures are oriented in the expected direction. The ellipticity values are reported in Tables 5-3 (HPX) and 5-4 (HNX).

The twisted $HPCH_2$ and $HPSiH_2$ geometries, and the hypervalent $HPSH_2$ species, have much lower ellipticities than the planar analogues. In $HPCH_2$ the softer curvature (broader density distribution) is in the plane containing the lone pairs on P and C and the H atom on P. In $HPSiH_2$ the softer curvature is in the plane containing the H atoms on Si and the 'lone pair(s)' on P, leaving a slightly narrower density in the plane containing the 'bridging' H atom. The P-S bond in $HPSH_2$ has a very large ellipticity and the softer curvature is in the hypothetical π-plane despite the apparent lack of a double bond, again associated with two non-bonding charge concentrations on P.

The observed ε values in the planar systems range from 0.12 in HP=O to 0.76 in $HP{=}SiH_2$. It is interesting that the highest electron density values are found in the bonds with the lowest ellipticities and most positive Laplacian values. The ε and $\nabla^2\rho_b$ values might be seen as evidence for near ionic character of P=O bonds, however, the high BCP density is indicative of a shared interaction. Electrostatic attraction shortens the very polar bond and reinforces the covalent interaction. This must be seen as a very polar covalent interaction. At the other extreme, the bond shortening and increase in ρ_b for P=Si bonds *vs.* P-Si bonds, with high ellipticity, seems to relate strongly to double bond character that could be described in terms of *p-p* π-like overlap.

The influence of lone pairs on the phosphorus atom may also serve to lower the BCP ellipticity, as these can extend into the bonding region, in directions orthogonal to the *p-p* overlap. As seen in section 5.2, the BCP moves from inside the valence shell of P in the P-O bond (where there is strong interaction with the lone pair and low ellipticity) to inside the valence shell of Si in the P-Si bonds (where the lone pair has little effect and the ellipticity is high).

5.6. Integrated populations and charges

Atomic and group charges and energies (K= -*E*) are given in Table 5-5 for phosphinylidenes and in Table 5-6 for imines. See Chapter 4 for the interpretation of the integrated Laplacian, L. The trends in the charges on the phosphorus atom and the substituent group are plotted in Figures A4-6 and A4-7, respectively.

5.6.1. Charges

Hydrogen atoms bonded to phosphorus accept approximately 0.6 electrons each, in line with the phosphine results. The second row phosphinylidenes, $HP=LH_{n-1}$, transfer from less-than-one up to one-and-a-half electrons across the P=L bond. The charge transfer in HP=S is similar to that in $HP=CH_2$. Symmetry requires that there is no charge transfer in HP=PH, except from P to H. One electron is transferred *to* phosphorus in $PH=SiH_2$.

Most of the substituent group charges q(X) in PH=X are from 65 to 85% larger in magnitude than q(R) in PH_2-R, but the charge on S is more than double that on SH. Whereas in the phosphines one pair of electrons is unequally shared, here two pairs of electrons are unequally shared, but the polarity per bonding pair has apparently decreased.

The combined effect of q(H) and q(X) is that q(P) ranges from -0.5 (X = SiH_2) to +2.0 (X = O). The charge on phosphorus in $HP=MH_{n-1}$ is similar to q(P) in the disubstituted phosphines, $HP(MH_n)_2$, as might be expected as a result of *two* polar P-M bonds and one P-H bond, while q(P) in $HP=LH_{n-1}$ is similar to q(P) in the monosubstituted phosphines, H_2P-LH_n, due to the above mentioned decrease in P-E bond polarity.

We saw in section 5.2 that MP2 correlation shifts the BCP towards a more central position, *i.e.* towards the more electronegative atom. The net effect is that about 0.3 electrons fewer electrons are transferred across the P=X bond at the MP2 level than at the Hatree-Fock level. This occurs even when both bonding radii are increased. The change due to correlation in the phosphines is about 0.1 electrons, so correlation decreases the difference in charge between the phosphine and the phosphinylidene, further lowering the charge ratio, q(X)/q(XH).

The twisted structures of $HPCH_2$ and $HPSiH_2$ transfer 0.3 and 0.2 additional electrons, respectively, to the more electronegative atom, relative to the planar systems. Amino-substitution of the phosphaalkene donates 0.6 electrons to the phosphorus atom, and removes a total of 1.6 electrons from the carbon atom as a result of the polar N-C bonds. Thus, while the transfer of density to P is presumably due to increased valence of the atom C when the lone pairs on N are shared, the net effect of amino-substitution is a decreased charge at carbon.

5.7. Localization and Delocalization

The trends in the delocalization index, δ(P,X), are plotted in Figure A4-8. The δ(P,X) values are given in Table 5-3a, with σ and π contributions enumerated separately in Table 5-3b. The δ(N,X) values are given in Table 5-4.

5.7.1. Comparison to phosphines

The percent localization of the P atom in phosphinylidenes ranges from 90% to 92%; slightly less than in the phosphines. The delocalization index between P and the directly bonded hydrogen atom ranges from 0.77 to 1.1, compared with 0.79 to 0.96 in the phosphines, probably due to the slightly higher population on P. The delocalization index δ(P,X) (including the substituent H atoms) ranges from 1.26 in HPO to 2.06 in HP=PH. In all cases this is 1.74 (O, S) to 1.86 (NH, PH) times the δ(P,R) values in the monosubstituted phosphines. If we consider only the substituent atom, the δ(P,E) ratio ranges from 1.78 for δ(P,O) to 2.37 for δ(P,Si).

As in the phosphine case, the non-polar HP=PH system reaches the ideal value of 2.0 for δ(P,PH) and in fact surpasses it, though this should decrease with correlation. Unlike the phosphine case, δ(P,S) does not attain this value. Again, δ(P,X) correlates well with q(X), though δ(P,CH_2) is an apparent outlier, having a somewhat low delocalization index for the degree of charge transfer.

5.7.2. Relationship to bond order

A plot of δ(P,X) and δ(N,X) *versus* q(X) is shown in Figure 5-1. The H_2PR and H_2NR series are shown for comparison, along with the ideal double bond curve. The HPX and HNX data have each been divided into two sets.

Set 1 of HPX includes all the planar systems except $HPCH_2$, which lies a little below the curve. Set 2 includes both the planar and pyramidal geometries of $HPCH_2$ and $HPSiH_2$. The curve for these four points lies very close to the curve for the linear systems. The best-fit equations for these two series are:

$\delta(\text{set 1}) = -0.4299q^2 - 0.0486q + 2.0507;\ R^2 = 0.9955$
$\delta(\text{set 2}) = -0.4002q^2 - 0.0197q + 1.9803;\ R^2 = 0.9980.$

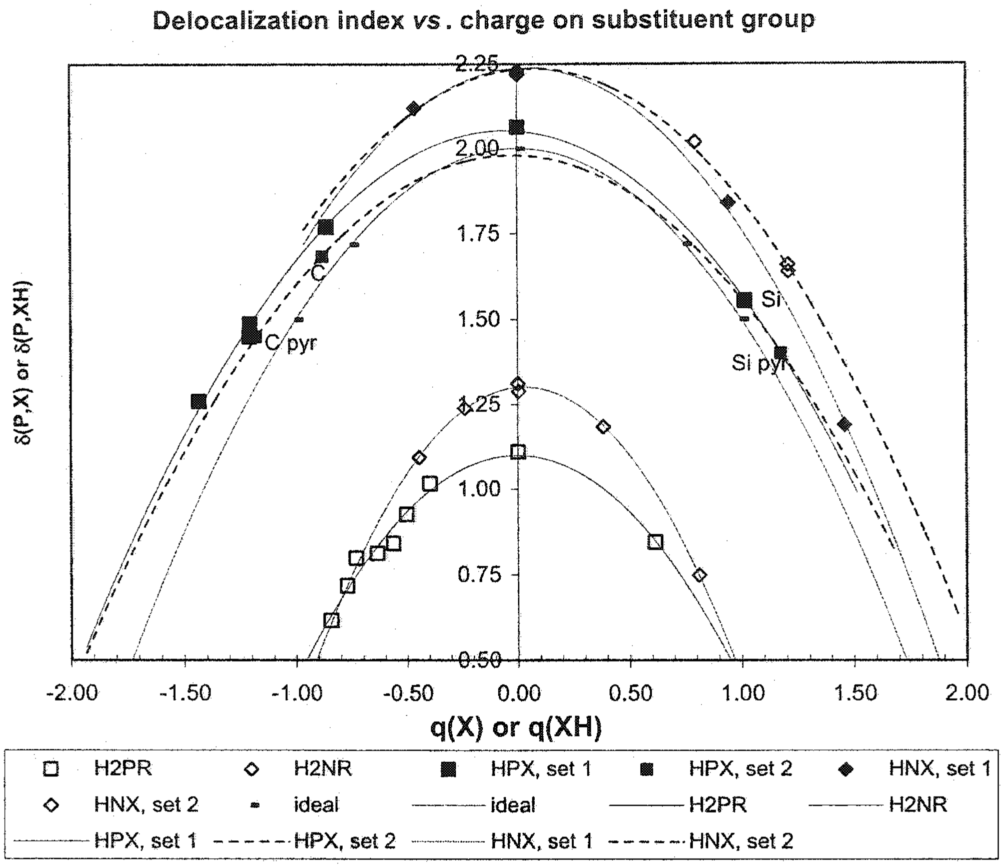

Figure 5-1: Plot of delocalization index *versus* charge transfer for PH_2R, NH_2R, HPX and HNX. The curves correspond to best-fit quadratic equations. The ideal curve, $\delta = 2 - 0.5q^2$, is also shown, for comparison. The doubly bonded series are each divided into two sets. **HPX set 1** includes X = O, NH (*cis* and *trans*), S, PH (*trans*), and *planar* SiH_2. **HPX set 2** includes X = CH_2, (*pyramidal* and *planar*) and SiH_2, (*pyramidal* and *planar*). **HNX set 1** includes X = O, NH (*cis* and *trans*), CH_2 and SiH_2. **HNX set 2** includes X = O, NH (*cis* and *trans*), S and PH (*cis* and *trans*). The H_2NH data set excludes R = SH, PH_2.

We see that these systems have a bond order of two, with a small excess delocalization, and the curve is shifted towards (electro)negative substituents. As in the phosphines, this may be associated with 'lone pair' delocalization. The second

HPX set, which includes high-energy C_s-twisted geometries, shows that a planar arrangement is not necessary for electron delocalization, only for energetic stabilization of the interaction.

Assuming that the delocalization maxima for HPX and the phosphines should be 2 and 1, respectively, and should occur when q(X) is zero, the fitting equations can be approximated as $\delta = 2 - 0.4q^2$ and $\delta = 1 - 0.7q^2$. Just as the phosphines can be described as involving polar single P-E bonds supplemented by delocalization of the lone pairs, the phosphinylidenes can be well described as having a polar double bond between P and a substituent atom. The involvement of lone pairs is smaller in these doubly bonded species. While the curvatures of these graphs are not those expected based on the derivations for the ideal cases, the relative curvatures for the phosphines and phosphinylidenes are in the expected 1:2 ratio.

Considering that phosphorus and sulphur substituents were left out of several other fitting procedures in this thesis, the HP=X fit was reconsidered. If instead of removing CH_2 we remove PH and S, the curve is still a good fit, giving $\delta(P,X) = -0.3409q^2 + 0.0242q + 1.9302$, or about $2 - 0.34q^2$. The slight drop below 2.0 could be explained by the loss of electron density to the H on phosphorus. The data points for X = PH and S both lie above this curve, giving additional delocalization from the readily available lone pairs.

The imine data are consistent with the amine results, as shown in Figure 5-1. Again the nitrogen analogues give a delocalization maximum about 0.2 higher than the phosphorus systems. While the HPX curve is shifted slightly towards negative charge transfer, the nitrogen analogue is shifted towards positively charged substituents. Because the S and PH substituents (set 2) have similar charges to the CH_2 and SiH_2 substituents (set 1) it is clear that they lie on two separate curves, with the NH and O ligands fitting equally well on either curve. Since both curves include the HN=NH and HN=O data near the maximum, they differ mainly in the curvature. The best-fit equations for the two sets of imine data are:

$$\delta(\text{set } 1) = -0.5158q^2 + 0.0412q + 2.2375;\ R^2 = 0.9984$$
$$\delta(\text{set } 2) = -0.4474q^2 + 0.0598q + 2.2350;\ R^2 = 0.9972.$$

Clearly, nitrogen systems involve more lone pair delocalization than phosphorus systems and this is reduced when the substituent atom is a group 4A element that does not have lone pairs to contribute. From the phosphine and amine data, it appears that P, S and N are better lone pair sharers than Cl, O and F. The first imine curve can be approximated as $\delta = 2.2 - 0.5q^2$. The approximate equation of the second set, with additional lone pair contributions, is $\delta = 2.2 - 0.4q^2$.

5.7.3. Separation into sigma (σ) and pi (π) components

It was found in the study by Fradera *et al.* (1999) that the when the delocalization index is separated into terms arising from π-like orbitals and σ-like orbitals, the σ-type delocalization is typically greater than the π-type delocalization. The discrepancy increases as the bond polarity increases. For example, in N_2 the σ contribution is 1.042 and each π component is 1.000, while in CO the σ contribution is 0.646 and each π component is 0.464. In the essentially ionic LiF, the contributions are 0.126 and 0.026, respectively. An exception is the slightly polar CN^-, which has a σ-delocalization of 0.734 and a slightly higher π-delocalization of 0.738.

For most of the relatively polar planar species in this investigation, the σ-delocalization is somewhat greater than the π-delocalization. The two contributions, and their ratio, are shown in Table 5-3b. In HPNH the π contribution is only 2% less than the σ contribution, but in $HPCH_2$ it is 10% *greater*. In the remaining systems, including the non-polar HPPH, the π- delocalization is 80(±5)% of the σ-delocalization. In all but $HPCH_2$, the σ-delocalization is quite similar to the total delocalization in the phosphines. In $HPCH_2$ the π contribution to the delocalization is quite similar to the phosphine delocalization. Within the MO model, the π-density is more localized on the more electronegative atom than is the shared σ-density. If the extra delocalization from σ-like lone pairs is accounted for, by subtracting 0.1 from the σ indices, then the π/σ ratio rises to greater than 90%.

5.8. Laplacian Distributions

Figure 5-4 shows contours of the Laplacian in the symmetry plane and has been introduced in section 5.4.

Figure 5-5 shows isovalue envelopes for the Laplacian scalar field, $\nabla^2\rho(\mathbf{r})$. The value plotted is $\nabla^2\rho(\mathbf{r}) = 0$, which is often associated with a so-called reactive surface. The position and some properties of the non-bonded charge concentration on phosphorus are given in Table 5-7. The corresponding imine data are in Table 5-8. The position and some properties of the P-E bonding charge concentrations are given in Table 5-9. Table 5-10 gives the properties of the non-bonding charge concentrations on the substituent atoms in the HPX systems.

5.8.1. Non-planar systems

The non-planar $PHCH_2$ has a single non-bonding CC on phosphorus, and a non-bonding concentration on carbon. This corresponds to a zwitterionic structure with the negative charge on the CH_2 group, $[HP^+\text{-}CH_2^-]$. Based on the good fit with the delocalization *vs.* charge transfer curve, the 'lone pair' on carbon may be significantly delocalized.

Non-planar $PHSiH_2$ and potentially 'hypervalent' $PHSH_2$ each have two symmetry equivalent non-bonded CCs on phosphorus, in and out of the plane. There is no non-bonding concentration on Si and only one on S. The two non-bonding CC's on the P atom correspond to two distinct electron pairs, as a single electron pair would be expected to lie in the symmetry plane, whether the P-E bond is single or double. These are zwitterionic structures with the negative charge on the PH group.

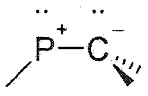

twisted

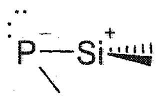

twisted

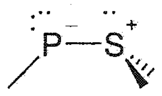

hypervalent

These high-energy zwitterionic structures arise when the *p-p* π-like interaction is interrupted. In each case, the resulting lone pair is found on the more electronegative group. Clearly C is more electronegative than P, leading to a tetrahedral arrangement of electron pairs in the valence shell of the carbon atom. Similarly, P is more electronegative than Si, so it accepts the non-bonding electron pair, leaving Si with three valence electron pairs, in a planar arrangement. Considering the position of the lone pairs on P, one could further suggest that there are three valence electron pairs in the valence shell of the phosphorus atom, and the fourth electron pair resides almost exclusively on the hydride, interacting from above the $PSiH_2$ plane, see Figure 5-4j and Table 5-7.

While S is more electronegative than P, the hypervalent $\{=:SH_2\}$ group is effectively less electronegative. Hypervalency is supported by bonds that are polar, with the bonding electrons pulled away from the hypervalent atom. Both P and H tend to donate charge to sulfur. The second 'bonding' electron pair is therefore donated from S to P. While the bond critical point is shifted towards P, relative to the H_2PSH, the net charge transfer across the P-S bond is nearly zero in this system, *i.e.* some electron density has been shifted towards phosphorus also. The bond is longer than in H_2PSH and the BCP density is even lower. This system does not form a double bond, and the extra pair of electrons resides on the tetrahedral, trivalent phosphorus atom. The effects of hypervalency will be discussed further in the next two chapters.

5.8.2. Planar Systems – general features

Looking at the isovalue envelopes, Figure 5-5, one of the first features that jump out is that in HPO and $HPSiH_2$ there are two distinct, unconnected regions: a PH region and an X region. The oxygen atom is nearly spherical, with a small bonding appendage. As in all of the phosphinylidenes, this bonding region is clearly elliptical, being much wider in the expected π-like plane. The SiH_2 group is reduced to a silicon core and two hydride valence regions. The bonding region of this molecule is connected to the valence shell of phosphorus, but seems to 'cradle' the silicon core with density in the silicon valence region.

We may also notice that the 'hydrides' attached to phosphorus and silicon look qualitatively different from the hydrogen atoms on N and C. Indeed, no bonding concentrations can be found in the P and Si valence shells corresponding to the hydride, while C and N show bonding CC's for the C-H and N-H bonds. The hydrogen atoms themselves have only one shell and the maximum is located at the nucleus regardless of the atomic charge.

Let us choose the non-polar HP=PH, Figure 5-5e, as a reference from which to discuss the trends through each period. The isosurface of the *trans* isomer might be described as S- or Z-shaped. As the human brain is designed to recognize faces, this imagery will be used to identify salient features. Turn the figure upside-down and look at the 'back' view, to see the faces. The lone pair on each phosphorus atom appears as a chin, above which there is a hint of a dimple. Above this, appears a smiling mouth (a region of electrophilicity) with puffy cheeks behind (the lone pair on the other P atom) and a bulbous nose in front is the hydride.

As the substituent becomes more electronegative, the chin juts upward; the dimple becomes a hole and the mouth on phosphorus gapes ever wider. The hydride nose does not appear to change significantly. Having mentioned that the lone pair 'chin' juts more upward as the substituent changes, it should be mentioned that the actual angle formed by E, P and the non-bonding maximum follows this trend only if we average the *cis* and *trans* values, see Table 5-7.

We may also consider the 'waist' of each molecule, which separates the valence region of the phosphorus atom from the valence region of the substituent atom. As the substituent becomes more electronegative, the waist becomes narrower, particularly in the wider, π-like, dimension. This supports the idea that the ratio of π-type to σ-type bonding is decreasing as the bond becomes more polar. In the exceptional $HP=CH_2$, the valence sphere is distorted, such that there is a depletion of charge in the π-like plane on the H side of C, and an extra concentration in the P-C π-bonding region.

5.8.3. Planar systems – bonding charge concentrations

A look at the bonding charge concentrations reveals a single charge concentration (CC), in the valence shell of the second row atom, for HPO, HPNH and $HPCH_2$. For the third row substituents there are two bonding CC's, one in the valence shell of each atom. There is a more obvious pattern here than in the phosphines.

Looking at the bonding CCs in the valence shell of phosphorus, we see that the maximum moves away from phosphorus as the BCP moves towards P, from E = Si to P to S. In the imines, the bonding CC on nitrogen is furthest from N in the non-polar HN=NH and closest to N in HN=PH. There is only minimal variation in the distance to N among the N=L bonds, and similar consistency among the N=M bonds. It is interesting that the maximum magnitude of the Laplacian does not correlate with its distance from N. This emphasizes the *bonding* nature of this charge concentration. The non-bonding concentrations do show a strong correlation between distance to the nucleus and the Laplacian and density values.

5.8.4. Planar systems – non-bonding charge concentrations

The non-bonded charge concentrations on the phosphorus atoms of the phosphinylidenes are very similar to those of the phosphines, in fact the 'lone pair' on a given $HP=EH_{n-1}$ is more similar (in terms of distance to the nucleus, density, Laplacian, *etc.*) to that of the corresponding $H_2P\text{-}EH_n$ and $P(EH_n)_3$ than to other phosphinylidenes.

Considering the similarities of the lone pairs in these species to the lone pairs in phosphines, it is not surprising that they undergo very similar reactions, including oxidative 1,1-addition and complexation to transition metals. Perhaps the presence of the double bond adds extra lability, allowing the addition reaction to begin at the electrophilic 'chin dimple' as well as at the nucleophilic lone pair.

Group 6A, having no substituent to sterically protect this electrophilic region, is so susceptible that no stable examples of the P^{III} species (YPO, YPS) are known.

The imine non-bonded charge concentrations on the nitrogen atoms are about 0.01 au closer to the nucleus than in the amines, so that $HN{=}CH_2$ most resembles NH_2NH_2 (and so on) in its lone pair properties. Interestingly $HNSiH_2$ follows this trend for $r(N\text{-}r_{nb})$ and for $\mu_3(\mathbf{r}_{nb})$ – being similar to NH_2PH_2 – but remains very similar to NH_2SiH_2 in its density and Laplacian values at the non-bonded charge concentration.

In each of the planar systems, we see one non-bonding charge concentration on phosphorus and the expected number on the substituent atom (two minus the number of E-H bonds), confirming the doubly bonded nature of these species. In HPO and HPS there are two distinct non-bonding maxima in the valence shell of the terminal E atom. The density and Laplacian at the saddle points on oxygen are very similar to those properties at the P-O bonding concentration and much smaller than the values at the non-bonding concentrations.

5.9. Conclusions

Based on the delocalization index *versus* charge transfer curves, Figure 5-1, we can conclude that the planar species, HPX and HNX, all involve the (unequal) sharing of two Lewis pairs of electrons between P and X, or N and X. In comparison to the singly bonded phosphines and amines, the bonds are shorter and the BCP density and ellipticity are higher. Within each series, the delocalization index decreases as the charge transfer increases demonstrating the predicted quadratic relationship. Both q(X) and δ(P,X) are somewhat less than double the phosphine values, q(R) and δ(P,R). While the P=C bond is apparently the most stable (commonly isolable) of the P^{III}=E bonds, the delocalization index is small for the polarity of this bond, falling below the best-fit parabola for the other species. This may be due to a lack of lone pair delocalization, as suggested by the unusually high $\delta^{\pi}/\delta^{\sigma}$ ratio. Among the planar $HP{=}EH_{n-1}$ species studied here the chalcogens (and particularly S) have the largest increase in charge transfer and the smallest increase in delocalization index relative to the mono-substituted phosphines, H_2P-EH_n.

The delocalization index increases by a smaller factor between the amines and the imines than for the phosphorus species. The charge transfer increases by a comparable factor. This is probably due to the additional lone pair delocalization, which does not get doubled when the bond order doubles, and in fact seems to be reduced, based on the maximum delocalization observed in each series.

5.10. Additional figures

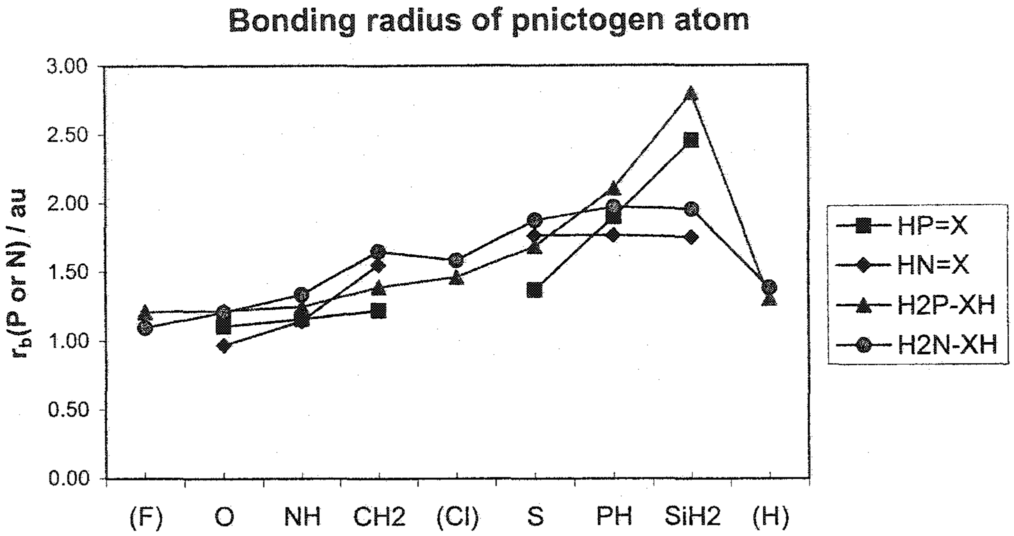

Figure 5-2: Bonding radius of the central pnictogen atom (P or N) in single (H_2PR and H_2NR) and double (HPX and HNX) bonds.

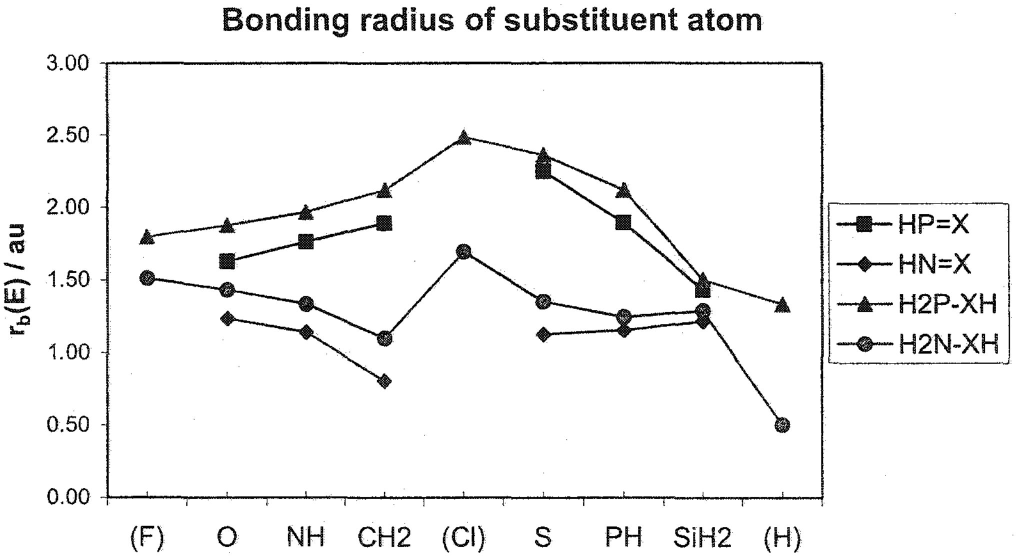

Figure 5-3: Bonding radius of the substituent atom (E) in single (H_2PR and H_2NR) and double (HPX and HNX) bonds.

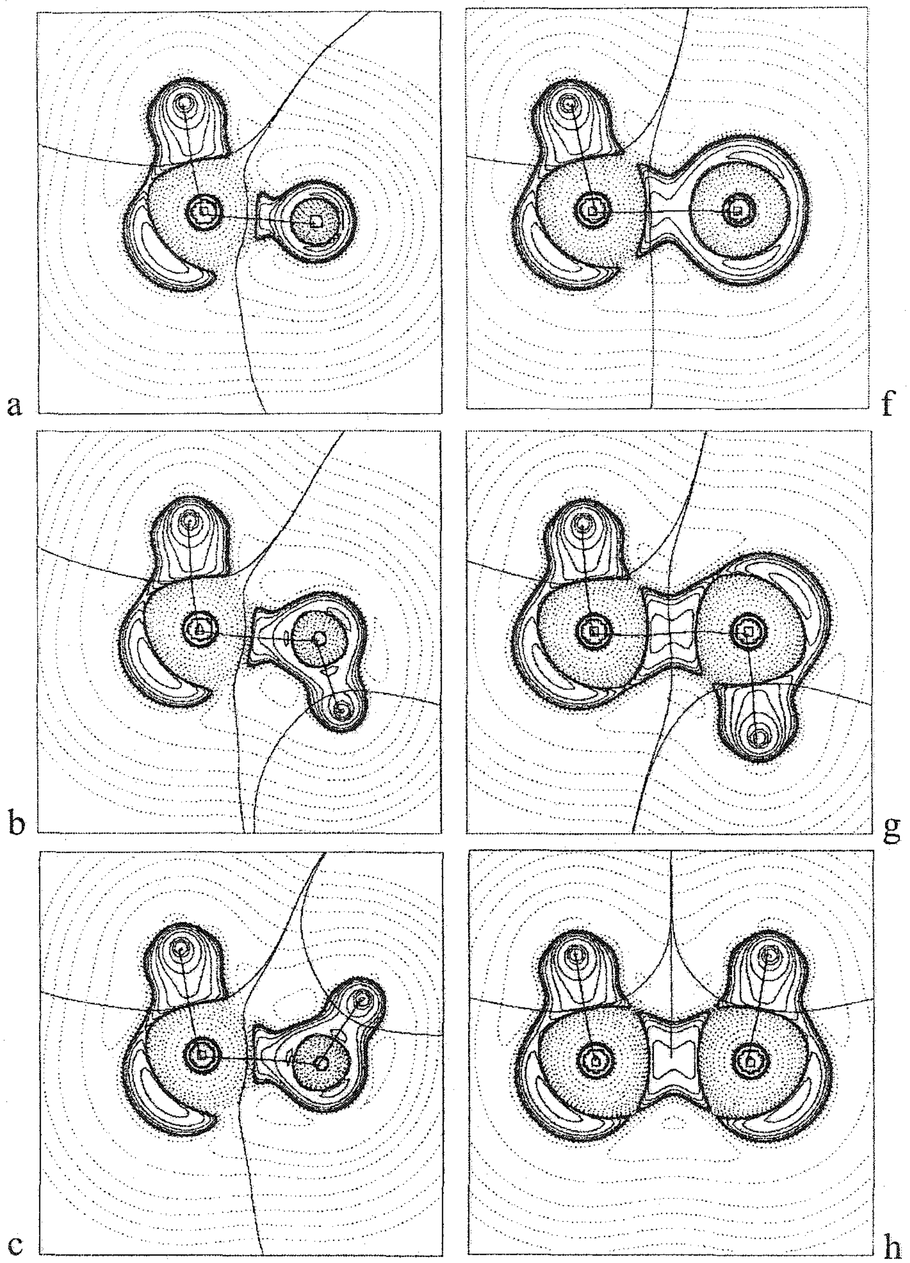

Figure 5-4: Continued on next page.

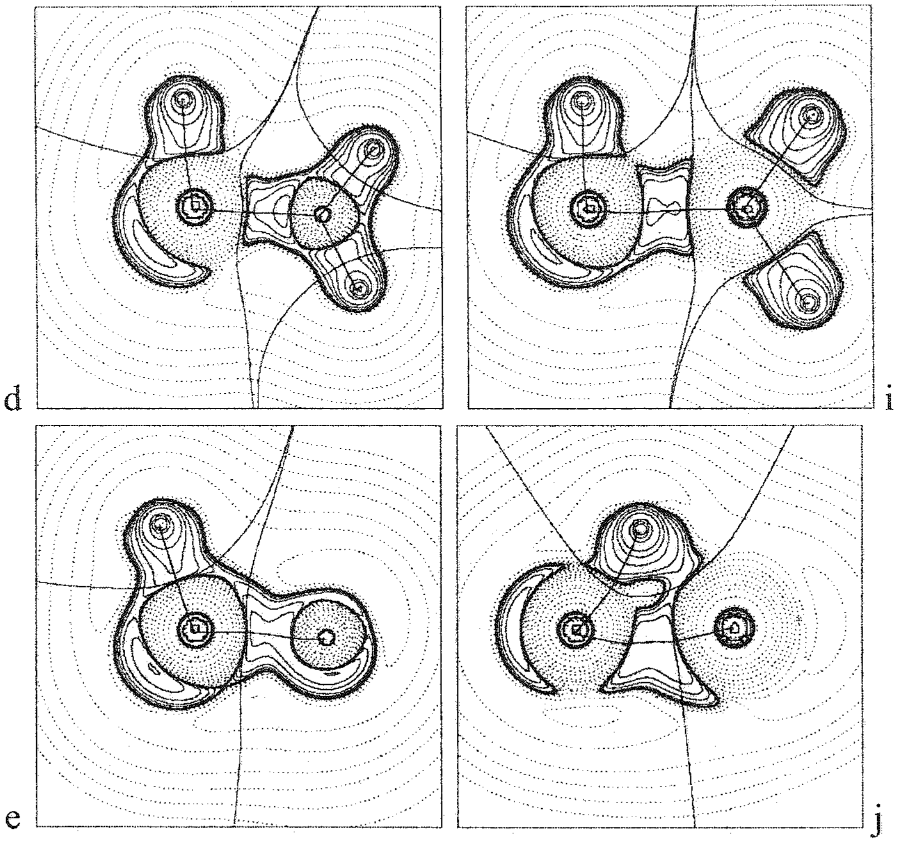

Figure 5-4: Contour maps of $\nabla^2\rho(\mathbf{r})$ in the symmetry plane of HPX: **a**) HPO, **b**) HPNH *trans*, **c**) HPNH *cis*, **d**) $HPCH_2$ *planar* **e**) $HPCH_2$ *twisted*, **f**) HPS, **g**) HPPH *trans*, **h**) HPPH *cis*, **i**) $HPSiH_2$ *planar* **j**) $HPSiH_2$ *twisted*. Solid contours indicate negative values (concentration) and dashed lines indicate positive values (depletion). The outermost contour is +0.002 au. Isovalue contours increase and decrease from the $\nabla^2\rho(\mathbf{r}) = 0$ contour in the order $\pm2\times10^n$, $\pm4\times10^n$, $\pm8\times10^n$, beginning with $n = -3$ and increasing in steps of unity. Each map is overlaid with the bond paths and with the intersection of the interatomic surfaces with the displayed plane.

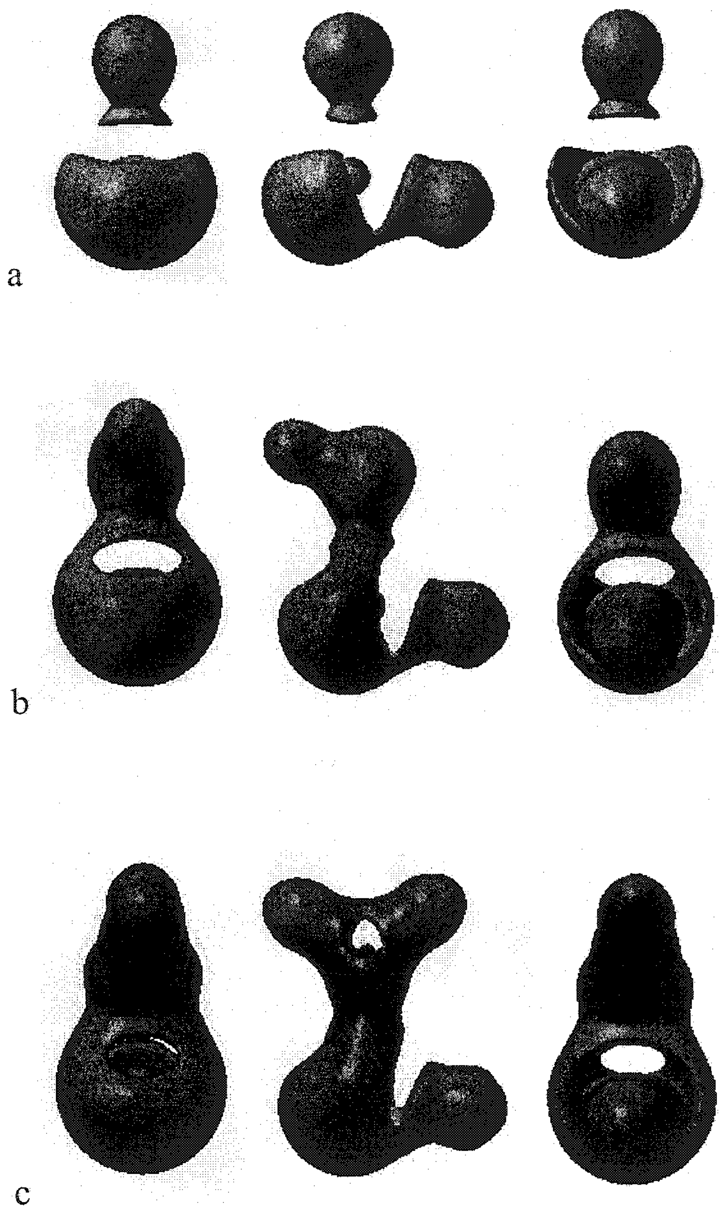

Figure 5-5: Continued on next page.

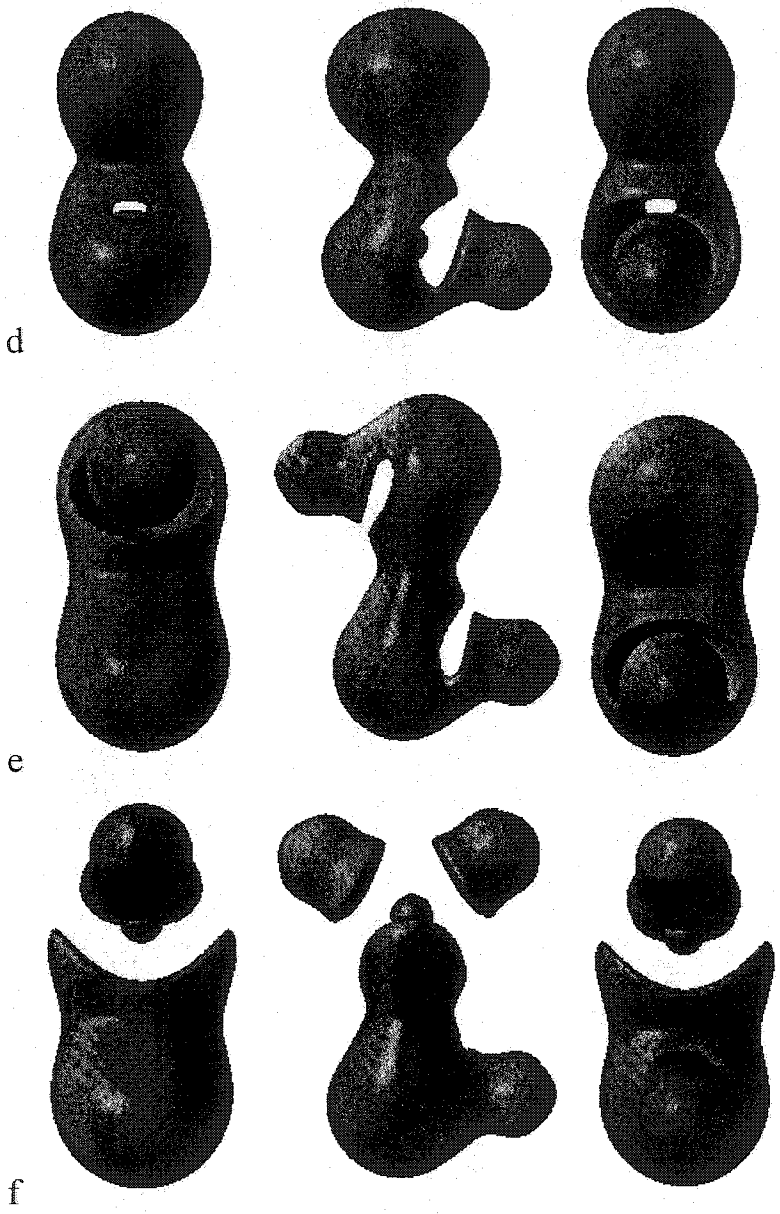

Figure 5-5: Isovalue envelopes of $\nabla^2\rho(\mathbf{r}) = 0$; ‘front’, ‘side’ and ‘back’ views of planar HPX: **a**) HPO, **b**) HPNH *trans*, **c**) $HPCH_2$, **d**) HPS, **e**) HPPH *trans*, **f**) $HPSiH_2$.

5.11. Data Tables

Table 5-1: Optimized geometries of phosphinylidenes and related systems, $HP=EH_{n-1}$, at HF/6-311++G(2d,2p) and at MP2 (in italics). Related experimental values are given where available.

Phosphinylidene	**r(P-E)**	**r(P-H)**	**∠ HPE**	**-Energy /au**
HP=O	144.80	143.85	104.78	416.18896
	150.10	*144.81*	*104.27*	*416.69383*
CASPT2[a]	*149.0*	*145.2*	*104.1*	
Exp't [b]	148.0 ± .5	145.6 ± .3	103.5 ± 2.5	
HP=NH *trans*	154.40	141.61	100.14	396.33674
	159.55	*141.99*	*97.85*	*396.81758*
Deriv. Exp't[c]	(155.6 ± .5)		(100.6 ± .3)	
HP=NH *cis*	153.80	143.14	105.06	396.33511
	158.44	*143.78*	*104.88*	*396.81522*
$HP=CH_2$	164.61	141.03	99.03	380.33111
	167.03	*141.34*	*96.89*	*380.77476*
Exp't[d]	167.3 ± 2	142.0 ± .6	97.4 ± .4	
Exp't[e]	167.1 ± .1	142.5 ± .2	95.5 ± .3	
$HP\text{-}CH_2$ *twisted*[f]	168.43	145.33	111.54	380.18792
HP=S	191.43	141.70	102.67	738.84983
	196.06	*142.52*	*101.39*	*739.38965*
HP=PH *trans*	200.41	140.83	95.87	682.62921
	205.33	*141.42*	*93.18*	*683.16173*
Deriv. Exp't[g]	(203.4 ± .2)		(102.8 ± .1)	
HP=PH *cis*	201.27	140.63	100.45	682.62357
	206.41	*141.12*	*98.04*	*683.15538*
$HP=SiH_2$	205.84	140.95	92.29	631.39190
	208.07	*141.52*	*88.03*	*631.90264*
Deriv. Exp't[h]	(209.4 ± .3)		(104.2 ± .2)	
$HP\text{-}SiH_2$ *twisted*[i]	206.41	155.48	56.2	631.34843
$HP\text{-}SH_2$	218.51	140.86	92.95	739.96259
$HP=C(NH_2)_2$	175.42	140.78	94.60	490.45163

- Bond lengths in picometers and angles in degrees.

a) Luna, Merchan and Roos (1995). CASPT2 calculations.
b) *Rotational analysis of vibrational bands in the 520 nm emission system of phosphorus oxyhydride.* Larzilliere, Damany and My (1980).
c) *X-ray for* ***Mes*P=N^{t}Bu*** Chernega, *et al.* (1987).
d) Kroto *et al.* (1981). Microwave.
e) Brown *et al.* (1981). Microwave.
f) The sum of the angles about C is 320.68°.
g) *X-ray for* ***Mes*P=PMes**** Yoshifuji *et al.* (1981).
h) *X-ray for* ***Mes*P=Si(^{t}Bu)(PMes*-PPh$_2$)*** Bender *et al.* (1993). Slightly pyramidal Si. Others difficult to crystallize – oils.
i) The sum of the angles about Si is 359.42°.

Table 5-2: Optimized geometries of imines, $HN{=}EH_{n-1}$, at HF/6-311++G(2d,2p). Related experimental values are given where available.

Imine	**r(N-E)**	**r(N-H)**	**∠ HNE**	**-Energy /au**
HN=O	116.78	102.87	109.24	-129.83419
Exp't[a]	120.58 ± .27	106.28 ± .25	109.09 ± .24	
HN=NH *trans*	120.95	101.08	108.12	-110.03826
HN=NH *cis*	121.11	101.42	112.84	-110.02786
$HN{=}CH_2$	124.70	100.26	111.78	-94.06585
Exp't[b]	127.3 ± .4	102.3 ± 2.0	110.5 ± 1.5	
HN=S	152.85	100.58	111.12	-452.51152
HN=PH *trans*	154.40	100.18	112.42	-396.33674
HN=PH *cis*	153.80	99.84	118.87	-396.33511
$HN{=}SiH_2$	156.77	99.35	125.54	-345.10854
Deriv. Exp't[c]	(156.8 ± .3)			

- Bond lengths in picometers and angles in degrees.

a) Hirota, Eizi (1986). Microwave.
b) Pearson, R. and F.J. Lovas (1977). Microwave.
c) *For* $(t\text{-}Bu)_3Si\text{-}N{=}Si(t\text{-}Bu)_2$: Wiberg *et al.* (1986). The SiNSi angle is 177.8 ± .3.

Table 5-3a: Properties of P-E BCPs in $HPEH_{n-1}$ systems. MP2 values in italics.

Phosphinylidene	$\rho(r_b)$	$\nabla^2\rho(r_b)$	$\varepsilon\ (r_b)$	$r(P\text{-}r_b)$	$r(E\text{-}r_b)$	**δ(P,E)**	**δ(P,X)**	**Ratio to H_2PEH_n**
HP=O	0.257 *0.225*	+1.593 *+1.079*	0.117 *0.073*	1.108 *1.149*	1.629 *1.688*	1.260	1.26	1.75
HP=NH *trans*	0.226 *0.203*	+0.809 *+0.455*	0.293 *0.215*	1.157 *1.203*	1.761 *1.813*	1.459	1.49	1.86
HP=NH *cis*	0.227 *0.206*	+0.827 *+0.493*	0.302 *0.227*	1.156 *1.198*	1.752 *1.798*	1.434	1.47	1.84
$HP{=}CH_2$	0.198 *0.188*	+0.264 *+0.081*	0.485 *0.366*	1.220 *1.261*	1.891 *1.896*	1.581	1.68	1.82
HP=S	0.167 *0.151*	-0.180 *-0.196*	0.310 *0.182*	1.366 *1.567*	2.251 *2.138*	1.771	1.77	1.74
HP=PH *trans*	0.153 *0.135*	-0.235 *-0.153*	0.503 *0.335*	1.894 *1.940*	1.894 *1.940*	1.912	2.06	1.86
HP=PH *cis*	0.151 *0.133*	-0.230 *-0.150*	0.521 *0.348*	1.902 *1.950*	1.902 *1.950*	1.892	2.04	1.84
$HP{=}SiH_2$	0.122 *0.114*	-0.015 *-0.074*	0.758 *0.638*	2.455 *2.431*	1.435 *1.501*	1.226	1.55	1.84
$HP{=}C(NH_2)_2$	0.158	+0.245	0.633	1.267	2.048	1.211	1.51	1.63
$HP\text{-}CH_2$ twisted	0.208	-0.283	0.189	1.285	1.902	1.164	1.34	1.45
$HP\text{-}SiH_2$ twisted	0.116	-0.076	0.076	2.456	1.487	0.920	1.18	1.40
$HP\text{-}SH_2$	0.090	+0.013	1.770	1.528	2.594	0.976	1.09	1.03

- All properties, including distances from nuclei to BCPs, are in atomic units.
- Delocalization indices for Hartree-Fock results only.
- The ratios relative to the phosphines are for the indices, $\delta(P,EH_{n-1})$ *vs.* $\delta(P,EH_n)$
- The delocalization index between Si and its H atoms, in twisted $HPSiH_2$ is 0.526. The delocalization between Si and the bridging H is 0.245. For (P,H) the delocalization indices are 1.006 and 0.131.

Table 5-3b: Delocalization indices, separated into σ and π contributions.

Phosphinylidene	δ^{σ} (P,X)	δ^{π} (P,X)	Ratio π to σ
HP=O	0.719	0.541	0.75
HP=NH *trans*	0.752	0.735	0.98
HP=CH_2	0.800	0.884	1.10
HP=S	0.991	0.781	0.79
HP=PH *trans*	1.128	0.935	0.83
HP=SiH_2	0.858	0.696	0.81
HP-CH_2 *twisted*	1.087	0.253	0.23

Table 5-4: Properties of N-E bond critical points in imines, NH=EH_{n-1}.

Imine	**ρ(r_b)**	**$\nabla^2\rho(r_b)$**	**ε (r_b)**	**r(N-r_b)**	**r(E-r_b)**	**δ(N,E)**	**δ(N,X)**	**Ratio to H_2NEH_n**
HN=O	0.575	-1.984	.087	0.970	1.237	2.120	2.12	1.71
HN=NH *trans*	0.526	-1.682	.162	1.143	1.143	2.174	2.23	1.70
HN=NH *cis*	0.521	-1.643	.170	1.145	1.145	2.152	2.22	1.69
HN=CH_2	0.415	-0.929	.248	1.548	0.809	1.620	1.84	1.55
HN=S	0.266	+0.284	.161	1.760	1.129	2.015	2.02	1.61
HN=PH *trans*	0.226	+0.809	.293	1.761	1.157	1.459	1.66	1.50
HN=PH *cis*	0.227	+0.827	.302	1.752	1.156	1.434	1.64	1.49
HN=SiH_2	0.183	+1.065	.238	1.745	1.220	0.879	1.19	1.59

- All properties, including distances, are in atomic units.
- The ratios relative to the amines are for the delocalization indices, δ(N,EH_{n-1}) *vs.* δ(N,EH_n).

Table 5-5a: Atomic and group properties of phosphinylidenes, HP=EH_{n-1}. MP2 values in italics.

Phosphinylidene	**q(P)**	**q(E)**	**q(X)**	**K(P)**	**L (P)**	**L (E)**	**Ratio to H_2PEH_n**
HP=O	+2.030 *+1.721*	-1.434 *-1.210*	-1.434 *-1.210*	339.922 *340.305*	2.1 e-3 *-1.4 e-4*	-1.9 e-4 *-6.1 e-5*	1.86 *1.70*
HP=NH *trans*	+1.798 *+1.510*	-1.589 *-1.348*	-1.206 *-0.999*	340.025 *340.407*	1.7 e-3 *1.3 e-4*	-4.6 e-4 *1.5 e-4*	1.65 *1.53*
HP=NH *cis*	+1.812 *+1.537*	-1.609 *-1.380*	-1.208 *-1.016*	340.019 *340.398*	-1.9 e-3 *1.2 e-3*	-2.8 e-3 *2.9 e-4*	1.65 *1.55*
HP=CH_2	+1.470 *+1.249*	-0.925 *-0.835*	-0.880 *-0.746*	340.168 *340.533*	1.5 e-3 *-2.1 e-4*	-1.8 e-4 *-8.4 e-4*	1.75 *1.93*
HP=S	+1.437 *+1.004*	-0.862 *-0.515*	-0.862 *-0.515*	340.167 *340.593*	-2.9 e-4 *-1.2 e-3*	-6.1 e-4 *-6.7 e-4*	2.17 *1.72*
HP=PH *trans*	+0.572 *+0.483*	+0.572 *+0.434*	0.000 *0.000*	340.516 *340.812*	-1.4 e-3 *3.5 e-4*	-1.4 e-3 *3.5 e-4*	-
HP=PH *cis*	+0.570 *+0.480*	+0.570 *+0.480*	0.000 *0.000*	340.513 *340.808*	-8.8 e-3 *-1.1 e-3*	-8.8 e-3 *-1.1 e-3*	-
HP=SiH_2	-0.461 *-0.294*	+2.462 *+2.099*	+1.015 *+0.746*	340.828 *341.051*	4.9 e-4 *-7.4 e-4*	1.3 e-3 *3.1 e-4*	1.66 *1.45*

- The ratios relative to the phosphines are for the group charges, q(EH_{n-1}) *vs.* q(EH_n).
- P_2H_2: P charges recorded as negative of H charges, since these are determined more accurately. Charge transfer should be 0.000 by symmetry; actual sum of charges is non-zero.

Table 5-5b: Atomic and group properties of other HP=EH_{n-1} species

Phosphinylidene	**q(P)**	**q(E)**	**q(X)**	**K(P)**	**L (P)**	**L (E)**	**Ratio to H_2PEH_n**
HP=$C(NH_2)_2$	+0.844	+0.672	-0.246	340.357	-2.4 e-3	-8.3 e-4	0.49
HP-CH_2 twisted	+1.761	-1.198	-1.179	340.059	7.1 e-4	-1.3 e-3	2.34
HP-SiH_2 twisted	-0.639	+2.604	+1.174	340.895	-4.8 e-3	7.7 e-5	2.08
PH-SH_2	+0.508	+0.268	+0.080	340.434	-3.0 e-3	3.1 e-3	-0.20

Table 5-6: Atomic and group properties in imines, NH=EH_{n-1}.

Imine	**q(N)**	**q(E)**	**q(X)**	**K(N)**	**L (N)**	**L (E)**	**Ratio to H_2NEH_n**
HN=O	+1.577	-0.464	-0.464	54.214	1.4e-4	2.4e-5	1.94
HN=NH *trans*	-0.341	-0.341	0.000	54.511	9.4e-5	9.4e-5	-
HN=NH *cis*	-0.315	-0.315	0.000	54.495	-7.8e-5	-7.8e-5	-
HN=CH_2	-1.290	+0.973	+0.944	55.064	2.9e-4	9.9e-4	2.47
HN=S	-1.194	+0.797	+0.797	54.896	-5.3e-3	-1.1e-4	1.93
HN=PH *trans*	-1.589	+1.798	+1.206	55.019	-4.6e-4	1.7e-3	1.65
HN=PH *cis*	-1.609	+1.812	+1.208	55.035	-2.8e-3	-1.9e-3	1.65
HN=SiH_2	-1.852	+2.899	+1.458	54.966	-9.8e-5	1.4e-3	1.80

- The ratios relative to the amines are for the group charges, q(EH_{n-1}) *vs*. q(EH_n).
- *Trans* N_2H_2: N charges recorded as negative of H charges, since these are determined more accurately.

Table 5-7: Properties of non-bonded charge concentrations on P in phosphinylidenes, compared to phosphine.

Phosphinylidene	**r(P-r_{nb})**	**$\nabla^2\rho(r_{nb})$**	**$\rho(r_{nb})$**	**$\mu_3(r_{nb})$**	**E angle**	**H angle**
PH_3	1.443	-0.340	0.132	-9.58		
HP=O	1.422	-0.401	0.143	-11.25	133.6	121.6
HP=NH *trans*	1.434	-0.360	0.136	-10.23	135.5	124.4
HP=NH *cis*	1.430	-0.368	0.137	-10.53	131.7	123.3
HP=CH_2	1.446	-0.315	0.129	-9.27	134.3	126.7
HP=S	1.433	-0.354	0.135	-10.25	134.4	122.9
HP=PH *trans*	1.451	-0.294	0.124	-8.85	138.8	125.3
HP=PH *cis*	1.448	-0.303	0.126	-9.09	133.4	126.2
HP=SiH_2	1.465	-0.245	0.116	-7.81	139.7	128.0
HP-SiH_2 twist	1.472	-0.248	0.118	*1.43 au in and out of plane*		

- Distances from nuclei to maxima in atomic units.
- Angles between the maximum, the P nucleus and the attached atoms are shown in degrees.

Table 5-8: Properties of non-bonded maxima on N in imines, compared to amine.

Imine	**r(N-r$_{nb}$)**	**$\nabla^2\rho(r_{nb})$**	**$\rho(r_{nb})$**	**$\mu_3(r_{nb})$**
NH_3	0.748	-2.65	0.556	-165.7
HN=O	0.717	-4.02	0.653	-235.2
HN=NH *t*	0.727	-3.48	0.616	-208.4
HN=NH *c*	0.725	-3.58	0.625	-214.1
HN=CH_2	0.738	-2.98	0.580	-185.4
HN=S	0.728	-3.34	0.608	-204.1
HN=PH *t*	0.743	-2.73	0.559	-175.2
HN=PH *c*	0.743	-2.72	0.560	-173.7
HN=SiH_2	0.759	-2.18	0.513	-148.4

- All properties, including distances from nuclei to maxima, are in atomic units.

Table 5-9: Properties of P-E bonding maxima in phosphinylidenes.

Phosphinylidene	**r(P-r$_b$)**	**r(E-r$_b$)**	**$\nabla^2\rho(r_b)$**	**$\rho(r_b)$**
HP=**O**	2.041	0.698	-3.63	0.809
HP=**NH** *trans*	2.123	0.798	-2.25	0.516
HP=**NH** *cis*	2.119	0.798	-2.23	0.515
HP=**CH**$_2$	2.171	0.940	-1.20	0.314
HP=**S**	2.240	1.379	-0.378	0.201
HP=**PH** *trans*	2.257	1.532	-0.293	0.156
HP=**PH** *cis*	2.270	1.534	-0.290	0.154
HP=**SiH**$_2$	2.146	1.744	-0.209	0.126
HP=S	1.521	2.097	-0.277	0.168
HP=PH *trans*	1.532	2.257	-0.293	0.156
HP=SiH$_2$	1.565	2.328	-0.240	0.138
HP-SiH$_2$ *twist*	1.580	2.446	-0.184	0.126
HP-**SiH**$_2$ *twist*	2.329	1.705	-0.190	0.115

- The bolded element is the atom in whose valence shell the charge concentration is located.
- The shaded rows correspond to the maxima in the valence shells of substituent atoms.
- All properties, including distances from nuclei to maxima, are in atomic units.

Table 5-10: Properties of non-bonding maxima on substituent atoms, E, in $HPEH_{n-1}$ systems.

Phosphinylidene	**r(E-r$_b$)**	**$\nabla^2\rho(r_b)$**	**$\rho(r_b)$**	**Z**
HP=O	0.651 0.653	-5.036 -4.989	0.915 0.912	0 0
HP=NH *trans*	0.743	-2.732	0.559	0
HP=NH *cis*	0.743	-2.720	0.560	0
HP=S	1.302 1.300	-0.549 -0.567	0.191 0.194	0 0
HP=PH *trans*	1.451	-0.294	0.124	0
HP=PH *cis*	1.448	-0.303	0.126	0
HP-CH_2 *twist*	0.914	-0.848	0.264	0
HP-SH_2	1.281	-0.702	0.209	0

- All properties, including distances, are in atomic units.
- Z is the distance from the maximum to the molecular symmetry plane.

Bibliography

References are listed alphabetically by first author and then by date, with the references in the Data Tables sections listed separately.

Appel, R., J. Menzel, F. Knoch, P. Volz (1986). *Z. Anorg. Allg. Chem.* **534**, 100.

Appel, R. (1990). *Phosphaalkenes, Phosphacarbaoligoenes, and Phosphaallenes* Chapter D4 in Multiple Bonds and Low Coordination in Phosphorus Chemistry, Chapter D4, M. Regitz and O.J. Scherer, editors. Stuttgart: Verlag.

Arduengo *et al.* (1997*a*). *J. Chem. Soc. Chem. Commun.* **1997**, 981.

Arduengo *et al.* (1997*b*). *Inorg.Chem.* **36**, 2151.

Binnewies, M., B. Solouki, H. Bock, R. Becherer and R. Ahlrichs (1984). *Angew. Chem. Int. Ed. Engl.* **23**, 731.

Cowley, A.H. (1986). *Phosphorus and Sulfur* **26**, 31, and references therein.

DeFrees, D.J.; B.A. Levi, S.K. Pollack, W.J. Hehre, J.S. Binkley and J.A. Pople (1979). *J. Am. Chem. Soc.* **101**(15), 4085.

Fradera, X.; M.A. Austen, R.F.W. Bader, (1999). *J. Phys. Chem. A* **103**, 304.

Gillespie, R.J. and E.A. Robinson (1998). *Adv. Mol. Struct. Res.* **4**, 1.

Gusel'nikov, L.E. and N. S. Nametkin (1979). *Chem. Rev.* **79**, 529

Kutcha, M.C. and G. Parkin (1998). *Coord. Chem. Rev.* **176**, 323.

Lacombe, S., D. Gorbeau, J.-L. Cabioch, B. Pellerin, J.-M. Denis and G. Pfister-Guillozo (1988). *J. Am. Chem. Soc.* **110**, 6964.

Larzilliere, M., N. Damany and L.T. My (1980). *Chem. Phys.* **46**, 401.

Luna, A., M. Merchan and B.O. Roos (1995). *Chem. Phys.* **196**, 437.

Malcolm, N.O.J.; R.J. Gillespie and P.L.A. Popelier (2002). *J. Chem. Soc., Dalton Trans.* **2002** 3333.

Nagase, S., S Suzuki and T Kurakake (1990). *J. Che. Soc. Chem. Commun.* **1990**, 1724.

Niecke, E. (1990). *Iminophosphines*, Chapter D8 in Multiple Bonds and Low Coordination in Phosphorus Chemistry, M. Regitz and O.J. Scherer, editors. Stuttgart: Verlag.

Neicke, E. and D. Gudat (1991). *Angew. Chem. Int. Ed. Engl.* **30**, 217.

Noury, S; B. Silvi and R.J. Gillespie (2002). *Inorg. Chem.* **41**, 2164.

Power, P.P. (1999). *Chem. Rev.* **99**, 3463.

Regitz, M. and O.J. Scherer editors. (1990). Multiple Bonds and Low Coordination Chemistry in Phosphorus Chemistry. Stuttgart: Georg Thieme Verlag.

Saito, S.; Y. Endo and E. Hirota, (1986). *J. Chem. Phys.* **84**, 1157.

Scherer, O. and M. Regitz (1990). *Historical Introduction*, Chapter A in Multiple Bonds and Low Coordination in Phosphorus Chemistry, M. Regitz and O.J. Scherer, editors. Stuttgart: Verlag.

Schoeller, W.W. (1990). *Double Bonded Phosphorus,* Chapter B5 in Multiple Bonds and Low Coordination in Phosphorus Chemistry, M. Regitz and O.J. Scherer, editors. Stuttgart: Verlag.

Schoeller, W.W.; T. Busch, E. Niecke (1990). *Chem. Ber.* **123**, 1653.

Schoeller, W.W.; C. Begemann, U. Tubbesing and J. Strutwolf, (1997). *J. Chem. Soc., Faraday Trans.* **93**, 2957.

Yoshifuji, M.; K. Toyota, K, Shibayama, N. Inamoto (1983). *Chem. Lett.* **1983**, 1183.

Yoshifuji, M.; K. Toyota, K, Shibayama, N. Inamoto (1985). *Tetrahedron Lett.* **26**, 1727.

Zurmühlen, F. and M. Regitz (1987). *Angew. Chem. Int. Ed. Engl.* **26**, 83.

Table References

Bender, H.R.G.; E. Niecke and M. Nieger (1993). *J. Am. Chem. Soc.* **115**, 3314.

Brown, R.D.; P.D. Godfrey and D. McNaughton (1981). *Aust. J. Chem.* **34**, 465.

Chernega, A.N.; M.Y. Antipin, Y.T. Struchkov, A.V. Ruban and V.D. Romanenko (1987). *Zh. Strukt. Khim. (J. Struct. Chem)* **28**, 105.

Hirota, E. (1986). *Nippon Kagaku Kaishi* **11**, 1438.

Kroto, H.W.; J.F. Nixon and K. Ohno (1981). *J. Mol. Spectrosc.* **90**(2), 367.

Larzilliere, M.; N. Damany and Lam Thanh My (1980). *Chem. Phys.* **46**, 401.

Luna, A.; M. Merchan and B.O. Roos (1995). *Chem. Phys.* **196**, 437.

Pearson, R. and F.J. Lovas (1977). *J. Chem. Phys.* **66**, 4149.

Wiberg, N., K. Schirz, G. Reber and G. Muller (1986). *J. Chem. Soc. Chem. Commun.* **1986**, 591.

Yoshifuji, M.; I. Shima, N. Inamoto, K. Hirotsu and T. Higuchi (1981). *J. Am. Chem. Soc.* **103**, 4587.

6. Phosphorane Results

6.1. General bonding considerations

We can define the *valence* of an atom (with a formal charge of zero) as the number of (Lewis) bonds formed (coordination is the number of atoms bonded) to that atom. The typical valence for main group elements is the *smaller of* group number (#A) and eight minus group number (8-#). We then define hypervalence as a valence greater than this typical valence (Musher, 1969). Similarly, one could define hypovalence as a valence less than this same number. An alternative definition identifies a hypervalent atom as one with more than four pairs of electrons in its valence shell (Noury *et al.*, 2002). The phosphorus atom in PCl_5 would be hypervalent under either of these definitions, forming five bonds with five pairs of valence electrons.

Phosphoranes, $Y_3P{=}X$, have a four coordinate phosphorus atom that is formally pentavalent. This is a higher valence than 'normal' trivalent phosphorus, but such 'hypervalence' is not uncommon for atoms of the third and higher rows. Pentacoordinate phosphorus halides, such as PCl_5, are well known and hexacoordinate forms, such as in solid $PCl_4^+PCl_6^-$, also exist. While hypervalent compounds have previously been explained by occupation of *d* orbitals, it is now fairly well established that the inclusion of high energy *d*-polarized basis functions are important for a sufficiently flexible basis set but their occupation is quite low for non-metal atoms. Therefore, hybridization such as sp^3d^n is not an appropriate description of the bonding in these molecules (Gilheany, 1994).

Molecular orbitals to describe the bonding can be constructed from just the s and p atomic-orbital-like functions on the central (hypervalent) atom and appropriate basis functions on the ligands. Participation of four atomic orbitals in five or six molecular orbitals requires that the MOs have larger contributions from ligand basis functions, *i.e.* that the bonds are polarized towards the ligands. This requirement suggests that hypervalent molecules will be most stable when the ligands are more electronegative than the central atom. In addition, steric crowding of the ligands disfavours high coordination numbers for small central atoms.

Both steric and electronic effects suggest that hypervalent, high-coordinate compounds will be less stable for the small electronegative centres (F, O and N) than for heavier atoms. Tetracoordinate nitrogen is well known, as NR_4^+, but pentavalent, formally neutral nitrogen is much less common. $F_3N=O$ (note the very electronegative ligands) is known but, in accordance with the octet rule, is typically described as zwitterionic: $F_3N^+\text{-}O^-$, and is thus not hypervalent. Musher's definition of hypervalent should be limited to formally neutral atoms, so it does not apply to the zwitterionic description of F_3NO. Pentacoordinate nitrogen is not known.

Tetracoordinate, pentavalent phosphorus atoms are much more common, in the form of phosphine oxides and phosphine sulfides. The electronegativity difference between P and O is much larger than between N and O, thus suggesting a more polar bond. The phosphine oxides are often described as a having a polar covalent double bond.

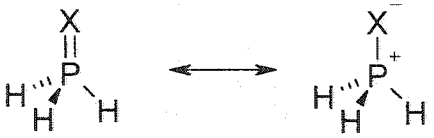

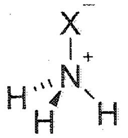

Recalling the discussion of Lewis structures from the introductory chapters, we realize that the first structure above is sufficient to describe a polar double bond. On the other hand, if the delocalization index does not reach two in the non-polar limit we would have reason to include the second resonance structure. Conversely, if the delocalization index is greater than one in the non-polar limit for H_3NX, we should include the doubly bonded resonance structure in its description. The results of this chapter will give us an indication of the importance of the octet rule, *versus* formal charge minimization, in the Lewis description of these systems.

Phosphoranes, $H_3P{=}X$, differ from phosphines, $H_2P\text{-}XH$, by a simple 1,2-shift of a hydrogen atom. The unsubstituted systems are generally unstable with respect to the phosphines, and thus are not well known. Many examples are known in which the hydrogen atoms are replaced by other groups, such as aryl groups, $(Ar)_3P{=}CR_2$, or halides, $Y_3P{=}NR$. A few examples of 'phospha-Wittig' reagents, $Y'P{=}PY_3$, are also known, where Y is a small alkyl group and Y′ is CF_3 or a large aryl group, giving electronic stability or steric protection, respectively. These decompose at room temperature (Schmidpeter, 1990, §10.3). While the P=C bond in $R_3P{=}CR_2$ is fairly reactive (this is the Wittig reagent), the P=O bond in $R_3P{=}O$ is very stable; in fact its formation seems to be a driving force in many reactions.

The unsubstituted phosphine chalcogenides have previously been studied by Atoms in Molecules analysis (Dobado *et al.*, 1998). A large variety of P-substituted phosphine chalcogenides are known (Walker, 1972;). Trivalent hydroxyl phosphines undergo rearrangement to give $Y_2HP{=}O^*$ and much of the chemistry of other trivalent phosphorus compounds involves oxidation to the P(V) state (Walker, 1972, p.48). The chemistry of the phosphine chalcogenides typically involves the P-H bond (Hamilton and Landis, 1972).

6.2. Energies relative to phosphines and amines

The Hartree-Fock calculated tautomerization energy varies widely. See Table 6-1. For X = O and S, the phosphines are 9 and 18 kJ/mol lower in energy than the phosphoranes, H_3PO and H_3PS, respectively. This small energy difference is unsurprising given the well-known strength of the P=O and P=S bonds. The recent observation of the transient species H_3PO in a dc glow discharge (Ahmad *et al.*, 1999) led to the suggestion that it is stable relative to H_2POH in the gas phase. At the MP2 level of theory, H_3PO is lower in energy by 0.2 kJ/mol.[†] On the other hand, correlation slightly increases the energy separation between H_3PS and thiophosphine. For the remaining systems, the phosphine is clearly more stable than the phosphorane. The energy difference for the methyl(ene) systems is over 200 kJ/mol, while the pnictogen systems (X = NH, PH) have energy differences on

---

[*] $(CF_3)_2POH$ and $(CF_3)_2PSH$ are exceptions.

[†] Previous calculations at the MP4 level have found the phosphine to be more stable (Kwiatkowski and Leszczynski, 1992).

the order of 100 kJ/mol.

The H_3PSiH_2 system with a planar arrangement about Si is 300 kJ/mol higher than the phosphine. A more stable pyramidal H_3PSiH_2 is 160 kJ/mol higher in energy than silylphosphine, but does not appear to involve a double bond. Rather this system appears to be a complex between phosphine and the carbene analogue, SiH_2. To help verify this description, the borane complex, H_3PBH_3 was studied.[*] To investigate the effect of putting two formally hypervalent atoms together, the systems $H_3P{=}PH_3$ and $H_3P{=}SH_2$ were studied. While H_3PSH_2 formed a bound molecule, H_3PPH_3 dissociated into two phosphine molecules.

A pyramidal geometry of NH_3SiH_2 is 166 kJ/mol higher in energy than H_2NSiH_3 (similar to the phosphorus congeners), but *pyramidal* NH_3CH_2 is 276 kJ/mol higher than H_2NCH_3 and *planar* H_3NCH_2 52 kJ/mol higher in energy than *pyramidal* NH_3CH_2. The preference for pyramidal geometries is evidence of zwitterionic structures in these systems. Alternatively, they could be described as coordination complexes. The greater stability of NH_3SiH_2 *vs.* NH_3CH_2 could then be explained by the greater stability of the closed shell SiH_2 relative to CH_2. While H_3NS was only 47 kJ/mol higher in energy than H_2NSH, the remaining H_3NX species (X = O, NH, PH) are 100 to 200 kJ/mol higher in energy than the amine tautomers.

---

[*] The NH_3BH_3 system was also optimized as an example of an amine complex.

6.3. Geometry

For Pn = P and N, $H_3Pn=O$, $H_3Pn=S$ and H_3PnBH_3 were optimized in the C_{3v} point group. All the remaining phosphoranes and their nitrogen congeners were optimized within the C_s point group. Optimized bond lengths and bond angles about P are given in Table 6-1, along with experimental values for some related systems. The values for the nitrogen analogues are given in Table 6-2. Where both *trans* (*E*, **1a**) and *cis* (*Z*, **1b**) (staggered and eclipsed) isomers are possible, the *trans* isomer is lower in energy by 6 to 8 kJ/mol. As in HP=NH, the *trans-Z* arrangement of $H_3P=NH$ has a shorter P-N bond than the *cis-E* arrangement.

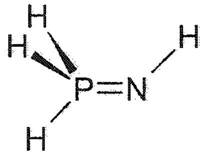

1a

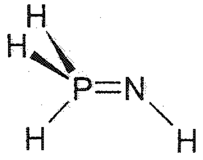

1b

6.3.1. Pyramidalization of group 4A substituents

For H_3PSiH_2, the planar Si geometry (as **2a** below) was used in the series trends, though two pyramidal geometries (**2c**, **2d** below) were found to have much lower energy. This is an early indication of localization of electron density on the silicon atom, rather than delocalization to hypervalent phosphorus. Hypervalence and multiple bonding are supported by electronegative atoms, while silylene is an electropositive ligand. We saw in the previous chapter that the *formally* hypervalent sulfur atom did not form a double bond with the electropositive PH group in $HPSH_2$. Rather the electrons remained localized on the phosphorus atom.

Higher valence atoms apparently have lower electronegativity than the same atom in a lower valence state.

One way of understanding these observations is that two reasonably electronegative atoms are required to hold two electron pairs in the bonding region, against the Pauli repulsion forces (Malcolm *et al.*, 2002). Since the phosphorus atom in H_3PSiH_2 has a complete octet without the second P-Si bond pair, the additional electron-electron repulsion in forming it would be too great. The second electron pair remains localized on silicon, rather than forming a bond that would be polarized towards P. For the more electronegative substituents, the P-E bonds are polarized towards the substituent, relieving some of the repulsion by the three P-H bonding electron pairs.

Based on the silylene results, and in consideration of previous experimental and computational results, a pyramidal geometry for H_3PCH_2 was also investigated. The degree of pyramidalization in H_3PCH_2 is much less than in H_3PSiH_2. The sum of bond angles about C is 353°, while about Si it is 272°. The pyramidal silicon atom (in **2c** & **2d**) suggests four valence electron pairs, while the nearly planar carbon atom (in **2b**) appears to have only three valence electron pairs, or four pairs with two pairs involved in P-C bonding (as in. **2a**).

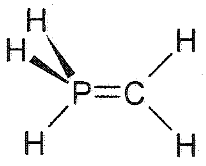
2a

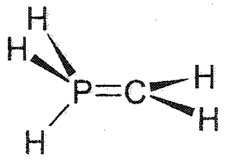
2b

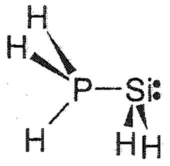
2c

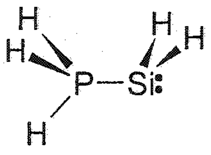
2d

Unlike the HPX systems, there is no obviously preferred arrangement of the P-H bonds relative to the E-H bonds. If there are five pairs of electrons in the valence shell of phosphorus, we expect a distorted square-based pyramidal (**a**), or a distorted trigonal bipyramidal (**b**), arrangement of the pairs.

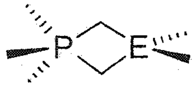

a

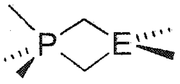

b

The distorted planar geometry (**2b**) of H_3PCH_2, which arises from the trigonal bipyramid, was found to be slightly lower in energy than the planar geometry (**2a**), which arises from the square based pyramid, at both the HF (3.9 kJ/mol) and MP2 (4.7 kJ/mol) levels of theory. This is comparable to the energy difference between the two geometries of $H_3P{=}PH$ and of $H_3P{=}NH$, which have a similar relationship to each other. These results are consistent with experimental geometries (Mitzel *et al.*, 1998) and with previous calculations, which have shown the pyramidal structure to be the minimum energy for simple ylides (Bachrach, 1992). The C-P bond may be up to 30° out of the CH_2 plane depending on the level of theory. This suggests different polarities for the two P-C bonding electron pairs. So-called 'stabilized' ylides have a planar arrangement about carbon, but the substituents are still arranged as in **2b** rather than **2a**.

The optimized P-C bond length in **2b** is 1 pm longer than in **2a**, possibly due to weaker electrostatic attraction of the less charged groups (see atomic properties below). The unique P-H bond is significantly (3 pm) longer in **2b**, while the other two P-H bonds are shorter. A similar P-X bond lengthening is seen for the *trans* isomer of $H_3P{=}NH$ relative to the *cis* isomer, in each case the more stable geometry has a longer P-X bond (and lower atomic charges). The opposite is seen for $H_3P{=}PH$, the *trans* P-P bond being 1.5 pm shorter (with the same atomic charges). The pyramidal silicon, in **2c** (**2d**), is involved in a P-Si bond 25 (30) pm longer[*] than the planar Si in the **2a** analogue, and 12 (17) pm *longer than in the phosphine*, H_2PSiH_3.

For the nitrogen analogues, both C and Si prefer a pyramidal geometry. No planar $NH_3{=}SiH_2$ geometry could be converged, and the planar $NH_3{=}CH_2$ geometry is 52 kJ/mol higher in energy than the pyramidal geometry. The pyramidal Si atom has a sum of bond angles of 274°, very similar to the phosphorane case. The pyramidalization of C is much more pronounced than for the phosphoranes, with a sum of bond angles of 312°, suggesting a tetrahedral arrangement of four electron pairs around the C atom, including one 'non-bonding' pair. The pyramidal C-N bond is 9 pm longer than the planar C-N bond. This is consistent with the tendency for second row atoms such as nitrogen to avoid hypervalent environments, particularly when the ligands are less electronegative than the central atom.

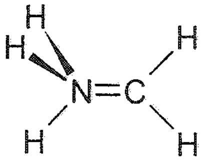

3a

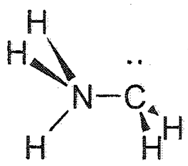

3b

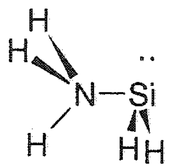

3c

---

[*] The difference drops to 20 (24) pm at MP2

Since the other substituent atoms are only one- or two-coordinate, there is no opportunity to directly observe (or prevent by symmetry) pyramidalization of the pnictogens or chalcogens. The electronic density about each atom will be further discussed below.

6.3.2. MP2 correlation effects and comparison with experiment

Where available, related experimental geometrical parameters are shown in Table 6-1. MP2 geometries are shown for each H_3PX system, and the QCISD parameters are given for H_3PO. Including correlation at the MP2 level of theory generally increases bond lengths and decreases bond angles (Teppen *et al.*, 1994). For the phosphoranes studied here, MP2 increases the P-L bond lengths by 1 to 4 pm but *decreases* the P-M bond lengths, as seen for the P-Si bond in H_2PSiH_3. The P-S bond length is almost unchanged, while the P-P bonds shorten by 2 pm. The bond between P and planar Si shortens by 1 pm, while the pyramidal Si-P bonds shorten by 7 pm. It appears that MP2 increases the extent of multiple bonding in these $H_3P{=}MH_{n-1}$ systems – or it may be a result of less polar bonds and therefore less electrostatic repulsion between positively charged atoms.

A recent structure determination of H_3PO found a P=O bond length of 147.6 pm and an HPO bond angle of 114° (Ahmad *et al.*, 1999). The current calculations show a P=O bond length of 145.3 pm by HF theory, 148.7 pm by MP2 and 148.1 pm by QCISD. The highest-level r_e(PO) results are in reasonable agreement with the experimental results (+0.5 pm), but the optimized HPO angle was found to be 2° to 2.5° larger than the experimental value and the P-H bond length was found to be 4 pm shorter than the experimental value, at all three levels of theory.

The experimental structural parameters for $Me_3P{=}O$ (Wilkins *et al.*, 1975) are very similar to those of $H_3P{=}O$, so one would expect that the $Me_3P{=}S$ geometry is a good model for $H_3P{=}S$. The optimized P-S bond is 1 pm too long (at HF and MP2) and the bond angles are very similar to the oxide results in terms of absolute value and magnitude of error. The $Me_3P{=}CH_2$ geometry has also been determined experimentally and it shows that the optimized bond length in H_3PCH_2 is 1 pm (HF) or 2 pm (MP2) too long. An X-ray structure for $Me_3P{=}PDmp$ has a P-P bond length in good agreement with the MP2-optimized value for H_3PPH. The trivalent phosphorus atom in the experimental system is substituted with the very bulky dimesitylphenyl group.

6.3.3. *Comparison with $HP{=}X$, HNX and H_2NXH*

The P-E bond lengths for each series are plotted in Figure A4-1. The P-M bond lengths in the phosphoranes are 5 to 10 pm longer than the corresponding phosphinylidene bond lengths. In the planar geometry, the P-Si bond length is only 9 pm longer than for $HP{=}SiH_2$, but in the more stable pyramidal geometry, **2c**, it is 34 pm longer than the phosphinylidene value and, as mentioned above, *12 pm longer* than the phosphine ($H_2P\text{-}SiH_3$) bond length. The P-O and P-C bond lengths in the phosphoranes are about 1 pm longer than the corresponding phosphinylidene bond lengths. The smallest difference is for the P-N bond, which is actually *shorter* by 0.4 pm at the HF level and by 3 pm at MP2, compared to HP=NH. The significant lengthening of P-M bonds is evidence for a decrease in overall bond strength, relative to $HP{=}MH_{n-1}$.

The formally pentavalent $Y_3N{=}X$ systems have only one experimentally known representative, F_3NO, whose bond lengths and angles are shown in Table 6-2. The N-O bond in F_3NO is shorter than the experimental N-O bond length in HN=O, suggesting a double bond, shortened by electrostatic effects. The calculated N-E bond lengths in H_3NX are up to 50 pm longer than the trivalent HN=X bonds. The calculated N-O bond in H_3NO is 20 pm longer than in HN=O, and just 3 pm shorter than in $H_2N{-}OH$. The remaining N-E bonds are 3 to 25 pm *longer than in the amines*, the discrepancy increasing as the electronegativity of E decreases. The N-C bond with the planar C atom is just 3 pm longer than in H_2NCH_3. For the pyramidal C atom it is 12 pm longer. This is consistent with the $HPSH_2$ and pyramidal H_3PSiH_2 data, where the substituent atom is less electronegative than the (formally hypervalent) central atom. In each of these cases, the bond is longer than a single bond between the same two atoms. When the substituent atom from group 4A is forced to be planar, the bond shortens, reflecting an increase in N-E bond strength, accompanied by an overall increase in molecular energy.

The HF optimized HPH[*] bond angle is about 101° to 102°, except for the

---

[*] Angle between two inequivalent H nuclei.

pyramidal SiH_2 and CH_2 cases where it is 99° to 100°. The MP2 angles are about 1° narrower. HPX angles[*] range from 106° to 120° and up to 127° for pyramidal structures. The P-H bond lengths are shorter and the HPH bond angles larger than in PH_3.[†] The HNX angles range from 105° to 118°. All the r(N-H) and $\angle$HNH values are very similar to the NH_3 parameters.

6.4. Position of the Interatomic Surface: Bonding Radii

Properties and positions of the bond critical points (BCPs) are given in Tables 6-3 (P-L, P-M) and 6-4 (N-L, N-M). Bond paths are found between all atoms that we expect to be bonded. There are no ring or cage critical points in the molecules studied. The phosphorus and substituent bonding radii, for each phosphorus series, are plotted in Figures A4-2 and A4-3, respectively. Figure 6-6 shows contour plots of $\nabla^2\rho(\mathbf{r})$ in the symmetry plane of each phosphorane. These plots are overlaid with bond path trajectories and the intersection of the interatomic surfaces with the plane.

The second row substituents of H_3PX have P-E BCPs in or near the core region of phosphorus, where the Laplacian is positive. In H_3PS the BCP lies between the two valence shells. For H_3PPH and H_3PSiH_2 the BCP falls in or near the core region of the substituent atom. The bonding radii of phosphorus and of the pyramidal silicon in **2c** and **2d** are 0.3 and 0.2 au longer than those of phosphorus

---

[*] Angle between X and the H nucleus lying in the symmetry plane.

[†] Note that the experimental P-H bond length in $H_3P{=}O$ is *greater* than the experimental bond length in PH_3.

and planar silicon in **2a**, respectively.

For the P=L bonds (second row atoms), the bond lengths and the positions of the bond critical points are very similar to the HP=X values. In $H_3P=O$ both the P and O radii are 0.005 au longer than in HP=O. In $H_3P=NH$ the BCP shifts about 0.01 au towards N, compared to HP=NH. In planar $H_3P=CH_2$, the P bonding radius lengthens by 0.032 au and $r_b(C)$ shortens by 0.015 au. Overall, we see a shift towards the second row atom.

The P=M bonds (third row atoms) are much longer than those in HP=X. The planar Si radius is just 0.005 au longer than in $HP=SiH_2$, so the lengthening is mainly in phosphorus, where the radius increases by 0.16 au. In pyramidal H_3PSiH_2, both radii are about 0.13 au greater than the *phosphine* (H_2PSiH_3) radii. In $H_3P=S$ and $H_3P=PH$, the pentavalent P bonding radius is greater than in the corresponding *phosphine*, by 0.16 au and 0.39 au respectively. The substituent radii are each 0.4 au shorter than in HP=X, however. Thus the bond lengthening in these two systems, relative to HP=X, is accompanied by a strong shift of the bond critical point towards the substituent group, *suggesting* charge transfer into the atomic basin of the pentavalent phosphorus.*

When correlation is included, the P-M BCPs shift towards the pentavalent phosphorus atom, with overall bond shortening. The P-L BCPs exhibit the behaviour observed for the HPX series: a shift towards the electronegative ligand and an increase in the P-L bond length. For both $H_3P=CH_2$ geometries, correlation

---

* We will see below that the opposite is true for all but H_3PS; the ligands become more negatively charged.

shortens the C bonding radius and lengthens the P bonding radius. For $H_3P{=}NH$ and $H_3P{=}O$ both bonding radii increase, but P more so, shifting the BCP away from the pentavalent phosphorus at the MP2 level.

In the nitrogen systems, H_3NX, the BCP lies in the bonding region between the two valence shells for X = O, NH and CH_2. For E = O, N and planar C, the substituent bonding radius is similar to its HN=X value, but the pentavalent nitrogen bonding radius is about 0.4 au longer than in the trivalent HNX and 0.2 to 0.3 au longer than the amine values. The bonding radius of nitrogen is similar in *planar* and *pyramidal* NH_3CH_2, while the bonding radius of pyramidal C is much longer than that of planar C. For planar CH_2 and the third row ligands, the BCP lies closer to the valence shell of the ligand than to that of nitrogen. For the third row substituents, both the nitrogen and substituent radii have increased significantly, compared to the HNX and H_2NR values.

6.5. Properties at the Bond Critical Points

6.5.1. Density, $\rho(r_b)$

The P-E bond critical point densities are plotted in Figure A4-4. Values are given in Table 6-3. The N-E BCP densities are given in Table 6-4. The P-L BCPs have $\rho(r_b)$ values ranging from 0.26 to 0.20 au – very smilar to, but slightly *higher* than, the phosphinylidenes. The P-M BCPs have $\rho(r_b)$ values ranging from 0.16 to 0.09 au. For $H_3P{=}S$ this is slightly smaller than for HP=S, consistent with the slightly longer bond. For the P=P and planar Si=P bonds, whose lengths lie between the single and double bond values, $\rho(r_b)$ is very similar to the phosphine values. In pyramidal H_3PSiH_2, the P-Si BCP density is only 0.05 au. This is even lower than the P-B BCP density in the PH_3BH_3 complex, which has a value of 0.09 au. The difference is attributable to the fact that B is a second row atom and Si a third row atom.

Relative to HF calculations, MP2 calculations shorten the P-L bonds and increase the density. The P-S bond is very similar in length at the HF and MP2 levels, however the density is significantly lower at MP2, as the BCP shifts towards P. For the P-P and P-Si bonds, MP2 shortens the bond and increases the density at the bond critical point (much more so for the pyramidal structures).

The nitrogen analogues have BCP densities 0.1 to 0.2 atomic units less than the respective imines. Consistent with the longer bonds, for all but H_3NO (which is shorter), this is even lower than the BCP density in the amine tautomers. While the two PH_3CH_2 isomers have similar BCP densities, the pyramidal NH_3CH_2 has a much lower ρ_b(N-C) than the planar arrangement about carbon.

6.5.2. Laplacian

In the phosphoranes, $\nabla^2\rho_b$ of the P-L bonds is slightly less positive than in the phosphinylidenes, and decreases from +1.41 for O to –0.10 for C. For the third row substituents, the Laplacian drops from 0.0 to –0.2, as the electronegativity of M increases, as seen for the MP2 results in phosphinylidenes. With the exception of $H_3P{=}S$, correlation makes the Laplacian values more negative.

In the H_3N=X species, for X = O, NH and *pyramidal* CH_2, the BCP lies within the bonding charge concentration and the Laplacian is negative, about –0.16. For the remaining species, the BCP lies closer to the ligand core and the Laplacian is small and positive, the smallest magnitude being for H_3NS, the largest for $H_3N=CH_2$ with the planar C atom. This is somewhat surprising, since in $HNCH_2$ the N-C BCP is even closer to the carbon nucleus, yet the Laplacian is large and negative. There has clearly been a significant rearrangement of the density about the planar C atom.

6.5.3. Ellipticity

The 'double' bond ellipticities of PH_3O and PH_3S are zero by symmetry, and so cannot tell us anything about the extent of π-like bonding. The symmetry planes of the remaining phosphorane species are conducive to larger ellipticities than those found in the phosphines, though the approximate three-fold symmetry about P may lower the ellipticity relative to HP=X. The observed curvatures are all oriented in the expected direction. This includes the pyramidalized PH_3CH_2 **(2b)** and PH_3SiH_2 **(2c)** structures, for which the density is enhanced in the plane containing the imagined π-bonding or lone pair, respectively. This is consistent with the twisted geometry for $HPCH_2$, which has the softer curvature in the plane containing the 'lone pairs', and a lower ellipticity, than the planar conformer does.

The P-N ellipticities are similar to the *cis* and *trans* aminophosphines. Both the P-C ellipticities are just slightly smaller than in the planar phosphaalkene,

$HPCH_2$. The planar $H_3P{=}SiH_2$ and the two isomers of PH_3PH, have exceptionally large ellipticities. For planar H_3PSiH_2 the ellipticity is 1.42 and drops to 1.26 at the MP2 level. The $H_3P{=}PH$ ellipticities are considerably reduced at MP2, while the ellipticities below 0.5 are only slightly lowered with the inclusion of correlation.

As for the phosphinylidenes, the highest electron density values are found in the bonds with the lowest ellipticities, and vice versa, except for pyramidal PH_3SiH_2, which has the lowest density and intermediate ellipticity.

The pyramidal H_3NX systems have similar ellipticities to the imines, and the H_3NNH ellipticities are actually higher than the $NH{=}NH$ values. The H_3NPH and the planar H_3NCH_2 ellipticities are extremely high. Even if the electron density is being transferred to the substituent, rather than shared, there is still considerable π-like density near the BCP, in the valence (or core) region of the substituent. The BCP is particularly close to the carbon nucleus in planar H_3NCH_2. The same argument may explain the high ellipticities in H_3PPH and H_3PSiH_2.*

6.6. Atomic and Group Charges

Atomic and group charges and energies ($K = G = -2V = -E$) are given in Tables 6-5 (H_3PX) and 6-6 (H_3NX). See Chapter 4 for the significance of the Laplacian, L. The atomic charges on phosphorus, and on the substituent group, are plotted in Figure A4-6 and A4-7, respectively, for each phosphorus series.

The heavy atoms in H_3PSiH_2, H_3PSH_2 and in H_3NCH_2 were reintegrated

---

* We will find below that there are two 'non-bonding' maxima on the PH in H_3PnPH, on the planar SiH_2 in PH_3SiH_2 and on the planar CH_2 in NH_3CH_2.

using the ‘Promega’ algorithm and with more rays followed than the default. This was done because the L values were greater than 10^{-2} and the magnitude of the total charge on each molecule was greater than 10^{-3}. The difficulty in integrating these atoms was most likely related to the high ellipticity at the BCP, reflecting unusual topology in these molecules. Atomic charges on P and Si each increased by about 0.1 electron and δ(P,Si) decreased by 0.2 due to the improvement in integration.

The expected increase in q(P) relative to the phosphinylidenes – due to the additional (electron withdrawing) H atoms – is further increased by additional charge transfer to X. Only S is less negative than in HP=X. The total increase in q(P), from HPX to H_3PX, is between 0.9 and 1.7 electrons, and reaches 2.2 electrons for the pyramidal silylene species.

One might expect that the substituents, X, would accept less charge density than in the phosphinylidenes, in order to moderate the atomic charge on phosphorus, but this is not the case (except when X = S). One interpretation of this is that the second shared pair of electrons in $H_3P{=}X$ is more localized on X than it is in HP=X. This might be described, in the Lewis model, by zwitterionic (ylidic) resonance contributions.

In H_3PX, unlike HPX, O and NH take 2.0 times the charge of OH and NH_2 in the phosphine tautomers. The planar and pyramidal CH_2 groups take almost 2.5 times the charge of CH_3, while the electropositive (planar) SiH_2 group gives only 0.5 times the charge of SiH_3. Recall that HP=S had a charge transfer that was more than twice that in H_2PSH. The charge transfer to S in $H_3P{=}S$ is 1.65 times that for the phosphine, which was typical for the other phosphinylidenes. It is as if the charges in HP=S and H_3P=S have switched roles.

The PH substituent is slightly electronegative relative to H_3P (and NH_3), taking on a small negative charge of –0.11 (–0.12 in the *cis* forms). In staggered H_3PSiH_2 (and H_3NSiH_2), pyramidal SiH_2 has a small charge of –0.04, giving evidence that the electronic structure is quite different in these molecules than in the other systems studied. In H_3PBH_3 the charge on BH_3 is also small and negative, despite the expected electronegativity difference. The other substituent groups change their charge in response to the central atom, but a -PH group accepts 0.11 electrons and a pyramidal silylene group, -SiH_2, accepts 0.4 electrons from a PnH_3 group, regardless of electronegativity differences. These molecules may all be described as donor-acceptor complexes, PH, SiH_2 and BH_3 acting as the acceptors, NH_3 and PH_3 as the donors.

As seen previously, MP2 reduces the magnitude of most charges. Interestingly, in the pyramidal H_3P=SiH_2 molecules, the electron transfer to the hydrogen atoms is significantly decreased, but the essential neutrality of the PH_3 and SiH_2 moieties is unchanged. In planar PH_3SiH_2 and both PH_3PH molecules, the population on PH_3 decreases with inclusion of correlation, even when this increases the magnitude of charge transfer. It appears that if the PH_3PH molecules can be considered as coordination complexes, then correlation increases the extent of donation from PH_3.

For H_3NO and H_3NNH, the charges on X are about 0.2 to 0.4 electrons more negative than for HNO and HNNH. For methylene and the third row ligands however, the charge difference is much bigger: from 1.0 to 1.5 electrons, suggesting that the degree of electron sharing is significantly reduced in these species relative to the others. Indeed, while all these X groups have large positive charges in the imines they have smaller negative charges here.

It is interesting to compare the properties of the P-N bonds in $H_3P=NH$ *vs.* $H_3N=PH$. Clearly, the second system has a much longer, weaker bond, with the BCP lying much closer to the nitrogen atom. The total charge transferred across the P-N bond in H_3PNH is 1.46 electrons, but in H_3NPH it is only 0.11 electrons. We may also recall from chapter 5 that in $H_2S=PH$, the PH group accepts 0.08 electrons. In each case the electron transfer is away from the formally hypervalent atom.

6.7. Delocalization Indices

The delocalization index between P and the directly bonded hydrogen atom ranges from 0.61 to 0.79 *vs.* 0.84 in PH_3 (& 0.79 to 0.96 in other phosphines). This reflects the variation in atomic charge on phosphorus; the more valence density is available, the more it will be shared with the neighbouring atoms. The $\delta(P,X)$ values are plotted in Figure A4-8, and reported in Table 6-3. The $\delta(N,X)$ values are reported in Table 6-4.

6.7.1. Comparison to other systems

While the phosphorus substituent ($X = PH$, $R = PH_2$) has given the largest delocalization for each of the series in previous chapters (and will in all subsequent chapters) the largest (P,X) delocalization index is for sulphur in this series. The delocalization index, δ(P, X), ranges from 0.81 in $H_3P{=}O$ to 1.45 in $H_3P{=}S$. These values are 61% (NH), 64% (O, CH_2, PH) and 82% (S, SiH_2) of the phosphinylidenes delocalization indices. The value for planar $H_3P{=}SiH_2$ is 1.29 (the same as *cis* $H_3P{=}PH$). The value for the non-planar H_3PSiH_2 is 0.8, (the same as $H_3P{=}O$), and only 45% of the $HP{=}SiH_2$ value.

For the second row substituents, the delocalization index is only 15% higher than in the phosphines. The delocalization index for pyramidal $H_3P{=}SiH_2$ is even lower than the phosphine value, again indicating that the electronic structure is significantly different in this species. The significant reduction of δ(P, X) in all phosphoranes, relative to HP=X, is only partly due to greater positive charge on the phosphorus atom, which was seen to affect the P-H bond delocalization. As the degree of phosphine substitution increases, from H_2PSiH_3 to $P(SiH_3)_3$, $\delta(P,SiH_3)$ varies only slightly, while the charge on phosphorus changes by a larger amount than between HPX and H_3PX. The significant decrease in delocalization index must therefore be due to real changes in the equality (polarity) and/or extent of electron pair sharing between the phosphorus atom and the substituent, X.

6.7.2. Relationship to bond order

Again the delocalization index was plotted *vs*. the charge transfer, q(X), in Figure 6-1 (H_3PX) and Figure 6-2 (H_3NX). Most of the 'planar' PH_3X points fall reasonably close to a quadratic function, the clearest exception being PH_3PH. A good fit is only obtained by removing one other point, either X = S (set 1) or X = CH_2 (set 2).

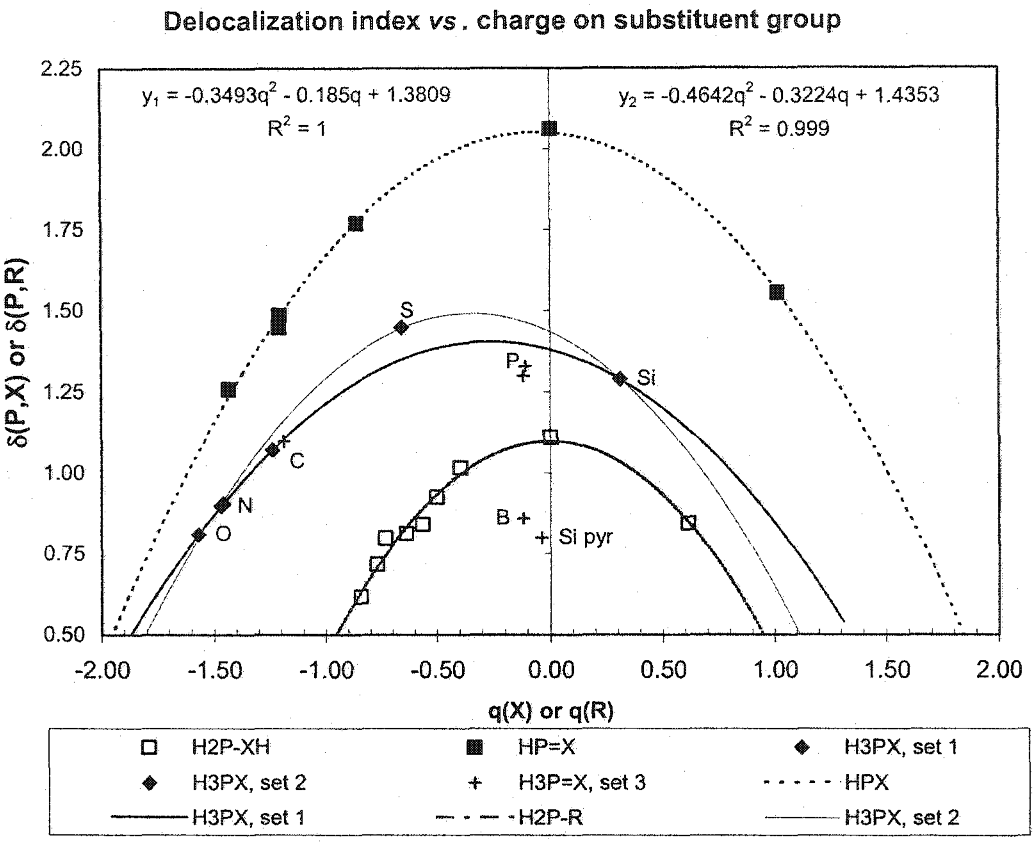

Figure 6-1: Delocalization versus charge curves for H_2PH, HPX and H_3PX. The H_3PX data are separated into three sets. Set 1: X = O, NH, CH_2 *planar* and SiH_2 *planar*. Set 2: X = O, NH, S and SiH_2 *planar*. Set 3: X = CH_2 '*pyramidal*', PH *cis* and *trans*, SiH_2 *pyramidal*, BH_3.

Both fitting schemes are shown in Figure 6-1. Considering that the planar arrangement of CH_2 is well established, and is even maintained when not required by symmetry, it seems most reasonable to remove the X = S point from the fitting procedure. The 3-fold symmetry about the S atom is enforced by the molecular symmetry and so little can be inferred about the type of bonding from the topology.

Since the S atom showed unusual trends in the charge transfer it is likely deviating from the electronic structure of the planar and very electronegative substituents, along with PH. The parabola then fits the remaining data very well, including both isomers of PH_3NH and of PH_3CH_2. The best-fit equation for this curve (set 1) is: $\delta_1 = -0.3493q^2 - 0.185q + 1.3809$; $R^2 = 1.0$ ($q_{max} = -0.265$, $\delta_{max} = 1.405$)

The PH data point lies a little below the curve and the S data point above. The best-fit equation for the set-2 data is: $\delta_2 = -0.4642q^2 - 0.3224q + 1.4353$; $R^2 = 0.999$ ($q_{max} = -0.347$, $\delta_{max} = 1.491$). The pyramidal SiH_2 data point has no connection to these curves at all. Like the $HPSH_2$ data in the previous chapter, and like the H_3PBH_3 data, the charge transfer is close to zero and the delocalization index is much lower than expected.

The H_3NX data show a very different trend. The maximum in the $\delta(N,X)$ *vs.* q(X) curve is near the H_3NO data point and corresponds most closely to a zwitterionic structure for these systems, Figure 6-2. Recognizing this, the data are shifted over, by plotting $\delta(N,X)$ *vs.* [q(X)+0.7], so that the maximum lies near the y-axis, and the curve coincides closely with the amine curve. The maximum delocalization is 1.3 and occurs when q(X) = -0.68. This maximum is about the same as that for the amines, but shifted towards negative substituents, as expected for the 'octet-rule' Lewis structure. The excess 0.3 of delocalization now arises from donation of the lone pairs on the substituent, rather than sharing lone pairs from both the central atom and the ligand, thus there is about 30% contribution from the doubly bonded structure, giving only 70% of the expected formal charge.

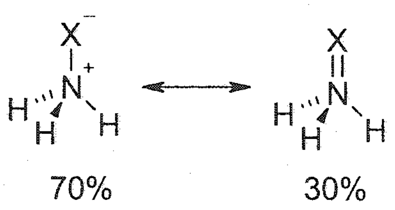

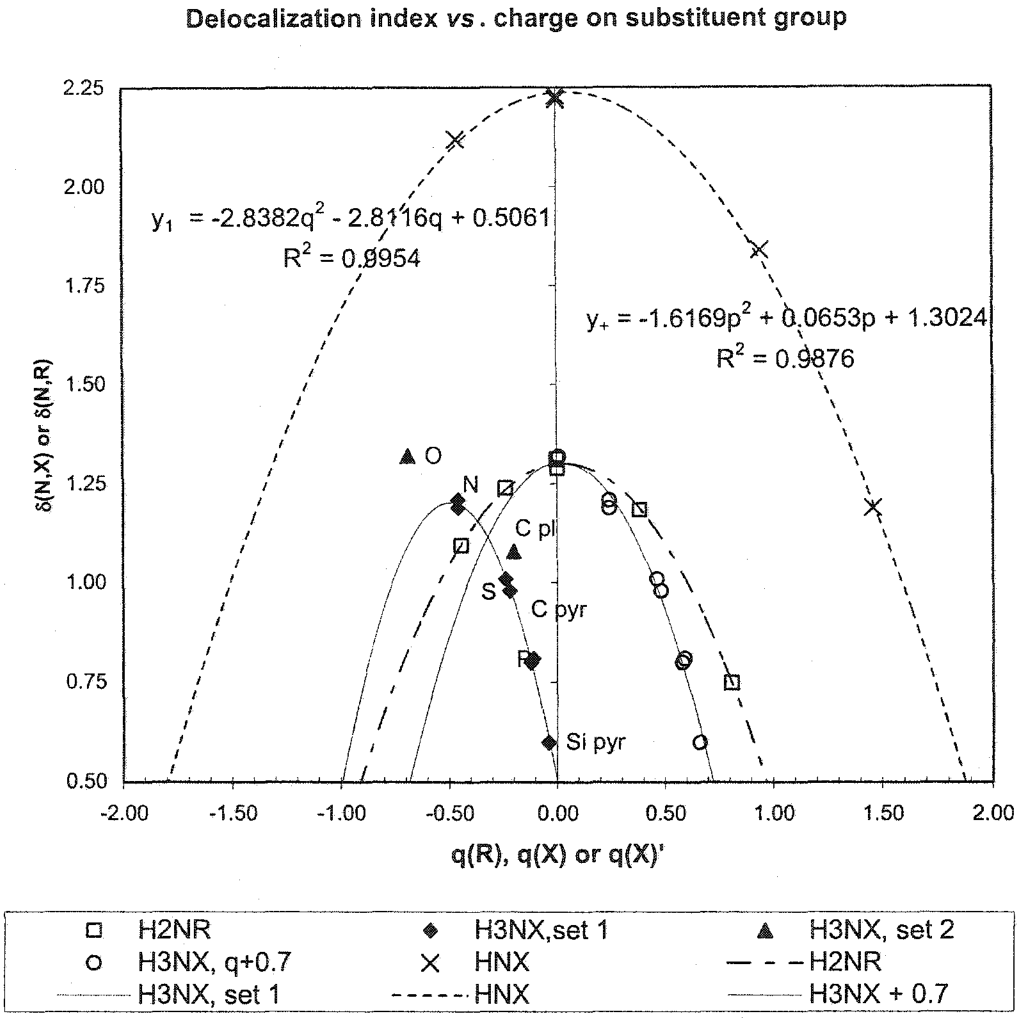

Figure 6-2: Delocalization *versus* charge transfer curves for H_2NR, HNX and H_3NX. The H_3NX was initially separated into two sets. Set 1: X = NH, CH_2 *pyramidal*, S, PH, and SiH_2 *pyramidal*. Set 2: X = O, CH_2 *planar*. Recognizing the zwitterionic nature of the system, the data are shifted over by plotting δ(N,X) *vs.* [q(X) + 0.7] for X = O, NH, CH_2 *pyramidal*, S, PH, and SiH_2 *pyramidal*. Both *cis* and *trans* data are plotted for NH and PH in each set.

6.8. The Laplacian and Lewis Structures

Figure 6-7 shows isovalue envelopes for the Laplacian, $\nabla^2\rho(\mathbf{r}) = 0$, from three perspectives, for H_3PX. Properties of the P-E bonding charge concentration maxima are given in Table 6-7. Properties of the non-bonding maxima (and some saddles) on the substituent atoms are given in Tables 6-8 and 6-9.

6.8.1. Standard phosphoranes

As expected, there are no non-bonding maxima in the valence shell of C when in a planar arrangement. The same is true for the slightly pyramidalized CH_2 group, consistent with the maintenance of a near-planar arrangement. The Lewis structures of $H_3P{=}O$ and $H_3P{=}S$ would have two lone pairs, but three (or one) non-bonding charge concentrations are required by the molecular symmetry. Saddles in the valence shell concentration are found between the three observed maxima. These six critical points have very similar density and Laplacian values, suggesting a slightly perturbed torus of valence density about the O and S atoms Table 6-8.

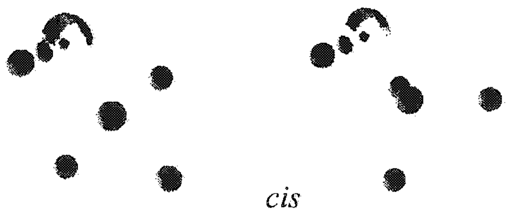

trans *cis*

Figure 6-3: Isovalue envelopes of *trans* and *cis* PH_3NH, for $\nabla^2\rho = -1.5$ a.u. There are no significant differences in the nitrogen lone pair regions of these two systems.

The number of non-bonding CC maxima is deceiving in PH_3NH, also. By noting the similarity of the one CC on *cis* PH_3NH to the two CCs on *trans* PH_3NH

we can conclude that there is only one electron pair represented. A saddle point in the Laplacian is found in the symmetry plane of the *trans* species, whose properties are almost identical to those of the maxima. This is in fact one slightly distorted charge concentration.

In H_3PPH however, both isomers have two non-bonding CCs, which are positioned almost opposite each other on the trivalent P. In addition, the trivalent P has no bonding CC along the P-P bond axis, which is unusual for a P-P bond, Table 6-7. The lone pairs are a bit further away than usual, probably due to excess density on the trivalent atom, but closer than typical bonding CCs. The saddles for these molecules have significantly different properties from the CC maxima. A negative Laplacian isovalue envelope makes it clear that the two maxima do in fact represent two Lewis non-bonding pairs.

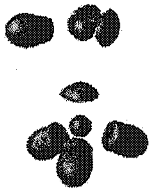

Figure 6-4: Isovalue envelope of *trans* H_3PPH, for $\nabla^2\rho = -0.2$ au. Two non-bonding maxima are seen in the valence shell of the trivalent P atom. The same is found for *cis* H_3PPH.

We thence have further evidence, along with the anomalous delocalization index, that the bonding in H_3PPH is not like that in the more electronegatively substituted phosphoranes. There is a larger contribution from the singly bonded structure, putting two lone pairs on the trivalent phosphorus atom. We add to this the unusually long bonding radius of the pentavalent P, in PH_3PH and in pyramidal PH_3SiH_2, and we may consider describing this phosphinylidene phosphorane as a coordination complex, see below.

Besides the two Si-H bonds, we find two charge concentrations in the valence shell of planar Si. The CC-Si-CC angle is 132.5°. While the PH group in H_3PPH has its three valence charge concentrations arranged trigonally, with PH_3 interacting at a position of low concentration, the SiH_2 group has four charge concentrations arranged in a distorted tetrahedron. The distortion is opposite to what would be expected for an electronegative atom involved in multiple bonding, where the angle should be less that 109°, so that the two charge concentrations fuse, giving a single maximum along the bond axis. The Laplacian isovalue envelopes in Figure 6-7**f** show that these two 'non-bonding' maxima are part of a continuous region of charge concentration, including the bonding charge concentration in the valence shell of phosphorus. The interaction looks distinctly π-like. The two Si maxima could correspond to a single pair of localized electrons; with the bonding pair localized more on phosphorus. If so, the bonding pair is considerably broadened in the valence region of phosphorus. This topology seems more consistent with distortion **a** of the non-polar model below than with **b**.

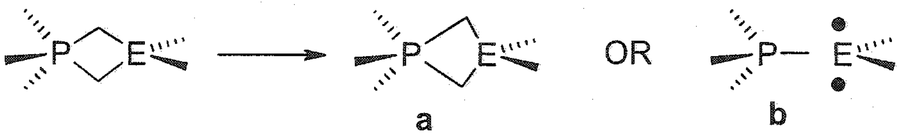

For all of the phosphoranes discussed in this section (X = O, S, NH, PH, CH_2 and *planar* SiH_2), we could describe the bonding as involving at least partial delocalization of two pairs of electrons. In a somewhat counterintuitive trend, the second pair of electrons becomes more localized on the substituent as the substituent becomes less electronegative. This is seen in the appearance of two non-bonding maxima for X = PH, and the preference for a pyramidal arrangement when X = SiH_2, to be discussed further below.

6.8.2. Nitrogen analogues

The arrangement of charge concentrations about the substituent atoms in the H_3NX series is quite different than in the H_3PX series. The most significant difference is for the X = CH_2 systems. We have seen that in H_3PCH_2, the methylene group remains essentially planar, even when not required by symmetry, and exhibits no non-bonding maxima about C in either geometry. In contrast, the methylene group in H_3NCH_2 is significantly pyramidalized when not constrained by symmetry, and non-bonding charge concentrations are observed about C in *both* geometries. For the pyramidalized methylene group, in **3b**, one non-bonding charge concentration is observed, similar to H_3NSiH_2 and to pyramidal H_3PSiH_2, **2c**, discussed below.

For the planar methylene group, in **3a**, two symmetry-equivalent non-bonding maxima are observed, above and below the CH_2 plane, analogous to the topology about planar SiH_2 in H_3PSiH_2 described above. There are differences, however. The maxima on Si are tipped towards the P-Si bond, and may be considered as part of a ‘banana bond’. The non-bonding maxima on C are tipped slightly *away* from the N-C bond, making a CC-C-CC angle of 169°. Furthermore, there is a N-C bonding maximum, along the bond axis, in the valence shell of the carbon atom. As discussed in Chapter 3, this is the expected result of forcing a non-bonding electron pair into a symmetric arrangement.

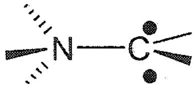

In H_3PNH, we saw that the single lone pair on N was easily distorted, giving one maximum in the *cis* (**1b**) arrangement and two maxima in the *trans* (**1a**) arrangement. In H_3PPH, there are two distinct non-bonding charge concentrations in the trivalent P in each arrangement. Similarly, there are two distinct non-bonding maxima on the trivalent N in each geometry of H_3NNH and on the P in NH_3PH. The properties of the saddle point linking the maxima are significantly different from those at the maxima, indicating the presence of two lone pairs on the substituent, and so confirming the involvement of only one primarily bonding pair in each of these H_3N-PnH systems, Pn = N or P.

Once again, the symmetries about O and S are uninformative. Once again, we see a weakly distorted torus of electron density around each chalcogen atom. Since F_3NO is a known compound, it would be interesting to apply the delocalization *versus* charge approach to the F_3NX series, to see if electronegative ligands can increase the delocalization between N and the divalent X substituent. For the H_3NX systems, the Laplacian confirms the conclusion from the delocalization indices: the N-X bonds are single bonds with a possible small contribution from delocalization of the substituent lone pairs.

6.8.3. Coordination complexes

It appears from the Laplacian envelopes in Figure 6-7 that the pyramidal PH_3SiH_2 is a complex between PH_3 and the closed-shell molecule, SiH_2. The PH_3 groups looks very similar to the PH_3 group in PH_3BH_3. The PH group in PH_3PH looks very similar to that group in $HPSH_2$, having a hole in the valence shell both above and below the P-H bond. Both molecules have two non-bonding maxima on the trivalent P atom, as in *twisted* HP-SiH_2. All three systems, we might describe as complexes of the closed shell molecules, PH_3, SH_2 and SiH_2, with PH.*

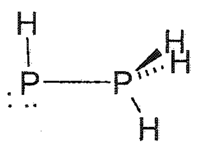
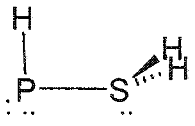
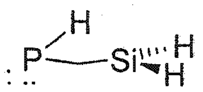

In *twisted* HP-SiH_2, Chapter 5, both moieties are electron acceptors and the hydrogen on phosphorus swings around to interact with silicon. A strong P-Si bond is formed, similar in length and polarity to the planar case. In *twisted* HP-CH_2, the carbene moiety is the acceptor, with the second Lewis pair being localized on carbon. Although the P-C bond is somewhat longer than in the doubly bonded planar system, the BCP density is actually higher. It is interesting that in both twisted species, $HPCH_2$ and $HPSiH_2$, 1.2 electrons are transferred, but in opposite directions, and this is the same magnitude as the charge transfer in H_3PCH_2. In those cases where both moieties are 'electron deficient' there is considerable charge transfer to the more electronegative atom or group.

---

* The PH would have one occupied p-π orbital and accept density into the vacant p-π orbital.

In $HPSH_2$, the charge transfer is minimal, as it is in H_3PBH_3, H_3PPH and pyramidal H_3PSiH_2. In each species with one donor molecule and one acceptor molecule, the charge transfer is from an electronegative atom to an electropositive atom, and is therefore minimal. The PH_3SH_2 system appears to be made up of two donor molecules. The charges show significant transfer of electron density (0.9 e) to the more electronegative SH_2 group.

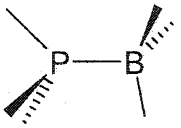

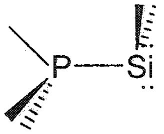

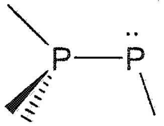

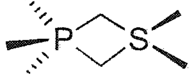

In fact, SH_2 accepts more charge from PH_3 than does divalent S, half of the excess going to the H atoms. The H atoms on S have a greater negative charge than they do in the thiophosphines, consistent with a hypervalent S atom. The H atoms on P have a similar charge to those in H_2PSH and in H_3PS. Each of the heavy atoms in H_3PSH_2 has two maxima in the bonding charge concentrations, located not along the bond axis, but on each side of the symmetry plane.

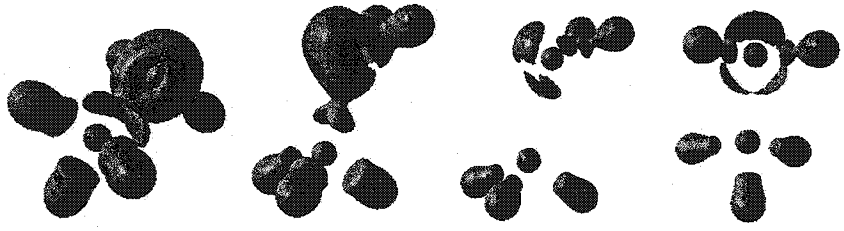

Figure 6-5: Isovalue envelopes of the Laplacian for PH_3SH_2 seen from various angles. The values are $\nabla^2\rho$ = -0.15 au (two left, we see the bonding maxima on P) and $\nabla^2\rho$ -0.34 au (two right, we see the bonding maxima, and non-bonding maximum, on S).

We might describe this as a 'banana bond' between two atoms, each with five pairs of electrons in their valence shell. The bonded atoms are not sufficiently electronegative to bring the two pairs of electrons into coincidence. Note that even when the Lewis pairs are apparently localized away from the bond axis, the maximum density (represented by the bond path) falls in the symmetry plane along a single path.

6.9. Summary

It seems clear that the CH_2 group shares two pairs of electrons with PH_3 in H_3PCH_2. The CH_2 group maintains an essentially planar arrangement even when the dihedral angle is changed. SiH_2 on the other hand forms a donor-acceptor complex with almost no charge transfer and a delocalization index of less than one. Only by restricting the symmetry can SiH_2 be made planar, and thus the (unequal) sharing of two electron pairs be enforced. When PH_3 is replaced by NH_3, neither CH_2 nor SiH_2 will form two bonds, even when the planar geometry is enforced by symmetry. The planar geometry for NH_3CH_2 does exhibit a slightly higher delocalization index than the pyramidal, with little change in charge transfer. The similarity in charge transfer is surprising, given that in the planar case the bond critical point is much closer to the carbon atom. Apparently, the density within the carbon atomic basin has shifted away from the bond axis, into the π-like region above and below the plane.

The NH group in PH_3NH exhibits a single non-bonding charge concentration, though this can be distorted to give two maxima. Again two pairs of electrons are unequally shared with the PH_3 group. The PH group exhibits two distinct non-bonding concentrations and a delocalization index that is lower than expected for the small charge transfer (though higher than the phosphines). It appears that the second pair of electrons is much more localized on the trivalent phosphorus. When PH_3 is replaced by NH_3 both NH and PH exhibit two distinct lone pairs.

The phosphine chalcogenides and amine chalcogenides each have a torus of non-bonding charge concentration, which is typical for terminal atoms. The tori are distorted by the three-fold symmetry and thus exhibit three local maxima. While the Laplacian distribution tells us little about the number of bonding *vs*. non-bonding Lewis pairs, the quality of fit on the delocalization *vs*. charge transfer curve gives some clues. H_3PO falls on the best-fit curve and the other properties are in line with H_3PNH and H_3PCH_2. It is thus reasonable to assume that two Lewis pairs are unequally shared between PH_3 and O. H_3PS falls above the best-fit curve, giving a greater than expected delocalization index. This behaviour has been seen for both P and S substituents in the other series and is attributed to additional delocalization of the lone pairs.

The best-fit delocalization *vs*. charge transfer curve for H_3PX suggests that the two bonding pairs are differently polarized, so that the maximum delocalization is less than 1.5 and occurs when 0.3 electrons are transferred to the substituent. When the total charge transfer is zero, the delocalization drops to 1.4 and so the Lewis bonds are actually more polarized (towards the central P) in this situation. The phosphoranes thus exhibit incomplete double bonds for the electronegative second row substituents and S, but single bonds for PH_3PH and PH_3SiH_2 (except when symmetry restricted). This conclusion is further supported by bond lengths and BCP densities very similar to the HP=X values, for all but X = PH and SiH_2, where the densities are similar to, or less than, the phosphines.

Double bonds, and thus zero *formal* charges are preferred by substituents with large group charges. As the substituent charge becomes less negative, the delocalization index is reduced relative to the formal double bond value. Because of the two opposing trends in bond polarity and localization as the substituent electronegativity changes, it is difficult to relate both the formal charge and bond order to a single resonance scheme. The maximum delocalization suggests 40% to 50% double bonding, while the charge transfer at the maximum suggests 65% to 75% double bonding (25% to 35% zwitterionic).

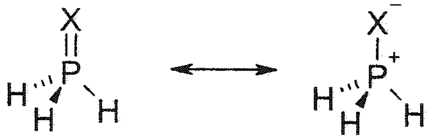

Using only the X = O, NH and S data points gives a quadratic with a maximum delocalization of 1.70, at $q = +0.39$. The positive substituent charge may correspond to additional donation of lone pair density. The most that can be said about this series is that there are two pairs of electrons involved in bonding, with different polarization trends. The first bonding pair presumably follows the predicted increase in localization as the substituent electronegativity increases. The second pair follows the opposite trend due to excessive electron-electron (Pauli) repulsion. The overall result of these two opposing trends is a maximum delocalization index near 1.5, when the substituent electronegativity is between than of S and PH.

The bonding in the H_3NX species is much less effective. Only H_3NO has a shorter bond than its tautomer (H_2NOH), though H_3NS has the smallest tautomerization energy[*]. The charge concentrations about all the remaining substituents show evidence that the second 'N=E' bonding pair of electrons is actually localized on the substituent. This is confirmed by the negative charges on the electropositive substituents. Since the BCPs lie closer to the substituent valence shells, the ellipticities are quite large, even though the π-like density is fairly localized.

The delocalization *vs.* charge curve for this series reaches the same maximum delocalization as the amines, 1.3, but with a formal charge of –0.7, suggestive of a single bond, weakened by steric crowding, but with some donation and delocalization of the substituent 'lone pairs'. Thus we find that the octet rule is more applicable to the second row atom, N, than to its third row congener, P. The reason behind this difference is probably a combination of size and electronegativity effects. It would be interesting to study the F_3NX series and determine whether the octet rule is obeyed in that series.

---

[*] Again there appears to be something special about sulfur

6.10. Laplacian Contours and Isovalue Envelopes

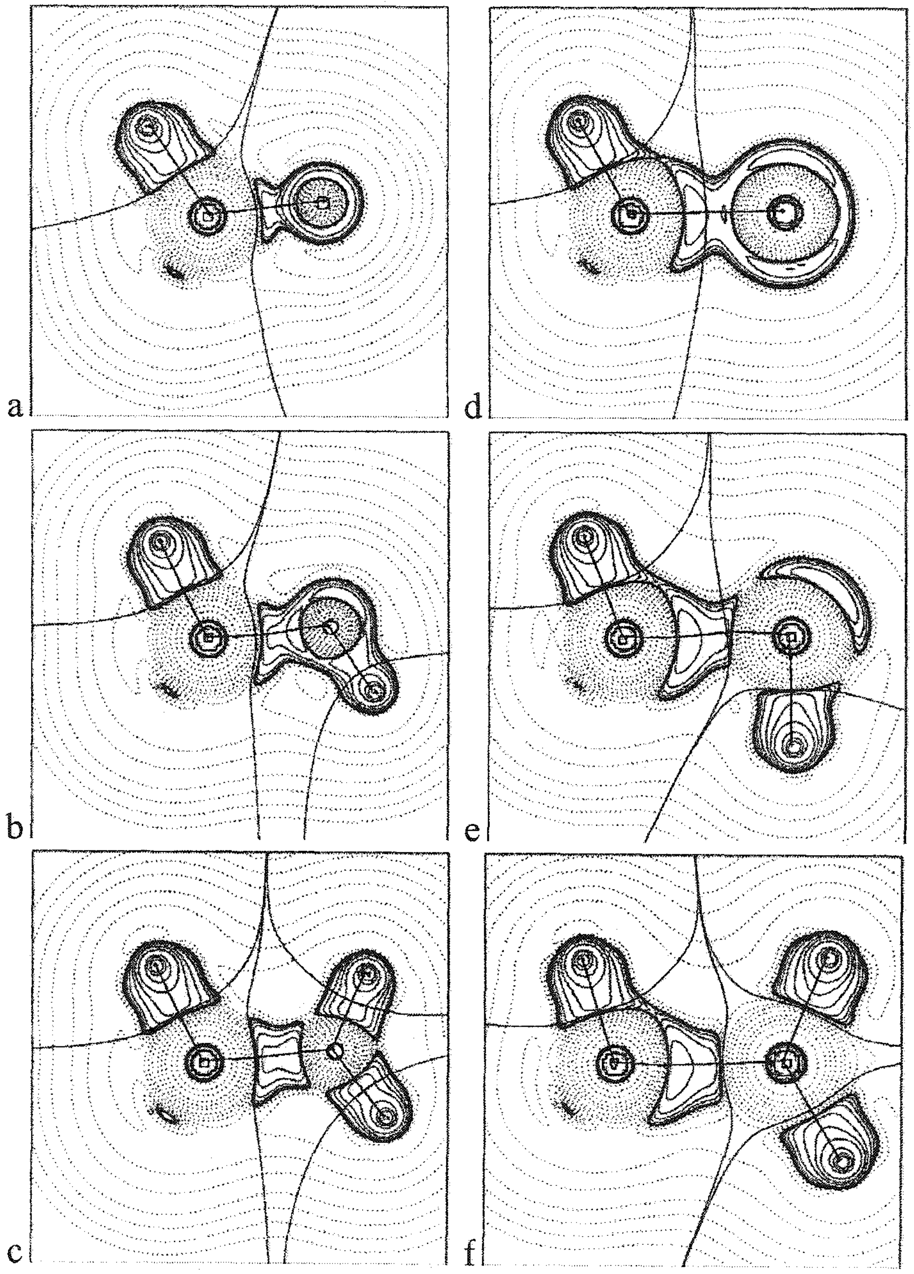

Figure 6-6: Continued on the next page.

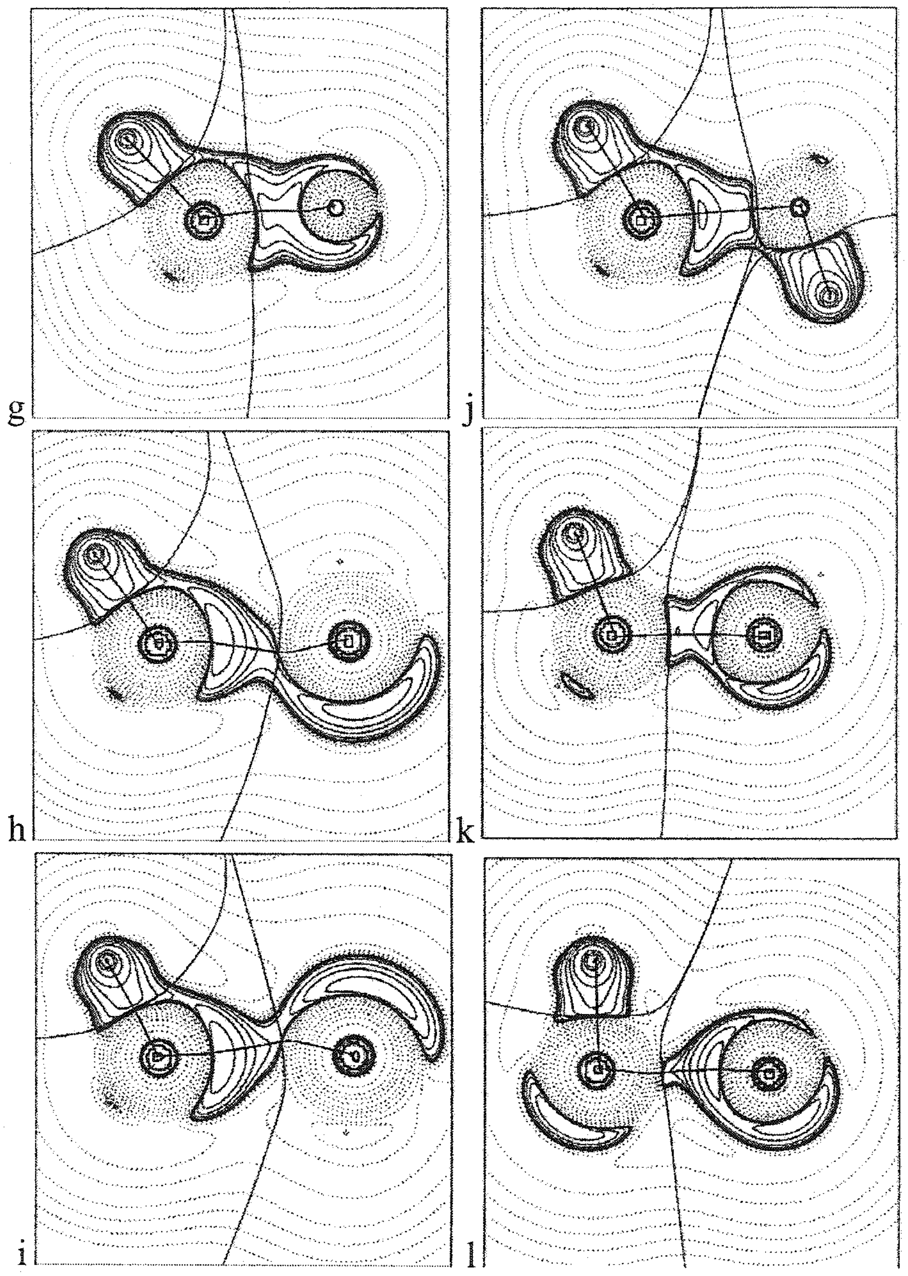

Figure 6-6: Contour maps of $\nabla^2\rho(\mathbf{r})$ in the symmetry plane of H_3PX: **a)** H_3PO, **b)** H_3PNH *trans*, **c)** H_3PCH_2 *planar*, **d)** H_3PS, **e)** H_3PPH *trans*, **f)** H_3PSiH_2 *planar* **g)** H_3PCH_2 *twisted* **h&i)** H_3PSiH_2 *twisted*, **j)** PH_3BH_3 **k)** H_3PSH_2 **l)** $HPSH_2$. Solid contours indicate negative values (concentration) and dashed lines indicate positive values (depletion). The outermost contour is +0.002 au. Isovalue contours increase and decrease from the $\nabla^2\rho(\mathbf{r}) = 0$ contour in the order $\pm2\times10^n$, $\pm4\times10^n$, $\pm8\times10^n$, beginning with $n = -3$ and increasing in steps of unity. Each map is overlaid with the bond paths and with the intersection of the interatomic surfaces with the displayed plane.

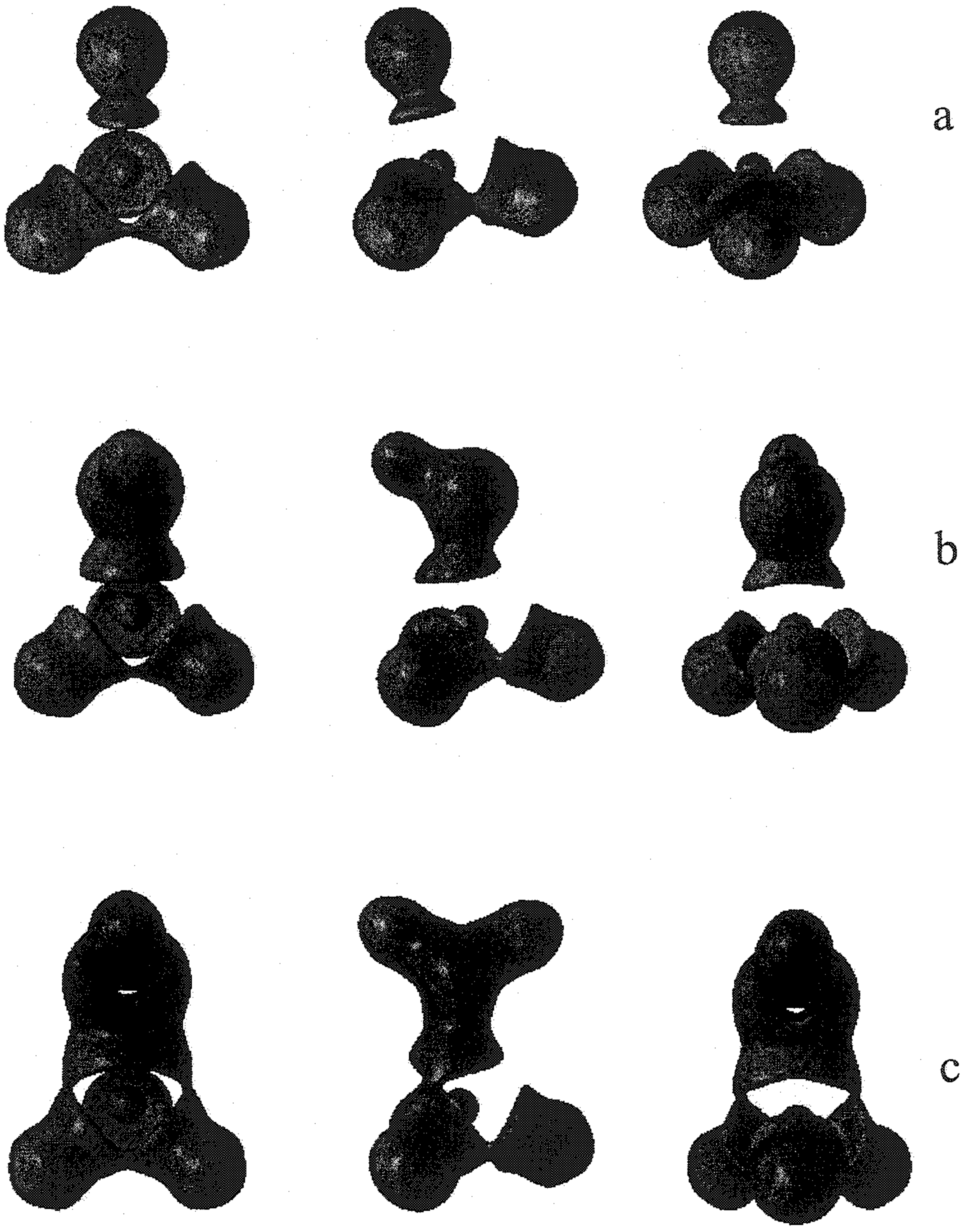

Figure 6-7: Continued on next page.

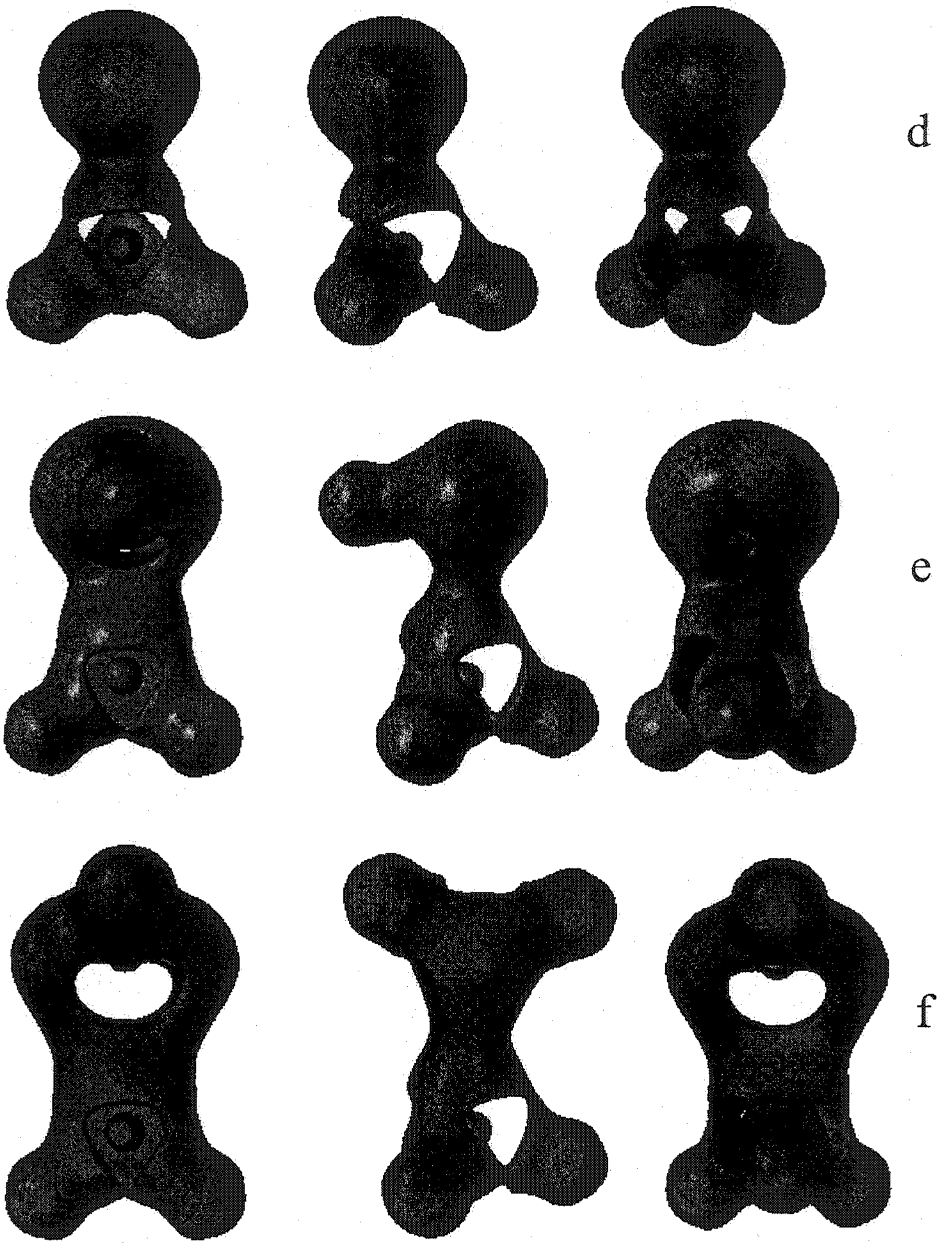

Figure 6-7: Continued on next page.

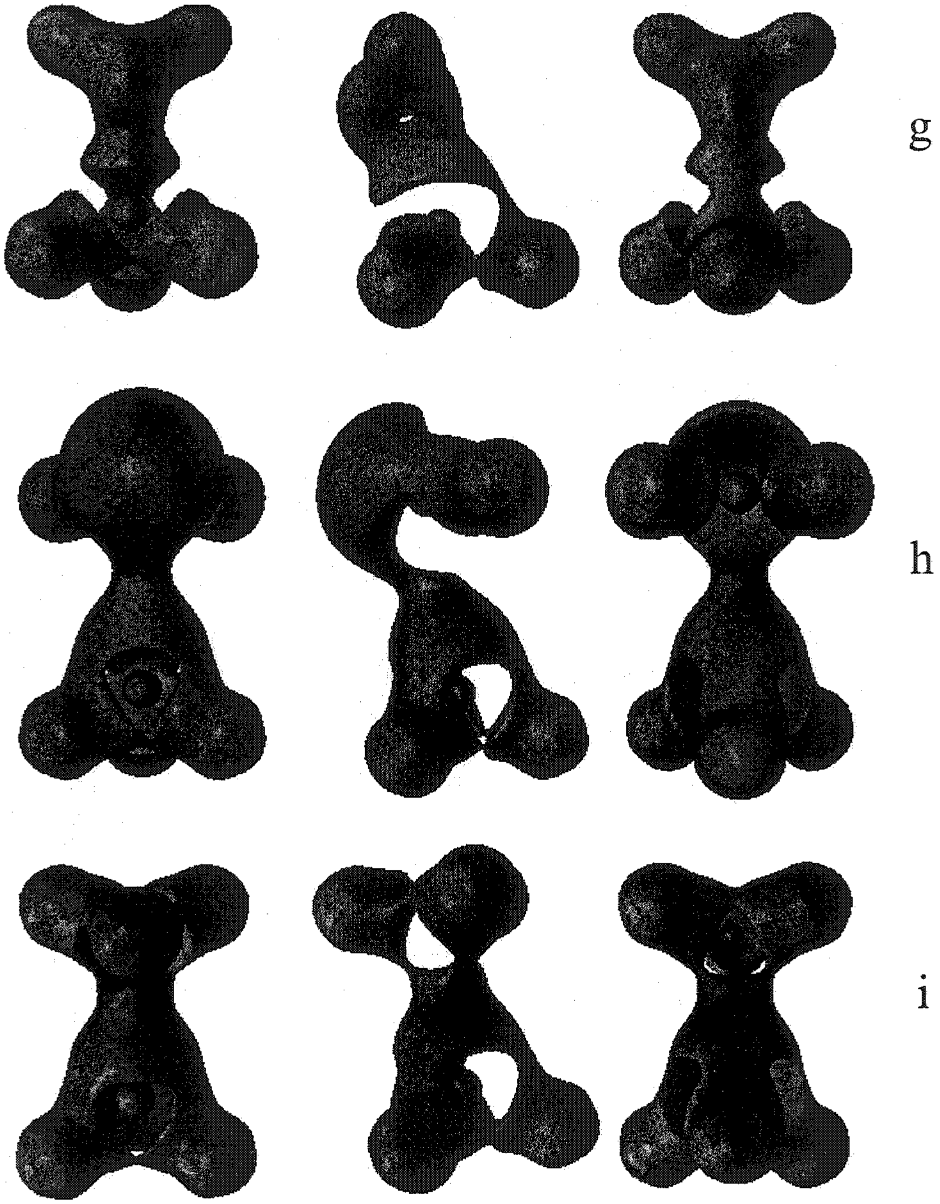

Figure 6-7: Continued on next page.

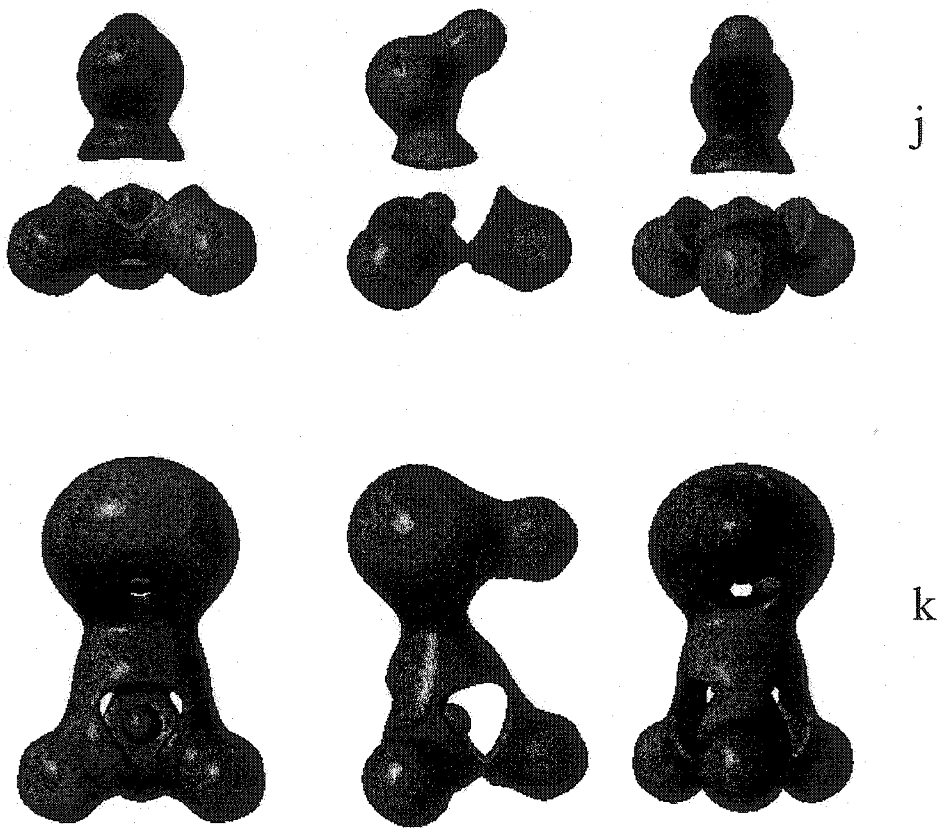

Figure 6-7: Isovalue envelopes of $\nabla^2\rho(\mathbf{r}) = 0$; 'front', 'side' and 'back' views of H_3PX: **a)** H_3PO, **b)** H_3PNH *trans*, **c)** H_3PCH_2*planar*, **d)** H_3PS, **e)** H_3PPH *trans*, **f)** H_3PSiH_2*planar*, **f)** H_3PCH_2*pyramidal* **h)** H_3PSiH_2*pyramidal* **i)** PH_3BH_3 **j)** H_3PNH *cis* **k)** H_3PPH *cis*.

6.11. Data Tables

Table 6-1: Optimized geometries of phosphoranes and related systems, PH_3EH_{n-1}, at the HF and MP2 (in italics) levels, compared to phosphine, PH_3.
Related experimental values are given where available.

Phosphorane	**r(P-E)**	**r(P-H)^1**	**∠ HPH^2**	**∠ HPE^1**	**-Energy /au**	**ΔE^5 / kJ/mol**
PH_3		140.43	95.44		342.47746	
		140.71	*93.52*		*342.76703*	
QCISD		*141.23*	*93.52*		*342.79392*	
Exp't^a		141.15 ± .05	93.36 ± .08			
PH_3O	145.32	139.46	101.84	116.32	417.38055	9.5
MP2	*148.72*	*140.06*	*101.15*	*116.88*	*417.90567*	*-0.2*
QCISD	*148.10*	*140.33*	*101.23*	*116.82*	*417.76630*	
Exp't.^{b}	147.63	144.06	104.29	114.26		
Deriv.Exp't.^{c}	(147.6 ± .2)		(104.1 ± .8)	(114.4 ± .7)		
PH_3NH (**1a**,	154.03	138.5	101.9	110.1	397.49679	118
trans)	*156.51*^{6}	*138.80*	*101.4*	*109.1*	*397.99992*	*105*
PH_3NH (**1b**,	153.73	139.90	101.1	119.75	397.49441	124
cis)	*156.07*^{6}	*140.53*	*100.5*	*121.5*	*397.99690*	*113*
PH_3CH_2 (**2a**,	165.44	138.59	102.3	110.65	381.44925	216
planar)	*166.03*	*138.90*	*101.99*	*110.31*	*381.91890*	*207*
PH_3CH_2(**2b**^{3},	166.5	141.66	98.62	126.86	381.45074	212
quasiplanar)	*167.39*	*142.56*	*97.96*	*128.67*	*381.92070*	*202*
DerivExp't.^{d}	(165.6 ± .2)		(101.0 ± 2.)	(122.4 ± .7)		
PH_3S	195.05	139.21	101.39	116.69	740.03361	18
	195.00	*139.83*	*100.28*	*117.58*	*740.59292*	*20*
Deriv.Exp't.^{c}	(194.0 ± .2)		(104.5 ± .3)	(114.1 ± .2)		
PH_3PH (**1a**,	210.91	138.84	101.68	109.97	683.77287	110
trans)	*208.94*	*139.21*	*100.53*	*109.96*	*684.32566*	*101*
Deriv.Exp't.^{e}	(208.4 ± .2)					
PH_3PH (**1b**,	212.56	138.85	101.59	114.6	683.76971	118
cis)	*210.33*	*139.23*	*100.55*	*115.55*	*684.32238*	*109*
PH_3SiH_2 (**2a**	214.66	138.84	102.49	106.25	632.48048	303
planar)	*213.52*	*139.24*	*102.01*	*104.81*	*633.01815*	*280*
PH_3SiH_2 (**2c**)	239.83	139.54	100.35	123.25	632.53512	159
staggered pyramidal^4	*233.10*	*139.97*	*99.11*	*125.08*	*633.06804*	*149*
PH_3SiH_2 (**2d**)	244.56	139.33	99.84	116.61	632.53250	166
eclipsed pyramidal^4	*237.27*	*139.69*	*98.47*	*117.50*	*633.06467*	*158*

- Bond lengths are in picometers and angles are in degrees.

1. Refers to the P-H bond in the plane of symmetry.
2. Refers to the angle between two inequivalent H's bound to P.
3. C_s symmetry with equivalent C-H bonds, sum of angles about C = 353.0° (*349.7°* at MP2)
4. C_s symmetry with equivalent Si-H bonds, sum of angles about Si = 272.1° (*staggered*), 269.7° (*eclipsed*).
5. Energy relative to phosphine tautomer; PH_2EH_n at the lowest energy conformation
6. Displacement not converged for the MP2 optimizations of PH_3NH.

Table 6-1 References:

a) Chu, F.Y. and T. Oka (1974). Microwave.
b) Ahmad, I.K., H. Ozeki and S. Saito (1999). Microwave.
c) *Electron diffraction for Me_3PS, Me_3PO*: Wilkins *et al.* (1975).
d) *Electron diffraction for Me_3PCH_2* : Ebsworth, Fraser and Rankin (1977). Modified analysis by Mitzel *et al.* (1998).
e) *X-ray for Me_3PPDmp* Shah, S, Yap and Protasiewicz (2000). Steric interaction with Dmp (dimesitylphenyl) makes angles unreliable.

Table 6-2: Optimized geometries of H_3NEH_{n-1} at the HF level, compared to amine. Experimental values are given where available.

H_3NX	**r(N-E)**	**r(N-H)^1**	**∠ HNH^2**	**∠ HNE^1**	**-Energy /au**	**ΔE^5 / kJ/mol**
NH_3 Exp't ^{a}		99.84 101.56	107.89 107.28		56.21864	
NH_3O DerivExp't^b	136.68 (115.8 ± .4)	100.62	107.41 (100.8 ± 1.1)	111.46 (117.1± .9)	131.00001	105
NH_3NH (*trans*)	147.19	100.02	107.10	105.24	111.14883	196
NH_3NH (*cis*)	148.29	100.26	107.27	114.84	111.14649	202
NH_3CH_2	148.57	100.13	106.30	107.83	95.12569	328
NH_3CH_2 *pyramidal*^{3}	157.39	100.51	108.22	117.67	95.14551	276
NH_3S	184.17	99.99	108.72	110.21	453.71725	47
NH_3PH (*trans*)	195.35	100.04	107.51	107.51	397.48881	139
NH_3PH (*cis*)	197.60	99.94	108.14	109.88	397.48747	142
NH_3SiH_2 *pyramidal*^{4}	206.14	99.94	108.53	111.86	346.28029	166

- Bond lengths are in picometers and angles are in degrees.

1. Refers to the N-H bond in the plane of symmetry.
2. Refers to the angle between two inequivalent H's bound to N.
3. C_s symmetry with equivalent C-H bonds, sum of angles about C = 311.7°.
4. C_s symmetry with equivalent Si-H bonds, sum of angles about Si = 273.8°.
5. Energy relative to amine tautomer; NH_2EH_n at the lowest energy conformation.

Table 6-2 References:

a) Helminger, DeLucia and Gordy (1971). Microwave, no uncertainties reported.
b) *Electron diffraction for F_3NO:* Plato, V., W.D. Hartford, and K. Hedberg (1970). Expect an electronic substituent effect to shorten the N-O bond and thus narrow FNF angle.

Table 6-3. Properties of P-E bond critical points and delocalization indices in PH_3X systems. MP2 values in italics.

Phosphorane	$\rho(r_b)$	$\nabla^2\rho(r_b)$	$\varepsilon(r_b)$	$r(P\text{-}r_b)$	$r(E\text{-}r_b)$	$\delta(P,E)$	$\delta(P,X)$
PH_3O	0.259	+1.41	0	1.112	1.634	0.81	0.81
MP2	*0.236*	*+1.08*	*0*	*1.143*	*1.665*		
QCISD	*0.239*	*+1.14*	*0*	*1.136*	*1.663*		
PH_3NH *trans*	0.233 *0.215*	+0.60 *+0.43*	0.16 *0.16*	1.165 *1.195*	1.750 *1.766*	0.89	0.91
PH_3NH *cis*	0.234 *0.217*	+0.62 *+0.45*	0.18 *0.18*	1.163 *1.192*	1.745 *1.760*	0.88	0.90
PH_3CH_2	0.207 *0.198*	-0.10 *-0.15*	0.47 *0.46*	1.251 *1.288*	1.876 *1.851*	1.01	1.07
PH_3CH_2 *quasiplanar*	0.205 *0.194*	-0.15 *-0.27*	0.44 *0.43*	1.264 *1.306*	1.885 *1.858*	1.03	1.10
PH_3S	0.163 *0.155*	-0.20 *-0.15*	0 *0*	1.843 *1.798*	1.843 *1.885*	1.45	1.45
PH_3PH *trans*	0.116 *0.117*	-0.07 *-0.09*	1.18 *0.74*	2.497 *2.315*	1.491 *1.636*	1.17	1.33
PH_3PH *cis*	0.113 *0.114*	-0.06 *-0.09*	1.15 *0.71*	2.526 *2.346*	1.497 *1.633*	1.14	1.30
PH_3SiH_2 [1] *planar*	0.092 *0.092*	+0.15 *+0.10*	1.42 *1.26*	2.618 *2.570*	1.440 *1.467*	1.00	1.29
PH_3SiH_2 *staggered*	0.059 *0.066*	+0.02 *+0.008*	0.36 *0.26*	2.933 *2.797*	1.640 *1.644*	0.50	0.80
PH_3SiH_2 *eclipsed*	0.054 *0.061*	+0.014 *+0.01*	0.29 *0.21*	2.985 *2.844*	1.684 *1.678*	0.46	0.75
PH_3BH_3	0.092	+0.13	0	2.732	1.048	0.33	0.86
PH_3SH_2 [1]	0.157	-0.05	2.72	1.350	2.288	1.22	1.37

- Distances from nuclei to bond critical points, $r(E\text{-}r_b)$, are given in atomic units.

1) P and E (Si or S) integrated by Promega in *planar* PH_3SiH_2 and in PH_3SH_2.

Table 6-4: Properties of N-E bond critical points and delocalization indices in H_3NX systems.

H_3NX	$\rho(r_b)$	$\nabla^2\rho(r_b)$	$\varepsilon(r_b)$	$r(N\text{-}r_b)$	$r(E\text{-}r_b)$	$\delta(N,E)$	$\delta(N,X)$
NH_3O	0.342	-0.16	0	1.354	1.229	1.32	1.32
NH_3NH *trans*	0.253	-0.165	0.24	1.576	1.205	1.16	1.21
NH_3NH *cis*	0.247	-0.14	0.24	1.589	1.213	1.14	1.19
NH_3CH_2 [1]	0.208	+0.17	3.30	1.932	0.875	0.94	1.08
NH_3CH_2 *pyramidal*	0.171	-0.16	0.23	1.971	1.017	0.82	0.98
NH_3S	0.127	+0.05	0	2.069	1.411	1.01	1.01
NH_3PH *trans*	0.086	+0.13	0.94	2.254	1.444	0.70	0.81
NH_3PH *cis*	0.084	+0.12	1.01	2.266	1.458	0.69	0.80
NH_3SiH_2 *pyramidal*	0.058	+0.16	0.27	2.386	1.522	0.38	0.60

- Distances from nuclei to bond critical points, $r(E\text{-}r_b)$, are given in atomic units.

1) N and C integrated by Promega in *planar* NH_3CH_2.

Table 6-5: Atomic and group properties in PH_3X systems, compared to PH_3. MP2 values in italics.

Phosphorane	**q(P)**	**q(E)**	**q(EH_n)**	**q(H)**	**K(P)**	**L (P)**	**L (E)**
PH_3	+1.695			-0.564	340.100	1.6 e-3	
MP2	*+1.46*			*-0.485*	*340.458*	*1.8 e-3*	
QCISD	*+1.45*			*-0.482*	*340.466*	*1.8 e-3*	
PH_3O	+3.37	-1.57	-1.57	-0.598	339.347	4.9 e-3	-2.3 e-4
MP2	*+3.01*	*-1.43*	*-1.43*	*-0.527*	*339.769*	*4.2 e-3*	*-1.1 e-4*
QCISD	*+3.06*	*-1.45*	*-1.45*	*-0.533*	*339.619*	*5.4 e-3*	*-1.3 e-4*
PH_3NH *trans*	+3.26	-1.84	-1.46	-0.599	339.403	7.6 e-3	-1.8 e-4
	+2.88	*-1.66*	*-1.30*	*-0.525*	*339.842*	*6.1 e-3*	*4.7 e-4*
PH_3NH *cis*	+3.27	-1.86	-1.47	-0.599	339.392	7.0 e-3	2.3 e-4
	+2.98	*-1.69*	*-1.31*	*-0.526*	*339.827*	*3.5 e-3*	*-2.8 e-4*
PH_3CH_2	+3.02	-1.22	-1.24	-0.592	339.553	7.1 e-3	7.4 e-4
	+2.63	*-1.14*	*-1.07*	*-0.517*	*339.998*	*4.8 e-3*	*2.8 e-4*
PH_3CH_2	+2.97	-1.16	-1.19	-0.591	339.580	2.3 e-3	-2.7 e-4
quasiplanar	*+2.56*	*-1.07*	*-1.01*	*-0.516*	*340.031*	*1.4 e-3*	*-5.3 e-4*
PH_3S	+2.36	-0.66	-0.66	-0.571	339.823	-2.6 e-4	1.5 e-4
	+2.10	*-0.60*	*-0.60*	*-0.500*	*340.175*	*2.8 e-3*	*1.2 e-4*
PH_3PH *trans*	+1.82	+0.46	-0.11	-0.566	340.059	7.2 e-3	-5.6 e-4
	+1.64	*+0.31*	*-0.16*	*-0.492*	*340.383*	*4.9 e-3*	*3.6 e-4*
PH_3PH *cis*	+1.82	+0.45	-0.12	-0.565	340.055	7.1 e-3	1.1 e-3
	+1.64	*+0.31*	*-0.16*	*-0.492*	*340.379*	*3.6 e-3*	*5.6 e-4*
PH_3SiH_2[1]	+1.37	+1.76	+0.31	-0.563	340.161	5.6 e-4	-4.1 e-3
planar	*+1.17*	*+1.60*	*+0.28*	*-0.483*	*340.516*	*5.4 e-3*	*-1.5 e-3*
PH_3SiH_2	+1.72	+1.44	-0.04	-0.557	340.126	5.8 e-3	4.8 e-3
staggered	*+1.49*	*+1.32*	*-0.03*	*-0.481*	*340.479*	*7.5 e-3*	*4.5 e-3*
PH_3SiH_2	+1.74	+1.43	-0.07	-0.555	340.123	4.8 e-3	4.7 e-3
eclipsed	*+1.51*	*+1.31*	*-0.06*	*-0.479*	*340.470*	*7.6 e-3*	*4.6 e-3*
PH_3BH_3	+1.82	+1.96	-0.12	-0.566	340.154	2.7 e-3	3.9 e-3
PH_3SH_2[1]	+2.56	-0.46	-0.88	-0.562	339.626	1.8 e-4	4.9 e-4

- q(H) refers to the average of the H atoms bonded to P.

1) P and E (Si or S) integrated by Promega in *planar* PH_3SiH_2 and in PH_3SH_2.

Table 6-6: Atomic and group properties in H_3NX, compared to amine.

H_3NX	**q(N)**	**q(E)**	**q(EH_n)**	**q(H)**	**K(N)**	**L(N)**	**L(E)**
NH_3	-1.044			+0.348	54.745	7.0 e-5	2.7 e-5
NH_3O	-0.51	-0.69	-0.69	+0.398	54.676	-1.6 e-3	-4.7 e-5
NH_3NH *trans*	-0.74	-0.72	-0.46	+0.402	54.789	1.9 e-4	-7.9 e-4
NH_3NH *cis*	-0.75	-0.73	-0.46	+0.405	54.793	2.0 e-4	3.2 e-4
NH_3CH_2[1]	-1.02	-0.14	-0.20	+0.404	54.938	6.1 e-4	-9.3 e-3
NH_3CH_2 *pyr*	-1.00	+0.01	-0.22	+0.407	54.915	1.0 e-4	-3.0 e-3
NH_3S	-1.07	-0.24	-0.24	+0.438	54.886	-2.3 e-3	7.5 e-4
NH_3PH *trans*	-1.16	+0.49	-0.11	+0.424	54.902	-5.6 e-4	-1.0 e-3
NH_3PH *cis*	-1.16	+0.49	-0.12	+0.426	54.899	1.2 e-4	-8.5 e-4
NH_3SiH_2 *pyr*	-1.19	+1.47	-0.04	+0.413	54.900	-4.5 e-4	1.0 e-3

- q(H) refers to the average of the H atoms bonded to N.

1) N and C integrated by Promega in *planar* NH_3CH_2.

Table 6-7: Properties of P-E bonding CC in PH_3X systems, at the HF level.

PH_3X	$\nabla^2\rho(r)$	$\rho(r)$	r(P)	r(E)
PH_3O $PH_3\mathbf{O}$	-0.362 -2.544	0.340 0.722	1.467 2.025	1.279 0.721
PH_3NH (*t*)	-1.413	0.440	2.075	0.8384
PH_3NH (*c*)	-1.420	0.442	2.071	0.8384
PH_3CH_2 (*pl*)	-0.732	0.259	2.116	1.011
PH_3CH_2 (*qp*)	-0.727	0.257	2.157	1.002
$PH_3\mathbf{S}$ PH_3S	-0.211 -0.354	0.172 0.168	2.246 1.475	1.450 2.211
PH_3PH (*t*)	-0.390	0.156	1.466	2.523
PH_3PH (*c*)	-0.391	0.155	1.466	2.560
PH_3SiH_2 (*pl*)	-0.371	0.151	1.474	2.594
PH_3SiH_2 (*s*)	-0.399	0.146	1.451	3.084
PH_3SiH_2 (*e*)	-0.396	0.145	1.451	3.170
PH_3BH_3	-0.455	0.161	1.444	2.336

- Distances from nuclei to maxima, r(E), are given in atomic units.
- The bolded element represents the atom in whose valence shell the CC is found.
- Bonding charge concentrations out of the symmetry plane are listed in Table 6-8.

Table 6-8: Properties of non-bonding charge concentrations *and intervening saddle points,* on the substituent atom, E, in H_3PX systems at the HF level.

PH_3X	$\nabla^2\rho(r)$	$\rho(r)$	Z	r(E)	# nb CC's; expected pairs
PH_3O *saddle*	-3.790 *-3.745*	0.830 **0.828**		0.666 *0.666*	3; (2)
PH_3NH (*t*) *saddle*	-1.812 -1.803	0.4818 0.4819	±0.396 0	0.770 0.769	2; 1
PH_3NH (*c*)	-1.832	0.484	0	0.769	1; 1
PH_3S *saddle*	-0.416 -0.399	0.174 0.172		1.322 1.324	3; (2)
PH_3PH (*t*) *saddle*	-0.253 -0.169	0.118 0.102	±1.358 0	1.473 1.488	2; 1
PH_3PH (*c*) *saddle*	-0.248 -0.091	0.117 0.100	±1.356 0	1.474 1.529	2; 1
PH_3SiH_2 (*pl*)	-0.068	0.056	±1.621	1.771	*2π-bond CC's, r(P)=3.72*
PH_3SiH_2 (*s*)	-0.132	0.074	0	1.665	1
PH_3SiH_2 (*e*)	-0.133	0.075	0	1.663	1
PH_3SH_2 PH_3SH_2 PH_3SH_2	-0.601 -0.404 -0.238	0.196 0.186 0.141	0 ±0.793 ±0.707	1.293 1.356 1.527	1; 1 *2 π-bond CC's, r(P)= 2.66* *2 π-bond CC's, r(S)= 2.39*

- Distances from nuclei to maxima, r(E), are given in atomic units.
- Z is the distance from the critical point to the molecular symmetry plane, in au.
- For PH_3O and PH_3S each CC makes a dihedral angle of 180° with an H bound to P, the saddles make dihedral angles of zero degrees with the H atoms, *i.e.* 180° with the maxima.
- The total number of non-bonding maxima is shown, along with the number of lone pairs expected from the doubly bonded Lewis structures.

Table 6-9: Properties of non-bonding CCs on E in H_3NX at the HF level.

NH_3X	$\nabla^2\rho(r_b)$	$\rho(r_b)$	Z	$r(E\text{-}r_b)$	# nb CC's, expected pairs
NH_3O saddle	-5.66 -5.61	0.949 0.947		0.6477 0.6479	3 (2)
NH_3NH (*t*) saddle	-2.887 -2.049	0.567 0.503	± 0.698 0	0.745 0.761	2, 1
NH_3NH (*c*) saddle	-2.901 -2.087	0.567 0.506	±0.696 0	0.745 0.760	2, 1
NH_3CH_2 (*pl*)	-0.694	0.249	± 0.929	0.933	2, 0
NH_3CH_2(*py*)	-1.234	0.294	0	1.008	1 (0)
NH_3S saddle	-0.550 -0.542	0.194 0.193		1.303 1.304	3 (2)
NH_3PH (*t*) saddle	-0.331	0.132	±1.367 0	1.451	2, 1
NH_3PH (*c*) saddle	-0.328 -0.155	0.132 0.102	±1.370 0	1.451 1.491	2, 1
NH_3SiH_2	-0.149	0.079	0	1.651	1 (0)

- Distances from nuclei to maxima, r(E), are given in atomic units.
- Z is the distance from the critical point to the molecular symmetry plane, in au.
- For NH_3O and NH_3S each CC makes a dihedral angle of 180° with an H bound to N, the saddles make dihedral angles of zero degrees with the H atoms, *i.e.* 180° with the maxima.
- The total number of non-bonding maxima is shown, along with the number of lone pairs expected from the Lewis structures.

Bibliography

References are listed alphabetically by first author and then by date, with the references in the Data Tables sections listed separately.

Ahmad, I.K.; H. Ozeki and S. Saito (1999). *J. Chem. Phys.* **110**, 912.

Bachrach, S.M. (1992). *J. Org. Chem.* **57**, 4367.

Dobado, J.A.; H. Martínez-García, J.M. Molina and M.R. Sundberg (1998). *J. Am. Chem. Soc.* **120**, 8461.

Ebsworth, E.A.V.; T.E. Fraser and D.W.H. Rankin (1977). *Chem. Ber.* **110**, 3495.

Gilheany, D.G. (1994). *Chem. Rev.* **94**, 1339.

Gillespie, R. J. (1972). Molecular Geometry. New York: Van Nostrand Reinhold.

Hamilton, L.A. and P.S. Landis (1972). *Phosphinous Acids and Derivatives*, in Organic Phosphorus Compounds , Volume 4, G. M. Kosolapoff and L. Maier editors. New York: Wiley Interscience.

Kwiatkowski, J. S.and J. Leszczynski. (1992). *Molecular Physics* **76**(2), 475.

Malcolm, N.O.J.; R.J. Gillespie and P.L.A. Popelier (2002). *J. Chem. Soc. Dalton Trans.* **2002**, 3333.

Mitzel, N.W. *et al.* (1998). *Angew. Chem. Int. Ed. Engl.* **37**, 1670.

Musher, J. I. (1969). *Angew. Chem. Int. Ed. Eng.* **8**, 54.

Noury, S; B. Silvi and R. J. Gillespie (2002) *Inorg. Chem.* **41**, 2164.

Power, P.P. (1999). *Chem. Rev.* **99**, 3463.

Schmidpeter, A (1990). *Phosphinylidene-σ^4-phosphoranes and phosphinylidenesulfuranes*, Chapter D10 in Multiple Bonds and Low Coordination in Phosphorus Chemistry, M. Regitz and O.J. Scherer, editors. Stuttgart: Verlag.

Teppen, B.J.; D.M. Miller, M. Cao, R.F. Frey, S.Q. Newton, F.A. Momany, M. Ramek and L. Schaefer, (1994). *THEOCHEM* **117**, 9.

Walker, B.J. (1972). Organophosphorus Chemistry. London: Penguin Books.

Wilkins, C.J.; K. Hagen, L. Hedberg, Q. Shan and K. Hedberg (1975). *J. Am. Chem. Soc.* **97**, 6352.

Table References

Ahmad, I.K.; H. Ozeki and S. Saito (1999). *J. Chem. Phys.* **110**, 912.

Chu, F.Y. and T. Oka (1974). *J. Chem. Phys.* **60**, 4612.

Ebsworth, E.A.V.; T.E. Fraser and D.W.H. Rankin (1977). *Chem. Ber.* **110**, 3495.

Helminger, P.; F.C. DeLucia and W. Gordy (1971). *J. Mol. Spectrosc.* **39**, 94.

Mitzel, N.W. *et al.* (1998). *Angew. Chem. Int. Ed. Engl.* **37**, 1670.

Plato, V.; W.D. Hartford, and K. Hedberg (1970). *J. Chem. Phys.* **53**, 3488.

Shah, S., G.P. Yap and J.D. Protasiewicz (2000). *J. Organomet. Chem.* **608**, 12.

Wilkins, C.J.; K. Hagen, L. Hedberg, Q. Shan and K. Hedberg (1975). *J. Am. Chem. Soc.* **97**, 6352.

7. Bis(ylene)phosphorane Results

While the phosphoranes have three single bonds and a potential double bond, the bis(ylene)phosphoranes, HPX_2, have one single bond and two potential double bonds to the phosphorus atom. Like the phosphoranes, they are formally pentavalent but may also be drawn with ylidic (zwitterionic) resonance structures. Since either one of the two ylene bonds can be drawn as a double bond in a tetravalent structure, the octet rule leads to an average P-X bond order of 1.5, *versus* 1.0 for the phosphoranes (H_3PX) and 2.0 for the phosphinylidenes (HPX).

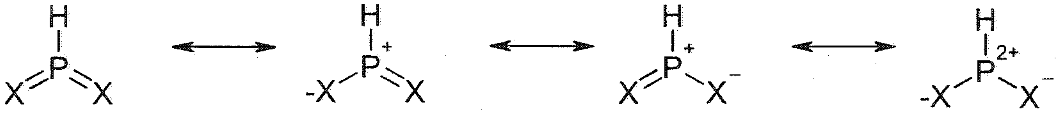

Bis(ylene)phosphoranes, $HP(=X)_2$, are experimentally known only when the hydrogen atoms are replaced by other groups (see Section E of Regitz and Scherer, 1990). Bis(methylene)phosphoranes are relatively well known, and bis(imino)phosphoranes have been isolated and structurally characterized. Mes^*PS_2 and Mes^*PSe_2 are known, but RPO_2 is highly reactive (Meisel, 1990). Some mixed bis(ylene)phosphoranes are known, such as $Y'P(X)=CY_2$ and $Y'P(X)=NY$ where X = NY, O, S or Se. These are typically made by oxidative addition to phosphaalkenes or phosphaimines. The C and N atoms are typically substituted with electron donating $SiMe_3$ groups, while the P may have a variety of sterically bulky and/or electron withdrawing substituents, Y′.

The same set of six molecules (X = O, NH, CH_2, S, PH, SiH_2) discussed here was studied computationally by Schoeller and Busch (1992) to determine their stability towards electrocyclization. They found that only HPS_2, HPO_2 and $HP(NH)_2$ prefer the open structure to the three-member ring. The major purpose for including this set of molecules in the current study is as a comparison with the phosphenium cations, Chapter 8. In Chapter 4, we saw systems with two single P-E bonds and here we see systems with, potentially, two P-E double bonds.

7.1. Geometry

7.1.1. Molecular symmetry

All the bis(ylene)phosphoranes were optimized within the C_2v point group. Previous calculations have shown all but bis(silylene)phosphorane to be planar (Schoeller, 1990). This is in contrast to the phosphorane case, which is found to be somewhat pyramidal at carbon, in H_3PCH_2. MCSCF calculations have found the C_2-twisted structure of $HP(SiH_2)_2$ to have biradical character (Schoeller and Busch, 1992). Optimized bond lengths and bond angles about P for the current study are given in Table 7-1. Where both *exo* (**1a**) and *endo* (**1b**) isomers are possible, the *endo* isomer is lower in energy by 15 to 30 kJ/mol, in agreement with an earlier study (Schoeller and Lerch, 1986). This preference is slightly increased at MP2. The *exo/endo* isomer (**1c**) was not investigated.

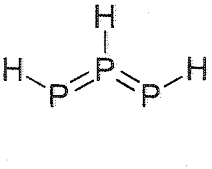
1a

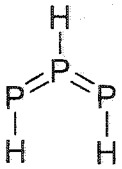
1b

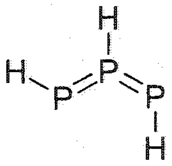
1c

At the Hartree-Fock level of theory, the preference for a C_2-twisted, pyramidal geometry at silicon is only half as strong, 70 kJ/mol, in the bis(silylene)phosphorane as in the silylenephosphorane, H_3PSiH_2.

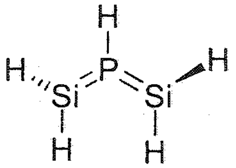

In contrast to the phosphorane case, optimal 'π-type' overlap in $HP(CH_2)_2$ requires a specific orientation of the CH_2 plane. In the Linnett (banana bond) model, we can describe the interaction of a square-based pyramid for the pentavalent P with a tetrahedron of electron pairs on each carbon atom.

The octet rule predicts less ylidic (zwitterionic) character in the bisylenes than in the phosphoranes, for all substituents. As in the phosphoranes, there is no opportunity to directly observe pyramidalization of the pnictogens or chalcogens from geometric parameters, but we will investigate the topology of the Laplacian below. Twisted structures or pyramidalization at phosphorus would indicate that the second bonding electron pair had become localized – on the substituent or central P atom, respectively. The vibrational frequency for inversion at the central phosphorus was calculated by Schoeller and Busch (1992). They found wavenumbers of: HPO_2 731 cm^{-1}, $HP(NH)_2$ 611 cm^{-1}, $HP(CH_2)_2$ 390 cm^{-1}, HPS_2 564 cm^{-1}, and $HP(PH)_2$ 331 cm^{-1}, indicating that the planar geometry was a minimum for all these species.

7.1.2. Comparison to related experimental structures

The experimental methylene derivative systems are planar at phosphorus and at carbon, but are twisted about the P=C bonds, perhaps due to steric constraints. The earliest bis(methylene)phosphoranes were substituted with *σ-donors,*[*] such as trimethylsilyl, on the carbon atoms; $YP[C(SiMe_3)_2]_2$, but with a range of substituents on the phosphorus atom. The X-ray determined P-C bond length ranges from 162 pm when Y = Cl to 170 pm when Y = $CHPh_2$. The optimized bond length for the unsubstituted system is 163 pm. The CPC angle ranges from 137° when Y = Cl to 127° when Y = $CHPh_2$ (Appel, 1990, p.370). The optimized bond angle is 135°, again in close agreement with the experimental data for $ClP[C(SiMe_3)_2]_2$.

The bis(imino)phosphoranes that have been studied experimentally are similar to the bismethylenes, in that there are typically electron-donating groups on nitrogen. The phosphorus substituent, Y, is often an amino group, $N(SiMe_3)_2$. The X-ray determined P=N bond length in $(SiMe_3)_2N\text{-}P(=NSiMe_3)_2$ is 151.5 pm and the NPN bond angle is 134.3°. The optimized values are 151 pm and 141°. The

---

[*] Methylene phosphoranes are stabilized by electron acceptors at C.

difference in angle is most likely due to steric effects, which also cause a torsion angle of 32° at the amino nitrogen atom for the experimentally observed endo/endo structure (Niecke and Gudat, 1990).

Steric stabilization is possible in place of electronic stabilization. Changing the substituents, to Mes-P(=$NSiMe_3$)(=$NMes^*$), increased the P-N bond lengths to 153.3 pm ($SiMe_3$) and 154.9 pm (Mes^*). We can expect that replacing the electron donating substituents ($SiMe_3$) at nitrogen (or carbon) and the electron donating group (NR_2) at phosphorus with hydrogen atoms would also lengthen the P=N (or P=C) bonds so that, as usual, the HF optimized bond lengths are short.

Dioxophosphoranes are only known as intermediates, so there is no experimental structural data. The dithioxophosphoranes, on the other hand, are stable, when the phosphorus substituent is a large aryl group such as supermesityl.* The X-ray structure of Mes^*PS_2 shows that the geometry is planar about P, with an SPS bond angle of 126° and a P-S bond length of 190 pm (Appel *et al.*, 1983).† This compares well with the optimized bond length of 189 pm, which is shorter than both the phosphinidene and the phosphorane bonds. Note that in the H_3PX series P-M bonds were found to be too long (compared to MP2 and experimental values) when optimized at the HF level. In this series, MP2 lengthens all the P-E bonds by 2 to 5 pm and P-H bonds by about 1 pm.

---

[*] The same synthetic approach [Ar-P$(TMS)_2$ + S_2Cl_2] leads to a four-membered ring dimer, when Ar = Ph.

[†] The aromatic ring makes an 80° dihedral angle with the PS_2 plane.

7.1.3. Comparison to other calculated P-E bonds

The P-E bond lengths are plotted, for all the series studied, in Figure A4-1. The P-L bond lengths in the bis(ylene)phosphoranes, HPX_2, are slightly shorter than the corresponding phosphinylidene (HPX) and phosphorane (H_3PX) bond lengths. The same is true of the P-S bond, but the P-P and P-Si bonds (in the planar geometries of HPX_2) are slightly longer than the phosphinylidene bonds. The phosphorane bonds are significantly longer. The twisted geometry has a P-Si bond 6 pm longer than the planar geometry, which is a much smaller difference than in the phosphoranes, H_3PHSiH_2.

The decreased ability of electropositive elements, P and Si, to form double bonds to hypervalent phosphorus is much less evident in the HPX_2 bond lengths (and deformation energies for silylene) than it was in the phosphoranes. The variation from the HP=X bond lengths is on the same order of magnitude as that between the differently substituted fluorophosphines. The same is true of the second row phosphoranes. Only $H_3P{=}PH$, $H_3P{=}SiH_2$ and *twisted* $HP(SiH_2)_2$ show significant bond lengthening relative to HP=X.

The XPX bond angles are consistent with one small and two large ligands around the phosphorus atom. The short P-H bonds are also consistent with little steric crowding, and may be further shortened by the large positive charges on P relative to the phosphinylidenes.

7.2. Bond Paths and Interatomic surfaces

Bond paths are found between all pairs of atoms that we expect to be bonded. Properties and positions of the P-E bond critical points (BCPs) are given in Table 7-2. There are no ring or cage critical points in the molecules studied. The bonding radii of the central phosphorus atom, and the substituent atom, E, are plotted *versus* E in Figures A4-2 and A4-3, respectively. The bonding radii of the substituents follow the same trends as in the phosphoranes.

The bonding radii of the phosphorus atoms along the P-L bonds are very similar to those in HP=X and H_3P=X. The bonding radii of P along the P-M bonds follow the same trend as H_3P=X, but are 0.24 to 0.08 au shorter. Sulfur has a somewhat longer bonding radius in HPS_2 than in H_3PS, while the other substituents have slightly shorter bonding radii than in H_3PX. When compared to HP=X, the P-P and P-S BCPs are significantly pushed towards the substituent, for both the phosphorane and bis(ylene)phosphorane series. For the bis(silylene)phosphorane, twisting lengthens both radii by about 0.07 au. The bonding radii in *twisted* $HP(SiH_2)_2$ are very similar to those in the H_3PSiH_2 system with a *planar* SiH_2 group.

Correlation at the MP2 level lengthens both radii relative to the HF values, for X = O and NH. When X = CH_2 and S, only the P bonding radius is significantly lengthened, so the BCP effectively shifts towards the substituent. In $HP(PH)_2$, correlation shortens the bonding radius of the central (pentavalent) phosphorus and lengthens those of the other (trivalent) P atoms. The same trend is seen for both planar and twisted $HP(SiH_2)_2$, but to a lesser extent.

7.3. Bond Critical Points

7.3.1. Density, $\rho(r_b)$

The BCP densities for the P-E bonds are plotted, for each series, in Figure A4-4. The values for the HPX_2 series are shown in Table 7-2. The P-L BCPs have $\rho(\mathbf{r}_b)$ values ranging from 0.28 to 0.21 au, very similar to the phosphinylidenes and phosphoranes, but slightly higher, consistent with the slightly shorter bonds. The P-M BCPs have $\rho(\mathbf{r}_b)$ values ranging from 0.18 to 0.10; lying between the phosphinylidenes and the phosphoranes for the planar P-P and P-Si bonds and above both for the P-S bonds.

While the P-Si bond length is similar to that in $HP{=}SiH_2$, the BCP density is much closer to the silyl phosphine values. The twisted geometry of $HP(SiH_2)_2$ has a slightly lower BCP density, again similar to planar H_3PSiH_2. Along with bond lengthening, MP2 reduces the density at the bond critical points, the smallest effects being for the twisted $HP(SiH_2)_2$.

7.3.2. Laplacian

The Laplacian at the P-E bond critical point is plotted in Figure A4-5. As in the other series, the Laplacian decreases sharply from O to C and increases slowly from S to Si. For F and O, the values are very similar to the phosphinylidenes. For C, P and Si, the values are between the phosphoranes and the phosphinylidenes (though the overall ordering switches between the second and third row). As in the phosphoranes and phosphinylidenes, correlation makes the Laplacian values more negative (except for the most negative value which becomes more positive) while the overall trend is preserved.

7.3.3. Ellipticity

The observed curvatures are all oriented in the expected direction. The values range from quite low for the chalcogens (O and S) to quite high for the P-P and P-Si bonds. The large ellipticity is maintained for the twisted silylene, along with the reasonably high density. The P-P and P-Si bonds have very large ellipticities, in all the formally double-bonded species.* The largest ellipticities (> 0.5) are reduced significantly by MP2 correlation, but planar Si and C remain highly elliptical. It was seen in H_3PX and H_3NX that these high ellipticities are associated with essentially non-bonding π-like density on the substituent atoms, when the bond critical point lies within the core region of the substituent.

7.4. Atomic and group charges

Atomic and group charges and energies (K= $G = -2V = -E$) are given in Table 7-3. See Chapter 4 for the interpretation of the integrated Laplacian, L. The

---

*The actual curvatures are quite small compared to P-L values. For H_3PCH_2 the values are about –0.3 and –0.2, while in H_3PSiH_2 the values are –0.05 and –0.04.

atomic charge on P and the group charge on X are plotted in Figures A4-6 and A4-7, respectively.

The charge transferred to each LH_{n-1} group lies between the phosphinylidene and phosphorane values; closer to H_3PNH for X = NH, and very close to $HPCH_2$ for X = CH_2. The trend is less obvious for the third row ligands. The charge on planar SiH_2 is also between the H_3PX and HPX values and is just above $q(SiH_3)$ in the phosphines. The twisted SiH_2 group* donates less charge to the PH group, having a positive charge intermediate between the H_3PSiH_2 and phosphine values. The charge on S in HPS_2 is similar to that in H_3PS, and less negative than that in HPS. The charge on the terminal PH in $HP(PH)_2$ is positive while in $H_3P{=}PH$ it is negative. This suggests that the bonding in $HP(PH)_2$ is more like that in HPS_2 and H_3PS than like the P-P bonding in H_3PPH.

The atomic charge on phosphorus is similar to that in the phosphoranes (H_3PX) for the second row ligands (significantly higher than in HPX and HPR_2). For the third row ligands, q(P) follows a similar trend to the phosphinylidenes (HPX) and to the disubstituted phosphines.

Correlation (MP2) reduces the magnitude of most charges, an exception being for X = PH where reduction of q(X) results in an increased positive charge on the central phosphorus atom. The PH groups become nearly neutral at the MP2

---

* It is important to keep in mind that a multiconfigurational treatment of this species may change the results considerably.

level, reminiscent of the H_3PPH and pyramidal H_3SiH_2 results. In another exception, the slightly decreased charge on twisted SiH_2 might be expected to decrease the negative charge on P, but the significantly decreased negative charge on the directly bonded H actually increases the charge on phosphorus.

7.5. Delocalization Indices and Bond Order

The delocalization indices between phosphorus and the substituent group are given in Table 7-2, and plotted in Figure A4-8. The delocalization index between P and the directly bonded hydrogen atom ranges from 0.65 to 1.00.

The delocalization index $\delta(P, X)$ ranges from 0.90 (HPO_2) to 1.66 (HPS_2 and $HP(PH)_2$). These values are from 70% (HPO_2 and $HP(NH_2)_2$) to 94% (HPS_2) of the phosphinylidene values. They are 33% (in HPO_2) to 60% (in HPS_2) greater than the disubstituted phosphine values, indicating a significant degree of multiple bonding.

Plotting a curve of delocalization, $\delta(P, X)$ *vs.* charge transfer, $q(X)$, as we have done for the previous series, all the points but planar CH_2 and twisted SiH_2 fall on a quadratic curve, Figure 7-1. Again, choosing two separate data sets better fits the data. For the H_3PX series, the H_3PO and H_3PNH data better matched the H_3PCH_2 data. For HPX_2, the $X = O$ and NH data seem to deviate less from the curve that includes the $X = S$ and PH data (set 1). The best-fit equation for set 1 is: $\delta = -0.4962q^2 - 0.1986q + 1.7204$; $R^2 = 0.9990$, which reaches a maximum of 1.74

when the charge transfer is 0.20 electrons to each of the substituents. Set 2, including the CH_2 data, but excluding the S and PH data also gave a good fit with a maximum delocalization index of 1.49, at a charge transfer of just 0.03 electrons, $\{\delta = -0.2628q^2 - 0.0160q + 1.4900;\ R^2 = 0.9963\}$. With the twisted SiH_2 data in place of the planar, the maximum drops to 1.44 at $q(X) = -0.2$ $\{R^2 = 0.9962\}$.

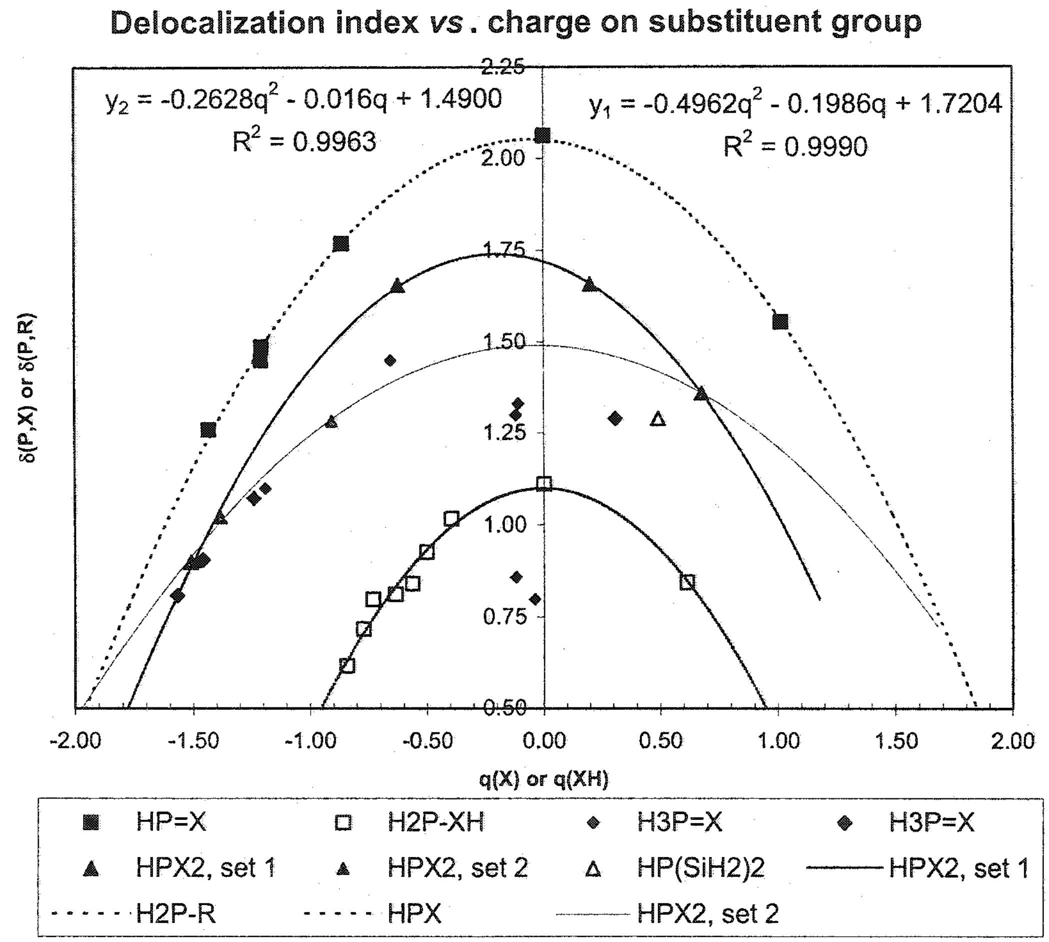

Figure 7-1: Delocalization *versus* charge curves for H_2PR, HPX and HPX_2. The HPX_2 data are split into two sets. Set 1 includes: X = O, NH, S, PH and *planar* SiH_2. Set 2 includes: X = O, NH, CH_2 and planar SiH_2. The twisted $HP(SiH_2)_2$ data point is also shown, without any connection to a best fit line. The data points for H_3PX are also shown, for comparison.

Many of the H_3PX data points lie quite close to the set-2 curve. The set-2 results have an appealing consistency with the predictions of the octet rule, that 1.5 bonds will be formed with each substituent, however we would then expect a formal charge of –0.5, not zero. The excluded S and PH indices are both 1.66. These substituents show the same unusual shift of the BCP towards the central P as in the phosphoranes and give excess delocalization in almost every series studied, though for the HP=X series it is only an additional 0.05.

The reduction of $\delta(P, X)$ in the phosphoranes and bis(ylene)phosphoranes, relative to HP=X, is *at least in part* due to the more positive charge on the phosphorus atom when X = O, NH and CH_2. For the third row substituents however, q(P) is very similar in HPX and HPX_2. The charge on P varies more with the degree of fluorine substitution in the phosphines, with much less effect on delocalization. There must be some real difference in the bonding to reduce the third row $\delta(P, X)$ values so that the HPX_2 curve lies halfway between HPX and H_3PX for X = S, PH and SiH_2.

Depending on which curve we believe is more representative of the series as a whole, we could say that the bond order for the planar, polar series is either 1.75, with a substituent formal charge of –0.2, or 1.5 with formal charge of zero. The curve including the PH and S data can be represented by a resonance scheme with 70 to 80% double bond character.

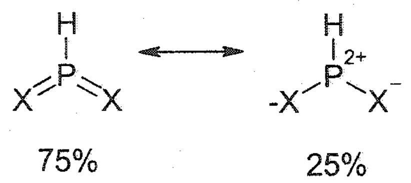

This could be equally well represented by inclusion of the octet rule structures, thus giving equal weighting to the structure that minimizes formal charges and the set of structures that obey the octet rule.

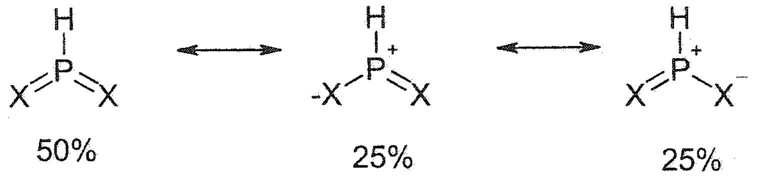

The curves including the CH_2 data do not correspond to any simple Lewis structure representation. A bond order of 1.5 should carry a formal charge of –0.5, so the decreased delocalization index in $HP(CH_2)_2$ must be due to something other than bond polarity. The effects at work here may be similar to those in the phosphoranes.

7.6. Topology of the Laplacian: Charge Concentrations

Figure 7-5 shows isovalue envelopes for the Laplacian scalar field, $\nabla^2\rho(\mathbf{r})$. The value plotted is $\nabla^2\rho(\mathbf{r}) = 0$. Table 7-4 shows the properties of the P-E bonding charge concentrations. Table 7-5 shows the properties and locations of the non-bonding charge concentrations on the substituent atoms.

The second row substituents each have a bonding maximum in their valence shell, but the phosphorus atom does not display a bonding maximum in those systems. For HPS_2, both P and S have bonding maxima in their valence shells. For X = PH and SiH_2, only the central P has bonding maxima in its valence shell. This is consistent with the bond polarity; only for HPS_2 does the BCP lie between the two valence regions. Similar observations are made in the H_3PX series. The bonding maximum in *twisted* $HP(SiH_2)_2$ is closer to the phosphorus nucleus and has a more negative Laplacian than the planar species. This observation is also made for twisted *versus* planar H_3PSiH_2.

At the Hartree-Fock level, all the planar substituents in HPX_2 exhibit the expected number of non-bonding maxima for doubly bonded systems: 2 for O and S, 1 for NH and PH, none for CH_2 and SiH_2. All charge concentrations are in the plane of symmetry, as expected. There is a non-bonding maximum in the Si valence shell for C_2-twisted $HP(SiH_2)_2$. A lone pair was also seen on pyramidal SiH_2 in H_3PSiH_2, but in twisted $HPSiH_2$ the lone pair resided on the more electronegative P. Since only Si has a preference for a pyramidal arrangement, we can conclude that the other substituents are involved in double bonds with the central, pentavalent phosphorus atom.

The positions of the maxima on O are interesting; they seem to be part of a 'cap' on the O atom, rather than the torus that is more typical about terminal atoms, Figure 7-2. In addition, there are two pairs of π-like maxima, one pair for each P-O bond, 1.68 au from the phosphorus nucleus, 1.62 au above and below the plane, making an angle of 150° with the P atom. A search out to 1.8 au did not reveal similar maxima on P for any of the other substituents.

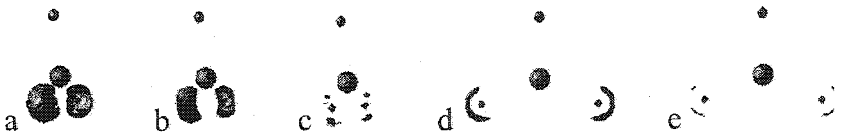

Figure 7-2: Isovalue envelopes for HPO_2, calculated at the HF level, from two different points of view. The structure of the cap-like non-bonding maxima on each O atom is revealed. $\nabla^2\rho$ = **a)** –3.0, **b)** –3.5, **c)** –4.0, **d)** –3.5, **e)** –4.0.

The MP2 wavefunction for HPO_2 shows a similar topology around phosphorus, but with the π-like maxima 0.1 au closer to the nucleus, and with the addition of P-O σ-bonding charge concentration maxima in the valence shell of phosphorus. The cap-like arrangement of the lone pairs on O is consistent with double bonds to P, or transfer of the second bonding electron pair from O to P, so that the lone pairs on O lie in the plane, rather than forming a torus of three non-bonding pairs. Based on electronegativity and valence arguments, the second possibility seems unlikely. The π-like maxima on P must then be due to the weak attraction of P for the bonding pairs, so that they don't coalesce into a single maximum.

The two lone pairs on S in HPS_2 are opposite each other (*endo* and *exo,* see Figure 7-3) with a significantly higher magnitude of the Laplacian than is found at the associated saddles in the valence shell, see Table 7-5. These two maxima represent well-resolved regions of charge localization on sulfur, rather than a torus of charge concentration.

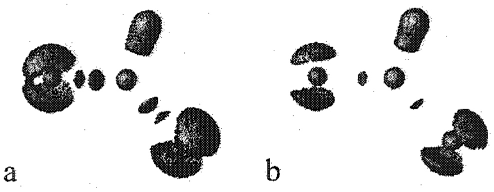

Figure 7-3: Isovalue envelopes for HPS_2, calculated at the HF level. The two non-bonding maxima on each S atom are apparent. $\nabla^2\rho$ = **a)** –0.25, **b)** –0.30.

In $HP(PH)_2$, MP2 correlation shifts charge back onto the substituent PH group, making each PH group essentially neutral. It also moves the BCP to a more neutral position nearer the central P, as it does for H_3PPH. Because correlation lowered the charge on the substituent PH to nearly zero, making it suspiciously like the H_3PPH system, the charge concentrations were checked for the MP2 wavefunctions of $HP(PH)_2$. Two maxima are found within the non-bonding concentrations on the substituent P atom, above and below the plane of symmetry. The density is very flat between the two maxima and the saddle between them has almost identical properties.

Figure 7-4: Isovalue envelopes for $HP(PH)_2$, calculated at the HF level, from two different points of view. The two non-bonding maxima on each trivalent P atom, in the MP2 wavefunction, are part of the same non-bonding charge concentration and apparently correspond to a single electron pair. $\nabla^2\rho$ = **a)** –0.10, **b)** –0.15, **c)** –0.20.

These maxima can be compared to those on N in H_3PNH, and on P in H_3PPH. In H_3PPH, there are two distinct maxima separated by a saddle whose properties are very different, as is seen above for HPS_2. In H_3PNH, the two maxima are connected by a saddle with very similar properties and we concluded that they represent one distorted electron pair. We make the latter conclusion here. The MP2 results are simply a small distortion of the single charge concentration observed at Hartree Fock. Even at the HF level there is a large density above and below the plane.

Looking at the -0.10 au envelope in Figure 7-4, one is tempted to describe the substituent as an HP molecule, displaying a torus of electron density, which is then distorted by the secondary interaction with the central HP group, also displaying a distorted torus. Besides HPO_2, twisted $HP(SiH_2)_2$ and $HP(PH)_2$, none of the remaining HPX_2 systems showed qualitative differences when correlation was included.

7.7. Summary

Considering that the experimental systems are twisted, such that the C (or N) bond plane is rotated relative to the P bond plane, it is not surprising that there is not complete sharing of two pairs of electrons in the HPX_2 systems studied. Once again, the third row ligands exhibit somewhat different bonding than the second row. Silicon prefers a twisted geometry with a non-bonding charge concentration, though it can be forced by symmetry to remain planar and seems to be involved in multiple bonding even when twisted. The arrangement of charge concentrations

(Lewis electron pairs) on the substituents PH and S cannot be completely controlled by symmetry. While the delocalization index at Hartree-Fock shows a high delocalization for X = S and PH, relative to the other bis(ylene)phosphoranes, there seems to be significant π-character in the lone pair localized on each substituent PH group at the HF and MP2 levels. This suggests that there may be a contribution from the polarized P-P bonding electron pairs to the 'non-bonding' concentration.

The extent of covalent bonding, as measured by the delocalization index, is definitely less in the phosphoranes and the bis(ylene)phosphoranes than in the phosphinylidenes. This can only partly be accounted for by differences in atomic charges and bond polarity, and must in part be related to the hypervalent nature of these compounds. The localization of what would otherwise be bonding electrons is more pronounced in the phosphoranes where even one double bond would exceed the Lewis octet on the central P atom, whereas in the bis(ylene)phosphoranes one double bond completes the octet and the second exceeds it.

There is considerable debate in the chemical education literature about whether Lewis structures should be drawn to complete the octet or minimize formal charges. It appears from these results that both are important for phosphorus, and presumably for other third row main group elements. From the delocalization *vs.* charge transfer curves we find that up to one and a half Lewis pairs are shared between P and X in H_3PX and up to 1.75 pairs are shared with each X in HPX_2. It can be concluded that there are both quantitative and qualitative differences in the bonding properties of pentavalent phosphorus systems compared to trivalent phosphorus systems. Furthermore, as the substituent becomes more electropositive than the central atom, the hypervalent bonding arrangement becomes less favourable. We saw in the previous chapter that the octet rule is much more important for nitrogen and that the bond orders in formally pentavalent H_3NX were no greater than in the formally singly-bonded amines. Choosing more electronegative substituents could potentially alter this. For example, the N-X bond order may be higher in the F_3NX series than in the H_3NX series.

Bibliography

References are listed alphabetically by first author and then by date. Data Table references are included.

Appel, R., F. Knoch and H. Kunze (1983). *Angew. Chem. Int. Ed. Engl.* **22**, 1004.

Appel, R. (1990). *Bis(methylene)phosphoranes*, Chapter E1 in Multiple Bonds and Low Coordination in Phosphorus Chemistry, M. Regitz and O.J. Scherer, editors. Stuttgart: Verlag.

Meisel, M (1990). *Dioxo- and Dithioxophosphoranes, including the Metaphosphate Anion*, Chapter E6 in Multiple Bonds and Low Coordination in Phosphorus Chemistry, M. Regitz and O.J. Scherer, editors. Stuttgart: Verlag.

Niecke, E. and D. Gudat (1990). *Bis(imino)phosphoranes*, Chapter E3 in Multiple Bonds and Low Coordination in Phosphorus Chemistry, M. Regitz and O.J. Scherer, editors. Stuttgart: Verlag.

Regitz, M and O.J. Scherer, editors (1990). Multiple Bonds and Low Coordination in Phosphorus Chemistry, Stuttgart: Verlag.

Schoeller, W.W. and C. Lerch (1986). *Inorg. Chem.* **25**, 576.

Schoeller, W.W. (1990). *Bonding Properties of Low Coordinate Phosphorus Compounds,* Section B in Multiple Bonds and Low Coordination in Phosphorus Chemistry, M. Regitz and O.J. Scherer, editors. Stuttgart: Verlag.

Schoeller, W.W. and T. Busch (1992). *Chem. Ber.* **125**, 1319.

7.8. Laplacian Isovalue Envelopes

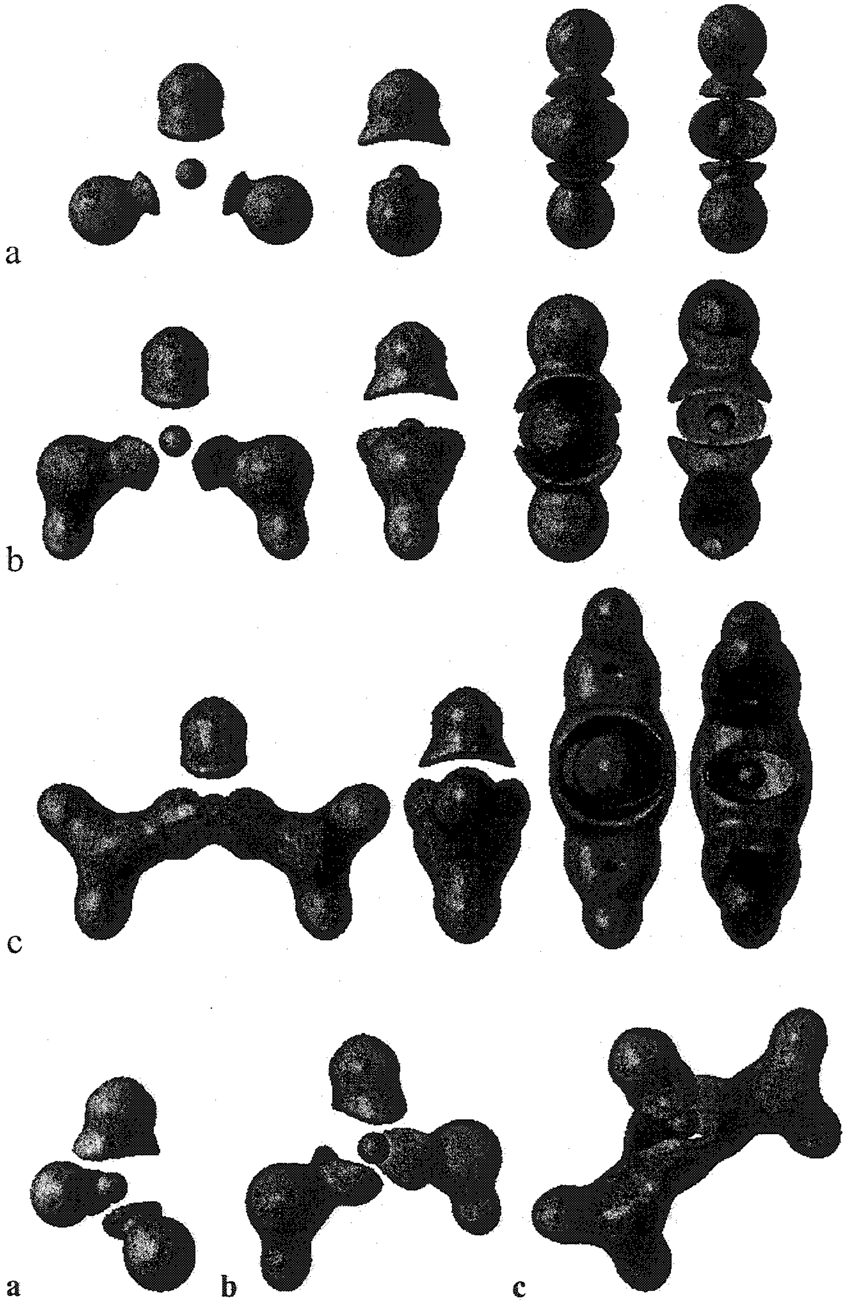

Figure 7-5: Continued on next page.

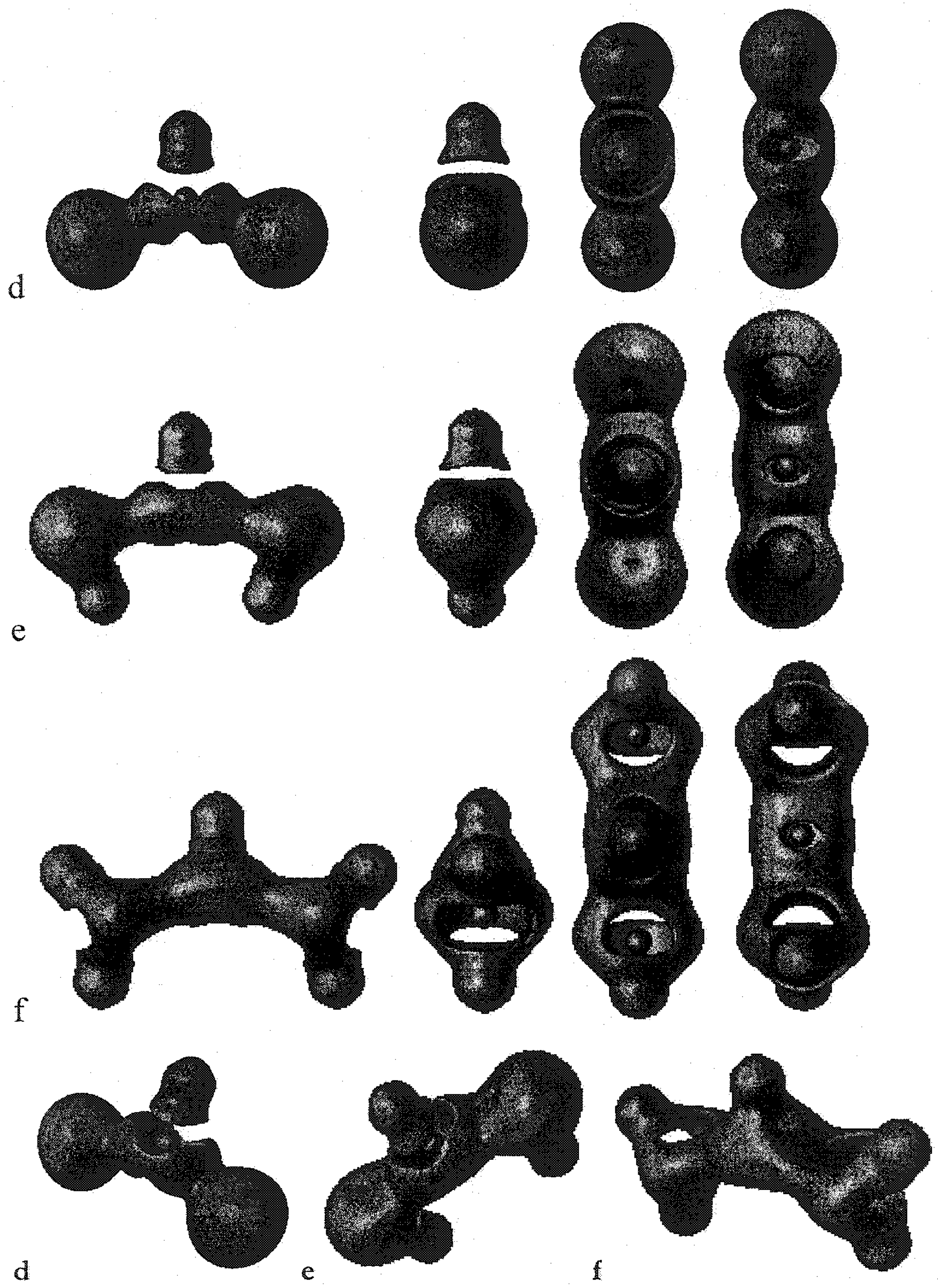

Figure 7-5: Isovalue envelopes of the Laplacian, $\nabla^2\rho = 0$, for HPX_2. Five views, where X is a) O, b) NH, c) CH_2, d) S, e) PH, f) planar SiH_2.

7.9. Data Tables

Table 7-1: Optimized geometries of bis(ylene)phosphoranes, $PH(EH_{n-1})_2$, at HF; MP2 values in italics. Related experimental values or ranges are given in parentheses.

bisylene	**r(P-E)**	**r(P-H)**	**∠EPE**	**∠HPE**	**-Energy /au**
PHO_2	142.35	138.17	134.21	112.89	491.12427
	146.62	*139.26*	*134.98*	*112.51*	*491.87478*
$PH(NH)_2$	151.23	137.34	140.69	109.66	451.38660
trans	*155.18*	*138.03*	*143.79*	*108.10*	*452.08957*
Deriv.Exp't[a]	(151.5)		(134.3)		
$PH(NH)_2$	150.90	139.45	127.49	116.26	451.37565
cis	*154.63*	*140.71*	*124.64*	*117.68*	*452.07736*
$PH(CH_2)_2$	162.97	138.09	135.37	112.32	419.31568
	165.00	*138.63*	*134.93*	*112.54*	*419.94709*
Deriv.Exp't[b]	(162 – 170)		(137 – 127)		
PHS_2	189.27	138.77	134.06	112.97	1136.41973
	192.07	*139.59*	*133.98*	*113.01*	*1137.24427*
Deriv.Exp't[c]	(190)		(126)	(117)	
$PH(PH)_2$	203.05	138.82	141.14	109.43	1023.93161
trans	*205.98*	*139.46*	*141.58*	*109.21*	*1024.74304*
$PH(PH)_2$	203.54	138.82	131.89	114.05	1023.92608
cis	*206.41*	*139.55*	*130.73*	*114.63*	*1024.73686*
$PH(SiH_2)_2$	209.74	138.74	141.07	109.47	921.39288
planar	*211.90*	*139.30*	*142.08*	*108.96*	*922.16380*
$PH(SiH_2)_2$	216.05	138.86	140.53	109.73	921.41968
twisted[1]	*216.55*	*137.38*	*137.38*	*111.31*	*922.19687*

- Bond lengths are in picometers and angles are in degrees.

1. C_2 symmetry with 2 types of Si-H bonds; sum of angles about P = 360.0°, about Si = 329.4°; HPSiH dihedral angles are 171.09° and 49.78°.

a) *X-ray for* $\mathbf{(SiMe_3)_2N\text{-}P(=NSiMe_3)_2}$: Neicke and Gudat (1990).
b) *X-ray data for a range of systems,* $\mathbf{YP(C(SiMe_3)_2)_2}$: Appel (1990). The twist angle varies from 37 to 50°.
c) *X-ray for* $\mathbf{Mes^*PS_2}$: Appel *et al.* (1983).
(See reference list in Bibliography, above)

Table 7-2: Properties of P-E bond critical points and delocalization indices in bis(ylene)phosphoranes; MP2 values in italics.

bisylene	$\rho(r_b)$	$\nabla^2\rho(r_b)$	$\varepsilon(r_b)$	$r(P\text{-}r_b)$	$r(E\text{-}r_b)$	$\delta(P,E)$	$\delta(P,X)$	**Ratio to HPR_2**
PHO_2	.276 *.245*	+1.70 *+1.25*	.14 *.13*	1.096 *1.131*	1.594 *1.640*	0.90	0.90	1.33
$PH(NH)_2$ *trans*	.242 *.218*	+0.81 *+0.55*	.36 *.33*	1.148 *1.185*	1.714 *1.751*	1.00	1.02	1.37
$PH(NH)_2$ *cis*	.246 *.224*	+0.82 *+0.54*	.38 *.36*	1.145 *1.180*	1.708 *1.743*	1.00	1.02	1.37
$PH(CH_2)_2$	.212 *.199*	+0.06 *+0.06*	.74 *.67*	1.227 *1.268*	1.853 *1.851*	1.17	1.24	1.43
PHS_2	.178 *.162*	-0.31 *-0.20*	.29 *.20*	1.602 *1.653*	1.975 *1.977*	1.66	1.66	1.60
$PH(PH)_2$ *trans*	.135 *.126*	-0.14 *-0.13*	1.00 *.53*	2.373 *2.145*	1.466 *1.748*	1.48	1.66	1.45
$PH(PH)_2$ *cis*	.134 *.126*	-0.13 *-0.13*	.93 *.49*	2.400 *2.181*	1.450 *1.721*	1.47	1.66	1.45
$PH(SiH_2)_2$ *planar*	.102 *.097*	+0.12 *+0.04*	1.17 0.90	2.536 *2.528*	1.428 *1.477*	1.04	1.36	1.54
$PH(SiH_2)_2$ *twisted*	.094 *.093*	+0.01 *-0.02*	.81 *.47*	2.608 *2.573*	1.492 *1.529*	0.96	1.29	1.47

- Distances from nuclei to bond critical points, $r(E\text{-}\mathbf{r}_b)$, are given in atomic units.
- The ratio relative to the phosphines is for the delocalization indices, δ(P.X) *vs*. δ(P.R)

Table 7-3: Atomic and group properties in bis(ylene)phosphoranes, compared to phosphine; MP2 values in italics.

bisylene	**q(P)**	**q(E)**	**q(X)**	**q(H)**	**K(P)**	**L(P)**	**L(E)**
PHO_2	+3.558 *+3.080*	-1.511 *-1.324*	-1.511 *-1.324*	-0.534 *-0.433*	339.24312 *339.71664*	1.7 e-3 *-1.1 e-3*	-3.1 e-4 *-1.6 e-4*
$PH(NH)_2$ *trans*	+3.343 *+2.809*	-1.804 *-1.555*	-1.388 *-1.167*	-0.565 *-0.479*	339.36649 *339.86459*	3.6 e-3 *-4.1 e-3*	-5.0 e-4 *1.8 e-4*
$PH(NH)_2$ *cis*	+3.342 *+2.824*	-1.797 *-1.565*	-1.380 *-1.174*	-0.578 *-0.473*	339.37239 *339.87497*	5.5 e-3 *2.5 e-3*	-1.6 e-4 *1.4 e-4*
$PH(CH_2)_2$	+2.827 *+2.321*	-1.169 *-1.035*	-1.121 *-0.911*	-0.580 *-0.493*	339.68842 *340.18123*	4.8 e-3 *4.0 e-3*	6.2 e-4 *4.0 e-4*
PHS_2	+1.787 *+1.396*	-0.625 *-0.477*	-0.625 *-0.477*	-0.541 *-0.446*	340.05016 *340.45637*	-3.6 e-3 *-3.4 e-3*	-3.5 e-5 *-6.1 e-5*
$PH(PH)_2$ *trans*	+0.164 *+0.341*	+0.752 *+0.481*	+0.202 *+0.033*	-0.557 *-0.469*	340.72099 *340.88041*	4.7 e-3 *-3.1 e-3*	1.5 e-3 *-2.3 e-3*
$PH(PH)_2$ *cis*	+0.116 *+0.349*	+0.767 *+0.500*	+0.216 *+0.050*	-0.546 *-0.449*	340.73748 *340.89375*	2.7 e-3 *-2.6 e-3*	-7.0 e-4 *6.2 e-4*
$PH(SiH_2)_2$ *planar*	-0.811 *-0.670*	+2.124 *+1.864*	+0.677 *+0.522*	-0.533 *-0.433*	340.97815 *341.21142*	5.7 e-3 *3.9 e-4*	3.7 e-4 *2.7 e-4*
$PH(SiH_2)_2$ *twisted*	-0.422 *-0.479*	+1.928 *+1.782*	+0.491 *+0.466*	-0.548 *-0.455*	340.87240 *341.16640*	3.4 e-3 *2.3 e-3*	1.8 e-3 *-1.7 e-3*

- q(H) refers to the H atom bonded to P.

Table 7-4: Properties of the P-E bonding charge concentration maxima.

bisylene	$\nabla^2\rho(r)$	$\rho(r)$	r(P)	r(E)
$\mathbf{P}HO_2{}^*$	+0.032	0.045	1.684	2.774
$PH\mathbf{O}_2$	-3.187	0.785	2.022	0.703
$PH(\mathbf{N}H)_2$ (*t*)	-1.744	0.478	2.043	0.821
$PH(\mathbf{N}H)_2$ (*c*)	-1.747	0.478	2.034	0.823
$PH(\mathbf{C}H_2)_2$	-0.867	0.278	2.090	0.990
$PH\mathbf{S}_2$	-0.288	0.192	2.160	1.417
$\mathbf{P}HS_2$	-0.340	0.178	1.480	2.097
$\mathbf{P}H(PH)_2$ (*t*)	-0.349	0.159	1.483	2.358
$\mathbf{P}H(PH)_2$ (*c*)	-0.358	0.160	1.481	2.366
$\mathbf{P}H(SiH_2)_2$ (*pl*)	-0.319	0.146	1.499	2.470
$\mathbf{P}H(SiH_2)_2$ (*tw*)[1]	-0.325	0.142	1.481	2.735

- Distances from nuclei to bond critical points, r(E), are given in atomic units.
- The bolded element represents the atom in whose valence shell the CC is found.

1) Above and below the symmetry plane by 1.622 au.

Table 7-5: Properties of the non-bonding CC maxima, *and intervening saddle points*, on the substituent atom, E.

bisylene	$\nabla^2\rho(r)$	$\rho(r)$	Z	r(E)	**# of nb CC's; # lp expected**
PHO_2 ***MP2***	-4.045	0.853	0	0.661	2; 2
endo	-4.347	0.873	0	0.656	
saddle	-3.709	0.829	0	0.663	(cap)
PHO_2 ***HF***	-4.433	0.875	0	0.657	2; 2
endo	-4.157	0.857	0	0.662	
saddle	-3.936	0.842	0	0.662	(cap)
$PH(NH)_2$ (*t*)	-2.094	0.508	0	0.760	1; 1
$PH(NH)_2$ (*c*)	-2.182	0.516	0	0.757	1; 1
PHS_2	-0.468	0.181	0	1.313	2; 2
endo	-0.481	0.182	0	1.310	
saddle	-0.259	0.148	±1.294	1.346	(torus)
$PH(PH)_2$ (*t*)	-0.221	0.112	0	1.470	1; 1
$PH(PH)_2$ (*c*)	-0.230	0.113	0	1.467	1; 1
$PH(PH)_2$ (*t*) ***MP2***	-0.187	0.106	±0.970	1.478	2; 1
saddle	-0.182	0.106	0	1.478	
$PH(PH)_2$ (*c*) ***MP2***	-0.190	0.108	±0.539	1.475	2; 1
$PH(SiH_2)_2$ (*tw*)	-0.097	0.065	3.531	1.708	1

- Distances from nuclei to maxima, r(E), are given in atomic units.
- Z is the distance from the critical point to the molecular symmetry plane, in au.
- The total number of non-bonding maxima are shown, along with the number of lone pairs expected from the doubly-bonded Lewis structures.

8. Phosphenium Cation Results

Phosphenium cations, PR_2^+, are experimentally known and characterized, where the R group is an electronegative potential π-donor; ideally an amino group with bulky substituents for steric (kinetic) protection (Cowley and Kemp, 1985). The phosphenium cations are often discussed as carbene analogues, being isolobal with $:CR_2$ and isoelectronic with silylenes, $:SiR_2$. While some carbenes have triplet ground states, the known phosphenium cations have singlet ground states, as do the silylenes.[*] The electrophilic chemistry is related to the formally vacant unhybridized *p* orbital on the phosphorus atom. Donation of the σ lone pair on phosphorus leads to complexation of transition metals.

Some particularly stable phosphenium cations incorporated the 'electron-deficient' phosphorus atom into apparently aromatic 6π-electron ring systems (Denk *et al.*, 1999).

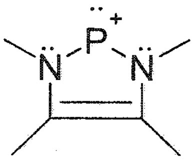

Stabilized phosphenium cations can be made from the chlorophosphine with a chloride-abstracting agent such as the Lewis acid Al_2Cl_6. The amino groups

---

[*] This is likely related to the types of stabilizing groups used and to the separation of *s* and *p* atomic orbitals in P and Si *versus* C (inert pair effect).

are planar, even when in a saturated and/or acyclic system. The planarity of the amino groups is explained by resonance structures in which the lone pairs on nitrogen are donated to phosphorus, delocalizing the formal positive charge over the three atoms. In the 6π-electron rings, the formal charge can be further spread out over all the atoms in the ring. Most other isolated phosphenium cations include a potential π donor as a substituent on phosphorus, such as a chlorine atom, an aromatic ring or a metallocene (Cowley and Kemp, 1985).

It has been suggested by Gudat (1998) that the stability of phosphenium cations depends both on the delocalization of π-like density from the substituent to the phosphorus atom and on electrostatic attraction arising from the polarity of the bonds. We have seen in previous chapters that there tends to be a relationship between these two parameters, with the delocalization of electrons decreasing as the bond polarity (atomic charge) increases. The amino group seems to have the optimum combination of π-donating ability, large charges and small bond lengths, leading to moderate Wiberg bond orders (see Appendix 3) and large electrostatic attractions (Gudat, 1998).

In this chapter we will examine the electronic structure of phosphenium cations to determine the extent of π-like bonding as measured by the delocalization index and the ability of each substituent to moderate the charge on phosphorus by either σ- or π-type donation of electron density. We will use the extrapolation method developed in the previous chapters to account for the effect of bond polarity on δ(P,R) and thus propose a Lewis structure representation, supported by an analysis of the charge concentrations on the substituents. We will be particularly interested to explain the extraordinary stabilization of aminophosphenium cations.

8.1. Geometry

8.1.1. Energy of conformers studied

All the phosphenium cations were optimized as singlets within the C_2v point group. No counter-ions were used. Optimized bond lengths and bond angles about P are given in Table 8-1, along with experimental values for some related systems. Where both *exo* (*E*, **1a, 2a**) and *endo* (*Z*, **1b, 2b**) isomers are possible, the *exo* isomer is lower in energy. The mixed *exo/endo* isomers were not investigated.

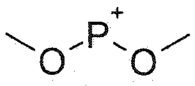

1a

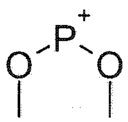

1b

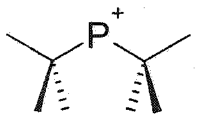

2a

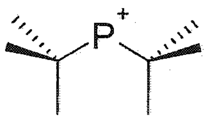

2b

The *exo versus endo* energy differences are 6, 28, 2 and 1 kJ/mol for the OH, SH, Me and SiH_3 substituents, respectively. It is interesting that only the thio substituent has a very strong preference for a particular conformer. The bond angle in both the hydroxyl- and thio- phosphenium cations increase by 10° between the *exo* and *endo* arrangements.[*] The changes in the methyl and silyl bond angles are smaller.

An additional C_2 geometry was investigated for the dimethylphosphenium cation, $P(CH_3)_2^+$, as this had previously been found to be the lowest energy structure (Gudat, 1998). It was found to be lower in energy than the C_2v geometries by an additional 2.7 kJ/mol. Due to the small difference in energy and similarity of geometry, the C_2v geometries are considered here for ease of analysis and comparison with the other systems. The slight twist (22° from *exo*) would help minimize the H···H repulsions but probably has little to do with electronic effects. The displacement would not converge for this geometry optimization despite vanishing forces, suggesting that the potential energy surface is very flat in this region. There is no experimental evidence that the phosphino ligands should be planar as the amino groups are, and a previous calculation had found a C_2 arrangement to be the lowest energy[†] (Schoeller and Busch, 1990). Therefore a cation with pyramidal phosphino groups (C_2, **3b**) was investigated, along with the planar diphosphinophosphenium cation (C_2v, **3a**).

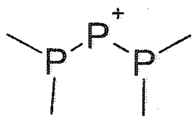
3a

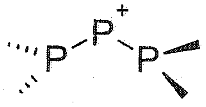
3b

The C_2 pyramidal geometry, **3b**, has the substituent 'lone pairs' pointing

---

[*] A similar 10 degree difference is seen between the conformers of $HP(PnH)_2$.

[†] Schoeller has also found a C_1 geometry, similar to the C_2 geometry (Schoeller and Tubbesing, 1995).

above and below the PPP plane, and is 78 kJ/mol *lower* in energy than the planar system. This energy difference is probably related to the inversion barrier for phosphines. The barrier to inversion, through a planar transition state, is 115 kJ/mol in PH_3 but only 25 kJ/mol in NH_3 (Emsley and Hall, 1976, p. 41). Therefore amines invert rapidly while phosphines do not. The pyramidalization energy of the phosphino substituent suggests that the planar arrangement imparts about 35 – 40 kJ/mol more stability in terms of P-P bonding, but this is overwhelmed by the destabilization of the substituent. A similar effect is seen in the pyramidalization of the SiH_2 substituents in H_3PSiH_2 and $HP(SiH_2)_2$.

8.1.2. Hydride transfer reactions

Hydride transfer reactions have been studied previously to determine the relative stabilizing effects of phosphenium cation substituents (Gudat, 1998; Schoeller and Tubbesing, 1995)

$$PR_2^+ + PH_3 \rightarrow HPR_2 + PH_2^+ + \Delta E_H$$

Equation 8-1

None of these calculations included F, Cl, SiH_3 or planar PH_2 substituents. The same energy difference was evaluated for the current calculations, though zero point energies and basis set superposition errors were not accounted for. These effects should not alter the overall trends. The reaction energy values, ΔE_H, are given in Table 8-1. It is clear that the amino group is a much more stabilizing substituent than the others, in agreement with previous experimental and theoretical results. The overall stabilizing trend found in the current study is:

$NH_2 \gg OH > SH, PH_2^{pyr}, CH_3 > PH_2^{plan}, Cl, SiH_3 > F > H.$

The previous study by Gudat (1998) found OH and SH to have similar ΔE_H values in PR_2^+ but found SH to be more stabilizing (by 25 kJ/mol) in PHR^+, and OH to be more stabilizing (by 15 kJ/mol) in $P(NH_2)R^+$. When the inversion barrier is subtracted from the hydride transfer energies of planar $P(PH_2)_2^+$, the effects of P-P bonding alone are found to be similar to those of P-S bonding in *exo* $P(SH)_2^+$.

8.1.3. Comparison to experiment

Of the substituents studied here, only amino- and thio-phosphenium cations have been structurally characterized, see Table 8-1. The X-ray determined P-N bond length of a diaminophosphenium cation (Cowley *et al.*, 1978) is in good agreement with the calculated value, where the only difference is replacement of the hydrogen atoms with the larger isopropyl groups on nitrogen. Presumably, the difference in bond angles is due to the differing steric sizes of the nitrogen substituents. The optimized P-S bond lengths are in good agreement with those from an X-ray structure of a cyclic derivative (Burford *et al.*, 1988). While the optimized bond angle is determined by steric interaction of the ligands and the lone pair, the experimental bond angle is constrained by being in a five-member ring, so the disagreement is not surprising.

8.1.4. Comparison to other calculated structures

The *endo* and *exo* bond lengths are quite similar in all cases. A plot of the P-E bond lengths in the cations, and in each of the other phosphorus series studied, is shown in Figure A4-1. Comparing the bond lengths in the cations with the single and double bonds calculated previously, all but the silyl and planar phosphino systems lie somewhere between single and double bonds. The P-P bond is approaching a true double bond while the P-H and P-Si bonds seem to be destabilized single bonds. The P-Si bond in $P(SiH_3)_2^+$ is longer than the single bonds, but it is shorter than the P-Si bond in the *pyramidal* PH_3SiH_2 geometry.

The P-P bonds in the planar cation (**3a**) are about the same length as the double bonds in HP=PH and $HP(=PH)_2$. The P-P bonds in the C_2 (**3b**) cation have a similar to the length to those in H_3PPH. Compared to the phosphine $HP(PH_2)_2$, the P-P bonds in $P(PH_2)_2^+$ are 5% shorter in the pyramidal arrangement and 9% shorter in the planar arrangement. The P-C bonds are about 3% shorter than in dimethylphosphine. The remaining P-E bonds are all about 6% shorter than the corresponding phosphine, but longer than the P=E double bonds.

The EPE bond angles range from 100° to 111° for the planar geometries, consistent with an AX_2E VSEPR geometry. The variation in the angle seems to be determined mainly by the size of the substituent group, as suggested by the *endo vs. exo* geometries.

Since bond lengths are shortened and strengthened by both covalent (electron sharing) and ionic (electron transfer) interactions, it is interesting to consider the extent of bond shortening as it compares to the hydride transfer energy, which should also have contributions from electron delocalization and bond polarity, according to Gudat (1998). No correlation is observed. The P-P bond in the planar cation is the one that shortens the most, relative to the phosphine, but is among the least stabilizing substituents, due to the high inversion barrier of phosphines. The pyramidal $P(PH_2)_2^+$ has much longer P-P bonds that the planar cation, but the pyramidal substituent is twice as effective at stabilizing the cation. The bonds that shorten the least (or lengthen) are those without lone pairs on the substituent: P-H, P-C and P-Si. Of these, CH_3 is an intermediate stabilizer, similar to pyramidal PH_2, and the SiH_3 group is a weak stabilizer, similar to the planar PH_2 group. The remaining bonds all shorten by about 6%. The halogens, F and Cl, are weak stabilizers. The chalcogens, OH and SH, are intermediate stabilizers – slightly better than methyl. Finally, NH_2 is a superb stabilizer, having the largest hydride transfer energy, but unremarkable bond shortening. Clearly, the stabilization of phosphenium cations is not reflected in the bond lengths.

8.2. Bond Paths and Interatomic surfaces

Bond paths are found between all pairs of atoms that we expect to be bonded. Properties and positions of the P-E bond critical points (BCPs) are given in Table 8-2. There are no ring or cage critical points in the molecules studied.

Figure 8-8 shows contour plots of $\nabla^2\rho(\mathbf{r})$, in the molecular plane of the phosphenium cations, overlaid with bond path trajectories and the intersection of the interatomic surface with the plane.

Plots of the bonding radii of the phosphorus and substituent atoms are shown in Figures A4-2 and A4-3, respectively. The bonding radius of the central phosphorus follows the same pattern as the total bond length. The bonding radius of the central P in planar $P(PH_2)_2^+$ is actually shorter than that in HP=PH, though the bonding radius of the substituent P atom is closer to that of the phosphines, giving a bond length just above HP=PH. In the C_2-twisted cation, **3b**, the bond critical point shifts considerably towards the substituent, relative to the planar cation, **3a**. The central P atom resembles the phosphines and the substituent P atom resembles the phosphinylidene, HP=PH, in terms of bonding radius.

All the substituent bonding radii are shorter than in the phosphines, except for SiH_3 and H, which are nearly identical to the phosphines. The greatest decreases in bonding radii are for the most electronegative atoms, perhaps because they have the most density available for transfer to the positively charged phosphorus. The entire P-Si bond lengthening, relative to the phosphines, appears in the phosphorus atom's bonding radius.

8.3. Properties at the Bond Critical Point

8.3.1. Density, $\rho(r_b)$

A plot of the density at the P-E bond critical points is shown in Figure A4-4. Values are given in Table 8-2. The P-L BCPs have $\rho(r_b)$ values ranging from 0.18 to 0.22 au, falling between the single and double bond values, as the bond lengths do. The P-M BCPs have $\rho(r_b)$ values ranging from 0.08 to 0.15. These values also mirror the bond length trends. The BCP density of the planar diphosphinophosphenium P-P bond is between the $HP(=PH)_2$ and HP=PH values. For the pyramidal cation the density is similar to that of $HP(=PH)_2$. The P-Si bond density falls below the single bond values.

8.3.2. Laplacian

A plot of the Laplacian of the density at the P-E bond critical point is shown in Figure A4-5. Values are given in Table 8-2. As in the other series, the Laplacian decreases sharply from F to C and increases slowly from S to Si. The trend is less clear when Cl is included.

The Laplacian in dimethylphosphenium, $P(CH_3)_2^+$, is more negative than for the methylphosphines, Y_2PCH_3. The same is true for R = SH, PH_2 and H. All the other second row substituents have values between the single bond and double bond values. The Laplacian at the P-Cl BCP is in the range of the chlorophosphines. The Laplacian at the P-S BCP has a value near that for HPS_2, which is more negative than all the other single and double P-S bonds.

8.3.3. Ellipticity

The observed curvatures are all oriented in the expected direction. The ellipticity is only significantly larger than typical single bond values for R = PH_2 (planar), NH_2, H (*!*) and to a lesser degree SH and pyramidal PH_2. The planar pnictogens are in geometries conducive to high ellipticities, while the bonds around the group 4 substituents are arranged tetrahedrally, leading to high local symmetry and thus low ellipticity. The preferred geometry for the amino group is planar, so there is clearly a preference for accumulation of charge above and below the bond plane in this system. The pyramidal phosphino group seems to achieve the same goal by a different approach, putting electron density in the form of 'lone pairs' either above or below the plane. The chalcogens and halogens have no particular arrangement of electron density imposed by the geometry. The moderate ellipticity in $P(SH)_2^+$ indicates that there is probably some π-like bonding in this system as well. The O, S, N and (planar) P ellipticities are all comparable to those in (MP2) HPX_2, suggesting a significant degree of π-character in the bonding. The P-H bond critical point is near the valence shell of phosphorus and it has a surprisingly high ellipticity.

The positions of, and properties at, the bond critical points, along with the bond length trends, are indicative of a single bond for $P(SiH_3)_2^+$, weakened by additional electrostatic repulsion, and less polar single bonds for PH_2^+ and $P(CH_3)_2^+$, with increased density and charge concentration at the BCP, relative to the phosphines. They indicate a slightly weakened double bond for planar $P(PH)_2^+$ and partial multiple bonding for the remaining cations.

8.4. Atomic and Group Charges

Atomic and group charges and energies are given in Table 8-3. See Chapter 4 for the interpretation of the integrated Laplacian, L. Plots of the atomic charges on phosphorus, q(P), and on the substituent groups, q(R), are shown in Figures A4-6 and A4-7, respectively, and compared to the charges in the other phosphorus series studied. All the substituents studied are reasonably effective at spreading out the positive charge. In each phosphenium cation, the charge transferred to the substituent is less than in the phosphines. This is consistent with a small transfer of charge towards the phosphorus atom when the third substituent (say a chloride or hydride) is lost, $YPR_2 \rightarrow Y^- + PR_2^+$.

We see in Table 8-3 the charge of the hydride before it leaves. When a hydride, H^-, is removed from PH_3, the remaining atoms experience a total charge increase of +0.436, but it is not totally localized on the phosphorus atom. Each remaining H atom becomes less negative by 0.063. For the remaining systems, the total change in charge may be more or less than in PH_2^+, but in each case more of it is shared with the substituent.

For the electronegative second row substituents, the contraction of the P atom means that the H in *H*PR_2 is more negative than it is in PH_3. Therefore, removal of the hydride transfers less charge to the remaining atoms (0.38 to 0.41). Each F and OH group takes only 0.09 of that, while the less electronegative NH_2 and CH_3 take an additional 0.125 and 0.131, respectively, in positive charge.

For the third row substituents, the total charge transferred from the hydride is about +0.43 to +0.44. Each Cl takes a little less of that than the P atom, and each SiH_3 group takes a little more than P. The planar PH_2 groups take the majority of additional charge in $P(PH_2)_2^+$, and in $P(SH)_2^+$ the SH groups actually take *all* of the additional charge, leaving the central P atom slightly *less positive* than it was in $HP(SH)_2$. The pyramidal PH_2 groups *each* transfer enough additional electron density to counteract the loss of hydride, the net result being that the each PH_2 is 0.39e more positive than in the phosphine while the central P atom is 0.35e *less positive* in the cation than in the phosphine*!*

In the planar systems, the donation may be σ- or π-type, or both. In the C_2 cation the distinction is technically meaningless. As we have seen for the other systems, P and S are much more effective than the other substituents at delocalizing their lone pairs, and in this case, it seems, donating them.

For the chloro and methyl substituents (and R = H), all the phosphines have similar q(P) values and the phosphenium value is slightly higher than this. For the C_2-twisted $P(PH_2)_2^+$, the charge on the central P atom is most similar to that in

$HP(=PH)_2$; between that in $HP(PH_2)_2$ and that in $P(PH_2)_3$. For the remaining third row ligands, q(P) is similar to the disubstituted phosphines. For the remaining second row ligands, the atomic charge on phosphorus is quite similar to the trisubstituted phosphines.

While two third row substituents contribute almost as much additional electron density to the phosphorus in PR_2^+ as a hydride would in forming the phosphine, the second row substituents are more electronegative and less generous. The two R groups together donate only as much as one similarly electronegative substituent would in forming the substituted phosphine. This is probably related to the polarizability of the ligands, large electropositive atoms being more polarizable than small electronegative atoms.

8.5. Delocalization Indices

For the C_2v cations, we can separate the molecular orbitals into σ-like (a_1 and b_2) orbitals that are symmetric with respect to the molecular plane and π-like orbitals (a_2 and b_1) that are antisymmetric with respect to the molecular plane. We can then separate the atomic overlap matrices (AOMs) into σ and π blocks and calculate the σ- and π-delocalization indices separately. Table 8-4 shows the σ-like and π-like contributions to the delocalization index δ(P,R), the total delocalization index δ(P,R) and δ(P,E) for each phosphenium cation. The ratio of δ(P,R) values for PR_2^+ over HPR_2 is also given.

8.5.1. Comparison to other systems

The total delocalization index (including the substituent H atoms), δ(P,R), is plotted in Figure A4-8, as a function of the substituent atom, and is compared to δ(P,R) and δ(P,X) values in the other systems studied. In the phosphenium cations, δ(P,R) ranges from 0.71 (PF_2^+) to 1.63 (planar $P(PH_2)_2^+$). The ratio of δ(P,R) values in PR_2^+ and HPR_2 is shown in Table 8-4. The delocalization to the silyl group, δ(P,SiH_3), is 5% less than in $HP(SiH_3)_2$, while the delocalization to the H atoms, δ(P,H), is 6% larger in PH_2^+ than in PH_3. The increase in δ(P,CH_3) is 16%. For the remaining second row substituents (F, OH, NH_2), the delocalization index increases by 22% to 25%. For the planar PH_2 group, δ(P,PH_2) increases by 42% relative to $HP(PH_2)_2$, and is very close to δ(P,PH) in $HP(=PH)_2$. For the remaining third row substituents (Cl, SH, pyramidal PH_2), the delocalization increases 29% to 33% over HPR_2. These values are similar to the phosphoranes, $H_3P{=}EH_{n-1}$ for E = O, N, C and S, but between $HP(=PH)_2$ and $H_3P{=}PH$ for the C_2-twisted $P(PH_2)_2^+$.

8.5.2. Separation into π and σ contributions

There is negligible π-type delocalization in PH_2^+. In other words, the π-like density is almost completely localized on phosphorus and is core density, arising from the 2*p* orbital on phosphorus. In $P(CH_3)_2^+$ and $P(SiH_3)_2^+$, the π-type delocalization is 11% and 17 % of the σ-type delocalization, respectively. For the C_2 systems there is no symmetry plane and no separation is possible. For the planar cations the delocalization index decreases with polarity but the π to σ ratio seems to depend more on the group number of the substituent, being about 0.3 for R = F and Cl, 0.4 for R = OH and SH and 0.5 for R = NH_2 and PH_2, with slightly higher ratios for the third period member of each group.

While the π/σ ratio is much lower in the cations than in HPX_2, which in turn is lower than in HPX, we need not take this orbital approach. The additional transfer, *and sharing*, of electron density in these molecules, whether through σ- or π-type interactions, does lead to a significant increase in the delocalization index over the phosphines, particularly when bond polarity is accounted for.

8.5.3. Correlation with charge transfer

In order to fit the data to $\delta(P,R)$ *vs.* q(R) curves, the cations must first be separated into two sets: those having substituents with lone pairs to donate and those without. The data points for R = H, CH_3 and SiH_3 each fall near the phosphine curve, but fitting a quadratic through those three points gives a curve which has a maximum very near the $P(PH_2)_2^+$ data points. The C_2-twisted $P(PH_2)_2^+$ data point was therefore included in the 'no lone pairs to donate' set, while the planar $P(PH_2)_2^+$ data point was included in the 'lone-pair donor' set.

After the hydride in PH_2^+, the fluoride substituent is the poorest stabilizer of phosphenium cations studied. The PF_2^+ data point lies within the phosphine curves and its removal from the cation data set gives some interesting results, shown in Figure 8-1.

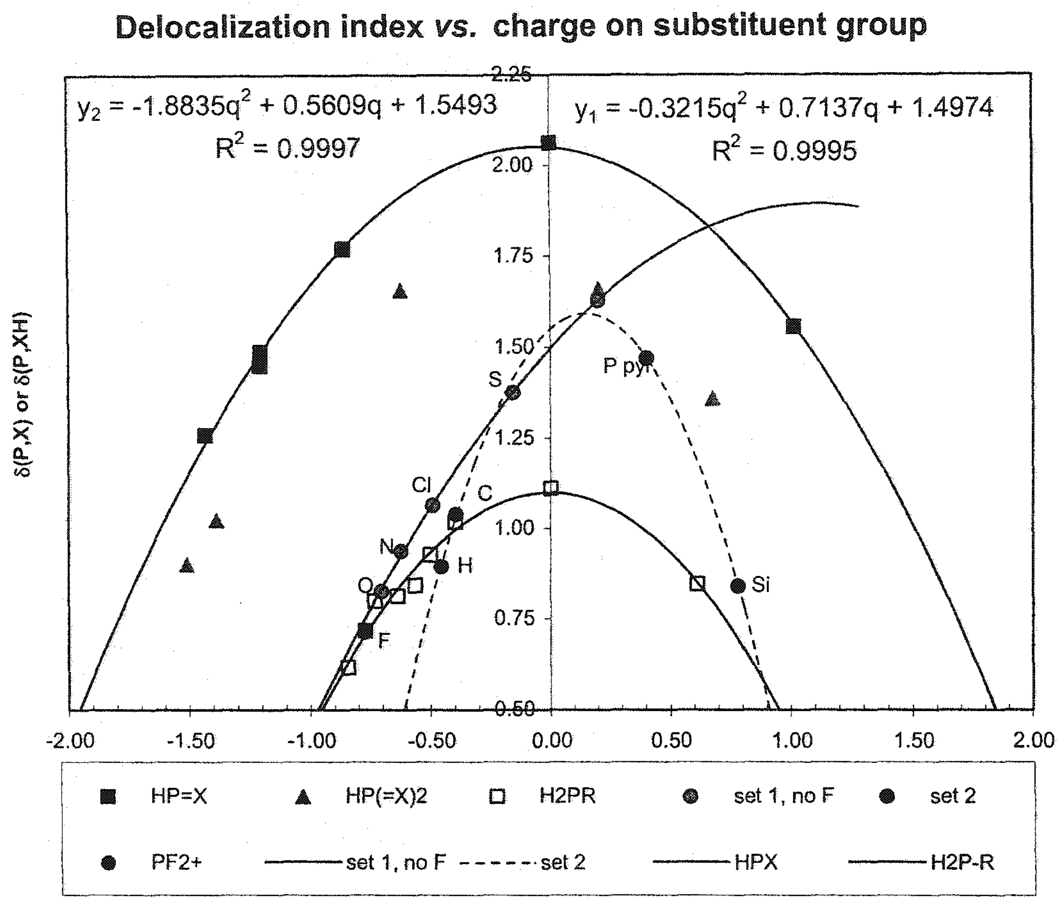

Figure 8-1: Plots of the delocalization index *versus* charge transfer in the phosphenium cations (•), compared to three other series: HPX, HPX_2 and H_2PR. The best-fit line for HPX does not include the anomalous X = CH_2 data point. The PR_2^+data are separated into two sets. Set 1 includes R = OH, NH_2, Cl, S and planar PH_2. Set 2 includes R = H, CH_3, SiH_3 and pyramidal PH_2.

The quadratic curve for R = OH, SH, Cl and planar NH_2 and PH_2 reaches a maximum δ(P,R) = 1.9. This is very similar to the phosphinylidenes, when HP=PH and HP=S are removed from the HP=X data set, as suggested for other series in this thesis. The charge on R corresponding to that delocalization maximum is displaced by 1.1 electrons, suggesting a Lewis structure with two full double bonds. A very electropositive atom would be needed to reach this maximum delocalization.

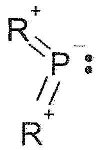

The PF_2^+ data fit into most of the observed trends in bond polarity and bond critical point properties. Despite the compelling similarity of the PR_2^+ curve and the HPX curve when R = F is excluded from the fit, one cannot quite convince oneself that the bonding in PF_2^+ is qualitatively different than in PCl_2^+ or $P(OH)_2^+$. The PF_2^+ data point was therefore included in the final fitting of the 'lone-pair donor' set. The Lewis structure shown above suggested shifting all the points over by subtracting one from the group charges, to give the bond polarity relative to the doubly-bonded structure. This plot of $\delta(P,R)$ *vs.* $q(R)'$ gives a curve that lies just slightly above the HPX_2 curve, as shown in Figure 8-2. In other words, there is at least as much double bond character in the 'electron deficient' phosphenium cations as in the 'hypervalent' bis(ylene)phosphoranes.

For the data set without lone pairs to donate, the curve looks very different. It is the most sensitive to atomic charge of any series studied in this thesis. The maximum (1.6) is reached for $q(R) = +0.15$, between R = pyramidal PH_2 and R = SH, which also lies quite close to this curve and very close to the pyramidal planar phosphino substituent. A transfer of just 0.5 electrons drops the delocalization index to 0.5. See Figure 8-1 or Figure 8-2.

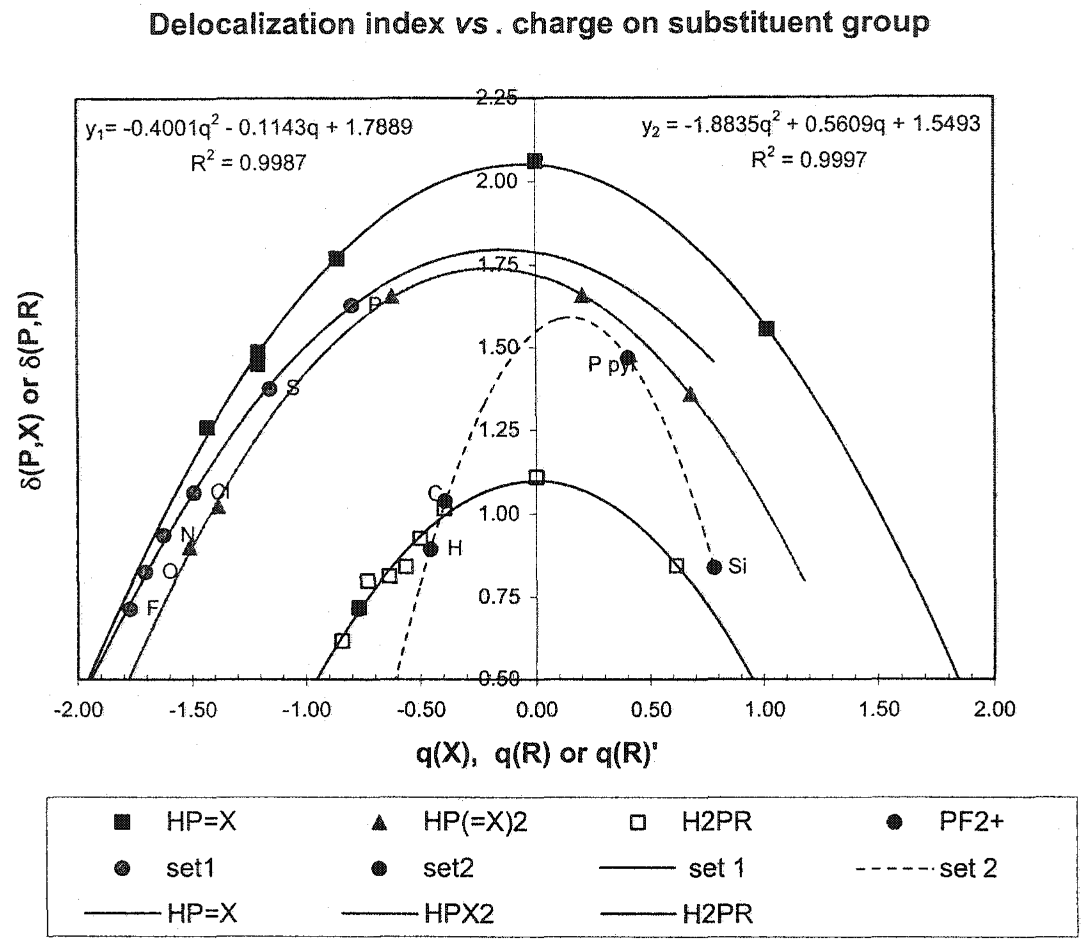

Figure 8-2: Plots of the delocalization index *versus* charge transfer in the phosphenium cations (•), compared to three other series: HPX, HPX_2 and H_2PR. The best-fit lines for HPX and HPX_2 do not include the anamolous X = CH_2 data points. The PR_2^+data are separated into two sets. Set 2 includes R = H, CH_3, SiH_3 and pyramidal PH_2. Set 1 includes R = F, OH, NH_2, Cl, S and planar PH_2. Set 1 is offset, so that q(R)' = q(R) – 1.0.

Without the inclusion of the pyramidal PH_2 data, the 'no lone pairs' curve, set 2, actually reaches a maximum above the planar $P(PH_2)_2^+$ data point. It is quite surprising that this curve reaches such a large maximum delocalization, but considering that the methyl phosphenium cation does not deviate significantly from most of the trends (density, bonding radius, charge, delocalization) established by the rest of the series, it seems that the additional charge transfer and delocalization need not be accomplished by 'lone pair' donation.

The deviation of the δ *vs.* q data for the methyl group can be seen as an exaggeration of the lower delocalization for C and Si throughout all the series studied in this thesis. In fact, if the data for set 2 are also shifted over by one charge unit, the R = CH_3 and H data points are found to lie quite close to the HPX_2 data. Thus only R = SiH_3 and pyramidal PH_2 need to be viewed as particularly special cases. The rest of the cations may be described as having two nearly full P-E double bonds.

8.5.4. The amino substituent – a special case?

Having established the degree of delocalization in the phosphenium cations as a series, it is time to consider whether the amino group is the most effective stabilizer due to effective electron donation, or due to other effects. It appears that there is nothing special in the delocalization index or charge transfer in $P(NH_2)_2^+$ compared to other PR_2^+ systems.

The differences that are seen in the other properties studied are even more pronounced for the planar phosphino substituent. These include bond shortening, relative to the phosphine, and a larger π to σ ratio for the delocalization index. It seems then that if the factors leading to pyramidalization of the phosphino group were removed, that could be an even more effective stabilizing force. However, given the small differences that are seen in this study, Gudat's proposition (1998) that electrostatic effects are important seems reasonable. While the charge on the amino group as a whole is less than on OH or F, the charge on the N atom is greater, due to the two polar N-H bonds. Both the P-N and P-O bonds are short and have large charge separation, which could lead to large electrostatic factors. The moderate ability of SH and PH_2 to stabilize cations, must be due to donation and/or delocalization effects as these have small or even repulsive electrostatic terms. It is unclear why the halides give such small hydride transfer energies.

8.6. The Laplacian and Electron Localization

Figure 8-9 shows isovalue envelopes for the Laplacian scalar field, $\nabla^2\rho(\mathbf{r})$. The value plotted is $\nabla^2\rho(\mathbf{r}) = 0$, which is often associated with a 'reactive surface'. Additional isosurfaces are shown for specific ions, in the figures below.

8.6.1. Phosphorus atoms and bonding concentrations

Table 8-5 gives properties of the non-bonding charge concentration maxima on the central P atom. This point lies on the C_2-axis for all the phosphenium cations. The position and maximum concentration vary with the electronegativity of the substituent. Electronegative substituents contract the valence shell of phosphorus, pulling the maximum in towards the nucleus, and increasing the magnitude of the Laplacian. It is interesting that the non-bonding CC in PCl_2^+ is in a very similar position to those on PMe_2^+ and $P(NH_2)_2^+$, yet has lower density and charge concentration. The longest non-bonding radius is for planar $P(PH_2)_2^+$.

Table 8-6 gives properties of the P-E bonding charge concentration maxima. For the C_2-twisted $P(PH_2)_2^+$ cation, these lie slightly out of the PPP plane. The CC of the central P is on the opposite side of the PPP plane to the bonding CC of the substituent, which is on the same side as the non-bonding maximum on the substituent. A top view is shown of the $\nabla^2\rho = -0.2$ isosurface in Figure 8-3.

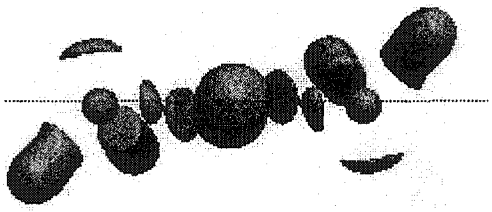

Figure 8-3: $\nabla^2\rho = -0.20$ isosurface for twisted $P(PH_2)_2^+$. A dashed line indicates the PPP plane.

8.6.2. Substituent atoms

Table 8-7 gives properties of the non-bonding charge concentration maxima on the substituent atoms. The methyl group has in- and out-of-plane C-H bonding CCs. No maxima were found around silicon. Planar PH_2 and NH_2 have only in-plane bonding CCs and no non-bonding maxima. In planar $P(NH_2)_2^+$ and $P(PH_2)_2^+$, the bonding charge concentration wraps around the substituent atom giving significant charge concentration above and below the plane.

The C_2-twisted cation, $P(PH_2)_2^+$, has a single non-bonding maximum on each substituent P atom, this maximum points in a direction perpendicular to the PPP plane, see Figure 8-4.

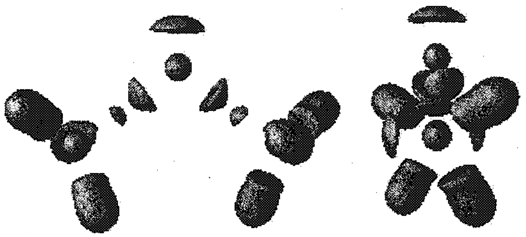

Figure 8-4: $\nabla^2\rho = -0.20$ isosurfaces for the pyramidal $P(PH_2)_2^+$ cation.

Both the S and O substituent atoms appear to have a distorted torus of charge concentration, but this is formed by the localization of the O-H and S-H bonds, not the localization of P-O and P-S bonds. The resulting torus is distorted by the interaction with the P atom, see Figure 8-5. Each $P(OH)_2^+$ species has a single in-plane non-bonding charge concentration on each oxygen atom.

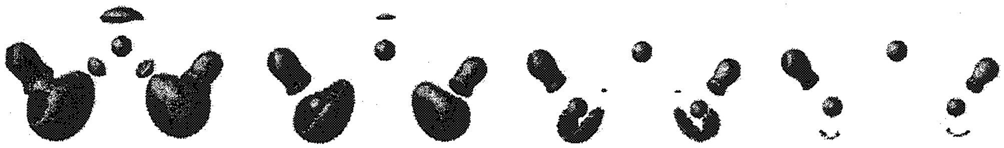

$\nabla^2\rho = -0.20$ -0.30 -0.40 -0.47

Figure 8-5: Laplacian isosurfaces for *exo* $P(SH)_2^+$.

The *exo* isomer of $P(SH)_2^+$ also shows only one non-bonding concentration on each sulfur atom. The *endo* isomer however has a symmetry-equivalent pair of out-of-plane maxima on each S atom. There is a saddle point between these maxima whose properties are quite similar to those of the maximum.

This suggests that there is a single region of charge concentration, which has been slightly distorted. Isovalue envelopes for *exo* $P(SH)_2^+$, with one non-bonded maximum per sulfur, are shown in Figure 8-5. Isovalue envelopes for *endo* $P(SH)_2^+$, Figure 8-6, show that the two maxima essentially constitute one slightly distorted region of charge concentration. This single non-bonding concentration is consistent with two bonding pairs being shared with the phosphorus atom.

$\nabla^2\rho =$ -0.20 -0.30 -0.40 -0.48

Figure 8-6: Laplacian isosurfaces for *endo* $P(SH)_2^+$.

In PF_2^+, each F has a nearly spherical reactive surface, with two in-plane non-bonding maxima. Saddles in the charge concentration lie above and below the plane and have significantly different properties from the maxima, suggesting that the charge concentration about the terminal F atom is well localized into two pairs, see Figure 8-7. This is strong evidence for localization of electron pairs due to two bonding pairs being formed. Each Cl in PCl_2^+ also has a near spherical reactive surface and two in-plane non-bonding maxima in its valence shell, see Figure 8-7. Slightly negative isosurfaces show a torus of charge concentration, but more negative Laplacian values show two distinct charge concentrations, again giving good evidence that the eight electrons in the valence shell of Cl have been localized into two bonding and two non-bonding pairs.

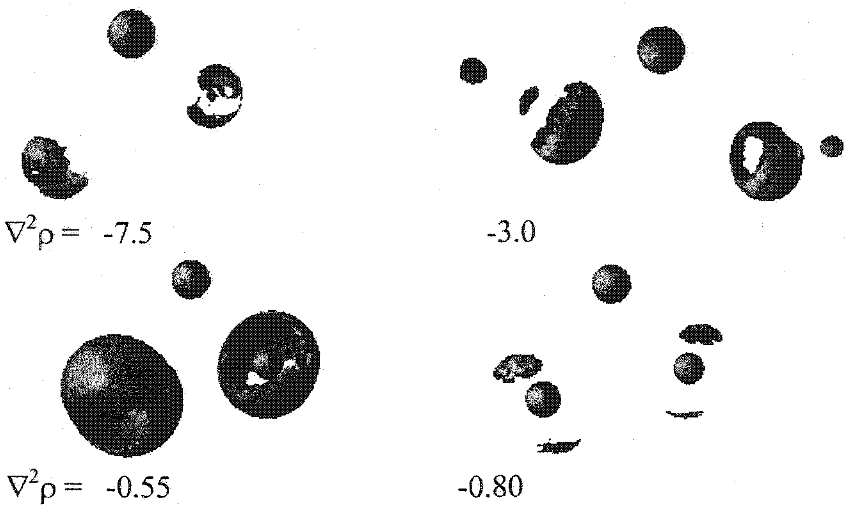

Figure 8-7: Laplacian isosurfaces for: *top* left PF_2^+, *top* right *exo* $P(OH)_2^+$, *bottom* PCl_2^+.

8.7. Summary

The phosphenium cations with lone pairs on the substituent exhibit a bond order greater than 1.75, but less than two. The corresponding formal charge is approximately plus one on each substituent group. One Lewis structure, with a small contribution from a second, could describe this situation:

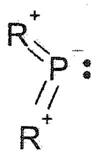

The planar amino group is the most effective substituent for stabilizing cations, according to experimental results and hydride transfer energies. The delocalization and charge transfer are not any more extensive in this cation than in the other members of the series. None of the other properties of the P-N bonding studied show significant deviation from the trends shown by the series as a whole. The P-F bond is the shortest. The P-O bond has the highest BCP density. The P-C bond has the most negative BCP Laplacian. The planar P-PH_2 interaction has the highest delocalization index, but is destabilized by the barrier to inversion at phosphorus. Other than planar PH_2, the NH_2 substituent shows the greatest $\delta^{\pi}/\delta^{\sigma}$ ratio, but the Cl and SH substituents show the greatest increase in $\delta(P,R)$ relative to the HPR_2 series. The one extremum exhibited by the amino group is the charge on nitrogen. Because of the three polar bonds to N, q(E) is most negative for E = N. Thus it seems that electrostatic factors play an important role in stabilizing aminophosphenium cations, as suggested by Gudat.

The ability of sulfur and phosphorus to delocalize their lone pairs has been observed throughout this thesis. In this series they also exhibit a large amount of charge transfer towards the central phosphorus atom, relative to the phosphines. The large barrier to inversion for phosphines seems to be responsible for the preferred pyramidalization of the phosphino group. While the delocalization index is smaller than in the planar system, the charge donation is greater.

Other systems that show significant charge transfer and delocalization through the P-E σ-bond are PH_2^+ and $P(CH_3)_2^+$. When compared to the 'lone pair donors' the methyl group shows similar changes in charge transfer and delocalization indices and just slightly less bond shortening and smaller increases in the BCP density, relative to the phosphines. The silyl group on the other hand is a poor cation stabilizer. It shows bond lengthening and reduction in BCP density relative to the phosphine. Like the other substituents, SiH_3 donates electron density to the phosphorus atom, relative to the phosphines.

It seems then that all the substituents studied, other than SiH_3 and possibly H, have significant ability to share electron density in order to increase the bond order in phosphenium cations well above that in the phosphines and potentially to a full double bond. This degree of delocalization is much more than was initially expected and indeed seems to exceed that in systems such as $HP(=X)_2$ where full double bonds seemed more likely.

Bibliography

References are listed alphabetically by first author and then by date. Data Table references are included.

Burford, N.; B.W. Royan, A. Linden, T.S. Cameron (1988). *J. Chem Soc. Chem. Commun.* **1988**, 842.

Cowley, A.H.; M.C. Cushner, J.S. Szobota (1978). *J. Am. Chem. Soc.* **100**, 7784.

Cowley, A.H. and R.A. Kemp (1985). *Chem. Rev.* **85**, 367.

Denk, M.K.; S. Gupta, A.J. Lough (1999). *Eur. J. Inorg. Chem.* **1999**, 41.

Emsley, J. and D. Hall (1976). The Chemistry of Phosphorus. New York: Wiley.

Gudat, D. (1998). *Eur. J. Inorg. Chem.* **1998**, 1087. [MP2/6-31+g(d)]

Schoeller, W.W. and T. Busch (1990). *Chem. Ber.* **123**, 971. (MCSCF calculations show biradical character for C_2 $P(PH_2)_2^+$.)

Schoeller, W.W. and U. Tubbesing (1995). *THEOCHEM* **343**, 49. [*ab initio* RHF/SCF level with inclusion of electron correlation treatment (MP4SDTQ(fc)/6-31+g(d)).]

8.8. Laplacian Contours and Isovalue Envelopes

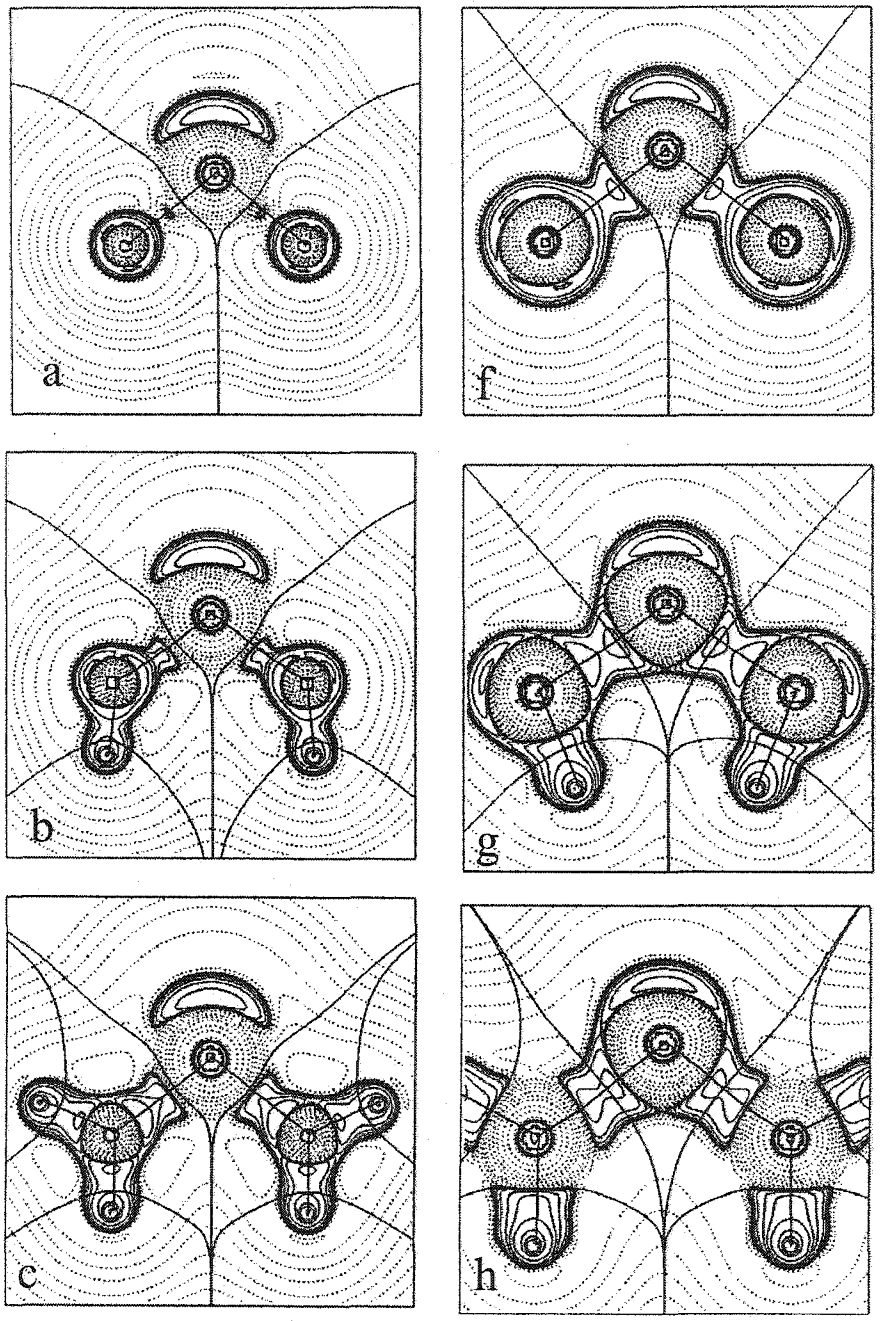

Figure 8-8: Continued on next page.

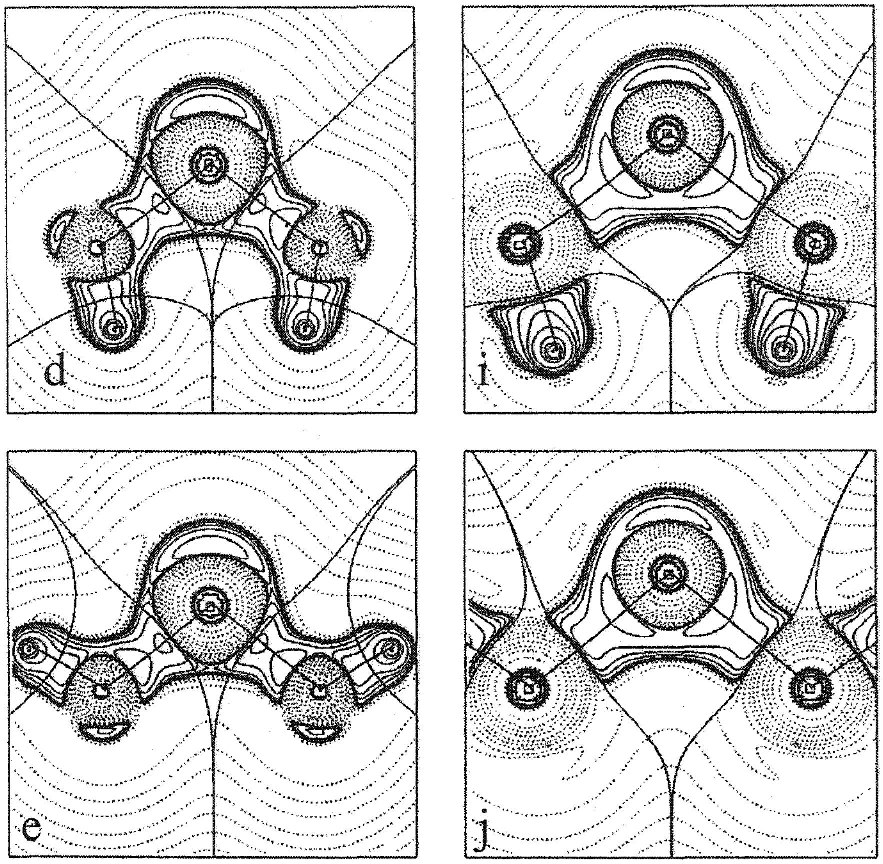

Above:

Figure 8-8: Contour maps of the $\nabla^2\rho(\mathbf{r})$, in the symmetry plane of the phosphenium cations, PR_2^+: **a)** PF_2^+; **b)** $P(OH)_2^+$, *endo*; **c)** $P(NH_2)_2^+$, planar; **d)** $P(CH_3)_2^+$, *endo*; **e)** $P(CH_3)_2^+$, *exo*; **f)** PCl_2^+; **g)** $P(SH)_2^+$, *endo*; **h)** $P(PH_2)_2^+$, planar; **i)** $P(SiH_3)_2^+$, *endo*; **j)** $P(SiH_3)_2^+$, *exo*. Solid contours indicate negative values (concentration) and dashed lines indicate positive values (depletion). The outermost contour is +0.002 au. Isovalue contours increase and decrease from the $\nabla^2\rho(\mathbf{r}) = 0$ contour in the order $\pm 2\times10^n$, $\pm 4\times10^n$, $\pm 8\times10^n$, beginning with $n = -3$ and increasing in steps of unity. Each map is overlaid with the bond paths and with the intersection of the interatomic surfaces with the displayed plane.

Below:

Figure 8-9: Isovalue envelopes of $\nabla^2\rho(\mathbf{r}) = 0$; 'front', 'top' and 'side' views of PR_2^+:
a) PF_2^+; **b)** $P(OH)_2^+$, *endo*; **c)** $P(NH_2)_2^+$, planar; **d)** $P(CH_3)_2^+$, *endo*;
e) PCl_2^+; **f)** $P(SH)_2^+$, *endo*; **g)** $P(PH_2)_2^+$, planar; **h)** $P(SiH_3)_2^+$, *endo*.

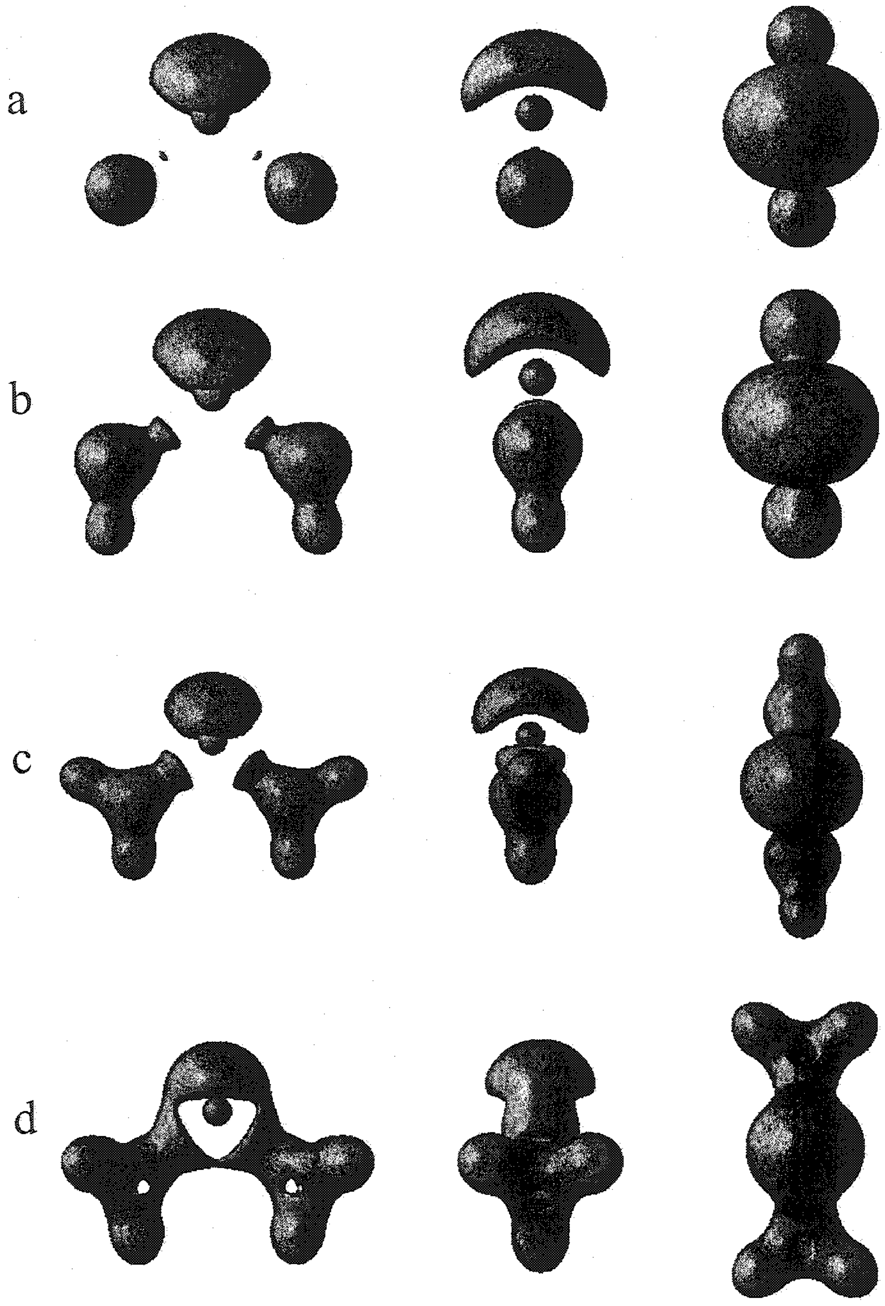

Figure 8-9: Caption above, continued on next page.

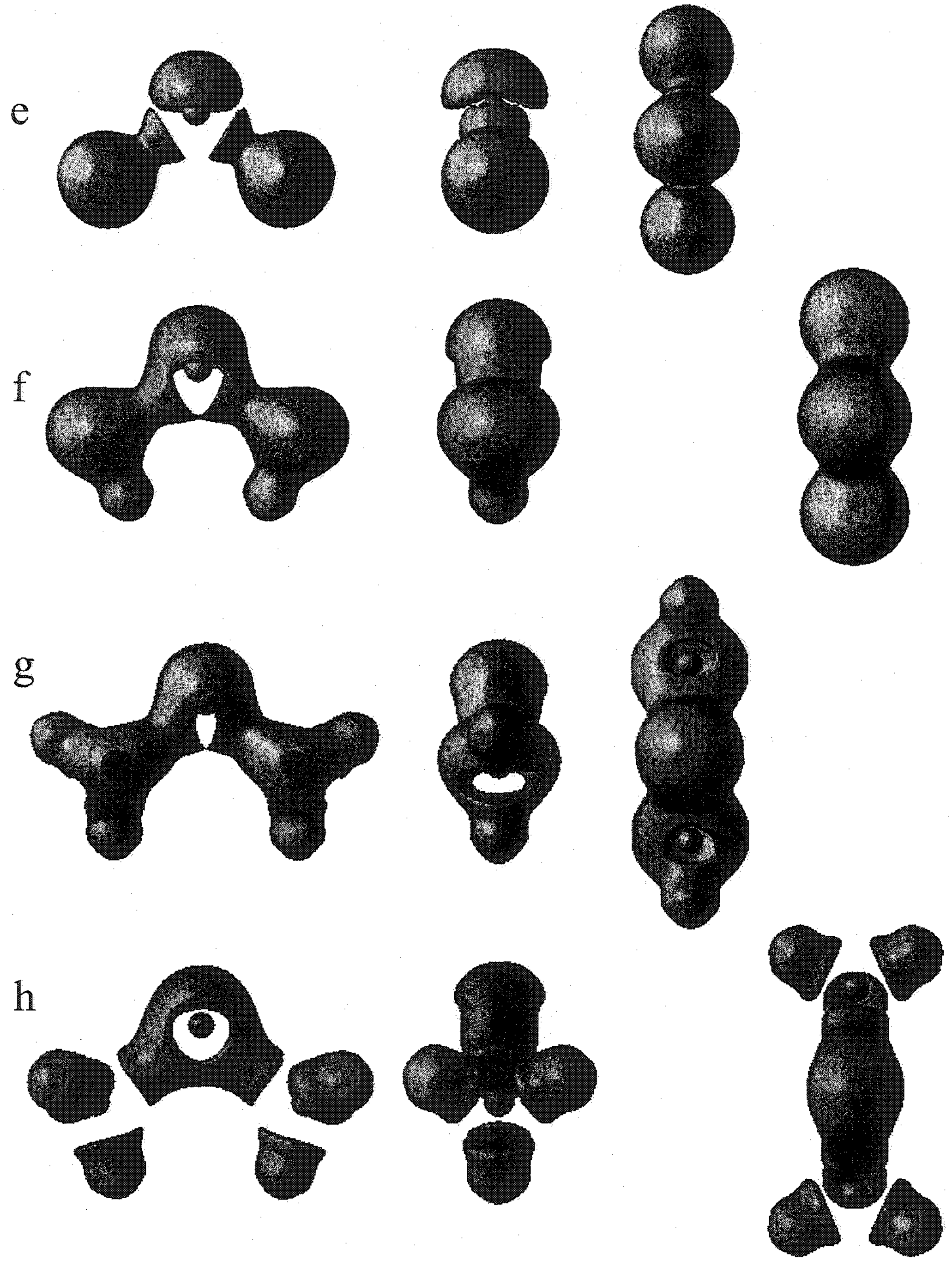

Figure 8-9: Caption above.

8.9. Data Tables

Table 8-1: Optimized geometries and energies of phosphenium cations, $P(EH_n)_2^+$, at HF/6-311++G(2d,2p) and related experimental values.

cation	**r(P-E)**	**∠ EPE**	**-Energy /au**	**ΔE_H / kJ·mol^{-1}**	**% Δ r(P-E)**[1]
PH_2^+	140.73	94.00	341.53910	0	+0.21
PF_2^+	147.85	101.54	539.40364	60.8	-5.61
$P(OH)_2^+$ *exo*	151.86	99.63	491.45559	233.5	-6.29
$P(OH)_2^+$ *endo*	151.78	109.44	491.45318	231.7	-6.23
$P(NH_2)_2^+$ Deriv.Exp't[a]	159.20 (161.1 ± .4)	105.01 (114.8 ± .2)	451.80751	349.4	-6.12
$P(CH_3)_2^+$ C_2	178.74	103.68	419.70279	152.7	-3.43
$P(CH_3)_2^+$ *exo*	179.39	102.99	419.70176	150.0	-3.08
$P(CH_3)_2^+$ *endo*	179.01	106.65	419.70090	147.8	-3.28
PCl_2^+	194.28	105.58	1259.48073	79.6	-6.07
$P(SH)_2^+$*exo*	201.39	101.58	1136.73928	202.8	-5.73
$P(SH)_2^+$ *endo* Deriv.Exp't[b]	201.67 (201.6 ± .3)	111.22 (97.59 ± .1)	1136.72845	231.7	-5.59
$P(PH_2)_2^+$ C_2 3b	211.81	105.14	1024.27105	160.9	-4.67
$P(PH_2)_2^+$	202.95	107.31	1024.24120	82.6	-8.66
$P(SiH_3)_2^+$ *exo*	234.98	100.81	921.80337	79.2	+3.38
$P(SiH_3)_2^+$*endo*	234.67	106.65	921.80299	78.2	+3.25

- Bond lengths are in picometers and angles are in degrees.
- The hydride shift energy is given, in kJ/mol, for the transfer of a hydride from PH_3.
- The percent change in the P-E bond length is given relative to the phosphine HPR_2.

1) The *endo* $P(OH)_2^+$ energy and bond length are compared to those in $HP(OH)_2$ with the H atoms pointing *down*, away from the lone pair, while the *exo* energy and bond length are compared to $HP(OH)_2$ with the H atoms pointing *up* towards the lone pair. For the remaining systems only one phosphine conformer was studied; *up* for R = SH, *staggered* (down) for CH_3 and SiH_3 and *gauche* for NH_2 and PH_2.

a) *X-ray structure for* $(^iPr_2N)_2P^+AlCl_4^-$: Cowley *et al.* (1978).
b) *X-ray structure for* $(C_6H_4)S_2P^+AlCl_4^-$: Burford *et al.* (1988).
See references in the bibliography, above.

Table 8-2: Properties of P-E bond critical points in phosphenium cations.

cation	$\rho(r_b)$	$\nabla^2\rho(r_b)$	$\varepsilon(r_b)$	$r(P-r_b)$	$r(E-r_b)$
PH_2^+	.185	-0.34	0.215	1.315	1.345
PF_2^+	.215	+1.37	0.033	1.136	1.659
$P(OH)_2^+$ *exo*	.218	+1.04	0.129	1.147	1.724
$P(OH)_2^+$ *endo*	.213	+1.05	0.121	1.150	1.710
$P(NH_2)_2^+$	.204	+0.56	0.248	1.184	1.824
$P(CH_3)_2^+$ *exo*	.182	-0.39	0.106	1.362	2.028
$P(CH_3)_2^+$ *endo*	.183	-0.37	0.083	1.356	2.027
PCl_2^+	.153	-0.11	0.037	1.348	2.324
$P(SH)_2^+$ *exo*	.152	-0.28	0.209	1.554	2.252
$P(SH)_2^+$ *endo*	.150	-0.27	0.203	1.562	2.251
$P(PH_2)_2^+$ C_2	.133	-0.20	0.202	2.134	1.871
$P(PH_2)_2^+$ *planar*	.143	-0.22	0.523	1.800	2.036
$P(SiH_3)_2^+$ *exo*	.078	+0.02	0.003	2.925	1.515
$P(SiH_3)_2^+$ *endo*	.078	+0.02	0.027	2.921	1.516

- Distances from nuclei to bond critical points, $r(A-r_b)$, are given in atomic units.

Table 8-3: Atomic and group properties in phosphenium cations, compared to phosphines, grouped by substituent atom.

cation	q(P)	q(E)	$q(EH_n)$	L (P)	L (E)	q(H) in ***HPR_2***	Δq(R) *vs.* ***HPR_2***	Δq(P) *vs.* ***HPR_2***
PH_2^+	+1.913	-0.457	-0.456	-3.6 e-4	2.0 e-5	-0.564	+0.063	+0.218
PF_2^+	+2.553	-0.776	-0.776	2.2 e-3	-8.7 e-5	-0.588	+0.090	+0.287
$P(OH)_2^+$ *exo*	+2.413	-1.449	-0.706	1.7 e-3	6.1 e-5	-0.596	+0.089	+0.230
endo	+2.446	-1.460	-0.722	1.8 e-3	-1.0 e-4	-0.619	+0.080	+0.222
$P(NH_2)_2^+$	+2.255	-1.602	-0.625	1.9 e-3	-5.8 e-4	-0.605	+0.125	+0.141
$P(CH_3)_2^+$ *exo*	+1.790	-0.648	-0.395	1.1 e-3	-3.8 e-4			+0.133
endo	+1.793	-0.661	-0.395	5.1 e-4	1.5 e-3	-0.596	+0.131	+0.136
PCl_2^+	+1.986	-0.493	-0.493	1.2 e-3	1.9 e-3	-0.563	+0.124	+0.183
$P(SH)_2^+$ *exo*	+1.315	-0.160	-0.157	1.0 e-3	-4.4 e-5	-0.563	+0.223	-0.011
endo	+1.308	-0.127	-0.155	4.7 e-3	-1.6 e-3			-0.018
$P(PH_2)_2^+$ C_2	+0.196	+1.380	+0.402	-5.9 e-5	-2.2 e-4	-0.568	+0.390	-0.351
planar	+0.605	+1.117	+0.200	3.9 e-3	2.0 e-3		+0.188	+0.059
$P(SiH_3)_2^+$ *exo*	-0.555	+2.824	+0.782	3.3 e-3	3.0 e-3			+0.139
endo	-0.559	+2.819	+0.781	3.0 e-3	1.4 e-3	-0.555	+0.156	+0.135

- q(H) refers to the H atom bonded to P in *H*PR_2.
- The atomic charges given for comparison with *endo* $P(OH)_2^+$ are those in $HP(OH)_2$ with the hydroxy H atoms pointing down, away from the lone pair, while the *exo* cation is compared to $HP(OH)_2$ with the hydroxy H atoms pointing up towards the lone pair. For the remaining systems only one phosphine conformer was studied; *up* for SH, *staggered* (down) for CH_3 and SiH_3, and *gauche* for NH_2 and PH_2.

Table 8-4: Sigma-like, pi-like and total delocalization indices in phosphenium cations.

cation	**δ^{σ} (P,R)**	**δ^{π} (P,R)**	**δ(P,E)**	**δ(P,R)**	**δ(P,R) ratio to HPR_2**	**Ratio π to σ**
PH_2^+	0.895	.0003	0.895	0.895	1.06	.0004
PF_2^+	0.545	0.169	0.714	0.714	1.22	0.31
$P(OH)_2^+$ *exo*	0.590	0.236	0.819	0.826	1.22	0.40
$P(OH)_2^+$ *endo*	0.577	0.237	0.798	0.814	1.25	0.41
$P(NH_2)_2^+$	0.626	0.310	0.900	0.937	1.25	0.49
$P(CH_3)_2^+$ C_2	-	-	0.919	1.047	1.16	-
$P(CH_3)_2^+$ *exo*	0.934	0.106	0.918	1.040	1.16	0.11
$P(CH_3)_2^+$ *endo*			0.926	1.057	1.17	
PCl_2^+	0.789	0.276	1.065	1.065	1.29	0.35
$P(SH)_2^+$ *exo*	0.973	0.402	1.332	1.376	1.33	0.41
$P(SH)_2^+$ *endo*	0.971	0.403	1.326	1.375	1.33	0.42
$P(PH_2)_2^+$ C_2	-	-	1.267	1.496	1.31	-
$P(PH_2)_2^+$ *planar*	1.063	0.566	1.463	1.629	1.42	0.53
$(SiH_3)_2^+$ *exo*	0.715	0.124	0.436	0.839	0.95	0.17
$(SiH_3)_2^+$ *endo*	0.748	0.136	0.441	0.844	1.00	0.18

- The ratios of delocalization indices, δ(P,R), are given relative to the disubstituted phosphines.

Table 8-5: Properties of non-bonding CC's on phosphorus, compared to PH_3.

cation	**r(P)**	**$\nabla^2\rho(r)$**	**ρ(r)**	**$\mu_3(r)$**
PH_3	1.443	-0.340	0.132	-9.58
PH_2^+	1.424	-0.364	0.137	-11.02
PF_2^+	1.407	-0.383	0.140	-12.38
$P(OH)_2^+$ *exo*	1.411	-0.398	0.143	-12.14
$P(OH)_2^+$ *endo*	1.408	-0.399	0.143	-12.38
$P(NH_2)_2$	1.416	-0.390	0.141	-11.65
$P(CH_3)_2^+$ C_2	1.419	-0.398	0.143	-11.54
$P(CH_3)_2^+$ *exo*	1.419	-0.399	0.143	-11.55
$P(CH_3)_2^+$ *endo*	1.418	-0.403	0.144	-11.66
PCl_2^+	1.417	-0.365	0.137	-11.48
$P(SH)_2^+$ *exo*	1.430	-0.337	0.132	-10.43
$P(SH)_2^+$ *endo*	1.425	-0.352	0.135	-10.86
$P(PH_2)_2^+$	1.444	-0.292	0.124	-9.26
$P(PH_2)_2^+$ C_2	1.437	-0.322	0.130	-9.89
$P(SiH_3)_2^+$ *exo*	1.438	-0.327	0.131	-9.85
$P(SiH_3)_2^+$ *endo*	1.438	-0.326	0.131	-9.82

- Distances to the phosphine nucleus are given in atomic units.

Table 8-6: Properties of P-E bonding charge concentrations.

cation	r(P)	r(E)	$\nabla^2\rho(r)$	$\rho(r)$
PF_2^{+} [1]	1.472		-0.042	0.303
$P(OH)_2^+$ *exo*	1.506		-0.297	0.291
		0.696	-3.652	0.808
$P(OH)_2^+$ *endo*	1.507		-0.255	0.283
		0.693	-3.678	0.812
$P(NH_2)_2$		0.804	-2.019	0.499
$P(CH_3)_2^+$ C_2	1.490		-0.464	0.184
		0.988	-0.822	0.252
$P(CH_3)_2^+$ *exo*	1.489		-0.464	0.183
		0.990	-0.808	0.250
$P(CH_3)_2^+$ *endo*	1.489		-0.463	0.183
		0.989	-0.816	0.251
PCl_2^+	1.521		-0.243	0.156
		1.247	-0.551	0.259
$P(SH)_2^+$ *exo*	1.521		-0.284	0.152
		1.370	-0.410	0.191
$P(SH)_2^+$ *endo*	1.523		-0.278	0.150
		1.372	-0.403	0.193
$P(PH_2)_2^+$		1.530	-0.285	0.150
$P(PH_2)_2^+$ C_2 [2]	1.509	2.514	-0.322	0.147
	2.453	1.552	-0.252	0.136
$P(SiH_3)_2^+$ *exo*	1.485		-0.327	0.142
$P(SiH_3)_2^+$ *endo*	1.484		-0.353	0.142

- The distance from the valence shell maximum to the nucleus is given in atomic units

1) There is a saddle point where the bonding maximum is expected in the valence shell of F.
2) The bonding CC's are slightly out of the PPP plane in C_2 $P(PH_2)_2^+$; see text. The central BCC is -0.19 au out of plane; the other BCC is +0.026 au out. The BCP is -0.04 au out of plane.

Table 8-7: Properties of non-bonding CC's, and intervening saddle points, on the substituent atoms, E.

cation	CC position	r(E)	$\nabla^2\rho(r)$	$\rho(r)$	Z
PF_2^+	endo	0.574	-9.245	1.467	0
	exo	0.575	-9.261	1.468	0
	saddle	*0.581*	*-7.751*	*1.342*	*±0.47*
$P(OH)_2^+$ *exo H*	endo	0.647	-5.160	0.934	0
$P(OH)_2^+$ *endo H*	exo	0.648	-5.133	0.935	0
PCl_2^+	endo	1.182	-0.865	0.274	0
	exo	1.181	-0.884	0.276	0
$P(SH)_2^+$ *exo H*	endo	1.301	-0.482	0.180	0
$P(SH)_2^+$ *endo H*	exo ×*2*	1.301	-0.493	0.182	±0.89
	saddle	*1.300*	*-0.486*	*0.181*	*0*
$P(PH_2)_2^+$ C_2	exo ×*1*	1.46	-0.274	0.119	1.43

- Distances from nuclei to maxima, r(E), are given in atomic units.
- Z is the distance from the critical point to the molecular symmetry plane, in au.

9. Summary and Conclusions

This thesis started with a series of questions about the electronic structure of phosphenium cations. These came down to: 1) What is the extent of multiple bonding in phosphenium cations in general? 2) Is it exceptionally high in amino-phosphenium cations? 3) Do amino-phosphenium cations exhibit any other major differences relative to less stabilized phosphenium cations? In order to answer these questions, it was necessary to consider the meaning of electron delocalization and its description at both the simple Lewis model level and at the level of *ab initio* electron structure calculations, in order to make a connection between these two descriptions. This connection was found to exist in the delocalization index, but only after it had been corrected for the effects of bond polarity.

A new relationship between the delocalization index and the polarity of the bonding has been discovered. A quadratic relationship has been derived for the case of one shared pair of electrons ($\delta = 1- q^2$) and for the case of two equally polarized shared pairs of electrons ($\delta = 2- q^2/2$). This derivation applies equally well to the bonding indices defined by Bader (Fradera *et al.*, 1999), by Mayer (Ángyán, Loos and Mayer, 1994) and by Fulton (Fulton and Mixon, 1993), which are all equivalent at the Hartree-Fock level of theory. A plot of previously published δ and q data for simple hydrides, AH_n, has shown that the derived expression is obeyed at the Hartree-Fock level of theory and that a quadratic relationship is maintained when correlation effects are included in the wavefunction. This is the first measure of bond order that does not depend on partitioning of the orbitals in some way, either by assigning density to atoms based on the atom-centred basis functions, or by transforming the molecular orbitals to correspond with a localized model.

Interactions (exchange and overlap) with other orbitals and additional delocalization of 'lone pairs' onto neighbouring atoms can alter the position and curvature of the parabolic δ *versus* q curve. Therefore, in order to establish the bond order for a species of interest, a series of related molecules should be studied and the data plotted to establish the best-fit line. The maximum of this curve will correspond to the formal charge (q) and bond order (δ) of the idealized 'non-polar' representative of the series. When there are no data points available near the maximum, the results can be quite sensitive to the choice of data points used.

In order to further establish the bonding pattern in a particular species, the arrangement of bonding and non-bonding charge concentrations may be analysed. Further evidence regarding the similarity of bonding arrangements in a series of molecules can be gained by studying the trends in the properties of the bond critical points, most notably the bonding radii and the density at the BCP. The Laplacian and the ellipticity are less reliable indicators of regularity, but can give general information in the cases of extremely polar (*e.g.* P=O) or extremely elliptical (*e.g.*

P=C) bonds, respectively.

9.1. *'Trivalent'* systems

The new methodology was tested on some standard systems involving trivalent phosphorus or trivalent nitrogen. We have seen that for the 'standard' single bond and double bond series (H_2PR, HPR_2, PR_3 and HPX, as well as NH_2R and HNX) there is a strong correlation between the square of the transferred charge and the delocalization index. While the observed curvatures of the δ *vs.* q graphs are less than expected for both single and double bonds to phosphorus, the ratio between them is the predicted 2:1 {0.66 : 0.34}. In each 'standard' series, the maximum delocalization is slightly greater than the integer. Both of these effects can be attributed to the interaction with other electron pairs in the molecule. Most significantly, the 'lone pairs' on the central atom and on the substituents may be partially delocalized.

By dealing with the charge on the entire substituent ($X = EH_{n-1}$ or $R = EH_n$), the effects of the E-H bond polarity are minimized and we are dealing primarily with the effects of the P-E bond polarity. The charge variation on P due to the *other* substituents (R or H) is expected to have some effect on the delocalization index, mainly associated with changes in the additional 'lone pair' delocalization, mentioned above. The effect must be very small however because the ($q(SiH_3)$, $\delta(P,SiH_3)$) data points for H_2PSiH_3, $HP(SiH_3)_2$ and $P(SiH_3)_3$ all fall very close together, while q(P) varies from +0.5 to –1.9.

The N-E delocalization indices are greater than the P-E delocalization indices for the same extent of charge transfer, particularly for the single bonds. This is attributed to more extensive delocalization of lone pairs between the nitrogen atoms and the substituents than between phosphorus and the substituents. The doubly bonded species are seen to have shorter bonds, with higher density at the bond critical point, and larger charges on the substituent groups, than the singly bonded species. This is as expected.

9.2. *'Hypervalent'* systems

The methodology was applied to some formally pentavalent environments of phosphorus and nitrogen. The results indicated less than a full double bond for the phosphorus-element bonds and not much more than a single bond for the nitrogen-element interactions. For the pentavalent phosphorus species, one might be tempted to attribute the decrease in the maximum delocalization to a decrease in the population on phosphorus. Based on the phosphine results, however, this does not seem reasonable.* The decrease in the delocalization index, for a given charge transfer, as the phosphorus environment changes from HPX to HPX_2 to H_3PX must be a real change in the number of shared electron pairs, or at least in the polarity of the second electron pair, relative to the first.

---

[*] Furthermore, q(P) in HPX_2 is similar to H_3PX for the second row substituents and similar to HPX for the third row substituents, yet $\delta(P,X)$ for HPX_2 lies between H_3PX and HPX for both the second and third period substituents.

Minimization of formal charge suggests the Lewis structures with double bonds.

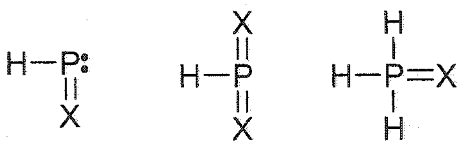

Meanwhile the octet rule (Lewis's rule of eight) suggests one P-E single bond for the pentavalent phosphorus systems, plus a P-E double bond in HPX_2.

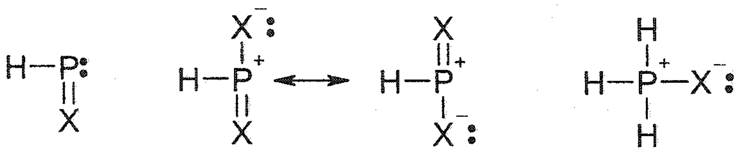

This gives a formal charge of +1 on phosphorus in both pentavalent systems. For HPX_2 the average formal charge on X from these two equivalent resonance structures is –0.5 and the average P-X bond order is 1.5. For H_3PX the formal charge on X is –1 and the P-X bond order is 1.0, if the octet rule is obeyed.

Taking the maximum of each curve as the point where the formal charges (equal sharing assumed) are most closely related to the actual charges, and the delocalization index most closely reflects the number of (equally) shared pairs, the approximate bond orders and formal charges from the quadratic fitting are shown in Table 9-1, below. The results depend on which points are included in the fit. Typically, E = C data points lie below the graph and E = S points lie above. Normally P follows the same trends as S, but in H_3PPH it is below the curve.

Series	HPX	HPX_2		H_3PX	
Substituent atoms excluded from the fitting procedure.		C	S, P	S, P	P
Formal Charge, $q_{max}(X)$	0	-0.20	-0.21	-0.26	-0.33
Bond Order, $\delta_{max}(P,X)$	2	1.74	1.44	1.40	1.48

Table 9-1
Formal charges and bond orders extracted from the best-fit equations of the delocalization *versus* charge transfer graphs for HPX, HPX_2 and H_3PX, as a function of the data points included in the fitting procedure.

The calculated properties are an approximately equal mixture of the predictions from the octet rule and the formal charge minimization. We see this trend most clearly for the substituents X = O, NH and planar SiH_2 where q(X) becomes more negative over the series HPX, HPX_2, H_3PX. The variations in q(X) where X = S, PH and planar CH_2 are less well understood. The CH_2 group is almost as 'neutral' in $HP(CH_2)_2$ as in $HPCH_2$. In HPPH, the substituent PH group donates density to the central P, though in H_3PPH the PH group accepts density and the delocalization index amplifies the effect. Sulfur seems to be particularly effective at transferring and delocalizing charge onto phosphorus and q(S) is actually less negative in HPS_2 and H_3PS than in HPS. The delocalization index follows the expected trend, HPX > HPX_2 > H_3PX for all planar substituents, X.

The nitrogen species have a different story to tell. The standard single and double bond curves have a delocalization maximum significantly above the expected integer and about 0.2 above the phosphorus curves. This suggests that there is more delocalization of the lone pairs in these trivalent nitrogen species than in the phosphorus analogues. While the H_3PX series has a bond order of approximately 1.5 (expected formal charge: -0.5), the H_3NX series maximum is *equal to* the amine maximum of 1.3, and corresponds to a formal charge of approximately -0.75 on the substituent. The very electronegative oxide substituent lies reasonably close to the H_3PX curve, and if this is removed from the H_3NX fitting the maximum lies near the H_3NNH data points, (-0.5, 1.2). Clearly there is only one fully shared electron pair in this series, with the second electron pair being no more delocalized than the lone pairs in the amines. In this case the lone-pair donation is one-way (from E to N only) and thus the charge on the substituents is smaller than the expected –1.0 for the octet structure.

An explanation for the lack of high-coordinate second-row atoms is that they are both too small to accommodate more ligands, and too electronegative to participate in the polar bonding needed when using four atomic orbitals (2s, 2ppp) to describe more than four bonding molecular orbitals. If the hydrogen atoms were replaced by fluorine atoms, the F_3NX series may be sufficiently polarized to display multiple N-E bonds. This would be an interesting series to study in the future.

9.3. *'Hypovalent'* systems

Turning now to the phosphenium cations, PR_2^+, placing the positive formal charge on the most electropositive element leads to single bonds for all R but PH_2 and SiH_3. In $P(PH_2)_2^+$ we may be equally justified in putting the positive charge on the substituents. The two structures with a double bond also obey the octet rule for all atoms.

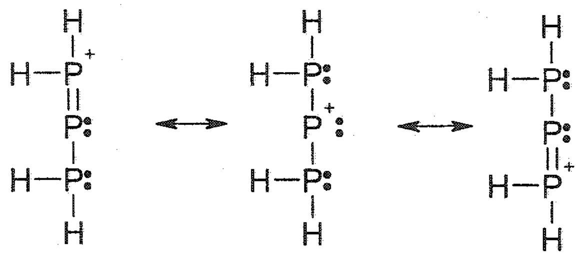

There are no lone pairs on SiH_3, however, and regardless of electronegativity differences the only 'reasonable' Lewis structure for R = H, CH_3 and SiH_3 is the singly-bonded structure with the positive formal charge on phosphorus.

For the substituents with lone pairs, R = F, Cl, OH, SH, NH_2 and PH_2, the octet rule indicates that the best resonance structures have one double bond, as shown at the far left and far right for R = PH_2, above. This would lead to a formal charge of zero on the central phosphorus and an average formal charge of +0.5 on the substituent, along with an average P-R bond order of 1.5. A complete sharing of two electron pairs per substituent is also a possibility and would give a bond order of 2 and a formal charge of +1 on each substituent and –1 on the central phosphorus.

Surprisingly, removal of the very electronegative F substituent from the planar set mentioned above gives a quadratic fit with a maximum very close to q(R) = +1 and $\delta(R,R) = 2$. Unfortunately, no data points are available near the maximum to verify the extrapolation. Inclusion of F in the fitting gives a curve that is slightly higher than for HPX_2 and shifted over by a charge of one electron; $q_{max}(R) = +0.86$, $\delta_{max}(P,R) = 1.80$. Once again, the octet is exceeded on the central phosphorus. We could describe the overall structures as 80% doubly bonded and 20% singly bonded with the appropriate contributions from the two symmetric structures.

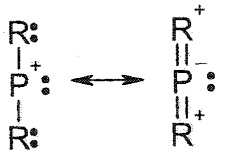

The distribution of valence shell charge concentrations around the substituent atoms is also consistent with two P-E bonding pairs and two non-bonding, or E-H bonding, electron pairs. Separating the delocalization indices into σ-like and π-like contributions gives a slightly different description. While δ^{π} is 75% to 110% of δ^{σ} in HPX, δ^{π} ranges from 30% to 50% of δ^{σ} in planar PR_2^+. For R = H, CH_3 and SiH_3 the percentages are 0.04%, 11% and 17%, respectively. These three species do not involve extensive multiple bonding, in the Lewis sense.

For a given substituent atom, [EH_n / EH_{n-1}] the σ-delocalization is slightly lower in PR_2^+ than in HPX (higher for E = C) but the π-delocalization is significantly lower. For example, $\delta^{\pi} / \delta^{\sigma}$ drops from 0.98 to 0.49 between HP=NH and $P(NH_2)_2^+$. This seems to suggest that the bond order is closer to 1.5 than to 1.8. On the other hand, the π-delocalization is known to decrease relative to the σ-delocalization as the total bond polarity increases, and since a non-polar double bond in PR_2^+ would require much more electropositive elements than those studied here, it is not surprising that the π-delocalization is lower in this series. Comparing HPX and PR_2^+ systems with similar delocalization indices, such as $HPCH_2$ (1.68) and $P(PH_2)_2^+$ (1.63), the δ^π / δ^σ ratio is still much higher for the HP=X series. It should be noted, however, that P-C and P-N σ-delocalization indices seem to be unusually low. In PCH and PN, which are formally triply bonded, the δ^π / δ^σ ratios are 0.84 / 0.63 and 0.89 / 0.65, respectively.

Returning to our original questions, while there is conflicting evidence regarding the exact bond order for the phosphenium cations it seems clear that the bond order is between 1.5 and 2, and may even be higher than in the pentavalent HPX_2 series. It is not unusually high in $P(NH_2)_2^+$. It seems likely then, that the thermodynamic stability of aminophosphenium cations arises from electrostatic attraction between the positively charged phosphorus atom and the negatively charged nitrogen atom. There may be additional steric and/or electronic effects that make aminophosphenium cations kinetically more stable as well – and therefore easier to isolate than other phosphenium cations.

While pentavalent phosphorus systems do exceed the octet rule, they do not form complete double bonds, and thus the formal charges are not completely reduced. The structures seem to be best described as somewhere between the octet and 'formal-charge-minimization' predictions. The hypervalent nitrogen systems studied appeared to be more controlled by the octet rule. This limitation may be lifted if more electronegative substituents (*e.g.* fluorine atoms) are used, and should be studied further.

It is hoped that the methods developed in this thesis will be used by other theoreticians and computational chemists when investigating Lewis bond orders. The regular decrease in the delocalization index (as well as the bond indices developed by Fulton, 1993, and Ángyán *et al.*, 1994) should be accounted for in any calculation of bond order using these indices. Furthermore, chemical educators should think carefully about how they present Lewis structures, and chemical bonding in general, to the next generation of chemists. What is the point of speaking a common language if there is no common lexicon?

Bibliography

Ángyán, I.; M. Loos and I. Mayer (1994). *J. Phys. Chem.*, **98**, 5244.

Fradera, X.; M. A. Austen and R. F. W. Bader, (1999). *J. Phys. Chem. A*, **103**, 304.

Fulton R.L. (1993). *J. Phys. Chem.*, **97**, 7516.

Fulton R.L. and S. T. Mixon (1993). *J. Phys. Chem.*, **97**, 7530

A1. Appendix 1: Glossary of terms and symbols used in this thesis

A1.1 Words and phrases

Additivity: A property can be expressed as a sum of contributions from its constituent groups. Additivity may be seen empirically, in which case each chemically similar group is seen to have an equal contribution, or computationally, in which case the additivity is rigourous, but the contribution of each group may vary somewhat (when groups are not perfectly transferable).

Antisymmetric function: a function whose sign changes when some operation is performed. In the Pauli sense, one that changes sign upon exchanging the labels of any two electrons.

Atom: 1) a region of real space bounded by surfaces of 'zero-flux' (interatomic surfaces). Equivalently, the union of an attractor (in the scalar electron density field) and its basin. 2) a nucleus and its associated electrons.

Attractor: a maximum in a scalar field, such as nuclear positions in the electron density.

Average value: See expectation value.

Basin: the region of real space containing all gradient paths terminating at a given nucleus.

Basis function: a mathematical function of real space (and/or spin) that is used in a linear expansion of some other function. Typically, a hydrogen-orbital-like atom-centred function used in the expansion of a molecular orbital.

Bond: an attractive interaction between two atoms indicated by the presence of a bond path in the electron density.

Bond Critical Point: the position of minimum density along the bond path. Also, a (3,-1) saddle point in the density.

Bond order: a) the number of pairs of electrons shared between two atoms in a Lewis structure, or the weighted average of this over two or more resonance structures. b) the maximum delocalization index for a delocalization *versus* charge plot, for a series of related molecules.

Bond path: a pair of trajectories of the gradient of the electron density, both originating at a (3,-1) critical point and terminating at two different nuclear attractors.

Bonded radius: the distance (reported in bohr) from the nucleus of interest to the bond critical point of interest.

Chalcogen: an element of group 6A (16).

Charge Concentration: a region of negative Laplacian, typically in the valence region of an atom.

Commuting operators: operators commute when the order of operation has no effect on the outcome, *i.e.* AB = BA

Complex conjugate: For a complex number (a + ib) we replace $i = +\sqrt{-1}$ with $-i = -\sqrt{-1}$ to get the complex conjugate.

Constant of Motion: an observable that commutes with the Hamiltonian, and for which the state function is an eigenfunction.

Correlation function: f(r_1, r_2) measures the difference between the correlated and uncorrelated density distributions of two electrons of given spin and is defined by $\rho^{\sigma\sigma'}(\mathbf{r}_1,\mathbf{r}_2) = \frac{1}{2}\rho^{\sigma}(\mathbf{r}_1)\rho^{\sigma'}(\mathbf{r}_2)\left[1 + f^{\sigma\sigma'}(\mathbf{r}_1,\mathbf{r}_2)\right]$.

Correspondence Principle: a postulate of quantum mechanics: for every classical observable there corresponds a quantum mechanical operator. Specifically, we write the classical observable in terms of position and momentum (x, p_x) and then replace position with the position operator ($\hat{x}$ = x·) and replace momentum with the momentum operator ($\hat{p} = -i\hbar\nabla$).

Covalent bond: a bonding interaction characterized by 'significant' delocalization of electrons between the two atoms of interest. Compare ionic bond.

Critical point: a point at which the gradient of some scalar field (such as the density) is equal to the zero-vector. The nuclear positions may be considered pseudo-critical points in the density, since these maxima are cusps, with undefined gradient vectors. Critical points are classified by their rank and their signature.

Curvature: the second derivative of a function with respect to a spatial (Cartesian) coordinate.

Delocalization: An electron is said to be delocalized when its Fermi hole is delocalized. We can measure atomic delocalization with the delocalization index, the Fermi hole integrated over two different atoms.

Density: electronic charge density, $\rho(\mathbf{r})$.

Density matrix: See Appendix A2.

Determinant: an antisymmetrized product of molecular orbitals, representing an uncorrelated molecular wavefunction.

Dressed density: a one-electron operator in which the mean field of the remaining electron has been accounted for, so that a local property density may be obtained.

Eigenfunction / Eigenstate: (a state described by) a function f(x) that obeys the equation $\mathbf{A}f(x) = a\, f(x)$, for the operator of interest, **A,** where a is a scalar value.

Eigenvalue: the scalar value (a) in the equation above, which corresponds to the well-defined value of the property A in the state described by f(x).

Exchange Energy: the energy difference between a simple Hartree product of molecular orbitals and an antisymmetrized product of these MOs.

Expectation value: the average value of some observable for the given state.

Fermi hole: the same-spin correlation function weighted by the density at $\mathbf{r}_2$. A measure of the reduction of same-spin density at position $\mathbf{r}_2$ due to the presence of an electron at $\mathbf{r}_1$.

Fermion: a particle with half-integer spin, such as an electron, which obeys Fermi-Dirac statistics.

Formal Charge: the hypothetical atomic charge arising from a Lewis structure when all the bonds are assumed to be non-polar, or a weighted average of this property over two or more Lewis structures.

Gradient path / gradient trajectory: a path of maximum increase in a scalar property. Gradient vectors begin (originate) at a critical point (or infinite distance) and end (terminate) at a critical point in the scalar field of interest.

Gradient vector operator: $\nabla = \left(\frac{\partial}{\partial x}, \frac{\partial}{\partial y}, \frac{\partial}{\partial z}\right)$

Group number: There are two group number systems for the periodic table in common use. 1) The A/B system in which main groups run from 1A to 8A, while transition metals run from 3B to 8B, then 2B and 3B. 2) The 18-group system, in which the main and transition groups are numbered in order from 1 through 18, and the main groups are 1, 2 and 13 through 18. The A/B system will be used in this thesis.

Halogen: an element of group 7A (17).

Hamiltonian operator: an operator whose expectation value, or eigenvalue, is the total energy. H = K + V. The kinetic energy operator in the Hamiltonian corresponds to the local property density, K(r), while the kinetic energy in Schrödinger's energy functional corresponds to G(r). The Hamiltonian is also the generator of time evolution, as expressed in the time-dependent Schrödinger equation.

Hartree-Fock: a method of approximating the wavefunction as an antisymmetrized product (a Slater determinant) of molecular orbitals.

Heisenberg's Uncertainty Principle: The momentum and position of a particle cannot be simultaneously known (measured) with infinite precision. This measurement limitation can be extended to other pairs of observables by considering the commutator of the two operators.

Hilbert Space: The multidimensional space spanned by the eigenvalues of all the observables. For an approximate, numerical wavefunction we can also discuss the basis functions in terms of a Hilbert space. When we *partition a wavefunction in Hilbert space* we assign the partial properties arising from a given basis function to the atom about whose nucleus the function is centred. Note that this does not apply to non-atom-centred basis functions.

Hypervalent: a) the property of an atom in a molecule whose valence is greater than its principal valence. b) having more than eight electrons in the valence shell (applies to main group atoms).

Indistinguishable particles: particles in a system whose observable properties would not change if two of the particles were exchanged.

Interatomic surface: the set of gradient vectors of the electron density terminating at a bond critical point. The bounding (zero-flux) surface between two proper open systems.

Ionic bond: a bonding interaction characterized by electrostatic attraction between 'significantly' charged atoms with 'minimal' electron delocalization between them. Compare covalent bond.

Kinetic energy: the energy of a system due to motion of the particles.

Laplacian: the sum of the curvatures. It results from the square of the gradient vector operator, particularly when it operates on the electron density.

Local property density: a function of real space describing the local contribution to some total (molecular) property.

Localization: the extent to which the Fermi hole for a reference electron in a given basin remains within that basin.

Mesityl: 2,4,6-trimethylphenyl (Mes), a substituent used for its steric bulk.

Molecular Orbital: a one-electron wavefunction for an electron in a molecule. The Hartree-Fock wavefunction can be written as an antisymmetrized product (a Slater determinant) of these molecular orbitals.

Observable: a measurable property of the system.

Open system: a system that exchanges energy and particles with its surroundings. See proper open system.

Operator: a mathematical functional that operates on the wavefunction to obtain a value for the corresponding observable.

Pauli Principle: the requirement that a system of indistinguishable fermions be antisymmetric with respect to exchanging the labels of any two such particles.

Pnictogen: an atom of group 5A (15).

Post-Hartree-Fock: A computational method (level of theory) that accounts for Coulomb correlation between electrons, *e.g.* MP2 or CI.

Polar bond: a covalent bond in which the two atoms have different electronegativities, and thus different degrees of attraction for the bonding electrons. At the extreme polar end of the covalent spectrum is the ionic bond.

All covalent bonds are to some extent polar unless the bond critical point intersects some symmetry element of the molecule such as a mirror plane or an inversion center (or a C_2 rotation axis perpendicular to the bond path).

Principal valence: the 'normal' valence of an atom, determined by the number of unpaired electrons in the Lewis dot symbol for the isolated atom. For main group elements this is the lesser of the group number (A/B system) or eight minus the group number.

Probabilistic Interpretation (of the wavefunction): The probability of finding the state in the multidimensional volume of state-space, $d\tau$, is $\Psi^2(\tau)d\tau$.

Proper open system: an open system bounded by a zero-flux surface, whose physics is thus well defined.

Property density: see local property density

Rank: ω, the number of non-zero curvatures at a critical point. This is typically 3 for scalar functions of real space.

Saddle point: a critical point that is a minimum is some direction and a maximum in some other direction. Within the topology of the electron density, a saddle point may be either a (3,-1) critical point called a bond critical point or a (3,+1) critical point called a ring critical point.

Scalar field: a function of real space whose values have only sign and magnitude, not direction.

Schrödinger equation: time-dependent: Equation 1-1, time independent: Equation 1-2.

Signature: σ, the sum of the signs of the curvatures at a critical point.

Slater determinant: an approximate form of the wavefunction, written as an antisymmetrized product of molecular orbitals.

State function: the projection of the state vector onto the particle coordinates. See wavefunction.

State vector: a vector in Hilbert space, which describes the probability of observing each eigenvalue of each observable.

Stationary state: a state whose properties (and particularly the Hamiltonian operator) are independent of time.

Substituent atom: the atom, E = L, M or H, bonded directly to the central phosphorus or nitrogen atom in each of the molecules studied.

Substituent group: the group R = EH_n or X = EH_{n-1} bonded directly to the central phosphorus or nitrogen atom in each of the molecules studied.

Supermesityl: 2,4,6-tri-*tert*-butylphenyl (Mes^*) a substituent with even greater steric bulk than mesityl: 2,4,6-trimethylphenyl (Mes)

Transferability: When the electron density of a group is the same, in different chemical environments, all the other properties of the group will also be the same. Perfect transferability of electron density leads to perfect transferability of other properties. Near transferability of density and other properties is often seen, leading to empirical additivity schemes.

Valence: the number of bonds formed by an atom in a given molecule, as determined by the Lewis structure with no formal charges; *e.g.* 4 for carbon in methane, 2 for oxygen in water, 5 for phosphorus in H_3PO. Valence is less well defined for molecules with formal charges on one or more of the atoms, but we may define a 'formal valence' as the number of bonds an atom would form if its formal charge were zero.

Valence electron: an electron in the outer (valence) shell of an atom – either bonding or non-bonding.

Valence shell charge concentration – for atoms this is a spherical charge concentration. In molecules it is associated with the reactive surface.

Vector field: a function of real space whose values have magnitude and direction in real space.

Wavefunction: a function, obtained from the Schrödinger equation, of the particle space and spin coordinates that is postulated to contain all the measurable information about a system.

Zero-flux surface: a surface through which no gradient paths cross, defined by a set of gradient paths originating at a bond critical point (or ring critical point). The gradient at any point on the surface is parallel with the surface, so that the surface normal is orthogonal to the gradient at every point on the surface.

A1.2 'Atomic' symbols

E: Any atom, particularly the heavy atom (L or M) in the substituents X and R.

L: a main group element of the second row (the first heavy row), specifically C, N, O or F. An atom whose valence shell is the L shell (n = 2).

M: a main group element of the third row (the second heavy row), specifically Si, P, S or Cl. An atom whose valence shell is the M shell (n = 3).

Me: Methyl, CH_3.

Mes: Mesityl, 2,4,6-trimethylphenyl.

Mes*: Supermesityl, 2,4,6-tri-*tert*-butylphenyl

R: a substituent group of the central phosphorus atom that has a formal valence of 1, also represented by EH_n. Specific groups in this thesis are CH_3, NH_2, OH, F, SiH_3, PH_2, SH and Cl. R may also represent H in the molecules PH_3 and PH_2^+.

TMS: Trimethylsilyl, $Si(CH_3)_3$.

X: a substituent group of the central phosphorus atom that has a formal valence of 2, also represented by EH_{n-1}. Specific groups in this thesis are CH_2, NH, O, SiH_2, PH, and S.

Y: An atom or group replacing a hydrogen atom (H) in any of the general formulae: $P(EH_n)_3$, $HP(EH_n)_2$, H_2PEH_n, $HPEH_{n-1}$, H_3PEH_{n-1}, $HP(EH_{n-1})_2$, $P(EH_n)_2^+$.

A1.3 Acronyms

AO: atomic orbital

BCP: bond critical point

CC: charge concentration

HF: Hartree-Fock (method)

LCP: Ligand Close Packing (model)

MCSCF: MultiConfiguration Self-Consistent Field method

MO: molecular orbital.

MP2: Møller-Plesset (perturbation method), 2nd order

MP4: Møller-Plesset (perturbation method), 4th order

QCISD: Quadratic Configuration Interaction, Singles and Doubles

RHF: Restricted Hartree-Fock (method)

SCF: Self-Consistent Field

VSCC: valence shell charge concentration

VSEPR: Valence Shell Electron Pair Repulsion (theory)

A1.4 Local and atomic properties, arabic:

G(r): Kinetic energy density, positive definite form.

$h^{\sigma}(\mathbf{r}_1, \mathbf{r}_2)$: the Fermi hole at point $\mathbf{r}_2$ (for a spin σ reference electron at point $\mathbf{r}_1$).

$J_F(r)$: vector current density for property F.

J(r): vector current density.

$j_F(r)$: one-electron contribution to the vector current density for property F.

K(r): kinetic energy density.

L(Ω): the residual Laplacian of an open system due to integration errors.

N: the total number of electrons in a closed system.

N(Ω): the electron population of the open system Ω.

q(Ω): the electric charge on the open system Ω; q(Ω) = N(Ω) – Z.

$\mathbf{r}_b$: the position of a bond critical point.

$r_b(\Omega)$: the bonded radius of the atom Ω with respect to the bond path of interest.

$\mathbf{r}_{nb}$: the position of a non-bonding maximum in the charge concentration, $-\nabla^2\rho$.

$r_{nb}(\Omega)$: the distance of a non-bonding maximum from the nuclear position of atom Ω.

<T>, T(Ω): average kinetic energy.

<V >, V(Ω): average potential energy, atomic virial.

X: the set of nuclear spatial coordinates describing the nuclear configuration of the molecule.

x: the set of electronic spin and spatial coordinates.

Z: The atomic number, equal to the nuclear charge (in atomic units) of an atom.

A1.5 Greek Letters and other symbols:

α: a 'spin-up' spin function, $m_s = +1/2$

β: a 'spin-down' spin function, $m_s = -1/2$

χ: a spin (molecular orbital)

$\delta(\Omega,\Omega)$: delocalization index.

ε: ellipticity (at the BCP).

ϕ: a basis function (atomic centred).

Φ: a (spatial) molecular orbital.

γ: a density matrix.

η: a natural (molecular) orbital.

λ_i: component of the curvature of the density at a critical point – an eigenvalue of the Hessian matrix of ρ.

μ: dipole moment vector, or its magnitude.

μ_i: component of the curvature of the Laplacian of the density.

π: A symmetry representation that is antisymmetric about a symmetry axis, or more generically, a bond axis.

$\rho(\mathbf{r}; \mathbf{X})$: electron density, with parametric dependence on the nuclear configuration.

σ: a) A symmetry representation that is symmetric about a symmetry axis, or more generically, a bond axis. b) An electron spin-coordinate. C) Signature of a critical point.

τ: the set of all spin and spatial coordinates.

τ': the set of all spin coordinate and the spatial coordinates of all electrons but one.

ω: Rank of a critical point.

Ω: a proper open system.

Ξ: an arbitrary open system.

$\psi(\mathbf{x}, \mathbf{X})$: a time-independent wavefunction.

$\Psi(\mathbf{x}, \mathbf{X}, t)$: a time-dependent wavefunction.

$\nabla^2\rho(r)$: the Laplacian of the electron density.

$\nabla = \left(\frac{\partial}{\partial x}, \frac{\partial}{\partial y}, \frac{\partial}{\partial z}\right)$, the gradient vector operator.

A2. Appendix 2: Derivations

A2.1. Derivations for Closed Systems

A2.1.a. The Hyperviral Theorem, for a closed system, stationary state.

$$\left\langle \psi \middle| \left[\hat{H},\hat{A}\right] \middle| \psi \right\rangle \equiv \left\langle \psi \middle| \hat{H}\hat{A} \middle| \psi \right\rangle - \left\langle \psi \middle| \hat{A}\hat{H} \middle| \psi \right\rangle = \left\langle \hat{H}\psi \middle| \hat{A} \middle| \psi \right\rangle - \left\langle \psi \middle| \hat{A} \middle| \hat{H}\psi \right\rangle$$

$$= \left\langle E\psi \middle| \hat{A} \middle| \psi \right\rangle - \left\langle \psi \middle| \hat{A} \middle| E\psi \right\rangle = E\left\langle \psi \middle| \hat{A} \middle| \psi \right\rangle - E\left\langle \psi \middle| \hat{A} \middle| \psi \right\rangle = 0$$

And we have shown that $\left\langle \psi \middle| \left[\hat{H},\hat{A}\right] \middle| \psi \right\rangle = 0$ for a Hermitian operator.

A2.1.b. Time dependence of observables

Using the time-dependent Schrödinger equation we can write an expression for the time dependence of the observables for the total system.

$$\frac{d\langle A\rangle}{dt} = \frac{d\left\langle \Psi \middle| \hat{A} \middle| \Psi \right\rangle}{dt} = \int\left\{\left(\frac{\partial \Psi^*}{\partial t}\right)\hat{A}\Psi + \Psi^*\hat{A}\left(\frac{\partial \Psi}{\partial t}\right) + \Psi^*\left(\frac{\partial \hat{A}}{\partial t}\right)\Psi\right\}d\tau$$

$$= \int\left\{\left(\frac{\hat{H}\Psi^*}{-i\hbar}\right)\hat{A}\Psi + \Psi^*\hat{A}\left(\frac{\hat{H}\Psi}{i\hbar}\right) + \Psi^*\left(\frac{\partial \hat{A}}{\partial t}\right)\Psi\right\}d\tau$$

$$= \frac{1}{-i\hbar}\int\left\{\hat{H}\Psi^*\hat{A}\Psi - \Psi^*\hat{A}\hat{H}\Psi\right\}d\tau + \int\Psi^*\left(\frac{\partial \hat{A}}{\partial t}\right)\Psi d\tau$$

$$= \frac{i}{\hbar}\int\left\{\Psi^*\hat{H}\hat{A}\Psi - \Psi^*\hat{A}\hat{H}\Psi\right\}d\tau + \int\Psi^*\left(\frac{\partial \hat{A}}{\partial t}\right)\Psi d\tau$$

$$\frac{d\langle A\rangle}{dt} = \frac{i}{\hbar}\left\langle \Psi \middle| \left[\hat{H},\hat{A}\right] \middle| \Psi \right\rangle + \left\langle \frac{\partial \hat{A}}{\partial t} \right\rangle$$

A2.2. Derivations for Open Systems

A2.2.a. Non-Hermitian Operators in subspace integration

An operator is Hermitian if $\left(\hat{A}^*\right)^T = \hat{A}$. We define a property of the total system:

$$\langle A\rangle = \left\langle \Psi\middle|\hat{A}\middle|\Psi\right\rangle = \left\langle \Psi^*\left(\hat{A}\Psi\right)\right\rangle = \left\langle\left(\hat{A}\Psi\right)^*\Psi\right\rangle$$

The Hermitian quality may not persist for an open system. To ensure that the calculated property is real we add the complex conjugate and divide by two.

$$\langle A\rangle_\Xi = \frac{\left\langle \Psi^*\left(\hat{A}\Psi\right)\right\rangle_\Xi + \left\langle\left(\hat{A}\Psi\right)^*\Psi\right\rangle_\Xi}{2} = \frac{1}{2}\left\langle\Psi\left(\hat{A}\Psi\right)\right\rangle_\Xi + cc$$

A2.2.b. The Hyperviral Theorem, for an open system, stationary state.

$$\begin{aligned}\left\langle\psi\middle|\left[\hat{H},\hat{A}\right]\psi\right\rangle_\Xi &\equiv \left\langle\psi\middle|\hat{H}\hat{A}\middle|\psi\right\rangle_\Xi - \left\langle\psi\middle|\hat{A}\hat{H}\middle|\psi\right\rangle_\Xi \\ &= \left\langle\psi\middle|\hat{H}\hat{A}\middle|\psi\right\rangle_\Xi - E\left\langle\psi\middle|\hat{A}\middle|\psi\right\rangle_\Xi = \left\langle\psi\middle|\hat{H}\hat{A}\middle|\psi\right\rangle_\Xi - \left\langle\hat{H}\psi\middle|\hat{A}\middle|\psi\right\rangle_\Xi\end{aligned}$$

$$\hat{H} = \sum_i \frac{-\hbar^2}{2m}\nabla_i^2 + \hat{V}$$

The potential energy operator is a simple multiplicative operator (no derivatives). Therefore, it commutes with the other operators and those terms cancel. The following derivation is for a one-electron kinetic energy operator. For a many electron system, we can simply insert $N\int d\tau'$ into each integral below.

$$\left\langle\psi\left|\left[\hat{H},\hat{A}\right]\right|\psi\right\rangle_{\Xi}=\frac{-\hbar^{2}}{2m}\int_{\Xi}d\tau\left\{\psi^{*}\nabla^{2}\left(\hat{A}\psi\right)-\nabla^{2}\psi^{*}\hat{A}\psi\right\}=\frac{-\hbar^{2}}{2m}\int_{\Xi}d\tau\nabla\cdot\left[\psi^{*}\nabla\left(\hat{A}\psi\right)-\nabla\psi^{*}\hat{A}\psi\right]$$

$$=\frac{-\hbar^{2}}{2m}\oint dS(\Xi,\mathbf{r})\left[\psi^{*}\nabla\left(\hat{A}\psi\right)-\nabla\psi^{*}\hat{A}\psi\right]\cdot\mathbf{n}(\mathbf{r})=-i\hbar\oint dS(\Xi,\mathbf{r})\mathbf{j}_{A}(\mathbf{r})\cdot\mathbf{n}(\mathbf{r})$$

$$\mathbf{j}_{A}(\mathbf{r})=\frac{\hbar}{2mi}\left\{\nabla\psi^{*}\hat{A}\psi-\psi^{*}\nabla\left(\hat{A}\psi\right)\right\}$$

We ensure the expression is real, as described above.

$$\frac{1}{2}\left(\frac{i}{\hbar}\left\langle\psi\left|\left[\hat{H},\hat{A}\right]\right|\psi\right\rangle_{\Xi}+cc\right)=\frac{1}{2}\left(\oint dS(\Xi,\mathbf{r})\mathbf{j}_{A}(\mathbf{r})\cdot\mathbf{n}(\mathbf{r})+cc\right)$$

A2.2.c. Time-dependence in an open system

We must include the complex conjugate, to ensure that the property is real. We also include the time-dependence of the surface. For the one electron case we can write:

$$\frac{d\langle A\rangle_{\Omega}}{dt}=\frac{1}{2}\frac{d\left\langle\Psi\left|\hat{A}\right|\Psi\right\rangle_{\Omega}}{dt}+cc$$

$$=\frac{1}{2}\int_{\Omega}\left\{\left(\frac{\partial\Psi^{*}}{\partial t}\right)\hat{A}\Psi+\Psi^{*}\hat{A}\left(\frac{\partial\Psi}{\partial t}\right)+\Psi^{*}\left(\frac{\partial\hat{A}}{\partial t}\right)\Psi\right\}d\tau+cc+\frac{1}{2}\oint dS(\Omega)\left(\frac{\partial S}{\partial t}\right)\Psi^{*}\hat{A}\Psi+cc$$

We may substitute the time-dependent Schrödinger equation into the first integral above.

$$\int_{\Omega}\left\{\left(\frac{\hat{H}\Psi^{*}}{-i\hbar}\right)\hat{A}\Psi+\Psi^{*}\hat{A}\left(\frac{\hat{H}\Psi}{i\hbar}\right)+\Psi^{*}\left(\frac{\partial\hat{A}}{\partial t}\right)\Psi\right\}d\tau$$

$$=\frac{1}{-i\hbar}\int_{\Omega}\left\{\hat{H}\Psi^{*}\hat{A}\Psi-\Psi^{*}\hat{A}\hat{H}\Psi\right\}d\tau+\int_{\Omega}\Psi^{*}\left(\frac{\partial\hat{A}}{\partial t}\right)\Psi d\tau$$

For a stationary state, where $\hat{A}$ is also a time-independent operator, all the terms vanish.

$$\frac{1}{-i\hbar}\int_{\Omega}\left\{\hat{H}\psi^{*}\hat{A}\psi-\psi^{*}\hat{A}\hat{H}\psi\right\}d\tau=\frac{i}{\hbar}\int_{\Omega}\left\{E\psi^{*}\hat{A}\psi-\psi^{*}\hat{A}E\psi\right\}d\tau=0$$

For a time-dependent state, let us assume for the moment that the operator has no explicit time-dependence. Since the Hamiltonian is no longer Hermitian, we make a substitution into the volume integral.

$$\frac{i}{\hbar}\int_{\Omega}\left\{\hat{H}\Psi^{*}\hat{A}\Psi-\Psi^{*}\hat{A}\hat{H}\Psi\right\}d\tau$$

$$=\frac{i}{\hbar}\int_{\Omega}\left\{\hat{H}\Psi^{*}\hat{A}\Psi-\Psi^{*}\hat{H}\hat{A}\Psi+\Psi^{*}\hat{H}\hat{A}\Psi-\Psi^{*}\hat{A}\hat{H}\Psi\right\}d\tau$$

$$=\frac{i}{\hbar}\int_{\Omega}\left\{\hat{H}\Psi^{*}\hat{A}\Psi-\Psi^{*}\hat{H}\hat{A}\Psi\right\}d\tau+\frac{i}{\hbar}\left\langle\Psi^{*}\hat{H}\hat{A}\Psi-\Psi^{*}\hat{A}\hat{H}\Psi\right\rangle_{\Omega}$$

As in the total system above, the terms involving the potential energy operator cancel.

$$=\frac{i}{\hbar}\int_{\Omega}\frac{-\hbar^{2}}{2m}\left\{\nabla^{2}\Psi^{*}\hat{A}\Psi-\Psi^{*}\nabla^{2}\hat{A}\Psi\right\}d\tau+\frac{i}{\hbar}\left\langle\Psi^{*}\left[\hat{H},\hat{A}\right]\Psi\right\rangle_{\Omega}$$

We have seen the first of these integrals in the open-system hyperviral theorem above.

$$\int_{\Omega}\frac{-\hbar^{2}}{2m}\left\{\nabla^{2}\Psi^{*}\hat{A}\Psi-\Psi^{*}\nabla^{2}\hat{A}\Psi\right\}d\tau=\frac{\hbar^{2}}{2m}\int_{\Omega}d\tau\nabla\cdot\left[\Psi^{*}\nabla\left(\hat{A}\Psi\right)-\nabla\Psi^{*}\hat{A}\Psi\right]$$

$$=\frac{\hbar^{2}}{2m}\oint dS(\Omega,\mathbf{r})\left[\Psi^{*}\nabla\left(\hat{A}\Psi\right)-\nabla\Psi^{*}\hat{A}\Psi\right]\cdot\mathbf{n}(\mathbf{r})=i\hbar\oint dS(\Omega,\mathbf{r})\mathbf{j}_{A}(\mathbf{r})\cdot\mathbf{n}(\mathbf{r})$$

Filling all of this in to the original expression:

$$\begin{aligned}
\frac{d\langle A\rangle_\Omega}{dt} &= \frac{1}{2}\frac{d\left\langle \Psi\middle|\hat{A}\middle|\Psi\right\rangle_\Omega}{dt} + cc \\
&= \frac{1}{2}\int_\Omega \left\{\left(\frac{\partial \Psi^*}{\partial t}\right)\hat{A}\Psi + \Psi^*\hat{A}\left(\frac{\partial \Psi}{\partial t}\right) + \Psi^*\left(\frac{\partial \hat{A}}{\partial t}\right)\Psi\right\}d\tau + cc + \frac{1}{2}\oint dS(\Omega)\left(\frac{\partial S}{\partial t}\right)\Psi^*\hat{A}\Psi + cc \\
&= \frac{1}{2}\left\{\frac{i}{\hbar}\int_\Omega \frac{\hbar^2}{2m}\left\{\Psi^*\nabla^2\hat{A}\Psi - \nabla^2\Psi^*\hat{A}\Psi\right\}d\tau + \frac{i}{\hbar}\left\langle \Psi^*\left[\hat{H},\hat{A}\right]\Psi\right\rangle_\Omega\right\} + cc \\
&\quad + \frac{1}{2}\int_\Omega \Psi^*\left(\frac{\partial \hat{A}}{\partial t}\right)\Psi d\tau + cc + \frac{1}{2}\oint dS(\Omega)\left(\frac{\partial S}{\partial t}\right)\Psi^*\hat{A}\Psi + cc \\
&= \frac{1}{2}\left\{\frac{i}{\hbar}i\hbar\oint dS(\Omega,\mathbf{r})\mathbf{j}_A(\mathbf{r})\cdot\mathbf{n}(\mathbf{r}) + \frac{i}{\hbar}\left\langle \Psi^*\left[\hat{H},\hat{A}\right]\Psi\right\rangle_\Omega + \left\langle\frac{\partial \hat{A}}{\partial t}\right\rangle_\Omega + \oint dS(\Omega)\left(\frac{\partial S}{\partial t}\right)\Psi^*\hat{A}\Psi\right\} + cc
\end{aligned}$$

$$\frac{d\langle A\rangle_\Omega}{dt} = \frac{1}{2}\left\{-\oint dS(\Omega,\mathbf{r})\mathbf{j}_A(\mathbf{r})\cdot\mathbf{n}(\mathbf{r}) + \frac{i}{\hbar}\left\langle \Psi^*\left[\hat{H},\hat{A}\right]\Psi\right\rangle_\Omega + \left\langle\frac{\partial \hat{A}}{\partial t}\right\rangle_\Omega + \oint dS(\Omega)\left(\frac{\partial S}{\partial t}\right)\Psi^*\hat{A}\Psi\right\} + cc$$

This is easily generalized to the many-electron case. The mathematical expressions in the above two sections are true for an arbitrary open system, but there is no guarantee that they are physically meaningful. To ensure a physical interpretation we must undertake a variational treatment.

A2.3. The calculus of variations

In variational calculus we want to find a path, $y(x)$, such that the integral J is extremized, given the known function $f(y, y_x, x)$, and known end points (x_1, y_1) and (x_2, y_2).

$$J = \int_{x_1}^{x_2} f(y, y_x, x)dx$$

We can describe any arbitrary path, $y(x, \alpha)$, in terms of the extremum path, $y(x,0)$, using some differentiable path, $\eta(x)$, and a scaling factor, α.

$$y(x,\alpha) = y(x,0) + \alpha\eta(x)$$
$$y_x(x,\alpha) \equiv \frac{\partial y(x,\alpha)}{\partial x} = y_x(x,0) + \alpha\eta_x(x)$$

$$\delta y \equiv y(x,\alpha) - y(x,0) = \alpha\eta(x)$$

We require that all paths have the correct end points: $\eta(x_1) = \eta(x_2) = 0$

For any path, the integral is: $J(\alpha) = \int_{x_1}^{x_2} f(y(x,\alpha), y_x(x,\alpha), x)dx$.

$$\frac{\partial J(\alpha)}{\partial \alpha} = \int_{x_1}^{x_2} \left[\frac{\partial f}{\partial y}\frac{\partial y}{\partial \alpha} + \frac{\partial f}{\partial y_x}\frac{\partial y_x}{\partial \alpha}\right]dx = \int_{x_1}^{x_2} \left[\frac{\partial f}{\partial y}\eta(x) + \frac{\partial f}{\partial y_x}\eta_x(x)\right]dx$$

Integration by parts yields:

$$\frac{\partial J(\alpha)}{\partial \alpha} = \int_{x_1}^{x_2} \left[\frac{\partial f}{\partial y}\eta(x) - \eta(x)\frac{d}{dx}\frac{\partial f}{\partial y_x}\right]dx + \eta(x)\frac{\partial f}{\partial y_x}\bigg|_{x_1}^{x_2} = \int_{x_1}^{x_2} \eta(x)\left[\frac{\partial f}{\partial y} - \frac{d}{dx}\frac{\partial f}{\partial y_x}\right]dx$$

The integral is extremized, $\frac{\partial J(\alpha)}{\partial \alpha} = 0$ for arbitrary $\eta(x)$ only if the bracketed factor in the integrand vanishes.

$$\left[\frac{\partial f}{\partial y}-\frac{d}{dx}\frac{\partial f}{\partial y_x}\right]=0$$

We apply the boundary conditions $y(x_1)=y_1$ and $y(x_2)=y_2$ and solve this resulting *Euler* equation. An example of this approach is the Schrödinger equation. Schrödinger's energy functional is extremized, subject to the normalization constraint.

$$\mathcal{G}[\psi]=\int_{-\infty}^{+\infty}\left\{\frac{\hbar^2}{2m}\nabla\psi^*\cdot\nabla\psi+\left(\hat{V}+\lambda\right)\psi^*\psi\right\}d\tau$$

The Euler equation is $\hat{H}\psi=E\psi$, where the Lagrangian multiplier, $-\lambda$, is identified with the energy, E.

A2.4. The variational definition of a subsystem

Schrödinger's variational approach can be generalized to an open system. This procedure leads to an open-system (stationary-state) analogue of the hypervirial theorem.

$$\delta\mathcal{G}[\psi,\Omega]=\frac{-\varepsilon}{2}\left\{\frac{i}{\hbar}\left\langle\hat{H},\hat{G}\right\rangle_\Omega+cc\right\}$$

The variation in the energy functional is caused by the operation of an infinitesimal operator, $\varepsilon\hat{G}/i\hbar$, on the wavefunction. The variational derivation of this expression only holds for proper open systems, *i.e.* for systems bounded by a surface of zero-flux. Only for proper open systems is the commutator of the operator $\hat{G}$ with the Hamiltonian physically meaningful. The commutator's relationship with the property flux through the surface can then lead to important atomic theorems describing the mechanics of an open system.

$$\frac{1}{2}\left(\frac{i}{\hbar}\left\langle\psi\left|\left[\hat{H},\hat{G}\right]\right|\psi\right\rangle_{\Omega}+cc\right)=\frac{1}{2}\left(\oint dS(\Omega,\mathbf{r})\mathbf{j}_{G}(\mathbf{r})\cdot\mathbf{n}(\mathbf{r})+cc\right)$$

The variational derivation of the hypervirial theorem follows for a stationary-state many-electron system. We start with Schrödinger's energy functional.

$$\mathcal{G}[\psi]=\int\left\{\frac{\hbar^{2}}{2m}\sum_{i}\nabla_{i}\psi^{*}\cdot\nabla_{i}\psi+\left(\hat{V}-E\right)\psi^{*}\psi\right\}d\tau=\int f(\psi,\nabla\psi)d\tau$$

We consider the variation in this function, due to a variation in the wavefunction, over an arbitrary open system, Ξ. This includes a variation in the surface, again through the variation in the wavefunction. Recall that $\int d\tau'$ indicates summation over all spins and integration over all spatial coordinates, except those of electron **1**. We will also use the notation $\int d\tau_{i}''$ to indicate summation over all spins and integration over all spatial coordinates, except those of electrons **1** and *i*.

$$\mathcal{G}[\psi,\Xi]=\int_{\Xi}d\tau_{1}\int d\tau'\left\{\frac{\hbar^{2}}{2m}\sum_{i}\nabla_{i}\psi^{*}\cdot\nabla_{i}\psi+\left(\hat{V}-E\right)\psi^{*}\psi\right\}=\int_{\Xi}d\tau_{1}\int d\tau' f(\psi,\nabla\psi)$$

$$\delta\mathcal{G}[\psi,\Xi]=\int_{\Xi}d\tau_{1}\int d\tau'\left\{\frac{\partial f}{\partial\psi}\delta\psi+\sum_{i}\frac{\partial f}{\partial\nabla_{i}\psi}\delta\nabla_{i}\psi\right\}+\oint_{\Xi}dS(\Xi,\mathbf{r}_{1})\int d\tau' f(\psi,\nabla\psi)\delta S(\Xi,\mathbf{r}_{1})+cc$$

We rid this expression of the terms involving $\delta\nabla_{i}\psi$ by integration by parts, followed by Gauss's theorem.

$$\int_{\Xi} d\tau_1 \int d\tau' \frac{\partial f}{\partial \nabla_i \psi} \delta \nabla_i \psi = \frac{\hbar^2}{2m} \int_{\Xi} d\tau_1 \int d\tau' \nabla_i \psi^* \cdot \delta \nabla_i \psi$$

$$= \frac{\hbar^2}{2m} \int_{\Xi} d\tau_1 \int d\tau' \left\{ \nabla_i \cdot \left(\nabla_i \psi^* \delta \psi \right) - \nabla_i^2 \psi^* \cdot \delta \psi \right\}$$

$$= \frac{\hbar^2}{2m} \int_{\Xi} d\tau_1 \int d\tau_i'' \left\{ \oint dS(\mathbf{r}_i) \left(\nabla_i \psi^* \cdot \mathbf{n}(\mathbf{r}_i) \delta \psi \right) \right\} - \frac{\hbar^2}{2m} \int_{\Xi} d\tau_1 \int d\tau' \left\{ \nabla_i^2 \psi^* \cdot \delta \psi \right\}$$

The surface integral vanishes for all electrons, $i \neq 1$, since the bounding surface is at infinity. For electron **1** the surface term does not vanish.

$$\int_{\Xi} d\tau_1 \int d\tau' \frac{\partial f}{\partial \nabla_1 \psi} \delta \nabla_1 \psi = \frac{\hbar^2}{2m} \int_{\Xi} d\tau_1 \int d\tau' \nabla_1 \psi^* \cdot \delta \nabla_1 \psi$$

$$= \frac{\hbar^2}{2m} \int_{\Xi} d\tau_1 \int d\tau' \left\{ \nabla_1 \cdot \left(\nabla_1 \psi^* \delta \psi \right) - \nabla_1^2 \psi^* \cdot \delta \psi \right\}$$

$$= \frac{\hbar^2}{2m} \oint dS(\Xi, \mathbf{r}_1) \int d\tau \nabla_1 \psi^* \cdot \mathbf{n}(\mathbf{r}_1) \delta \psi - \frac{\hbar^2}{2m} \int_{\Xi} d\tau_1 \int d\tau' \left\{ \nabla_1^2 \psi^* \cdot \delta \psi \right\}$$

We now return to the overall variation in the energy functional.

$$\delta G[\psi, \Xi] = \int_{\Xi} d\tau_1 \int d\tau' \left\{ \frac{\partial f}{\partial \psi} \delta \psi + \sum_i \frac{\partial f}{\partial \nabla_i \psi} \delta \nabla_i \psi \right\} + \oint_{\Xi} dS(\Xi, r_1) \int d\tau' f(\psi, \nabla \psi) \delta S(\Xi, r_1) + cc$$

$$= \int_{\Xi} d\tau_1 \int d\tau' \left\{ \hat{V} - E \right\} \psi^* \delta \psi - \sum_i \frac{\hbar^2}{2m} \int_{\Xi} d\tau_1 \int d\tau' \left\{ \nabla_i^2 \psi^* \cdot \delta \psi \right\}$$

$$+ \frac{\hbar^2}{2m} \oint dS(\Xi, \mathbf{r}_1) \int d\tau \nabla_1 \psi^* \cdot \mathbf{n}(\mathbf{r}_1) \delta \psi + \oint_{\Xi} dS(\Xi, \mathbf{r}_1) \int d\tau' f(\psi, \nabla \psi) \delta S(\Xi, \mathbf{r}_1) + cc$$

$$= \int_{\Xi} d\tau_1 \int d\tau' \left(\hat{H} - E \right) \psi^* \delta \psi + \oint dS(\Xi, \mathbf{r}_1) \int d\tau' \left\{ \frac{\hbar^2}{2m} \nabla_1 \psi^* \cdot \mathbf{n}(\mathbf{r}_1) \delta \psi + f(\psi, \nabla \psi) \delta S(\Xi, \mathbf{r}_1) \right\} + cc$$

We can drop the subscript on the operators and spatial coordinates. For the total system, all the surface terms vanish and we recover $\hat{H}\psi = E\psi$ and $\hat{H}\psi^* = E\psi^*$. Since this applies throughout the system, we find that the first integral above vanishes.

$$\delta\mathcal{G}[\psi,\Xi]=\oint dS(\Xi,\mathbf{r})\int d\tau'\left\{\frac{\hbar^2}{2m}\nabla\psi^*\cdot\mathbf{n}(\mathbf{r})\delta\psi+f(\psi,\nabla\psi)\delta S(\Xi,\mathbf{r})\right\}+cc$$

We must now consider the term involving the variation in the surface. When we include the complex conjugate we have two such terms. Considering the difference between the two forms of the kinetic energy density, K(r) – G(r) = L(r), we rewrite this as follows.

$$f(\psi,\nabla\psi)+cc=\left\{\psi^*\hat{H}\psi+\left(\hat{H}\psi\right)^*\psi\right\}-2E\psi^*\psi+2\frac{\hbar^2}{4m}\sum_i\nabla_i^2\left(\psi^*\psi\right)=\frac{\hbar^2}{2m}\sum_i\nabla_i^2\left(\psi^*\psi\right)$$

Once again, we have applied the time-independent Schrödinger equation.

$$\int d\tau' f(\psi,\nabla\psi)+cc=\int d\tau'\frac{\hbar^2}{2m}\sum_i\nabla_i^2\left(\psi^*\psi\right)$$

As seen for similar terms above, the volume integral becomes a vanishing surface integral for all $i\neq 1$. We define a charge density per electron, $\rho'(\mathbf{r})=\frac{\rho(\mathbf{r})}{N}=\int d\tau'\psi^*\psi$.

$$\int d\tau' f(\psi,\nabla\psi)+cc=\int d\tau'\frac{\hbar^2}{2m}\nabla_1^2\left(\psi^*\psi\right)=\frac{\hbar^2}{2m}\nabla_1^2\int d\tau'\left(\psi^*\psi\right)=\frac{\hbar^2}{2m}\nabla^2\rho'(\mathbf{r})$$

$$\oint dS(\Xi,\mathbf{r})\delta S(\Xi,\mathbf{r})\int d\tau' f(\psi,\nabla\psi)+cc=\frac{1}{2}\left\{\frac{\hbar^2}{2m}\oint dS(\Xi,\mathbf{r})\nabla^2\rho'(\mathbf{r})\delta S(\Xi,\mathbf{r})+cc\right\}$$

$$\delta\mathcal{G}[\psi,\Xi]=\oint dS(\Xi,\mathbf{r})\left\{\frac{\hbar^2}{2m}\int d\tau\nabla\psi^*\cdot\mathbf{n}(\mathbf{r})\delta\psi+\frac{1}{2}\nabla^2\rho'(\mathbf{r})\delta S(\Xi,\mathbf{r})\right\}+cc$$

We now consider the bounding surface more carefully. We apply some constraints in order to transform the expression for the variation in the energy functional into a physically meaningful form. All the variations above arise from a variation in the wavefunction, $\delta\psi(\mathbf{r})=\phi(\mathbf{r})-\psi(\mathbf{r})$. The trial function, $\phi(\mathbf{r})$, defines a trial density, $\rho'_\phi(\mathbf{r})=\int d\tau'\phi^*(x,\tau')\phi(x,\tau')$, and a region, $\Omega(\phi)$, bound by a zero-flux surface.

$$\nabla\rho'_\phi(\mathbf{r})\cdot\mathbf{n}(\mathbf{r})=0 \qquad \text{for all } \mathbf{r} \text{ in the surface } S(\Omega(\phi),\mathbf{r})$$

We require that as ϕ tends to ψ, the region $\Omega(\phi)$ is continuously deformable into the proper open system, $\Omega(\psi)$. This requires that, *at all stages* of the variation, the Laplacian of the trial density integrates to zero.

$$\int_{\Omega(\phi)}\nabla^2\rho'_\phi(\mathbf{r})d\tau=0$$

In order for this to be satisfied for all trial functions, $\phi(r)=\psi(\mathbf{r})+\delta\psi(\mathbf{r})$, we require the variation of the integral to vanish for the proper system.

$$\delta\int_\Omega\nabla^2\rho'(\mathbf{r})d\tau=0$$

$$\delta_\psi\int_\Omega\nabla^2\rho'(\mathbf{r})d\tau=\int_\Omega\delta_\psi\{\nabla^2\rho'(\mathbf{r})\}d\tau+\oint dS(\Omega,\mathbf{r})\delta_\psi S(\Omega,\mathbf{r})\nabla^2\rho'(\mathbf{r})=0$$

We rearrange to find an expression for the surface integral.

$$\begin{aligned}-\oint dS(\Omega,\mathbf{r})\delta_\psi S(\Omega,\mathbf{r})\nabla^2\rho'(\mathbf{r})&=\int_\Omega d\tau\delta_\psi\{\nabla^2\rho'(\mathbf{r})\}=\int_\Omega d\tau\delta_\psi\left\{\int d\tau\nabla^2(\psi^*\psi)\right\}\\&=\int_\Omega d\tau\delta_\psi\left\{\int d\tau\nabla\cdot[(\nabla\psi^*)\psi+\psi^*\nabla\psi]\right\}=\int_\Omega d\tau\int d\tau\nabla\cdot[(\nabla\psi^*)\delta\psi+\psi^*\delta\nabla\psi]\\&=\oint dS(\Omega,\mathbf{r})\int d\tau'[(\nabla\psi^*)\delta\psi+\psi^*\delta\nabla\psi]\cdot\mathbf{n}(\mathbf{r})\end{aligned}$$

The variation in the surface is effectively replaced by a variation in the Laplacian, when the conditions above are satisfied. This substitution is valid for *any* variation in the surface when the zero-flux condition is obeyed for all points on the surface.

$$\nabla\rho'(\mathbf{r})\cdot\mathbf{n}(\mathbf{r})=0 \quad \text{for all points on the surface.}$$

Thus if, and only if, the open system, Ξ, corresponds to a proper open system, Ω, bound by a surface of zero-flux, we can replace the surface term in the variation of the energy functional to get a physically meaningful expression:

$$\delta\mathcal{G}[\psi,\Omega]=\frac{\hbar^2}{2m}\oint dS(\Omega,\mathbf{r})\left\{\int d\tau'\nabla\psi^*\cdot\mathbf{n}(\mathbf{r})\delta\psi+\frac{1}{2}\delta S(\Omega,\mathbf{r})\nabla^2\rho'(\mathbf{r})\right\}+cc$$

$$=\frac{\hbar^2}{2m}\oint dS(\Omega,\mathbf{r})\int d\tau'\left\{(\nabla\psi^*)\delta\psi-\frac{1}{2}\left[(\nabla\psi^*)\delta\psi+\psi^*\delta\nabla\psi\right]\right\}\cdot\mathbf{n}(\mathbf{r})+cc$$

$$=\frac{\hbar^2}{2m}\oint dS(\Omega,\mathbf{r})\int d\tau'\left\{\frac{1}{2}(\nabla\psi^*)\delta\psi-\frac{1}{2}\psi^*\delta\nabla\psi\right\}\cdot\mathbf{n}(\mathbf{r})+cc$$

$$=\frac{\hbar^2}{4m}\oint dS(\Omega,\mathbf{r})\int d\tau'\{(\nabla\psi^*)\delta\psi-\psi^*\delta\nabla\psi\}\cdot\mathbf{n}(\mathbf{r})+cc$$

We define a single-particle vector current density, for a many-particle system.

$$\mathbf{j}(\mathbf{r})=\frac{\hbar}{2mi}\int d\tau'\{\psi^*\nabla\psi-(\nabla\psi^*)\psi\}$$

$$\delta_\psi\mathbf{j}(\mathbf{r})=\frac{\hbar}{2mi}\int d\tau'\{\psi^*\delta\nabla\psi-(\nabla\psi^*)\delta\psi\}=\frac{\hbar}{2mi}\int d\tau'\{\psi^*\nabla(\delta\psi)-(\nabla\psi^*)\delta\psi\}$$

$$\delta\mathcal{G}[\psi,\Omega]=-\frac{\hbar^2}{4m}\oint dS(\Omega,\mathbf{r})\int d\tau'\{\psi^*\delta\nabla\psi-(\nabla\psi^*)\delta\psi\}\cdot\mathbf{n}(\mathbf{r})+cc$$

$$=-\frac{i\hbar}{2}\oint dS(\Omega,\mathbf{r})\delta_\psi\mathbf{j}(\mathbf{r})\cdot\mathbf{n}(\mathbf{r})+cc$$

Finally, we write the variation in the wavefunction as a result of the action of an infinitesimal generator.

$$\delta\psi=\frac{\varepsilon}{i\hbar}\hat{G}\psi \qquad\qquad \delta\psi^*=-\frac{\varepsilon}{i\hbar}\hat{G}\psi^*$$

We recall the definition of a single-particle current density for the observable, G, now written for a many-particle system.

$$\mathbf{j}_G(\mathbf{r}) = \frac{\hbar}{2mi}\int d\tau' \left\{\psi^* \nabla\left(\hat{G}\psi\right) - \left(\nabla\psi^*\right)\left(\hat{G}\psi\right)\right\}$$

We may now identify the variation in the energy functional with the flux of the property G, though the bounding surface.

$$\begin{aligned}
&\delta G[\psi,\Omega] = -\frac{\hbar^2}{4m}\oint dS(\Omega,\mathbf{r})\int d\tau' \left\{\psi^* \nabla(\delta\psi) - \left(\nabla\psi^*\right)\delta\psi\right\}\cdot\mathbf{n}(\mathbf{r}) + cc \\
&= -\frac{\hbar^2}{4m}\oint dS(\Omega,\mathbf{r})\int d\tau' \left\{\psi^* \nabla\left(\frac{\varepsilon}{i\hbar}\hat{G}\psi\right) - \left(\nabla\psi^*\right)\left(\frac{\varepsilon}{i\hbar}\hat{G}\psi\right)\right\}\cdot\mathbf{n}(\mathbf{r}) + cc \\
&= -\frac{\hbar\varepsilon}{4mi}\oint dS(\Omega,\mathbf{r})\int d\tau' \left\{\psi^* \nabla\left(\hat{G}\psi\right) - \left(\nabla\psi^*\right)\left(\hat{G}\psi\right)\right\}\cdot\mathbf{n}(\mathbf{r}) + cc \\
&= -\frac{\varepsilon}{2}\oint dS(\Omega,\mathbf{r})\mathbf{j}_G(\mathbf{r})\cdot\mathbf{n}(\mathbf{r}) + cc
\end{aligned}$$

We are finally in a position to use the hypervirial theorem, derived for an arbitrary open system, with the assurance that the calculated properties are physically meaningful for a proper open system.

$$\left(\frac{i}{\hbar}\left\langle\Psi\middle|\left[\hat{H},\hat{G}\right]\middle|\Psi\right\rangle_\Omega + cc\right) = \left(\oint dS(\Omega,\mathbf{r})\mathbf{j}_G(\mathbf{r})\cdot\mathbf{n}(\mathbf{r}) + cc\right)$$

By choosing appropriate operators, G, we can derive a series of atomic theorems, such as the atomic force theorem, $\hat{G} = \mathbf{p}$ and the atomic virial theorem, $\hat{G} = \mathbf{r}\cdot\mathbf{p}$.

For the more general case of a time-dependent system, we extremize the action integral.

$$\mathcal{W}_{12}[\Psi] = \int_{t_1}^{t_2} \mathcal{L}[\Psi, t]dt = \int_{t_1}^{t_2} dt \int d\tau L[\Psi, \nabla\Psi, \dot{\Psi}, t]$$

$$L[\Psi, \nabla\Psi, \dot{\Psi}, t] = \frac{i\hbar}{2}\left(\Psi^*\dot{\Psi} - \dot{\Psi}^*\Psi\right) - \frac{\hbar^2}{2m}\sum_i \nabla_i \Psi^* \cdot \nabla_i \Psi - \hat{V}\Psi^*\Psi$$

$$\delta\mathcal{W}_{12}[\Psi] = \int_{t_1}^{t_2} dt \int d\tau \left\{\frac{\partial L}{\partial \Psi} - \nabla \cdot \frac{\partial L}{\partial \nabla\Psi} - \frac{d}{dt}\frac{\partial L}{\partial \dot{\Psi}}\right\}\delta\Psi + \int_{t_1}^{t_2} dt \oint dS \frac{\partial L}{\partial \nabla\Psi} \cdot \mathbf{n}\delta\Psi + \int d\tau \frac{\partial L}{\partial \dot{\Psi}}\delta\Psi\Big|_{t_1}^{t_2} + cc$$

For an open, time-dependent system:

$$\mathcal{W}_{12}[\Psi, \Omega] = \int_{t_1}^{t_2} \mathcal{L}[\Psi, \Omega, t]dt \qquad \mathcal{L}[\Psi, \Omega, t] = \int_{\Omega} d\mathbf{r} \int d\tau' L[\Psi, \nabla\Psi, \dot{\Psi}, t]$$

The hypervirial theorem then becomes:

$$\begin{aligned}
\frac{N}{\varepsilon}\delta\mathcal{W}_{12}[\Psi, \Omega] &= G(\Omega, t_2) - G(\Omega, t_1) \\
&\quad - \int_1^{t_2} dt \oint dS(\Omega, \mathbf{r})\left\{\frac{\partial S}{\partial t}\rho_G(\mathbf{r}, t) - \frac{1}{2}\left(\mathbf{J}_G(\mathbf{r}) \cdot \mathbf{n}(\mathbf{r}) + cc\right)\right\} \\
&= -\int_1^{t_2} dt \left\{\frac{1}{2}\frac{i}{\hbar}\left\langle \Psi \middle| \left[\hat{H}, \hat{G}\right] \Psi \right\rangle_{\Omega} + cc\right\}
\end{aligned}$$

A3. Appendix 3: Density Matrices and Population Analysis

A3.1. Density matrices and natural orbitals

Many expressions for atomic populations and bond orders are written in terms of the density matrix (Szabo and Ostlund, 1989, section 4.4; Springborg, 2000, chapter 14). For a Hartree-Fock wavefunction, $|\psi_0\rangle$, which is a single determinant of spatial molecular orbitals, $\Phi_i(r)$, the electron density of a closed shell molecule with N electrons can be expressed as:

$$\rho(r) = \sum_i n_i |\Phi_i(r)|^2 = 2\sum_i^{N/2} |\Phi_i(r)|^2$$

Equation A 3-1

Expanding the MO's in terms of basis functions, $\phi_\nu(\mathbf{r})$, we arrive at:

$$\begin{aligned}\rho(\mathbf{r}) &= 2\sum_i^{N/2} \Phi^*_i(\mathbf{r})\Phi_i(\mathbf{r}) = 2\sum_i^{N/2}\left(\sum_\nu C^*_{\nu i}\phi^*_\nu(\mathbf{r})\sum_\mu C_{\mu i}\phi_\mu(\mathbf{r})\right)\\ &= \sum_{\mu,\nu}\left[2\sum_i^{N/2} C_{\mu i}C^*_{\nu i}\right]\phi_\mu(\mathbf{r})\phi^*_\nu(\mathbf{r}) = \sum_{\mu,\nu} P_{\mu\nu}\phi_\mu(\mathbf{r})\phi^*_\nu(\mathbf{r})\end{aligned}$$

Equation A 3-2

The Hartree-Fock density matrix, **P**, consists of the components $P_{\mu\nu} = 2\sum_{i=1}^{N/2} C_{\mu i}C^*_{\nu i}$ where the C's are the coefficients of the basis functions in each doubly occupied MO. An important related matrix is the overlap matrix, **S**. The components of this matrix are $S_{\mu\nu} = \int d\mathbf{r}\,\phi_\mu(\mathbf{r})\phi^*_\nu(\mathbf{r})$. Written in terms of molecular orbitals, the overlap matrix is $S_{ij} = \int d\mathbf{r}\,\Phi_i(\mathbf{r})\Phi_j^*(\mathbf{r})$.

For multi-determinantal wavefunctions, we need to determine the fractional occupation numbers of each MO in order to determine the contribution of each basis function to the molecular properties. A more general way to write the reduced (one-electron) density function is $\rho(\mathbf{x}_1) = N\int d\mathbf{x}_2 \ldots d\mathbf{x}_N \psi(\mathbf{x}_{1,}\mathbf{x}_{2\ldots}\mathbf{x}_N)\psi^*(\mathbf{x}_{1,}\mathbf{x}_{2\ldots}\mathbf{x}_N)$ for any antisymmetric wavefunction, $\psi(\mathbf{x}_{1,}\mathbf{x}_{2\ldots}\mathbf{x}_N)$.

Similarly, the first-order reduced density *matrix* is defined as $\gamma_1(\mathbf{x}_1, \mathbf{x}_1') = N\int d\mathbf{x}_2 \ldots d\mathbf{x}_N \psi(\mathbf{x}_{1,}\mathbf{x}_{2\ldots}\mathbf{x}_N)\psi^*(\mathbf{x}_{1,}'\mathbf{x}_{2\ldots}\mathbf{x}_N)$. This can be expanded in terms of a set of molecular *spin* orbitals, $\{\chi_i\}$, as

$$\gamma_1(\mathbf{x}_1, \mathbf{x}_1') = \sum_{i,j} \chi_i(\mathbf{x}_1)\left[\int d\mathbf{x}_1 d\mathbf{x}_1' \chi_i^*(\mathbf{x}_1)\gamma(\mathbf{x}_1,, \mathbf{x}')\chi_j(\mathbf{x}_1')\right]\chi_j^*(\mathbf{x}_1') = \sum_{i,j} \chi_i(\mathbf{x}_1)\left[\gamma_{ij}\right]\chi_j^*(\mathbf{x}_1')$$

Equation A 3-3

If the wavefunction is the Hartree-Fock ground state and the molecular spin orbitals are orthonormal, then this reduces to

$$\gamma_1^{HF}(\mathbf{x}_1, \mathbf{x}_1') = \sum_{i,j} \chi_i(\mathbf{x}_1)\gamma_{ij}^{HF}\chi_j^*(\mathbf{x}_1') = \sum_i^{occ} \chi_i(\mathbf{x}_1)\chi_i^*(\mathbf{x}_1')$$

Equation A 3-4

The diagonal elements of this matrix, γ_{ii}^{HF}, are the occupation numbers of the spin orbitals, equalling zero or one.

In general the matrix γ_{ij} is not diagonal, but can be diagonalized by a unitary transformation (U) of the spin orbitals $\{\chi_i\}$ into the set of so-called natural orbitals (Lowdin, 1955), $\left\{\eta_k = \sum_i U_{ki}\chi_i\right\}$. These natural orbitals lead to the fastest convergence of a CI expansion. In this formalism, $\gamma_1(\mathbf{x}_1,\mathbf{x}_1') = \sum_k \lambda_k \eta_k(\mathbf{x}_1)\eta_k^*(\mathbf{x}_1')$ where the coefficients, λ_k are the diagonal elements of the diagonal matrix $\boldsymbol{\lambda} = \mathbf{U}^{+}\boldsymbol{\gamma}\mathbf{U}$. These coefficients are interpreted as the occupation numbers of the natural orbitals (Szabo and Ostland, 1989). With the natural orbitals expanded in a set of atomic functions, the contribution of each atom's functions to a given property can be calculated as shown in the next sections, with the SCF occupation numbers, n_i, replaced by λ_k.

We will later need the pair density, $\rho(\mathbf{r}_1,\mathbf{r}_2)$ which is related to the diagonal elements of the *second order* density matrix. In analogy with the first order density matrix, $\Gamma^{(1)} = \gamma_1(\mathbf{x}_1,\mathbf{x}_1') = N\int d\mathbf{x}_2 ... d\mathbf{x}_N \psi(\mathbf{x}_1,\mathbf{x}_2 ... \mathbf{x}_N)\psi^*(\mathbf{x}_1',\mathbf{x}_2 ... \mathbf{x}_N)$, we can write:

$$\Gamma^{(2)} = \gamma_2(\mathbf{x}_1,\mathbf{x}_1',\mathbf{x}_2,\mathbf{x}_2') = \int d\mathbf{x}_3 ... d\mathbf{x}_N \psi(\mathbf{x}_1,\mathbf{x}_2 ... \mathbf{x}_N)\psi^*(\mathbf{x}_1',\mathbf{x}_2' ... \mathbf{x}_N).$$

Equation A 3-5

The diagonal elements of this matrix give the probability of finding electron 1 at $\mathbf{r}_1$ and electron 2 at $\mathbf{r}_2$. In order to consider all possible pairs of indistinguishable electrons we multiply by $N(N-1)$ and divide by two to avoid double counting of pairs. This gives the *pair density*, which is required for calculating 2-electron properties, such as delocalization.

$$\rho(\mathbf{r}_1,\mathbf{r}_2) = \frac{N(N-1)}{2}\int d\sigma_1 d\sigma_2 d\mathbf{x}_3 ... d\mathbf{x}_N \psi(\mathbf{x}_1,\mathbf{x}_2 ... \mathbf{x}_N)\psi^*(\mathbf{x}_1,\mathbf{x}_2 ... \mathbf{x}_N)$$

Equation A 3-6

A3.2. Population Analysis

A3.2.a. Assigning electrons to atoms

Atomic Charge is a seemingly simple concept upon whose definition it has been surprisingly difficult to reach a consensus. Chemists can agree that the atomic charge is the nuclear charge minus the number of electrons associated with that nucleus (or atom). The problem is in agreeing upon which electrons (*i.e.* how many) are associated with each atom. The problem is evident even in the simplest approximations to atomic charge; the *formal charge* calculated from a Lewis structure assumes a non-polar bond while the *oxidation number* assumes a completely ionic bond. The 'truth' is usually somewhere in between. The Theory of Atoms in Molecules proposes one answer to this problem that is grounded in physics and derived using the calculus of variation. The partitioning of the electrons in real space was described in Chapter 2. A variety of other approaches will be described below.

Bond order is also defined differently within each particular model of electronic structure. As with many chemical concepts, it is most deeply rooted in the simple ideas of Lewis. When an experimentalist makes a new compound they draw a Lewis structure to summarize (and perhaps justify) the observed stability or reactivity and the spectroscopic data; such as X-ray structure, UV-visible, IR and Raman frequencies and NMR shifts and coupling constants. The (average) number of shared pairs in the Lewis structure is said to be the bond order, but this is usually only applied to 'covalent' interactions. In ionic interactions the charges are usually discussed rather than the bond order. When resonance averaging is invoked, the bond order and the formal charges are the weighted averages over the various resonance forms, but the weighting is often uncertain.

Bond order inferred from experimental bond length and strength data is often interpreted as covalent bond order, with the accompanying assumption that increased 'covalent character' means decreased 'ionic character'. However, this shortening and strengthening may be due either to increased sharing of electrons – more accumulation of electron density between the atoms – or increased charges – leading to increased electrostatic attraction – or both. The two effects may reinforce each other. The experimental data can be interpreted within any one of several models of chemical bonding.

Within the simplest molecular orbital models, bond order is equal to one half the sum of the occupation numbers of the bonding orbitals minus one half the sum of the occupation numbers of the antibonding orbitals. This is a useful definition only so long as the molecular orbitals are easily classified as bonding, non-bonding or antibonding with respect to the bond of interest. This is straightforward only in the case of homopolar diatomic molecules. In these cases the atomic charges are zero.

A3.2.b. Need for Advanced / Ab Initio Methods

The bond orders of polar bonds can be quite difficult to determine within either of the simple models (Lewis pairs or occupied molecular orbitals) described above. In the MO model most MOs are spread over the whole molecule and do not contribute a full electron pair to any one bond. In addition, for polar bonds it may not be clear whether the MO is non-bonding or (anti)bonding with respect to the bond of interest.

Many definitions of bond order have been proposed for both semi-empirical and *ab initio* wavefunctions. A number of definitions applying to single determinant and correlated wavefunctions were reviewed by Sannigrahi in 1992. Most of these definitions rely on the expression of the molecular orbitals (MO's) as linear combinations of atomic-orbital-like basis functions (LCAO). The total wavefunction is expressed as a Slater determinant of these MO's (Hartree-Fock, HF) or as a linear combination of determinants (Configuration Interaction, CI). Each MO is assigned an occupation number (an integer in HF or a fraction in CI) and all the properties of the system are written in terms of the basis functions. Each basis function is centred on a particular nucleus, and in this type of analysis all the electronic properties associated with a particular basis function are considered to 'belong' to the 'atom' on which it is centred.

A3.2.c. Hückel, Coulson and Wiberg

Within simple Hückel theory for planar hydrocarbons, the atomic p_z orbitals on the sp^2-hybridized carbons are assumed to be orthonormal. The π-like population on each atom, N^{π}_{A} and the π-like bond order, b^{π}_{AB}, are defined as:

$$N^{\pi}_{A} = P_{AA} = \sum_{i} n_i c^2_{iA} \qquad b^{\pi}_{AB} = P_{AB} = \sum_{i} n_i c_{iA} c^*_{iB}$$

Equation A 3-7

The occupation numbers, n_i are 2 for occupied MOs and 0 for unoccupied MOs. The populations and bond orders are components of the density matrix, **P**. This definition, originally proposed by Coulson (1939), marks the beginning of bond order definitions related to calculated wavefunctions. It applies only to orthonormal basis sets, with a single function centred on each atom. For several basis sets centred on each atom, one can sum the partial bond orders arising from each pair of atomic orbitals (Glendening and Weinhold, 1998), $b_{AB}^{(MO)} = \sum_{r}^{on\ A} \sum_{s}^{on\ B} P_{rs}$.

An alternative definition of bond order was proposed by Wiberg (1968) that avoids the possibility of a negative bond order, again assuming orthonormal basis sets: $b_{AB}^{(W)} = \sum_{r}^{on\ A} \sum_{s}^{on\ B} P_{rs}^2$. Many variations on Coulson's and Wiberg's definitions have been proposed for non-orthogonal basis sets, which incorporate the orbital overlap matrix, S, in some way. McWeeny (1951) has suggested the definition $B_{AB} = \left(\mathbf{S}^{1/2}\mathbf{P}\mathbf{S}^{1/2}\right)_{AB}$.

A3.2.d. Mulliken and Mayer

One approach that accounts for non-orthogonal basis sets is Mulliken analysis (Mulliken, 1955), which continues to be very popular despite its arbitrariness and basis set dependence (Springborg, 2000; Ostland and Szabo, 1989). For a single determinant of molecular orbitals, with occupation numbers n_i, expanded in a set of atom-centred functions ($\Phi_i = \sum_{\nu} c_{\nu i}\phi_{\nu}$), the gross Mulliken population on atom A is:

$$N_A = \sum_i n_i \left(\sum_{\mu \in A} \sum_{\nu} c_{\mu i} c_{\nu i} S_{\nu\mu} \right) = \sum_{\mu \in A} \sum_{\nu} P_{u\nu} S_{\nu\mu} = \sum_{\mu \in A} (\mathbf{PS})_{\mu\mu} \, .$$

Equation A 3-8

The sum over μ includes only those basis functions centred on atom A, while the sum over ν includes all basis functions. This can be separated into a population arising purely from orbitals centred on A ($\mu,\nu \in$ A) and a population arising from two orbitals on different atoms – a shared population. The overlap population, often interpreted as a bond order, is the sum over terms arising from basis functions on two separate atomic centers, A and B;

$$N_{AB} = 2\sum_i n_i \left(\sum_{\mu \in A} \sum_{\nu \in B} c_{\mu i} c_{\nu i} S_{\mu\nu} \right) = 2\sum_{\mu \in A} \sum_{\nu \in B} P_{\mu\nu} S_{\nu\mu} \, .$$

Equation A 3-9

Mayer (1983, 1985*a/b*, 1986*a/b*) has suggested keeping Mulliken's atomic populations, but replacing the overlap populations, which relate to electrostatic factors, with an alternative bond order index relating to the exchange effects from the bond. For single-determinant wavefunctions, the second order density matrix, Equation A 3-5, can be written as:

$$\begin{aligned} \gamma_2(\mathbf{x}_1, \mathbf{x}'_1; \mathbf{x}_2, \mathbf{x}'_2) &= \int d\mathbf{x}_3 \ldots d\mathbf{x}_N \psi(\mathbf{x}_1, \mathbf{x}_2 \ldots \mathbf{x}_N) \psi^*(\mathbf{x}'_1, \mathbf{x}'_2 \ldots \mathbf{x}_N) \\ &= \gamma_1(\mathbf{x}_1 : \mathbf{x}'_1) \gamma_1(\mathbf{x}_2 ; \mathbf{x}'_2) - \gamma_1(\mathbf{x}_2 ; \mathbf{x}'_1) \gamma_1(\mathbf{x}_1 ; \mathbf{x}'_2) \end{aligned}$$

Equation A 3-10

The second term is the exchange component. Integration of this term and expansion in the atomic orbital basis leads to:

$$\iint \gamma_1(2;1)\gamma_1(1;2)d\tau_1 d\tau_2 = \sum_{\mu,\nu} \left(\mathbf{P}^\alpha \mathbf{S}\right)_{\mu\nu}\left(\mathbf{P}^\alpha \mathbf{S}\right)_{\nu\mu} + \left(\mathbf{P}^\beta \mathbf{S}\right)_{\mu\nu}\left(\mathbf{P}^\beta \mathbf{S}\right)_{\nu\mu}$$

$$B_{AB} = 2\sum_{\mu\in A}\ \sum_{\nu\in B} \left(\mathbf{P}^\alpha \mathbf{S}\right)_{\mu\nu}\left(\mathbf{P}^\alpha \mathbf{S}\right)_{\nu\mu} + \left(\mathbf{P}^\beta \mathbf{S}\right)_{\mu\nu}\left(\mathbf{P}^\beta \mathbf{S}\right)_{\nu\mu}$$

Equation A 3-11

For closed shell systems Mayer's bond order index reduces to

$$B_{AB} = \sum_{\mu\in A}\sum_{\nu\in B} (\mathbf{PS})_{\mu\nu}(\mathbf{PS})_{\nu\mu}$$

Equation A 3-12

All the above methods define atomic properties by partitioning the Hilbert space. They depend on the assignment of particular basis functions to particular atom centres and are thus intrinsically basis set dependent. Angyan, Loss and Mayer (1994) later adapted Mayer's definition to real space partitioning, in place of Hilbert space partitioning, and that approach will be discussed below.

A3.2.e. Orbital Optimization: Löwdin Population Analysis

Löwdin's approach (Löwdin, 1950, 1970; Springborg, 2000) is the first to attempt an optimization of the orbitals to make the assignment of charge to atomic functions less arbitrary and less basis-set dependent. The population of each natural orbital is divided into one-atom and two-atom contributions. Symmetric transformation of the basis set (into the orthonormal set that most closely resembles the original atomic centred basis set) causes the two-atom contributions to disappear, leaving only atomic populations. This approach gives atomic charges, but not bond orders.

A3.2.f. Natural Population Analysis

In the related method, Natural Population Analysis (NPA), natural atomic orbitals (NAOs) are transformed into natural hybrid orbitals (NHOs) and then into natural bond orbitals (NBOs), which can in turn be analyzed as core, bonding or non-bonding. Note that while Löwdin transforms the basis set, in NPA it is formally the molecular orbitals that are transformed.

The NAO's are found by diagonalizing each block of atomic orbitals (basis functions) to produce 'molecular' orbitals centred on each nucleus and conserving the spherical symmetry of the atomic environment. These orbitals have non-integer occupancies in the molecular wavefunction. These pre-NAOs are then orthogonalized to remove interatomic overlap. The orthogonalization step is related to Löwdin's symmetrical transformation but is weighted to keep the occupied orbitals more closely related to the original atomic symmetry orbitals while allowing the virtual (Rydberg) orbitals to vary more from their original form (Reed *et al.*, 1985). The population on each atom is then found by integrating the NAO's for the given atom, A, over all space.

$$N_i^{(A)} = \left\langle \phi_i^{(A)} \middle| \Gamma \middle| \phi_i^{(A)} \right\rangle, \qquad N^{(A)} = \sum_i N_i^{(A)}, \qquad N = \sum_A N^{(A)}$$

Equation A 3-13

The NBO's are found (Reed, Weinhold *et al.*, 1980, 1983, 1985, 1988) by looping through the various blocks of the density matrix looking for components above a certain threshold. Within one-atom blocks core orbitals are taken out with occupancies above 1.999, then lone pairs are removed, with occupancies greater than 1.90. Two-centre blocks are then searched for bonding orbitals above some threshold occupancy. The orbitals found in this way are related to a 'natural Lewis structure' and the integer bond order is inferred from the best Lewis structure, or from a weighted average of integer values in the case of resonance. The resonance weighting is determined by natural resonance theory (NRT; Glendening and Weinhold, 1998).

A3.3. Real Space Population Analysis

The occupancy weighting of the NPA method makes it more stable to increasing the basis set size than Löwdin populations. Both 'optimal orthogonalization' approaches are less basis-set-dependent than Mulliken-type analyses (Levine, 2000, page 508). The basis set dependence can be further reduced by assigning properties to regions of real space rather than assigning orbitals to 'atoms'. In order to partition the bond orders in real space, as is done for atomic properties in the theory of atoms in molecules, we need a definition of bond order that defines an electron sharing (bonding) index as a function of real space. This function can then be integrated over the regions of interest.

A3.3.a. Cioslowski's Localized Orbitals

The population of an atom, defined as a proper open system, can be written in terms of natural spin orbitals: $\mathrm{N_A} = \sum_{k} \lambda_k^2 S_{kk}(A)^2$, we can further write the total number of electrons as $\mathrm{N} = \mathrm{N_a} + \mathrm{N_d} = \sum_{k} \lambda_k^2 \sum_{A} \sum_{B} S_{kk}(A) S_{kk}(B)$. The overlap integrals are now (natural) molecular orbital overlaps rather than atomic orbital overlaps and range over some open region of space, Ξ, instead of all space.

$$S_{ij}(\Xi) = \int_{\Xi} d\mathbf{r}\,\eta_i(\mathbf{r})\eta_j^*(\mathbf{r}).$$

The approach suggested by Cioslowski (1989, Cioslowski and Mixon, 1991) is to minimize the diatomic term, N_d (A≠B), *i.e.* to maximize the monatomic term, by unitary (or isopycnic) transformations of the orbitals. This method seems to be rather arbitrary in its definition, with no appeal to physical interpretation of the two components in terms of probabilities of any kind. This method still depends on an optimized orbital transformation to define the net atomic populations and the bond orders.

A3.3.b. Fulton Bond Index

Fulton (1993; Fulton and Mixon, 1993) has used the first-order density matrix, expressed in terms of natural orbitals, to define a *sharing index* between two atoms or any two regions of space, $I(A,B) = N\int_A d\mathbf{x}_1 \int_B d\mathbf{x}_1' i(\mathbf{x}_1;\mathbf{x}_1')$. He interprets the related function $i(\mathbf{x}_1;\mathbf{x}')d\mathbf{x}_1 d\mathbf{x}_1'$ as *"the probability that a single electron be found in the volumes* $d\mathbf{x}_1$ *and* $d\mathbf{x}_1'$ *about the points* $\mathbf{x}_1$ *and* $\mathbf{x}_1'$*."* Before defining this sharing index, Fulton imposed the constraint that $\int d\mathbf{x}_1' i(\mathbf{x}_1;\mathbf{x}_1') \propto \rho(\mathbf{x}_1)$, *i.e.* the single integral over all space is proportional to the probability of finding a single electron in the volume $d\mathbf{x}_1$ about the point $\mathbf{x}_1$. This constraint led Fulton to the definitions:

$$
\begin{aligned}
&i(\mathbf{x}_1;\mathbf{x}_1') \equiv \frac{1}{N}\gamma^{1/2}(\mathbf{x}_1;\mathbf{x}_1')\gamma_1^{1/2}(\mathbf{x}_1';\mathbf{x}_1) \\
&I(A,B) = N\int_A d\mathbf{x}_1 \int_B d\mathbf{x}_1' i(\mathbf{x}_1;\mathbf{x}_1') = \int_A d\mathbf{x}_1 \int_B d\mathbf{x}_1' \gamma_1^{1/2}(\mathbf{x}_1;\mathbf{x}_1')\gamma_1^{1/2}(\mathbf{x}_1';\mathbf{x}_1)
\end{aligned}
$$

Equation A 3-14

This final expression has the property that $\sum_B I(A,B) = N_A$, the population of region A, and $\sum_A \sum_B I(A,B) = N$, the total number of electrons in the system. Expanding out the expressions for the density matrix in terms of the natural spin orbitals, and performing the integrations gives:

$$
\begin{aligned}
I(A,B) &= \int_A d\mathbf{x}_1 \int_B d\mathbf{x}_1' I(\mathbf{x}_1;\mathbf{x}_1') = \int_A d\mathbf{x}_1 \int_B d\mathbf{x}_1' \gamma^{1/2}(\mathbf{x}_1;\mathbf{x}_1')\gamma^{1/2}(\mathbf{x}_1';\mathbf{x}_1) \\
&= \int_A d\mathbf{x}_1 \int_B d\mathbf{x}_1' \left(\sum_i \lambda_i \eta_i(\mathbf{x}_1)\eta_i^*(\mathbf{x}_1')\right)^{1/2} \left(\sum_j \lambda_j \eta_j(\mathbf{x}_1')\eta_j^*(\mathbf{x}_1)\right)^{1/2} \\
&= \int_A d\mathbf{x}_1 \int_B d\mathbf{x}_1' \left(\sum_i \lambda_i^{1/2} \eta_i(\mathbf{x}_1)\eta_i^*(\mathbf{x}_1')\right) \left(\sum_j \lambda_j^{1/2} \eta_j(\mathbf{x}_1')\eta_j^*(\mathbf{x}_1)\right) \\
&= \sum_i \lambda_i^{1/2} \sum_j \lambda_j^{1/2} \int_A d\mathbf{x}_1 \eta_i(\mathbf{x}_1)\eta_j^*(\mathbf{x}_1) \int_B d\mathbf{x}_1' \eta_i^*(\mathbf{x}_1')\eta_j(\mathbf{x}_1') \\
&= \sum_i \sum_j \lambda_i^{1/2}\lambda_j^{1/2} S_{ij}(A) S_{ij}(B)
\end{aligned}
$$

Equation A 3-15

For a Hartree-Fock wavefunction, all the occupation numbers are one or zero, and the sharing index reduces to $I(A,B) = \sum_i^{occ} \sum_j^{occ} S_{ij}(A)S_{ij}(B)$. Fulton further defined the *bond index*, $B(A,B) \equiv I(A,B) + I(B,A) = 2I(A,B)$. Note that this definition differs from Cioslowski's by the inclusion of off-diagonal terms, S_{ij}, and note the different treatment of the occupation numbers. While Cioslowski specifies that the regions should be proper open systems, Fulton suggests but does not require it.

A3.3.c. Mayer Bond Index

Ángyán, Loos and Mayer (1994) have extended Mayer's definition of bond order, which has a physical basis in the exchange energy, to an Atoms-in-Molecules partitioning scheme. For this analysis they replace Mulliken charges with Atoms-in-Molecules charges as determined by the integration of the electron density over proper open systems. The expression for the bond order now arises from an integration of the 'exchange part' $[\gamma_1(\mathbf{x}_2;\mathbf{x}'_1)\gamma_1(\mathbf{x}_1;\mathbf{x}'_2)]$ of the second order density matrix, Equation A 3-10. Expanding the density matrix in terms of molecular or natural orbitals one finds:

$$\gamma_1(2;1) = \sum_i \left\{ n_i^\alpha \alpha(s_1)\alpha^*(s_2) + n_i^\beta \beta(s_1)\beta^*(s_2) \right\} \phi_i(\mathbf{r}_1)\phi_i^*(\mathbf{r}_2)$$

Equation A 3-16

where n_i^σ is the occupation number of the spin orbital $\chi_i^\sigma(\mathbf{x}) = \phi_i(\mathbf{r})\sigma(s)$.

Inserting this expansion into the integral of the exchange density gives

$$\begin{aligned}\iint \gamma_1(2;1)\gamma_1(1;2)d\tau_1 d\tau_2 &= \sum_i \sum_j \left\{ n_i^\alpha n_j^\alpha + n_i^\beta n_j^\beta \right\} \langle \phi_i(\mathbf{r}_1) | \phi_j(\mathbf{r}_1) \rangle \langle \phi_j(\mathbf{r}_2) | \phi_i(\mathbf{r}_2) \rangle \\ &= \sum_A \sum_B \sum_i \sum_j \left\{ n_i^\alpha n_j^\alpha + n_i^\beta n_j^\beta \right\} \langle \phi_i | \phi_j \rangle_A \langle \phi_j | \phi_i \rangle_B \\ &= \sum_A \sum_B \sum_i \sum_j \left\{ n_i^\alpha n_j^\alpha + n_i^\beta n_j^\beta \right\} S_{ij}(A) S_{ij}(B)\end{aligned}$$

Equation A 3-17

$$B_{AB} = 2 \sum_i \sum_j \left\{ n_i^\alpha n_j^\alpha + n_i^\beta n_j^\beta \right\} S_{ij}(A) S_{ij}(B)$$

Equation A 3-18

For a single-determinant wavefunction, all the occupation numbers are one (or zero), and when the regions of space A and B are chosen to be proper open systems, the bond order expressions of Fulton and Mayer are identical. For Hartree-Fock wavefunctions these bond orders also reduce to the same expression as the delocalization index defined by Bader (Fradera *et al.*, 1999). Thus the Fulton, Mayer and Bader indices are all equivalent at that level of theory, although the philosophy and derivation of the three indices are quite different. For correlated wavefunctions the expressions are not equivalent. Important similarities in these approaches are that each defines atoms as regions of real space, rather than attempting to partition Hilbert space, each attempts some justification in terms of probabilities and/or exchange effects and each is invariant to unitary transformations of the orbitals.

It is of particular note that since these bonding indices all reduce to the same expression at the HF level of theory, the relationship between the delocalization index and charge transfer, derived in this thesis, also applies to the Fulton and Mayer indices.

Bibliography

References are listed alphabetically by first author and then by date.

Ángyán, I.; M. Loos and I. Mayer (1994). *J. Phys. Chem.* 98, 5244.

Cioslowski, J. (1989). *J. Am. Chem. Soc.* **111**, 8333.

Cioslowski, J. and S.T. Mixon (1991). *J. Am. Chem. Soc.* **113**, 4142.

Coulson, C.A. (1939). *Proc. Roy. Soc. (London)* **A169**, 413.

Foster, J.P. and F. Weinhold (1980). *J. Am. Chem. Soc.* **102**, 7211.

Fradera, X.; M.A. Austen and R.F.W. Bader (1999). *J. Phys. Chem. A* **103**, 304.

Fulton, R.L. (1993). *J. Phys. Chem.* **97**, 7516.

Fulton, R.L and S.T. Mixon (1993). *J. Phys. Chem.* **97**(29), 7530.

Glendening, E.D. and F. Weinhold (1998). *J. Comput. Chem.* **19**, 595 and 610.

Levine, I. (2000). Quantum Chemistry, 5th ed. Upper Saddle River, N.J.: Prentice Hall.

Löwdin, P.O. (1950). *J. Chem. Phys.* **18**, 365.

Löwdin, P.O. (1970). *Adv. Quantum Chem.* **5**, 185.

Mayer, I. (1983). *Chem. Phys. Lett.* **97**(3), 270.

Mayer, I. (1985*a*). *Chem. Phys. Lett.* **117**, 396. Mayer, I. (1985*b*). *Theoret. Chim. Acta* **67**, 315.

Mayer, I. (1986*a*). *Int. J. Quantum Chem.* **29**, 73. Mayer, I. (1986*b*). *Int. J. Quantum Chem.* **29**, 477.

McWeeny, R. (1951). *J. Chem. Phys.* **19**, 164.

Mulliken, R.S. (1955). *J. Chem. Phys.* **23**, 1841.

Reed, A.E. and F. Weinhold (1983). *J. Chem. Phys.* **78**, 4066.

Reed, A.E.; R.B. Weinstock and F. Weinhold (1985). *J. Chem. Phys.* **83**, 735.

Reed, A.E. and F. Weinhold (1985). *J. Chem. Phys.* **83**, 1736.

Reed, A.E.; L.A. Curtiss and F. Weinhold (1988). *Chem. Rev.* **88**, 899.

Sannigrahi, A.B. (1992). *Adv. Quantum Chem.* **23**, 301.

Springborg, M. (2000). Methods of Electronic Structure Calculations. West Sussex, England: Wiley.

Szabo, A. and N.S. Ostlund (1989). Modern Quantum Chemistry. New York: McGraw-Hill.

Wiberg, K.B. (1968). *Tetrahedron* **24**, 1083.

A4. Appendix 4: Plots of Calculated Data

In this appendix, graphs of calculated properties are presented for the phosphorus containing molecules. Each property is plotted as a function of the substituent group, X or XH = R. This allows a simple overview of the major trends in each series as the size and electronegativity of the substituent varies. For each property, all seven series are plotted on a single graph for easy comparisons between series. These graphs, Figures A4-1 through A4-8, are referred to throughout the results chapters (4 to 8). Each graph shows the properties for the lowest energy isomer (conformer) within the imposed symmetry. For example, only planar arrangements of X = CH_2 and SiH_2 are plotted for HPX, H_3PX and HPX_2, even when this is not the most stable form. Values of the plotted properties for all isomers studied can be found in the tables accompanying each chapter.

The systems whose properties are plotted are:

H_2PXH: H_2PF, H_2POH (anti-*eclipsed*), H_2PNH_2 (*gauche*), H_2PCH_3 (*eclipsed*), H_2PCl, H_2PSH (anti-*eclipsed*), H_2PPH_2 (*gauche*), H_2PSiH_3 (*eclipsed*), PH_3.

$HP(XH)_2$ (all C_s): HPF_2, $HP(OH)_2$ (‘*up*’), $HP(NH_2)_2$, $HP(CH_3)_2$, $HPCl_2$, $HP(SH)_2$ (‘*up*’), $HP(PH_2)_2$, $HP(SiH_3)_2$, PH_3.

$P(XH)_3$ (all C_3 or higher): PF_3, $P(OH)_3$ (‘*up*’), $P(NH_2)_3$ (*gauche*), $P(CH_3)_3$ (*eclipsed*), PCl_3, $P(SH)_3$ (‘*up*’), $P(PH_2)_3$ (*gauche*), $P(SiH_3)_3$ (*eclipsed*), PH_3.

HPX: HPO, HPNH (*trans*), $HPCH_2$ (*planar*), HPS, HPPH (*trans*), $HPSiH_2$ (*planar*).

H_3PX: H_3PO, H_3PNH (*trans*), H_3PCH_2 (*planar*), H_3PS, H_3PPH (*trans*), H_3PSiH_2 (*planar*).

HPX_2: HPO_2, $HP(NH)_2$ (*trans*), $HP(CH_2)_2$ (*planar*), HPS_2, $HP(PH)_2$ (*trans*), $HP(SiH_2)_2$ (*planar*).

$P(XH)_2^+$: PF_2^+, $P(OH)_2^+$ (*exo*), $P(NH)_2^+$ (*planar*), $P(CH_3)_2^+$ (*exo*), PCl_2^+, $P(SH)_2^+$ (*exo*), $P(PH_2)_2^+$ (*planar*), $P(SiH_3)_2^+$ (*exo*).

The properties plotted in each figure are as follows:

Figure A4-1: P-E bond length, in Ångstroms, (1Å = 100 pm)

Figure A4-2: Phosphorus bonding radius, $r_b(P) = r(P\text{-BCP})$, in atomic units.

Figure A4-3: Substituent atom bonding radius, $r_b(E) = r(E\text{-BCP})$, in atomic units.

Figure A4-4: Density at the P-E bond critical point, ρ_b, in atomic units.

Figure A4-5: Laplacian of the density at the P-E bond critical point, $\nabla^2\rho_b$, in atomic units.

Figure A4-6: Charge on the phosphorus atom, q(P), in electron units.

Figure A4-7: Charge on the substituent group, -q(X) or -q(R), in electron units.

Figure A4-8: Delocalization index, from the phosphorus atom to the substituent group, $\delta(P,X)$ or $\delta(P,R)$.

Figure A4-9 shows a plot of the delocalization index, $\delta(P,X)$ or $\delta(P,R)$, as a function of the charge transfer, -q(X) or -q(R), for each series. Best-fit quadratic curves are shown for each series, with some data points excluded from the fit. Similar plots are shown in each of the results chapters. Here $[P(XH)_2]^+$ includes XH = F, OH, NH_2, Cl and SH, while $[PR_2]^+$ includes R = H, CH_3, PH_2, and SiH_3. The HPX and HPX_2 curves do not include the X = CH_2 data. The H_3PX curve includes neither the X = CH_2 nor the X = PH data points.

Figure A4-1: Bond length between phosphorus and substituent atom

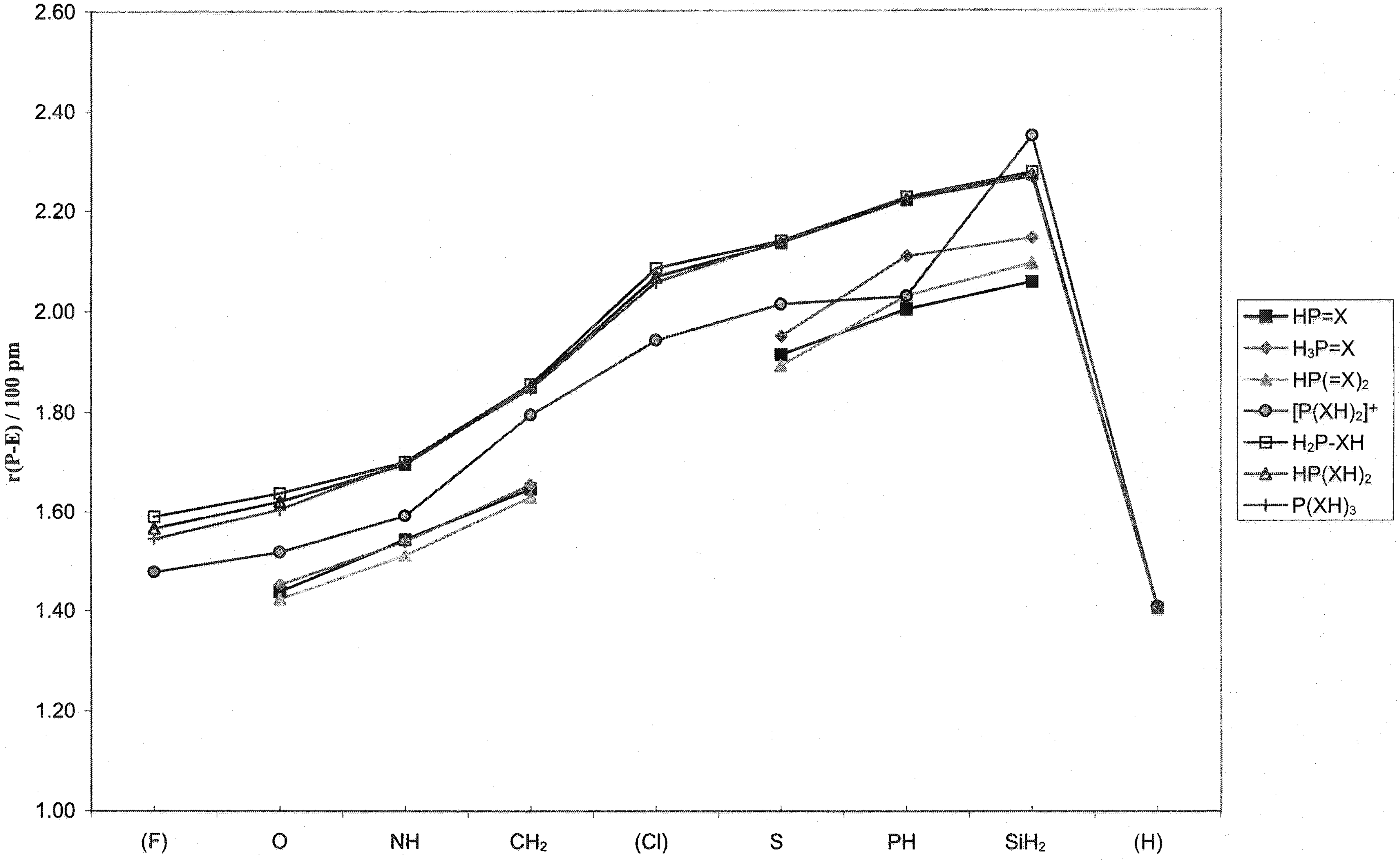

Figure A4-2: Bonding radius of phosphorus

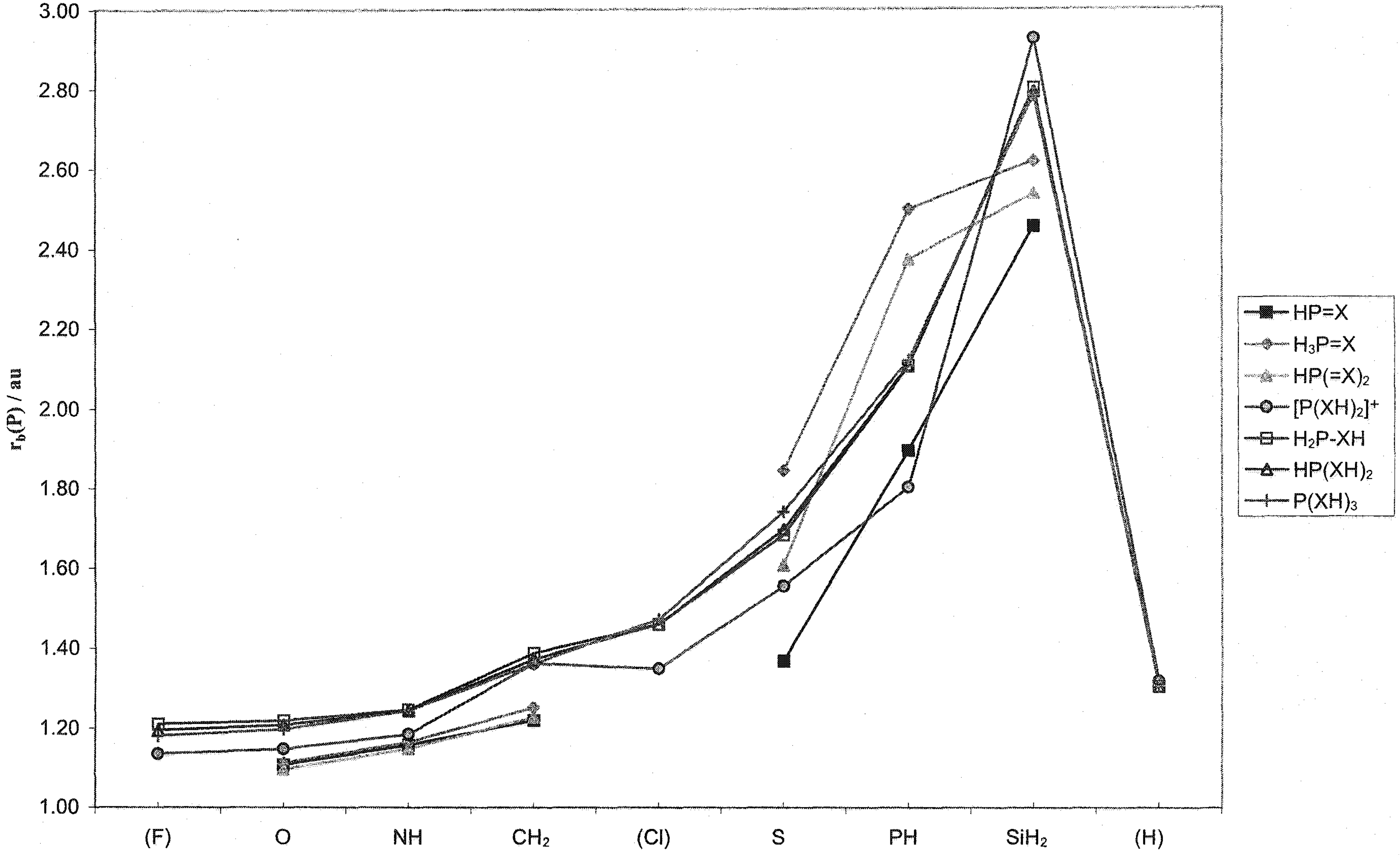

Figure A4-3: Bonding radius of substituent atom

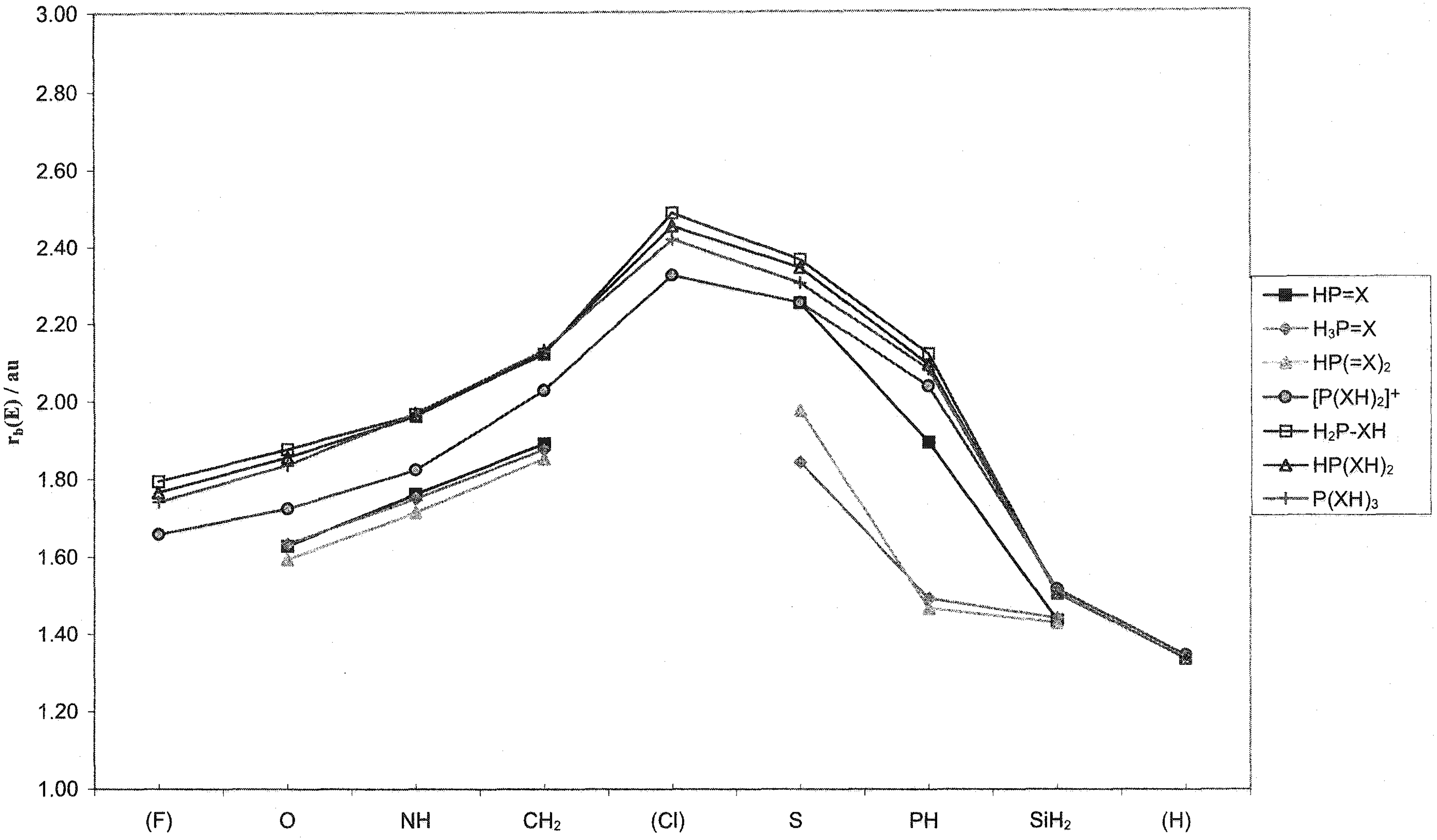

Figure A4-4: Electron density at the bond critical point

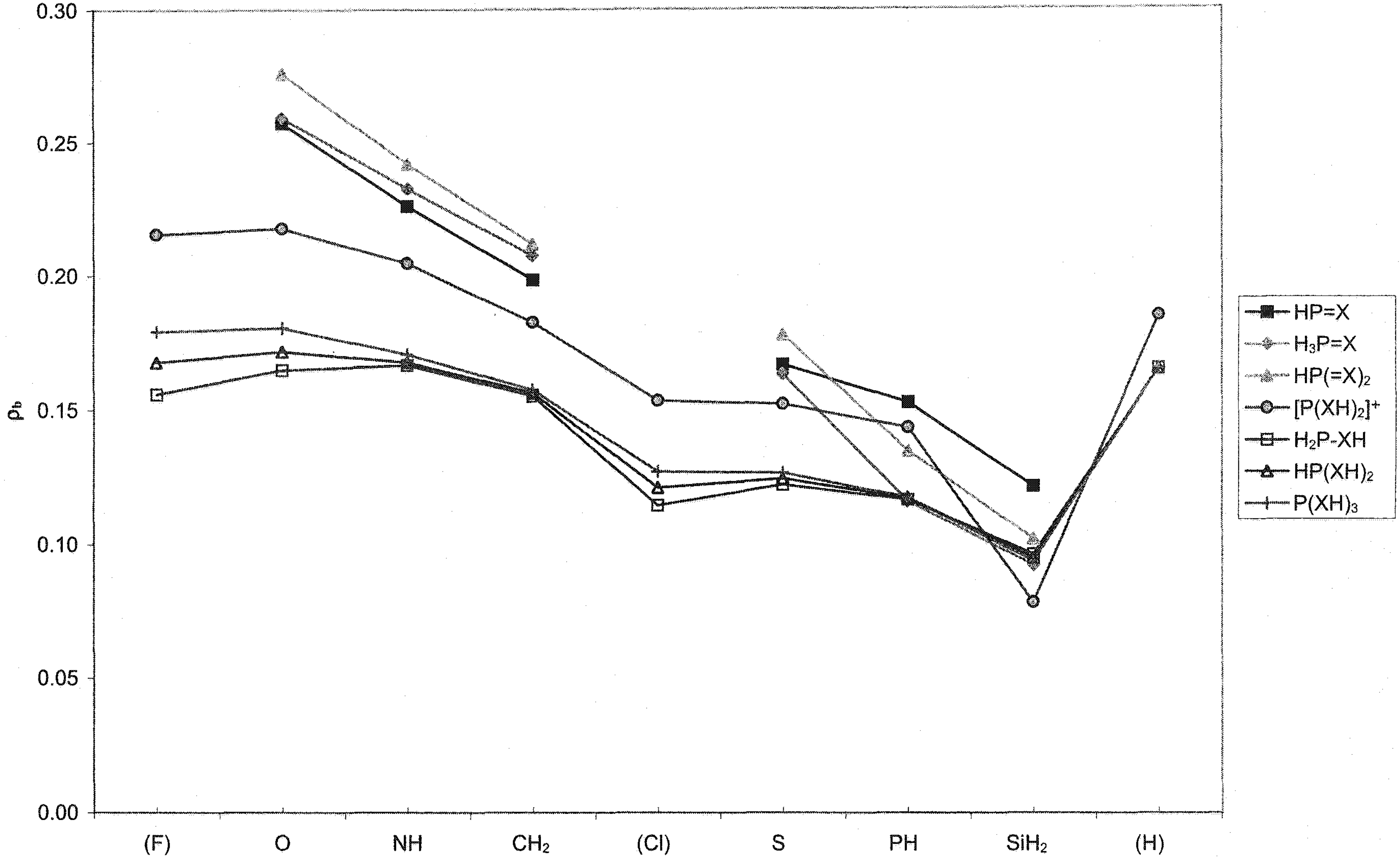

Figure A4-5: Laplacian of the electron density at the bond critical point

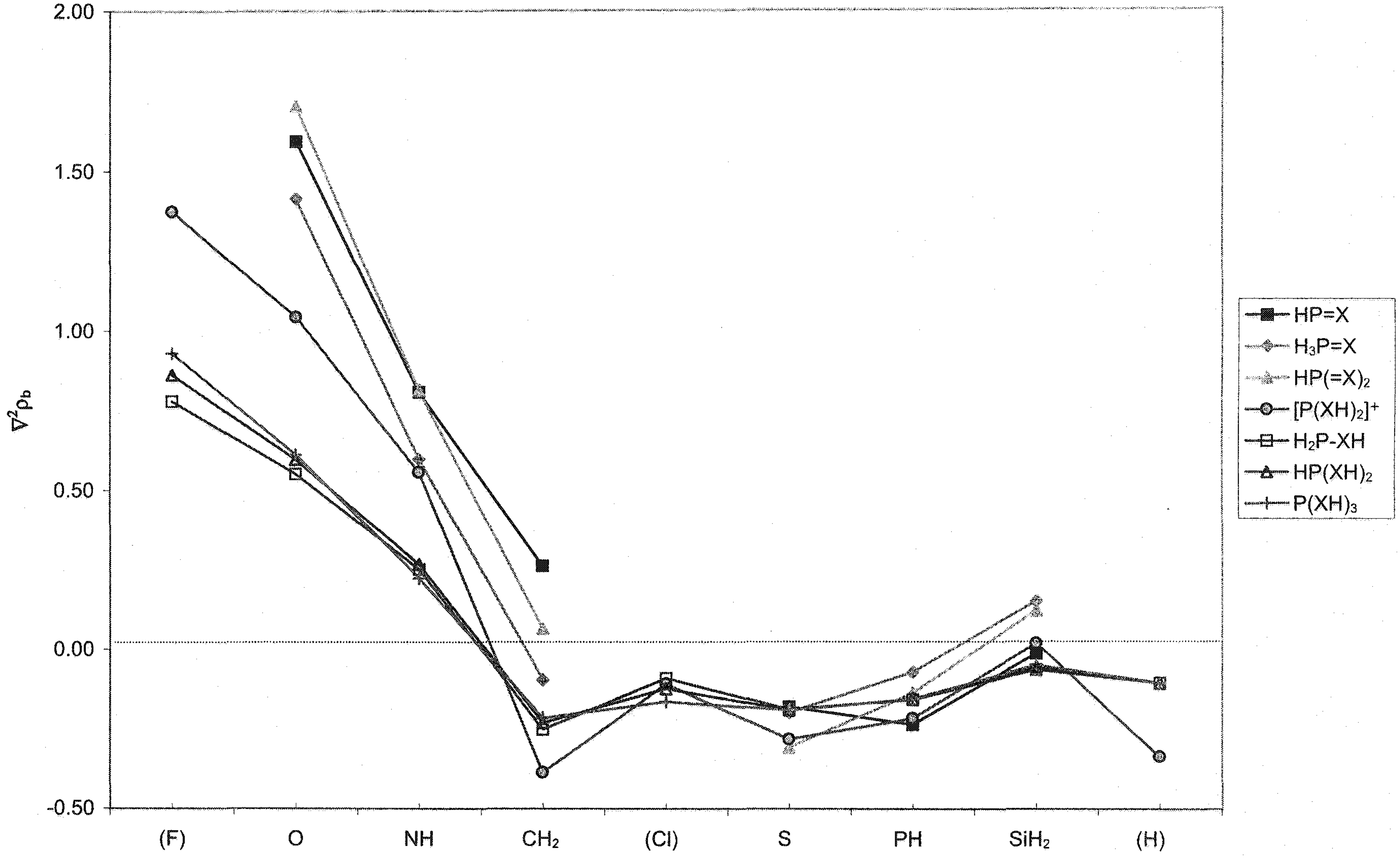

Figure A4-6: Atomic charge on phosphorus

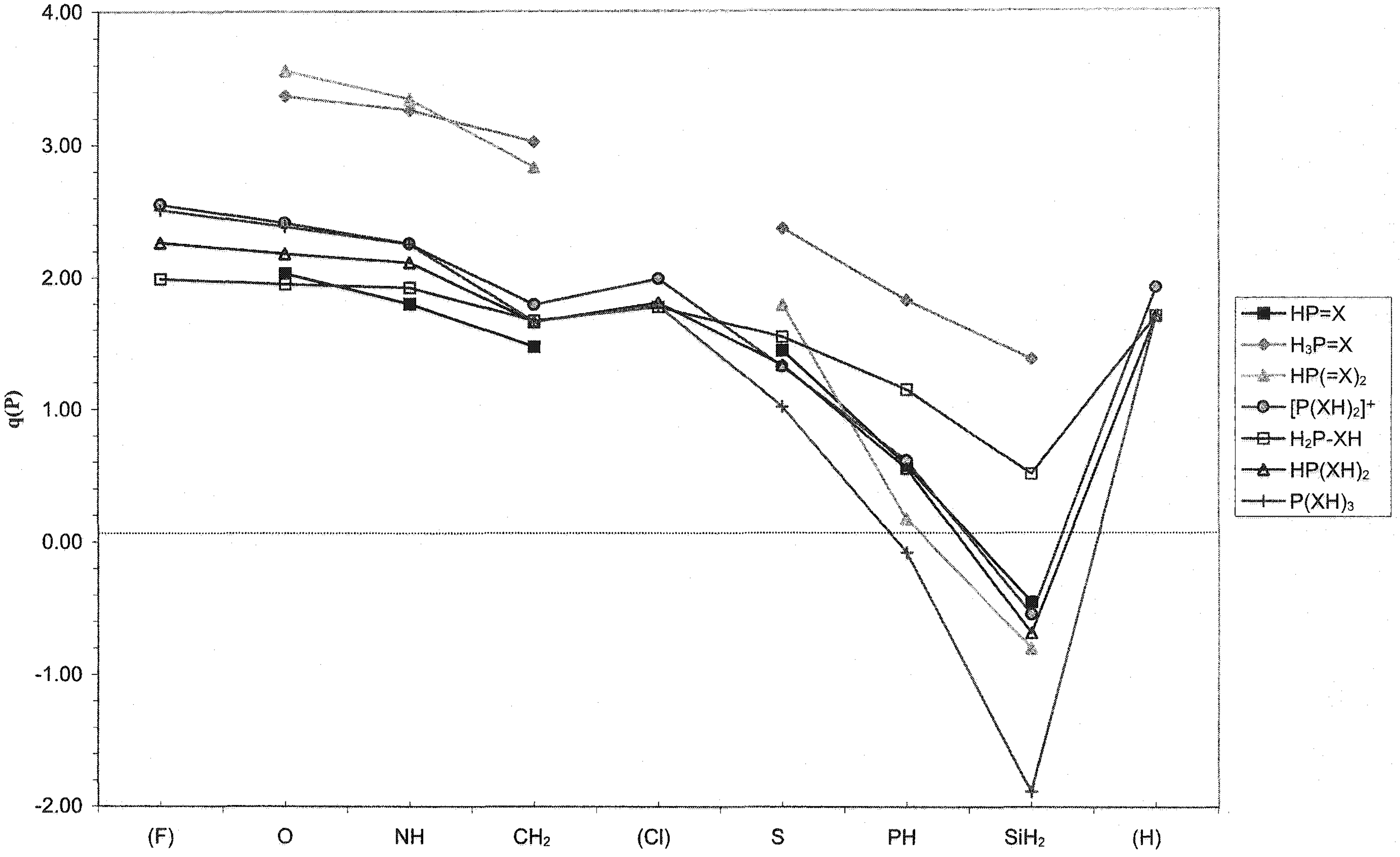

Figure A4-7: Charge transferred to substituent group

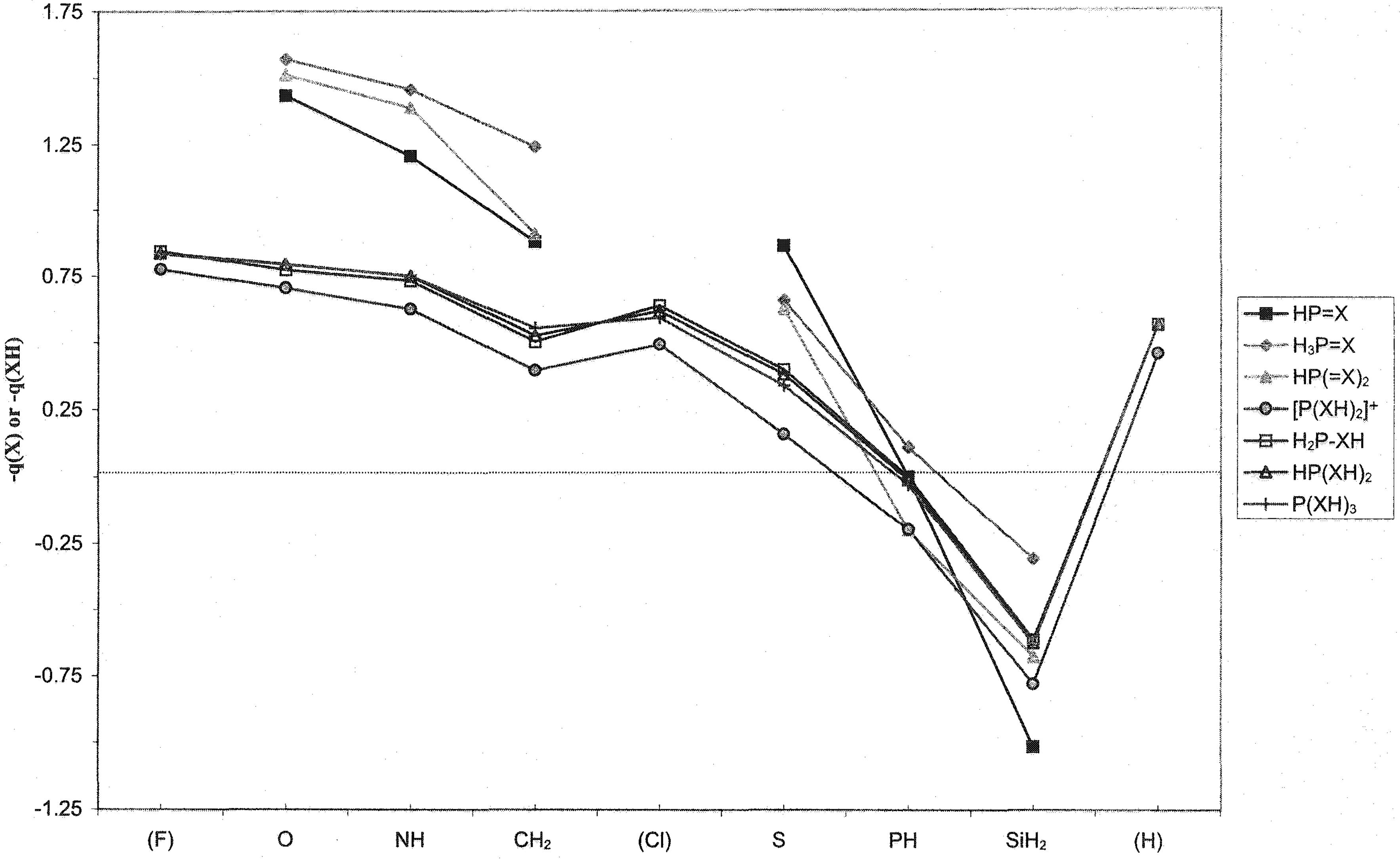

Figure A4-8: Delocalization index between phosphorus and substituent group

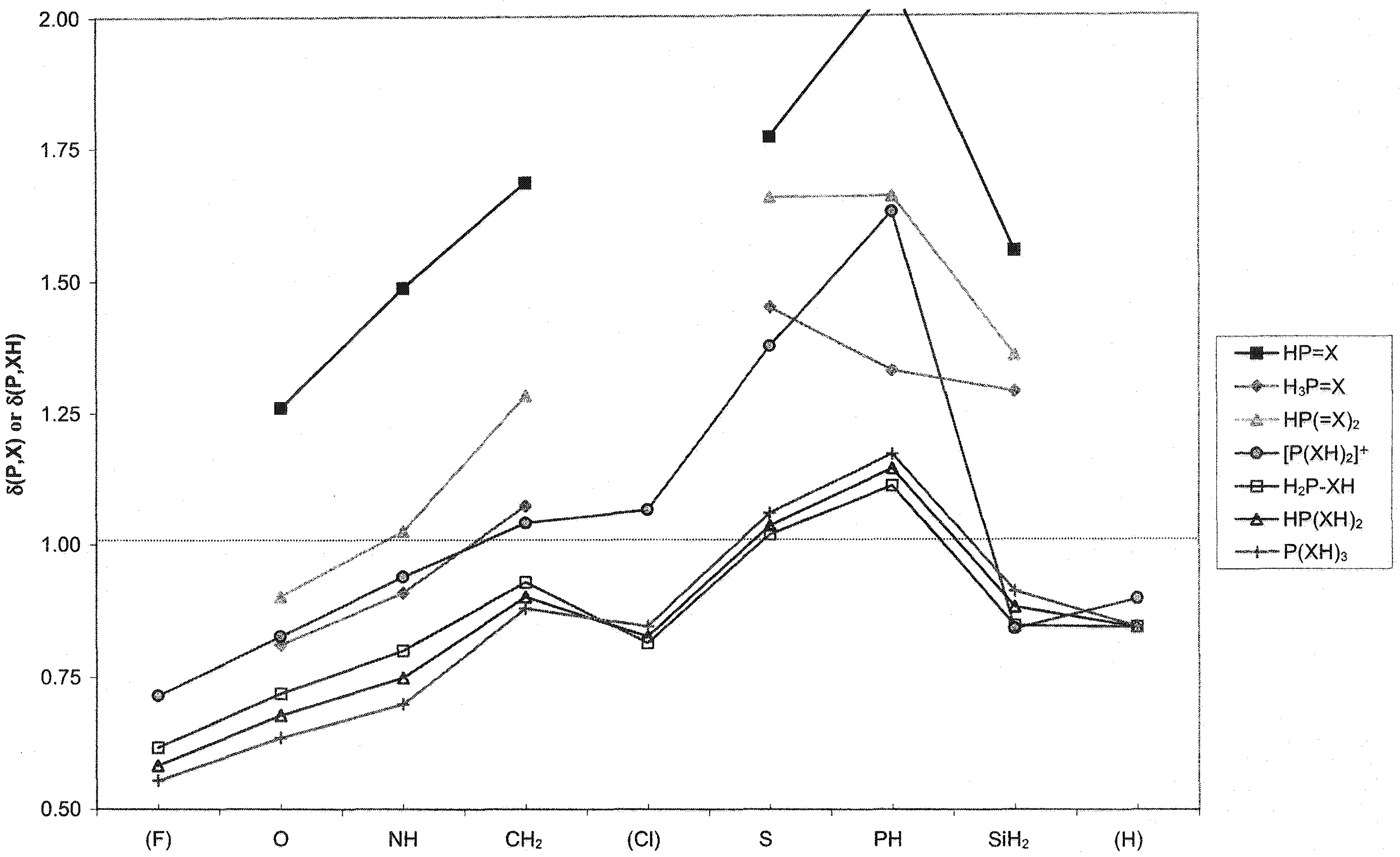

Figure A4-9: Delocalization index *vs*. charge on substituent group